Anthropogenic bromoform from industrial water treatment

Dissertation
zur Erlangung des Doktorgrades

der Mathematisch-Naturwissenschaftlichen Fakultät
der Christian-Albrechts-Universität zu Kiel
vorgelegt von

Josefine Maas

GEOMAR Helmholtz-Zentrum für Ozeanforschung Kiel

Kiel, Januar 2020

1. Gutachterin: Prof. Dr. Susann Tegtmeier
2. Gutachter: Prof. Dr. Arne Körtzinger

Tag der mündlichen Prüfung: 28.02.2020
Druckreife erhalten am: 28.02.2020

"Change will not come if we wait for some other person
or some other time. We are the ones we've been waiting for.
We are the change that we seek." – *Barack Obama*

Abstract

The control and ban of man-made long-lived ozone-depleting substances (ODSs) by the Montreal Protocol is expected to result in the recovery of the stratospheric ozone layer in the course of the 21st century. However, short-lived halogenated ODSs, which belong to the very short-lived substances (VSLSs), are not controlled and also participate in stratospheric ozone depletion through catalytic cycles. VSLSs are produced naturally from macroalgae and phytoplankton, and anthropogenically as disinfection by-products (DBPs) from chemical treatment of industrial water. Chemical treatment of seawater, e.g. cooling water of coastal power plants or ballast water of ships, mainly produces brominated VSLSs, with bromoform as the major DBP. Bromoform is also the largest source of organic bromine from biological marine sources to the atmosphere. Current estimates suggest that about 25 % of stratospheric bromine originate from naturally produced brominated VSLSs, while the contribution of anthropogenic VSLSs to the global bromine budget is still unclear.

Industrial water treatment has increased substantially over the last years due to strong economic growth and progressing industrialisation in East Asia and India. Furthermore, additional input of DBPs from ballast water treatment is expected in the near future as new regulations on ballast water discharge came into force in 2017. This increasing input of anthropogenic VSLSs from emerging industries and ballast water treatment to the environment has not been quantified yet. Given the growing importance of brominated VSLSs in the face of declining long-lived ODSs, a quantification of anthropogenic VSLS sources is urgently needed.

The aim of this thesis is to quantify the environmental input of anthropogenic brominated VSLSs from industrial water treatment, their distribution in the ocean and atmosphere, and their entrainment into the stratosphere. The assessment focusses on the major DBP bromoform. Its environmental input is quantified based on the estimation of treated seawater volumes from different industrial sectors, as well as the concentration of bromoform in treated waters. The derived global distribution of anthropogenic bromoform sources serves as the initial release field for Lagrangian simulations of bromoform pathways in the ocean and atmosphere, and as the basis for air-sea flux calculations. Different scenarios are run to capture the most likely range of the anthropogenic input of bromoform into the ocean and atmosphere. Oceanic trajectory simulations are performed with the ARIANE software to analyse seasonal to annual variations of bromoform distribution. Atmospheric bromoform mixing ratios are simulated with the FLEXPART model in order to analyse the tropospheric and stratospheric distribution.

The analyses show that the anthropogenic bromoform input from ballast water treatment in the near future will only have a minor contribution to the global atmospheric

bromine budget with 3–13 Mmol Br a^{-1} compared to a global climatological bromine flux of 1.7 Gmol Br a^{-1}. Current ballast water discharge volumes of 3.4 billion m^3 a^{-1} are too small to produce globally significant amounts of anthropogenic bromoform. Nevertheless, locally very high emissions of up to 3500 pmol m^{-2} h^{-1} can be well above background emissions around major harbours in Southeast Asia, e.g. Singapore and the Pearl River Delta. Hence, bromoform from ballast water treatment can be an additional input on local scales impacting tropospheric chemistry.

In contrast to the low ballast water volumes, coastal power plants globally discharge over 820 billion m^3 a^{-1} of treated cooling water. Combining the climatological bottom-up air-sea flux estimate with the bromoform flux from anthropogenic sources, the global bromine budget increases by 8–35 % to 1.9–2.2 Gmol Br a^{-1}.

Over 96 % of treated cooling water originate from the regions East-Southeast Asia, Europe, North America, India and Arabia. Bromoform is usually released to the atmosphere on short time scales of a few days and close to its source in the ocean. An effective transport into the stratosphere mainly takes place in the tropics, whereas in extratropical regions the majority of bromoform stays in the lower troposphere and is rapidly removed by deposition. For instance, there are large emissions over Europe without an effective bromoform transport into the stratosphere.

About half of the global anthropogenic bromoform is released in the region around East-Southeast Asia, which corresponds to an annual emission of 100–300 Mmol Br a^{-1}. The majority of this is discharged in the extratropics along the coasts of the Yellow, Japan and East China Seas. Still about 20 % of the bromoform from this region is entrained into the stratosphere during boreal winter due to transport towards the tropical West Pacific by northeasterly winds. The tropical West Pacific, as well as the Indian Ocean are the most efficient regions for stratospheric entrainment of bromoform. Over the Indian Ocean, tropical convection and the monsoon circulation during boreal summer transport 40–50 % of bromoform from the marine boundary layer to the stratosphere. Thereby, anthropogenic emissions contribute 10–43 % to stratospheric bromoform entrainment over the Indian Ocean, and 4–25 % over the global inner tropics.

The anthropogenic sources of brominated VSLSs are predicted to increase in the future. In particular, increased bromoform emissions from growing industries in tropical regions will likely lead to more bromine input into the stratosphere. In order to reduce the uncertainties of DBP concentration in treated seawater, as well as the number of missing sources in the bromoform air-sea flux estimate, additional observations along the coasts close to the industrial areas are necessary. A better understanding of all natural and anthropogenic sources of brominated VSLSs and their future trends will thus improve estimates of the global atmospheric bromine input.

Zusammenfassung

Aufgrund der Kontrolle und das Verbot von menschengemachten, langlebigen, ozonzerstörenden Substanzen (ODS), welche durch das Montreal-Protokoll geregelt sind, wird sich die stratosphärische Ozonschicht voraussichtlich im Laufe des 21. Jahrhunderts wieder erholen. Kurzlebige halogenierte ODS werden zwar nicht kontrolliert, sind aber auch am stratosphärischen Ozonabbau durch Katalysezyklen beteiligt. Diese kurzlebigen Substanzen entstehen natürlich durch Makroalgen und Phytoplankton, sowie als Desinfektionsnebenprodukte (DBP) bei der chemischen Behandlung von industriell genutztem Wasser. Dabei erzeugt die chemische Desinfektion von Meerwasser hauptsächlich bromierte Substanzen, was z.B. im Kühlwasser von Küstenkraftwerken oder im Ballastwasser von Schiffen auftritt. Bromoform kommt dabei am häufigsten vor und dessen biologische Quellen sind außerdem für den größten Eintrag von organischem Brom in die Atmosphäre verantwortlich. Aktuelle Schätzungen gehen davon aus, dass etwa 25 % des stratosphärischen Broms aus natürlichen Quellen von bromierten kurzlebigen Substanzen stammen, wohingegen der Beitrag anthropogener kurzlebiger Substanzen zum globalen Brombudget noch unklar ist.

Die industrielle Wasserbehandlung hat in den letzten Jahren aufgrund des starken Wirtschaftswachstums und der fortschreitenden Industrialisierung in Ostasien und Indien erheblich zugenommen. Darüber hinaus wird in naher Zukunft ein zusätzlicher Eintrag von DBP aus der Ballastwasserbehandlung erwartet, da seit 2017 neue Vorschriften zur Qualität von abgelassenem Ballastwasser eingehalten werden müssen. Dieser zunehmende Eintrag von anthropogenen kurzlebigen Substanzen in die Umwelt durch die wachsende Industrialisierung in Schwellenländern und die Ballastwasserbehandlung wurde bisher noch nicht quantifiziert. Angesichts der wachsenden Bedeutung bromierter kurzlebiger Substanzen durch den Rückgang langlebiger ODS, ist eine Quantifizierung der anthropogenen Quellen dieser Substanzen dringend erforderlich.

Ziel dieser Arbeit ist es, den Eintrag anthropogener bromierter Substanzen aus der industriellen Wasserbehandlung zu bestimmen, sowie ihre Verteilung im Ozean und in der Atmosphäre bis hin zum Eintrag in die Stratosphäre zu quantifizieren. Die Auswertungen konzentrieren sich dabei auf das am meisten verbreitete DBP Bromoform. Dessen Umwelteintrag wird anhand der abgeschätzten Menge an desinfiziertem Meerwasser aus verschiedenen Industriesektoren, sowie seiner Konzentration im behandelten Wasser bestimmt. Die daraus abgeleitete globale Verteilung anthropogener Bromoformquellen dient als Ausgangsfeld für Lagrange-Modellsimulationen von Transportwegen im Ozean und in der Atmosphäre, sowie als Grundlage für die Berechnung des Gasaustauschs an der Meeresoberfläche vom Ozean in die Atmosphäre. Anhand unterschiedlicher Modellszenarien wird die Menge des anthropogenen Bromoformeintrags in den Ozean und die Atmosphäre

durch einen Minimal- und Maximalwert abgeschätzt. Ozeansimulationen werden mit der ARIANE-Software durchgeführt. Die Bromoformverteilung in der Troposphäre und Stratosphäre wird mit dem FLEXPART-Modell simuliert.

Die Berechnungen ergeben, dass der zukünftige anthropogene Bromoformeintrag aus der Ballastwasserbehandlung auf Schiffen mit 3–13 Mmol Br a^{-1} nur einen sehr geringen Beitrag zum globalen atmosphärischen Brombudget leisten wird. Der bisher abgeschätzte Bromoformeintrag aller Quellen an der Meeresoberfläche in die Atmosphäre beträgt dagegen 1,7 Gmol Br a^{-1}. Das derzeitige globale Ballastwassergesamtvolumen von 3,4 Mrd. m^3 a^{-1} ist zu gering, um signifikante Mengen an DBP zu produzieren. Nichtsdestotrotz können die Emissionen lokal mit bis zu 3500 pmol m^{-2} h^{-1} sehr hoch sein und deutlich über den Hintergrundemissionen in großen Häfen in Südostasien liegen, z.B. in Singapur und im Perlflussdelta. Daher könnte das zusätzliche Bromoform aus der Ballastwasserbehandlung durchaus Einfluss auf die Atmosphärenchemie im lokalen Umfeld der Quellen nehmen.

Im Gegensatz zu den geringen Ballastwassermengen, leiten Küstenkraftwerke weltweit mehr als 820 Mrd. m^3 a^{-1} desinfiziertes Kühlwasser ab. Kombiniert man den bisherigen Bromoformeintrag von 1,7 Gmol Br a^{-1} mit dem industriellen Eintrag durch behandeltes Kühlwasser, erhöht sich das globale Brombudget um 8–35 % auf 1,9–2,2 Gmol Br a^{-1}.

Über 96 % des desinfizierten Kühlwassers stammt aus den Regionen Ost- und Südostasien, Europa, Nordamerika, Indien und Arabien. Bromoform wird normalerweise innnerhalb kurzer Zeit von wenigen Tagen und in der Nähe der Quellen im Ozean in die Atmosphäre ausgegast. Ein effektiver Transport in die Stratosphäre findet hauptsächlich in den Tropen statt, wohingegen in außertropischen Regionen der größte Teil des Bromoforms in der unteren Troposphäre verbleibt und durch Niederschlag schnell wieder aus der Luft entfernt wird. Beispielsweise gibt es in Europa große Emissionen ohne einen wirksamen Bromoformtransport in die Stratosphäre.

In der Region um Ost- und Südostasien wird etwa die Hälfte des globalen anthropogenen Bromoforms ausgegast, was einer jährlichen Emission von 100–300 Mmol Br a^{-1} entspricht. Das meiste davon wird außerhalb der Tropen entlang der Küsten des Gelben Meeres, des Japanischen Meeres und des Ostchinesischen Meeres freigesetzt. Dennoch wird etwa 20 % des Bromoforms aus dieser Region im borealen Winter in die Stratosphäre gebracht, da es durch Nordostwinde in Richtung des tropischen Westpazifik transportiert wird. Der tropische Westpazifik sowie der Indische Ozean sind die effizientesten Regionen für den Bromoformtransport in die Stratosphäre. Über dem Indischen Ozean können 40–50 % des Bromoforms aus der unteren Troposphäre mittels tropischer Konvektion und der Zirkulation des indischen Sommermonsuns in die Stratosphäre gelangen. Dabei tragen die anthropogenen Emissionen über dem Indischen Ozean zu 10–43 % zum stratosphärischen Bromoformeintrag in dieser Region bei. Die globalen anthropogenen Emissionen sind für 4–25 % des stratosphärischen Bromoforms über den Tropen verantwortlich.

In Zukunft werden die anthropogenen Quellen von bromierten kurzlebigen ODS voraus-

sichtlich weiter zunehmen. Insbesondere stärkere Bromoformemissionen durch ansteigende Industrialisierung in tropischen Regionen werden wahrscheinlich zu einem höheren Bromeintrag in der Stratosphäre führen. Um die Unsicherheiten der DBP-Konzentration in behandeltem Meerwasser zu verringern, sowie die Kenntnis des atmosphärischen Bromoformeintrags zu verbessern, sind zusätzliche Beobachtungen entlang der Küsten nahe der Industriegebiete erforderlich. Ein besseres Verständnis aller natürlichen und anthropogenen Quellen von bromierten VSLS und ihrer zukünftigen Trends kann daher die Abschätzungen des globalen atmosphärischen Bromeintrags deutlich verbessern.

Manuscript contribution

This thesis is based on the following manuscripts:

Maas, J., Tegtmeier, S., Quack, B., Biastoch, A., Durgadoo, J. V., Rühs, S., Gollasch, S., and David, M. (2019). Simulating the spread of disinfection by-products and anthropogenic bromoform emissions from ballast water discharge in Southeast Asia. *Ocean Science*, 15(4):891–904

Contribution: I designed the Ariane simulations, produced the data output and made all figures. JVD and AB provided the model code, JVD and SR set up the Lagrangian environment. ST and BQ designed the research question. ST and MD provided samples. I wrote the manuscript with the help of all co-authors.

Maas, J., Jia, Y., Quack, B., Biastoch, A., Durgadoo, J. V., and Tegtmeier, S. (2020). Simulations of anthropogenic bromoform reveal high emissions at the coast of East Asia. *Atmospheric Chemistry and Physics Discussions*, 1004:1–31, under review.

Contribution: I defined the research question and methodology with help of ST and BQ. I designed the Ariane simulations with help of JVD. AB and JVD provided ocean model code. I ran the oceanic ARIANE simulations, YJ did the atmospheric FLEXPART simulations. I analysed all data, made the figures and wrote the manuscript with the help of the co-authors.

Maas, J., Jia, Y., Quack, B., and Tegtmeier, S. (2020). Global emissions of anthropogenic bromoform from industrial seawater treatment. In prep.

Contribution: I defined the research question and methodology with help of ST. I designed the emission maps, made all the figures and wrote the manuscript. YJ ran the FLEXPART simulations.

Contents

1 Introduction

The ban of man-made ozone-depleting substances (ODSs) through the Montreal Protocol in 1987 to protect the ozone layer was a milestone of international research and politics. The control and gradual decline of long-lived ODSs (e.g. chlorofluorocarbons (CFCs)) has been predicted to lead to the recovery of the ozone layer by the second half of the 21st century (Engel and Rigby, 2018). Besides long-lived ODSs, there are additional, less abundant short-lived ODSs in the atmosphere which have both natural and anthropogenic sources in the ocean and are not controlled under the Montreal Protocol. Parts of the short-lived ODSs entrain into the stratosphere through tropical convection where they release the halogen and take part in ozone depletion through catalytic cycles. Thereby bromine is much more efficient in destroying ozone than chlorine (Sinnhuber et al., 2009) which makes brominated ODSs important for the recovery process of the ozone layer.
Certain short-lived brominated ODSs, like bromoform, are produced anthropogenically as by-products from industrial water treatment, e.g. in cooling water of power plants (Jenner et al., 1997). Moreover, an entirely new source of short-lived ODSs is emerging from the treatment of ballast water in ships to control the spread of invasive species (Werschkun et al., 2012). The atmospheric input of short-lived ODSs from industrial sources has been estimated to be a minor contribution compared to natural emissions (Quack and Wallace, 2003) due to a lack of global data. However, industrial growth and new emerging sources from ships might be larger than believed so far, and thus represent a relevant factor in the global estimates of bromine air-sea flux. Since the abundance of long-lived ODSs is declining, short-lived ODSs are gaining more importance and a quantification of anthropogenic sources becomes necessary.
In this chapter, I first present the industrial sectors and introduce the generating mechanism for brominated by-products; then I explain the role of short-lived brominated ODSs in the climate system, and finally, I motivate this work with my research questions.

1.1 Industrial water treatment

Whenever large volumes of water are used for industrial purposes, this water is withdrawn from natural reservoirs, such as the ocean, lakes or rivers. Waters from natural sources are characterised by their variety in properties, like temperature, salinity, organic matter and different types of biota. They usually have to be treated for different reasons, such

as disinfection, taste and odour control of drinking and tap water, and for bio-fouling control (Khalanski and Jenner, 2012) depending on the water application and the sector. Bio-fouling is understood as the unwanted accumulation of microorganisms, plants, algae and animals on submerged surfaces, e.g. water pipes or ship hulls. The main reason for industrial water treatment is the prevention of bio-fouling to avoid corrosion for proper functioning of the cooling system (Joint Research Council, 2001). In this thesis, the term water treatment refers to disinfection methods which minimise negative effects from marine biology. In many cases, treated water is returned to the environment and can thus change local water conditions.

1.1.1 Water treatment sectors

Ballast water

Ballast water is used for commercial vessels to maintain stability and draught during voyage and port operations. It acts as additional weight when a vessel is not fully loaded to compensate for increased buoyancy and stresses on the hull from unbalanced freight distribution (David, 2015). Thus, ballast water is indispensable for a save functioning of commercial vessels. Ballast water operations are usually executed in the port, where water is taken up during cargo unloading and discharged during loading of goods. The capacity of ballast water tanks depends on the cargo capacity of a vessel, which is given by its dead weight tonnage (DWT). Thus, the larger the vessel and its DWT, the more ballast water is needed to compensate the weight loss when cargo is unloaded (David, 2015) with tankers and bulk carriers having the largest ballast water volume. The global commercial fleet consists of over 94,000 vessels with a combined capacity of 1.92 billion DWT (UNCTAD, 2018). The volume of global ballast water is estimated to be around 3–5 billion m^3 per year (Tamelander et al., 2010; Endresen et al., 2004; David, 2015).
Not only ballast water is transported across the ocean but also marine organisms therein are spread into different ocean basins with the water. It has been known for decades, that commercial shipping is the main driver of global spread of marine invasive species, with negative impacts on ecosystems, economies and public health (Ruiz et al., 2000; Briski et al., 2012). The introduction of non-indigenous species to alien ecosystems is considered as one of the greatest threats to the ecological and economic well-being of the planet (GloBallast, 2013). Invasive species can be e.g. bacteria, like the *Vibrio cholerae*, which causes human epidemic cholera (Ruiz et al., 2000), or larger macroinvertebrates such as the zebra mussel *Dreissena polymorpha*. The invasion of the zebra mussel into North America caused major economic losses due to bio-fouling, and alterations of the food web by displacement of native species (Briski et al., 2012).
In 2004, the International Maritime Organization (IMO) adopted the Ballast Water Management (BWM) Convention, which entered into force on September 8^{th}, 2017 (IMO,

2004). The Convention obligates shipowners from ratified states to manage the ballast water in order to minimise the survival of organisms and to prevent new introduction of non-indigenous species. One proposed option of ballast water management is the on-board use of an approved ballast water treatment system (BWTS), which is based on physical or chemical treatment methods (e.g. David and Gollasch, 2015). In order to get approval for a BWTS by the Joint Group of Experts on the Scientific Aspects of the Marine Environmental Protection - Ballast Water Working Group (GESAMP-BWWG), the efficiency of the system in eliminating biological species has to be proven. To ensure that the IMO standards for treated ballast water are fulfilled, BWTSs usually use two or more treatment technologies, that will be explained in detail in Chapter 1.1.2. Systems that use chemical treatment methods or 'active substances' are required to show that the amount of residual oxidant and related chemicals is not environmentally harmful in terms of persistence, bioaccumulation and toxicity (PBT) (MEPC 57/21, 2008). The different types of BWTSs all have advantages and drawbacks in their usage and impact on the environment.

Ballast water treatment is a new sector of water treatment given the very recent ratification of the BWM Convention. The retrofitting of over 75,000 ships will be an ongoing process over the next years (David and Gollasch, 2015). Until now, it is unknown to what share the different treatment methods will be applied, thus the impact of treated ballast water on the environment is highly uncertain.

Cooling water

Cooling water is used in industry mainly by power plants to regulate the temperature in the system and keep the electric turbines running (Jenner et al., 1998). In particular, coal fired and nuclear power plants have a high demand of cooling water, usually $40\,m^3\,s^{-1}$ per 1000 MW, i.e. $144\,m^3$ of water per MWh (Jenner et al., 1998; Taylor, 2006). Such large capacity plants are often located at the coast where they can profit from an unlimited water supply. They mostly use a once-through cooling technique where the water passes from the heat exchangers directly back into the sea. This way, very large volumes of heated water, being 11–15 °C warmer than the surroundings, are discharged into the environment (Jenner et al., 1998), decreasing water density at the sea surface. This has a direct effect on the marine environment by affecting the physiology of species and reducing the oxygen solubility of the water (Joint Research Council, 2001). Such issues can be controlled by a suitable choice of the cooling water intake and outfall location, e.g. where tidal or estuarine flows ensure mixing and dispersion of the heated water (Joint Research Council, 2001).

In case a suitable water source is not available, recirculating systems are used, where the water is cycled through cooling towers via evaporative cooling (Joint Research Council, 2001). In contrast to recirculating systems, there is no water consumption in the once-

through system, which means the same amount of water withdrawn from the source is released back to the environment. On the downside, this also implies that bio-fouling and clogging of the water supply system and corrosion is a much more relevant threat.
At the coast, fish and other macro-organisms can be entrained into the cooling system at large water intakes. Moreover, the cooling systems are highly affected by accumulation of organisms, which can eventually lead to a failure of the system. Water treatment is necessary to reduce the development of bio-fouling and to prevent corrosion. It is therefore essential for maintenance of efficient heat transfer and securing the operability of the system, thus reducing the total energy consumption (Joint Research Council, 2001). Apart from other industrial sectors applying cooling water treatment, such as refineries or chemical plants, the biggest sector are electric power plants. In this thesis, the focus lies on DBPs from water treatment in coastal power plants. In the following, the term industrial cooling water refers to cooling water in coastal power plants.

Further water treatment applications

In addition to power plants and shipping industry, other industrial sectors also apply water treatment. These include desalination, wastewater treatment and recreational water treatment, as well as seawater toilets. These sources are only of minor importance with respect to the water volumes used and are not discussed further. Desalination plants require moderate amounts of seawater, however very limited data are available to evaluate the environmental impact from water treatment. The amount of treated water from desalination plants or brine is estimated to be around 50 billion $m^3\,a^{-1}$ (Jones et al., 2019). This is 10–15 times more than ballast water volumes and one order of magnitude less than cooling water volumes (see Chapter 2.1.2). Desalination plants can be of regional importance e.g. in the Arabian Peninsula, the Middle East and North Africa (Jones et al., 2019).

1.1.2 Water treatment methods

Ballast water and cooling water are treated with chemical or physical methods. Chemical treatment methods add a chemical disinfectant to the water stream which reduces accumulation of biology but also alters the chemical composition of the water. In contrast, physical methods cause no chemical reactions in the water and are thus more environmentally friendly but sometimes less effective. Often two or more treatment methods are combined in a treatment system.

Chlorination

Chlorination is the most common water treatment method to date, as chlorine is a powerful oxidising agent available at a reasonable cost that has been efficiently applied since

the end of the 19th century (Khalanski and Jenner, 2012). Chlorine is either added to the water by dissolution of chlorine gas (Cl_2) or addition of sodium hypochlorite (NaOCl). NaOCl can either be stored on-site or is generated by electrolysis from the electro-chemical reaction of sodium-chloride (NaCl) in the seawater (Khalanski and Jenner, 2012):

$$NaCl + H_2O \rightarrow NaOCl + H_2 \tag{1.1}$$

Both chemicals, NaOCl and Cl_2, further react in water to produce oxidants:

$$NaOCl \rightarrow Na^+ + ClO^- \tag{1.2}$$
$$Cl_2 + H_2O \rightarrow HCl + HOCl \tag{1.3}$$
$$HOCl \rightarrow H^+ + ClO^- \tag{1.4}$$
$$HOCl + Br^- \rightarrow HOBr + Cl^- \tag{1.5}$$
$$HOBr \rightarrow H^+ + BrO^- \tag{1.6}$$

Cl_2 and NaOCl react rapidly in the water which forms the oxidising agents hypobromous acid (HOBr), hypochlorous acid (HOCl), and also less commonly hypobromite ion (BrO^-) and hypochlorite ion (ClO^-) (1.2)–(1.6). During treatment of seawater, 99 % of these reactions happen within the first 10 seconds (Taylor, 2006; Khalanski and Jenner, 2012). Due to the elevated bromide ion content in seawater, the main oxidant for water chlorination is hypobromous acid (Werschkun et al., 2012).

Ozonation

Another frequently used treatment method is ozonation. Ozone (O_3) can be produced on-site from air or pure oxygen. Ozone is a stronger oxidant than chlorine and thus a very effective disinfecting agent, especially for drinking water (Rajagopal et al., 2012). Ozone treatment forms the hydroxyl radical (OH) which reacts with bromide ions in seawater to the disinfecting agents hypobromous acid or to hypobromite ion (Werschkun et al., 2012). However, ozonation is more expensive in its use than chlorination and the high volatility of ozone can be toxic for living organisms that come into contact with the treated water (Rajagopal et al., 2012).

Filtration

Among the physical water treatment methods, filtration is the most commonly applied method. It is usually used as a pre-treatment to other methods. Filters of different mesh size are in use with coarse grids >1 cm removing large debris, fish and large aquatic plants. Smaller filters <1 mm can even remove planktonic organisms or suspended matter.

However, such filters can also cause clogging in heavily turbid waters.

UV Radiation

Ultraviolet (UV) radiation is a physical treatment method often used for sterilisation purposes (Rajagopal et al., 2012). The high-energy light is capable of killing bacteria in the water. However, it is more complex in its use than other methods, which limits its applicability for very large water volumes. Moreover, the water clarity is important for proper functioning of UV-treatment because turbidity, sediments and dissolved organic matter (DOM) reduce the efficiency of UV radiation as disinfectant (Rajagopal et al., 2012). Therefore, the use in natural shallow waters, such as rivers or estuaries, is limited for UV-treatment, unless sediments and DOM are removed by filtration. Nevertheless it can be an environmentally-friendly alternative to oxidative water treatment methods.

Hydrogen peroxide and peracetic acid

The aqueous solution of peracetic acid (CH_3CO_3H) is an equilibrium mixture of acetic acid (CH_3CO_2H) and hydrogen peroxide (H_2O_2). Chemical disinfection by peracetic acid is due to the production of oxygen free radicals (Rajagopal et al., 2012).

Besides the methods presented here, there are various other physical and chemical disinfection techniques, which are less commonly used. In this thesis, the main focus lies on the chemical treatment methods from different chlorination techniques, which is used by most treatment systems. Therefore, in this thesis the terms 'industrial water treatment' or 'chemical water treatment' is considered here as equivalent and refer to the method of chlorination of seawater and brackish water.

1.1.3 Disinfection by-products

One major environmental issue of chemical water treatment is the generation of various compounds formed by the reaction of the oxidant with organic constituents in natural waters (Khalanski and Jenner, 2012). Especially chlorination and ozonation methods produce large amounts of DBPs. The general mechanism for the generation of DBPs is the reaction of HOBr or BrO^- with organic (mostly DOM) or inorganic moieties in the water (Fig. 1.1) producing different trihalomethanes (THMs), haloacetic acids and bromate (BrO_3^-) (Delacroix et al., 2013; Shah et al., 2015). Over 600 compounds have been identified in chlorinated water (Richardson et al., 2007) and some of the DBPs are suspected to be toxic, mutagenic or carcinogenic for humans (Khalanski and Jenner, 2012). For drinking water, maximum concentrations of DBPs are regulated (WHO, 2011). While treatment of freshwater mostly leads to chlorinated DBPs, elevated bromide levels in seawater of 65–68 $mg\,L^{-1}$ result in more bromine DBPs (Khalanski and Jenner, 2012;

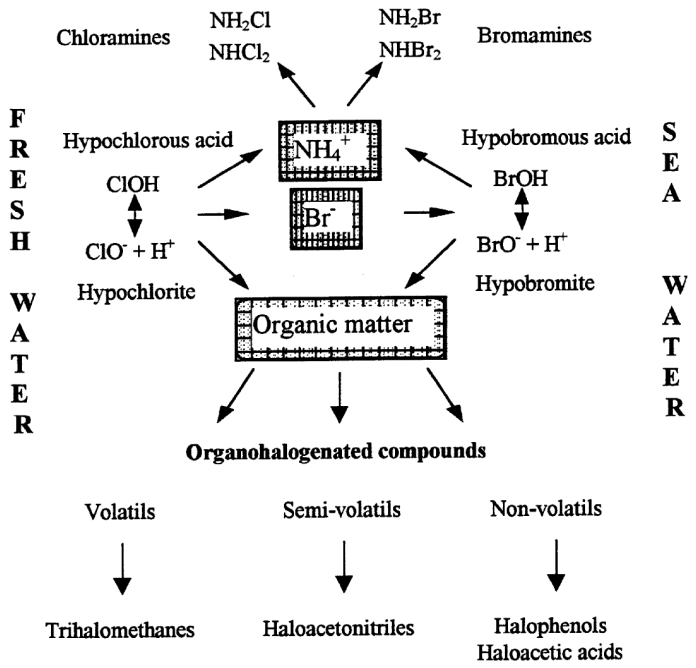

Figure 1.1: Main reactions forming disinfection by-products (DBPs) during water chlorination with HOCl/HCl in freshwater (left) and HOBr/HBr (right) in saline water (from Allonier et al., 1999).

Werschkun et al., 2012, Fig. 1.1). Brominated substances have been shown to be more cytotoxic and genotoxic than chlorinated DBPs (Richardson et al., 2007; Shah et al., 2015). No regulations exist that limit the DBP concentrations in saline waters.

The composition and amount of DBPs can vary depending on the sector of application or location even when the same techniques are used. DBP generation depends on many different factors such as oxidant type and dose, abundance and composition of DOM (Liu et al., 2015), as well as temperature and salinity of the treated water (Shah et al., 2015). Chlorination mainly leads to organohalogenated compounds (i.e. halocarbons) such as THMs, haloacetic acids and haloacetonitriles (Allonier et al., 1999, Fig. 1.1), while ozonation also produces bromate (Rajagopal et al., 2012). While these treatments are based on similar oxidants and generate DBPs of similar composition, other oxidation techniques such as peracetic acid or hydrogen peroxide produce different patterns of DBPs. Oxidative treatment in ballast water uses higher disinfection dosage and generates substantially larger quantities of DBPs than known from cooling water treatment in power plants or oxidation in desalination plants (Werschkun et al., 2012). The major THM found in treated seawater is bromoform ($CHBr_3$). Among the different treatment methods, chlorination produces the highest concentrations of bromoform. It is estimated that bromoform constitutes 93–97% of all THMs formed by seawater treatment (Rajagopal et al., 2012).

This raises concern about the fate of bromoform after treated water is discharged into the ocean. If substantial amounts of bromoform are released from the ocean into the atmosphere, this can increase the bromine abundance in the atmosphere and affect ozone

chemistry. Therefore, this thesis deals in particular with the environmental impact of anthropogenic bromoform, whose influence on the atmosphere is described in the following.

1.2 Short-lived bromocarbons in the environment

Apart from halocarbons produced from industrial water treatment, many substances have also natural abundances in the ocean and atmosphere. These volatile halocarbons have short lifetimes in the atmosphere of less than six months and belong to the very short-lived substances (VSLSs) (Carpenter and Reimann, 2014). Here, I describe the natural background of VSLSs by explaining their generation and degradation explicitly for brominated VSLSs, mainly bromoform and dibromomethane (CH_2Br_2). Then I present the current knowledge about atmospheric transport and chemistry of brominated VSLSs, which is relevant for both natural and anthropogenic sources of VSLSs.

1.2.1 Oceanic sources and sinks of natural bromocarbons

Bromocarbons such as bromoform and dibromomethane are assumed to have mainly natural sources in the ocean (Quack and Wallace, 2003). Bromoform is of biological origin produced in the surface water from macroalgae and phytoplankton. Bromoform production requires the oxidation of bromide to hypobromite (Quack and Wallace, 2003). Oxidation of bromide in marine species occurs via primary metabolic compounds with haloperoxidases in the presence of hydrogen peroxide (e.g. Theiler et al., 1978; Moore et al., 1996). Haloperoxidases are enzymes in seaweeds and phytoplankton, which induce the oxidation of halides (Cl^-, Br^-, I^-) by hydrogen peroxide (Geigert and Neidleman, 1986). The hypobromite reacts with many different organic substrates to unstable intermediates which hydrolyse to mainly bromoform and dibromomethane (Quack and Wallace, 2003). The natural generation of biogenic bromocarbons is still not fully understood which makes predictions about future changes of the biological source strength of bromocarbons difficult.

The spatial distribution of bromocarbons in the ocean surface is highly inhomogeneous due to the marine environmental conditions for macroalgae and phytoplankton habitats (Fig. 1.2a). Recent observations of bromoform in seawater suggest elevated abundances in coastal regions of 10–20 pmol L^{-1} and in equatorial and upwelling regions of 5–10 pmol L^{-1} (Quack and Wallace, 2003; Ziska et al., 2013; Fuhlbrügge et al., 2016). Values in coastal regions can also be much higher and at some coastlines, measurements have found concentrations above 100 pmol L^{-1}, e.g. in the Gulf of Mexico (Liu et al., 2011) and the Bay of Bengal (Yamamoto et al., 2001). There is a strong gradient of bromoform concentrations from the coast towards the open ocean, which contains little to no bromoform (Fig. 1.2a). Oceanic sinks include hydrolysis, dehalogenation, halogen-substitution and photolysis

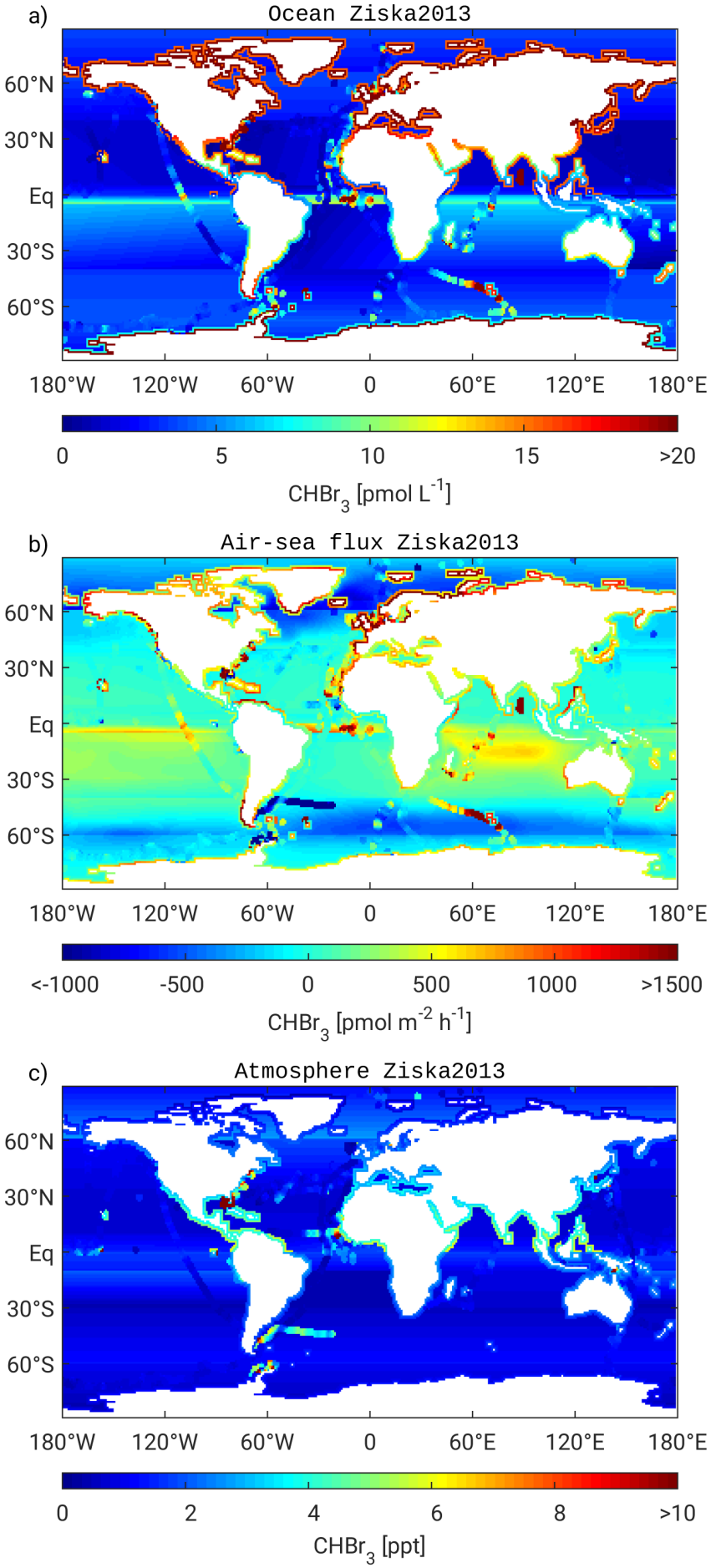

Figure 1.2: Global distribution of a) sea surface bromoform concentration [pmol L^{-1}], b) bromoform air-sea flux [pmol m^{-2} h^{-1}] and c) bromoform mixing ratio in the marine boundary layer [ppt] (updated from Ziska et al., 2013).

Table 1.1: Global annual atmospheric bromine input of bromoform given in Gg $CHBr_3$ a^{-1} and Gmol Br a^{-1}.

Gg $CHBr_3$ a^{-1}	**Gmol Br a^{-1}**	**Reference**
842	10	Quack and Wallace (2003)
864	10.3	Yokouchi et al. (2005)
595	7.1	Warwick et al. (2006)
400	4.8	Pyle et al. (2011)
842	10	Butler et al. (2007)
562	6.7	Ordóñez et al. (2012)
425	5.4	Liang et al. (2010)
174	2.1	Ziska et al. (2013)

(Quack and Wallace, 2003). All of these sinks are relatively slow processes with lifetimes of several years (Hense and Quack, 2009) and have little impact on time scales shorter than a few months. The lifetime is defined by the time scale when the amount has declined to 1/e of the initial value. Since bromoform is a volatile substance, air-sea flux into the atmospheric marine boundary layer occurs on relatively short time scales and presents the main pathway for oceanic loss (Quack and Wallace, 2003). Likewise, the air-sea flux into the atmosphere is the main pathway for anthropogenic bromoform from industrial water treatment after discharge into the ocean.

Air-sea flux is the gas exchange rate at the ocean-atmosphere interface usually given in orders of $\mathrm{mol\,m^{-2}\,h^{-1}}$. For bromoform the air-sea flux is mostly positive, i.e. directed from the ocean to the atmosphere, and is generally between 500 and 1500 $\mathrm{pmol\,m^{-2}\,h^{-1}}$ along the coast, and in tropical regions (Fig. 1.2b). Local emissions reach up to 10 $\mathrm{nmol\,m^{-2}\,h^{-1}}$. Global annual estimates of atmospheric bromine (Br) input from bromoform emissions have large uncertainties with a range of 2–10 Gmol Br (Tab. 1.1). This is due to the sparse observations in ocean and atmosphere, the high spatial variability, and different calculation methods (Ziska et al., 2013). A substantial difference in the calculation method is given by using either a bottom-up or a top-down approach. For the bottom-up approach, the air-sea flux is derived by spatially interpolating the distribution of measured sea surface concentrations (Ziska et al., 2013), while for the top-down approach the air-sea flux is calculated by fitting it to the atmospheric measurements using atmospheric transport models (Warwick et al., 2006; Butler et al., 2007; Liang et al., 2010; Ordóñez et al., 2012). In both cases, global estimates are based on too few measurements, and local hot spots of bromoform emissions are likely to be missed. Furthermore, it is not possible to distinguish between natural and anthropogenic bromoform from measurements alone, and it is unclear to what extent other sources such as industrial emissions are included in the current flux estimates.

Quack and Wallace (2003) made one attempt to quantify the global flux of anthropogenic bromoform from water treatment facilities based on simplified assumptions and few measurements. They found a contribution of 300 Mmol Br a^{-1} to the global air-sea flux of bromoform but without analysing the spatial distribution. There is still high uncertainty in the quantification and location of anthropogenic bromoform sources.

1.2.2 VSLS in the troposphere

Bromoform is the largest carrier of organic bromine from the ocean to the atmosphere (Quack and Wallace, 2003), contributing together with CH_2Br_2 up to 70 % of organic bromine to the marine troposphere (Hossaini et al., 2012). Atmospheric distributions of bromoform at sea level are highly variable being abundant near emission hot-spots and rapidly declining with distance (Fig. 1.2c). Highest mixing ratios in the marine boundary layer are mostly confined to the coastal areas with 4–10 ppt, while mixing ratios over the open ocean are rather small with only 0–1 ppt. Recently, elevated tropical abundances have been confirmed from ship campaigns in the near-coastal zones of the Yellow and South China Seas (Nadzir et al., 2014), and in coastal areas of the West Indian Ocean (Fiehn et al., 2017).

Once brominated VSLSs (or atmospheric source gases) are outgassed into the atmosphere they are mainly photolysed or oxidised by reaction with chlorine (Cl) and OH to reactive halogen species, often referred to as product gases (Quack and Wallace, 2003; Saiz-Lopez and von Glasow, 2012). For the source gas bromoform, the main degradation reaction is photolysis, and dibromomethane mainly reacts with OH (Hossaini et al., 2010). The main reaction products are carbonyl bromide (CBr_2O) and formyl bromide (CHBrO) which are photolysed to the inorganic product gases HBr, HOBr, or BrO, that are part of the inorganic bromine inventory Br_y (Fig. 1.3). The oxidation and photolysis of the source gases results in relatively short lifetimes of 15 days ($CHBr_3$) and 94 days (CH_2Br_2) in the atmospheric boundary layer.

In the troposphere, Br_y from VSLSs has a strong influence on the chemical composition of air and thus influences the fate of pollutants and greenhouse gases (GHGs), and may affect climate through direct and indirect radiative effects (Simpson et al., 2015). Reactive bromine (Br and BrO) reduces tropospheric nitrogen oxide radicals (NO_x = NO + NO_2, Jacob, 1999) by the formation of nitryl bromide ($BrNO_2$, Simpson et al., 2015) and alters tropospheric hydrogen oxide radicals (HO_x = OH + HO_2, Jacob, 1999) ratios towards OH (Sherwen et al., 2016).

The reactive brominated product gases Br_y cause ozone depletion in both troposphere and stratosphere. About 5–30 % of tropospheric ozone depletion is caused by bromine chemistry (Yang et al., 2005). Br_y from VSLSs contribute to direct catalytic ozone loss through reaction with BrO, and indirectly reduce ozone production by impacting nitrogen

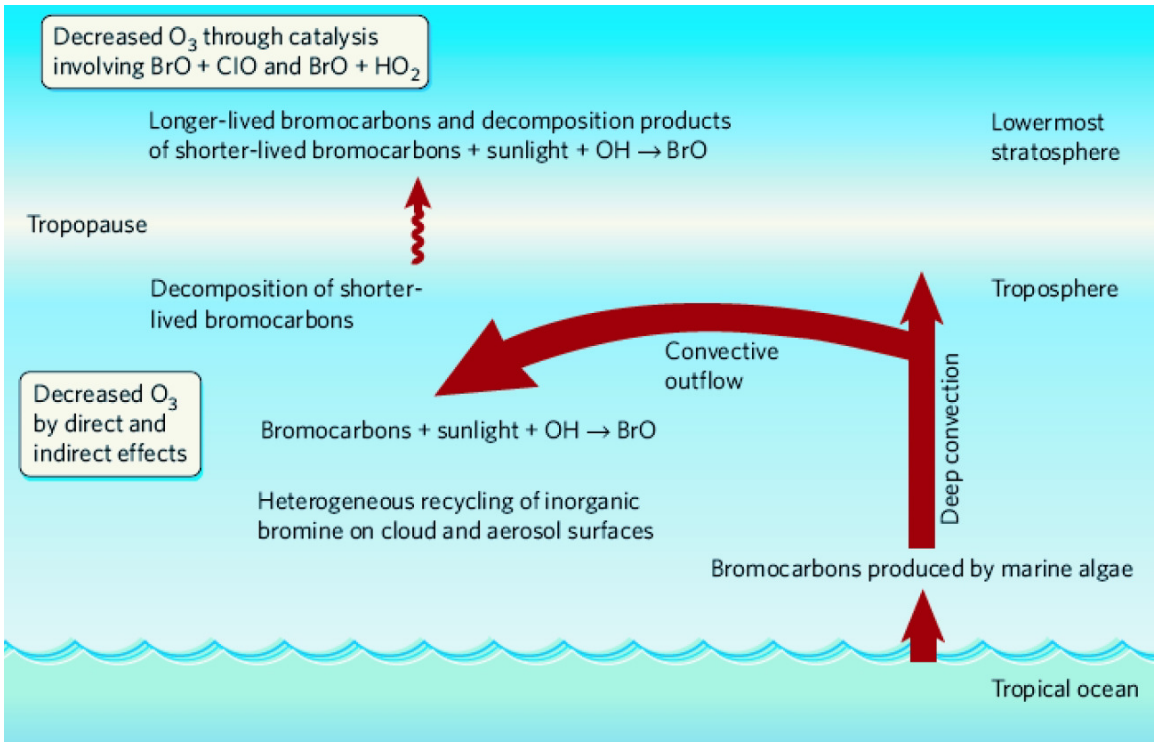

Figure 1.3: Role of bromocarbons in the troposphere and lower stratosphere (from Salawitch, 2006).

levels in the troposphere (Fig. 1.3). The atmospheric composition of ozone, OH and H_2O_2 determines the oxidising capacity of the atmosphere (Thompson, 1992). All of them play important roles in air quality. Especially, OH reacts with many GHGs and pollutants in the atmosphere and controls abundances of hydrogenated chlorofluorocarbons (HCFCs). Thus, stable OH abundances in the troposphere are favourable, especially since more OH leads to an increased formation of acids and acidic precipitation (Thompson, 1992).
Product gases of VSLSs further react with methane (CH_4), mercury and dimethyl sulfide (DMS) and change their lifetimes in the troposphere (Simpson et al., 2015; Saiz-Lopez and von Glasow, 2012). Therefore, additional input of VSLSs affects the oxidising capacity of the atmosphere, as well as the radiative forcing, since methane and ozone are strong GHGs.
In contrast to longer-lived species such as CFCs and methyl bromide (CH_3Br), VSLSs are mostly degraded in the troposphere to inorganic Br_y. Soluble species of Br_y (HBr and HOBr) are removed through wet deposition, i.e. precipitation, before they can reach the stratosphere. Heterogeneous reactions on aerosol surfaces release the inorganic bromine back to the gas phase so that more Br_y can enter the stratosphere (Salawitch et al., 2005, Fig. 1.3).
The impact of halogenated source gases on tropospheric and stratospheric chemistry is usually expressed by the total amount of bromine compared to chlorine. While most of atmospheric chlorine originates from anthropogenic sources, the majority of bromine is

expected to be of natural origin (Engel and Rigby, 2018). In the lower troposphere and marine boundary layer, sea-salt aerosol is the largest source of bromine (Yang et al., 2005; Dessens et al., 2009) while bromocarbons contribute to the bromine content in the middle to upper troposphere and lower stratosphere. Total organic bromine from VSLSs source gases in the marine boundary layer is on average 6.5 ppt Br with bromoform contributing 3×1.2 ppt and dibromomethane 2×0.9 ppt (Engel and Rigby, 2018). Total chlorine from VSLSs is 177 ppt Cl, of which 150 ppt originate from anthropogenic sources (Engel and Rigby, 2018). Tropospheric bromine from long-lived ODSs is 14.6 ppt Br from methyl bromide and halons, while long-lived chlorinated ODSs contribute 2621 ppt Cl to organic chlorine (Engel and Rigby, 2018). The abundances of long-lived ODSs are declining due to the effect of the Montreal Protocol while mixing ratios from VSLSs have been staying constant.

1.2.3 VSLS in the stratosphere

Stratospheric ozone chemistry

The stratosphere is characterised by a positive vertical temperature gradient caused by the absorption of UV radiation by ozone. The ozone layer comprises 90 % of atmospheric ozone and lies between 15–30 km (Fig. 1.4). Stratospheric ozone is formed and destroyed by photolysis of oxygen under high-energy UV radiation present at high altitudes. Thereby, the harmful UV radiation is absorbed and does not reach the Earth's surface, where it can cause skin cancer or damage plants, cells and organisms (Hegglin et al., 2015).
In a steady state, the Chapman Cycle describes the continuous production and depletion of ozone while the ozone mixing ratio stays constant (Jacob, 1999). However, stratospheric ozone abundances are smaller than what would result from Chapman chemistry. This is caused by catalytic ozone destruction with reactive halogen species at middle and high latitudes. In catalytic cycles, ozone reacts to molecular oxygen while the catalytic radical is not consumed by the reaction and is available for more reactions with ozone. The halogens, chlorine and bromine are important components of catalytic ozone depletion.
During polar spring, chemical reactions of halogenated molecules on the surface of Polar Stratospheric Clouds can substantially increase the abundance of the most reactive halogen species ClO and BrO (Solomon, 1999). The amount of Cl and ClO in the troposphere depends on the abundance of CFCs and halons in the stratosphere. The emission of anthropogenic CFCs from refrigerators and air-conditioning, and halons from fire-extinguishers in the 20^{th} century caused the ozone hole over Antarctica.
In 1987, CFCs and halons were banned by the Montreal Protocol, and the emission of long-lived ODSs is controlled. Since then, there is a steady decline of anthropogenic ODSs in the stratosphere. However, these molecules are so tightly bond and hydrophobic they can only be slowly removed from the atmosphere through photolysis with UV radiation in

the stratosphere, which will result in a delayed recovery of the ozone layer by the second half of the 21th century (Engel and Rigby, 2018).
Bromine is less tightly molecular-bound than chlorine, and thus rapidly available for ozone depletion (Solomon, 1999). Thereby, bromine is about 60 times more effective in destroying ozone than chlorine (Sinnhuber et al., 2009).

Stratospheric entrainment of VSLSs

The stratospheric entrainment efficiency of both short-lived source gases and the reactive product gases depends on the photochemical loss rate, the degradation and tropospheric removal processes and the time scale for direct transport into the stratosphere (Hossaini et al., 2010). Due to their short lifetime, the largest part of the VSLSs is already oxidised in the troposphere and removed through precipitation. In the tropics, stratospheric VSLS source gas injection due to strong convection has a much larger probability without being chemically altered than in other regions (Aschmann et al., 2009; Hossaini et al., 2013; Fernandez et al., 2017; Wales et al., 2018). Thereby the West Pacific is the most important region regarding the efficiency of vertical transport of VSLSs into the stratosphere

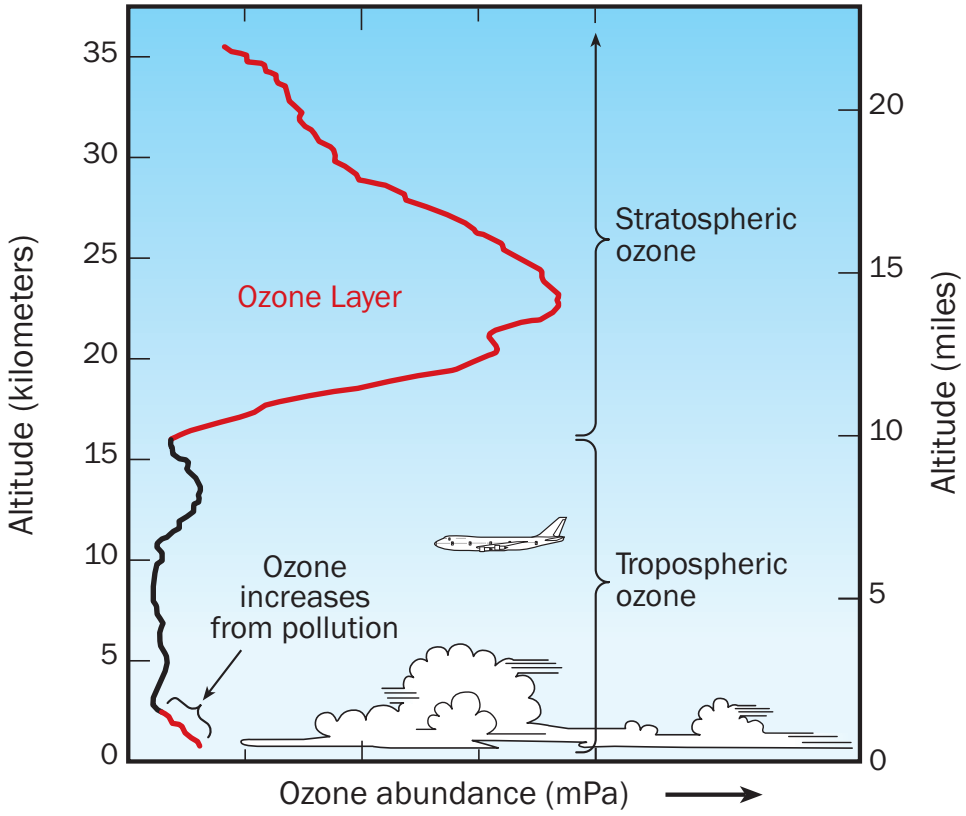

Figure 1.4: The ozone profile shows schematically how the ozone abundance (in mPa) changes with height. The sections with the red line show where ozone is most abundant: in the stratospheric ozone layer from Chapman chemistry and near the surface from pollution (from Hegglin et al., 2015).

(Tegtmeier et al., 2015; Hossaini et al., 2016). This is reflected in the ozone depletion potential of brominated VSLSs, which depends on the spatially and seasonally varying entrainment efficiency (Tegtmeier et al., 2015; Brioude et al., 2010).
Several measurement campaigns and modelling studies have estimated the contribution of VSLSs to stratospheric bromine from both source gas and product gas injection. They both contribute to a total stratospheric bromine of 5 ± 2 ppt Br (Engel and Rigby, 2018). Aircraft measurements estimate a source gas injection of 3 ppt Br (Navarro et al., 2015), and a total bromine contribution from VSLS source and product gases of 3.6–4.3 ppt Br to the lower stratosphere (Wisher et al., 2014). Modelling studies have estimated the contribution to stratospheric bromine by source gases and product gases. Source gas injection of 1.7–2.9 ppt (Hossaini et al., 2012; Wales et al., 2018; Engel and Rigby, 2018) and product gas injection of 2.1–2.7 ppt Br (Wales et al., 2018; Engel and Rigby, 2018) show a good agreement among the models. The source gases bromoform and dibromomethane contribute 84 % to the bromine loading from VSLSs in the lower stratosphere (Hossaini et al., 2016).
Stratospheric entrainment of brominated VSLSs is generally believed to increase by the end of the 21st century (Hossaini et al., 2012; Ziska et al., 2017; Fernandez et al., 2017). Due to changes in the tropospheric oxidising capacity and transport efficiency, source gas injection will increase stratospheric bromine levels from 1.7 ppt in 2000 to 2.0–2.7 ppt in 2100 under climate change scenarios (Hossaini et al., 2012). Moreover, enhanced tropical convection in the future can lead to an increase of 8 % of stratospheric bromine levels (Dessens et al., 2009). The effect of VSLSs on stratospheric bromine entrainment due to changes in the oceanic production is still uncertain. Oceanic bromocarbon production is sensitive to water temperature, nutrient supply and upwelling (Carpenter and Liss, 2000; Quack et al., 2004), and a future increase of natural VSLS production is possible. A stronger air-sea flux due to rising temperature and wind fields can also increase the VSLS entrainment into the stratosphere (Tegtmeier et al., 2015; Ziska et al., 2017).

Impact of VSLSs on stratospheric ozone

Currently, VSLSs contribute to 25 % of stratospheric bromine, and to less than 4 % of stratospheric chlorine (Engel and Rigby, 2018).
Brominated VSLSs which enter the stratosphere will release the bromine almost immediately (Engel and Rigby, 2018) and participate in ozone depletion at middle and high latitudes (Yang et al., 2014; Sinnhuber and Meul, 2015). Thus, catalytic ozone depletion cycles with bromine are most important in the lower stratosphere (Salawitch et al., 2005). Modelling studies which include VSLSs for ozone chemistry generally achieve a better agreement with observations than models without VSLSs (Salawitch et al., 2005; Sinnhuber and Meul, 2015). Models show a global stratospheric ozone loss due to VSLSs (Sinnhuber et al., 2009; Fernandez et al., 2017; Hossaini et al., 2015), which is strongest around

the South Pole of 20% (Sinnhuber and Meul, 2015) and has contributed -0.02 $W\,m^{-2}$ to global radiative forcing (Hossaini et al., 2015).
The influence of brominated VSLSs on future ozone abundances depends on trends in VSLS production, air-sea flux, atmospheric transport and chemical composition of the troposphere and stratosphere. It is predicted that stratospheric bromine from VSLS will increase in the future while long-lived ODSs are continuing to decline. Bromine chemistry from VSLSs is predicted to dominate Antarctic ozone depletion by the end of this century (Fernandez et al., 2017). Model results differ in the impact on the ozone layer due to an increase in the stratospheric bromine content. One study shows that by doubling the current brominated VSLS levels of 5 ppt to 10 ppt, the recovery of the ozone hole in this century can be delayed by up to 8 years (Yang et al., 2014). A different study predicts no delay in ozone hole recovery but instead an effect on the depth and duration of the Antarctic ozone hole (Fernandez et al., 2017). Modelling studies have shown that the impact of reactive bromine on lower stratospheric ozone depends on the depletion cycle by BrO and ClO, making bromine entrainment ineffective without chlorine (Yang et al., 2014). Recently, there is further evidence of increased input of anthropogenic CFCs into the stratosphere, which also contributes to a slowdown in the recovery of the stratospheric ozone layer (Hegglin, 2018; Montzka et al., 2018; Rigby et al., 2019). An increase of the stratospheric bromine loading from anthropogenic bromine sources, such as industrial water treatment, would contribute to the predicted trends.

1.3 Motivation and research questions

Over the last years, the importance of VSLSs for stratospheric ozone depletion has become more apparent. In the near future, the importance of VSLSs will continue to increase because of the decline of long-lived ODSs (Engel and Rigby, 2018). Due to the discovery of catalytic ozone destruction, there has been a rising awareness that molecules present at trace levels in the stratosphere can trigger chain reactions which lead to significant ozone depletion (Jacob, 1999). Thus, minor input from VSLSs into the stratosphere can significantly impact the process of ozone recovery.
So far, atmospheric research groups investigating volatile brominated VSLSs in the environment, have not tried to determine in detail the anthropogenic contribution of these species from water treatment technologies. At the same time, researchers who investigated the nature of DBPs from chemical water treatment, have neglected the large-scale environmental impact of brominated VSLSs but rather focussed on the local toxicological effects on humans and marine ecosystems.
This thesis aims to close the gap between the two fields by quantifying the amount of VSLSs produced from chemical water treatment and by investigating their transport pathways from the coastal discharge location into the ocean and atmosphere. There is

consensus that bromoform presents both a major species generated in oxidative water treatment technologies, as well as a major contributor of organic bromine to the atmosphere. Investigating the emission of anthropogenic bromoform can significantly improve the understanding of the environmental pressure by industrial water treatment.
I investigate the anthropogenic input of bromoform to the environment by simulating their distribution with transport models in the ocean and atmosphere. This method is widely accepted for analysing the transport pathways of a local source over a specific period of time (e.g. Durgadoo et al., 2017; Tegtmeier et al., 2012). The simulations are used to quantify regional aspects and global distributions, and allow to distinguish between anthropogenic abundances and background bromoform. This approach ultimately provides a first estimate of the anthropogenic source of organic bromine to the atmosphere, as well as a crucial information necessary for long-term risk assessments of DBPs from different water treatment sectors on regional to global scales.
To investigate the impact of anthropogenic bromoform from industrial water treatment, three research questions are addressed in this thesis:

1. Will treated ballast water from ships become an additional and relevant source of brominated VSLSs to the atmosphere?

2. How strong is the air-sea flux of bromoform produced from power plant cooling water treatment in comparison to recent bottom-up estimates?

3. What is the contribution of anthropogenic bromoform from industrial water treatment to stratospheric bromine entrainment?

I investigated these questions as part of the research project AVeSH (**A** new threat to the stratospheric ozone layer from **Ve**ry **S**hort-lived **H**alocarbons). The results of question 1 are presented in Chapter 3 *"Simulating the spread of disinfection by-products and anthropogenic bromoform emissions from ballast water discharge in Southeast Asia"*, where I focus on the oceanic spread of DBPs and the air-sea flux of bromoform in the case study of two major port regions, Singapore and Pearl River Delta.
Research questions 2 and 3 are addressed in Chapters 4 and 5. In Chapter 4 *"Simulations of anthropogenic bromoform reveal high emissions at the coast of East Asia"*, the anthropogenic production of bromoform in East-Southeast Asia, as well as the corresponding fluxes into the marine boundary layer and stratosphere in this region are quantified.
Based on the results of the regional simulations in Chapters 3 and 4, the air-sea flux and stratospheric input of anthropogenic bromoform from industrial water treatment is evaluated on a global scale in Chapter 5 *"Global emissions of anthropogenic bromoform from industrial seawater treatment"*. The global estimate of anthropogenic bromoform serves to assess, which regions are most important for anthropogenic emissions and the transport into the stratosphere.

The corresponding manuscripts of each chapter were or will be published in peer-reviewed journals. I summarise the results in Chapter 6 by answering the above stated research questions, and include a discussion of my findings and future research needs.

2 Data and methods

In this section, I describe in detail the data and methodology to obtain an estimate of the regional and global input of anthropogenic bromoform and other DBPs. The analysis requires the water volumes used in the different industrial sectors together with the amount of bromoform produced during the chemical treatment process.
Furthermore, I simulate the discharge of the bromoform in the surface ocean and model its oceanic distribution. I then derive the bromoform air-sea flux on regional to global scales. The obtained emission maps serve as the source function for atmospheric simulations of the bromoform pathways from the marine boundary layer into the stratosphere.

2.1 Global sources of anthropogenic bromoform

2.1.1 Ballast water

The aim is to derive a global map of ballast water discharge locations for the analysis of the DBPs and anthropogenic bromoform produced from ballast water treatment. This requires information on the location and size of harbours, which correlates to the volumes of ballast water discharge at each harbour, and also the typical bromoform concentration in treated ballast water.
Vessels always have to keep track of ballast water uptake and discharge but are not required to report ballasting operations to harbour officials. Therefore, detailed inventories of localised ballast water discharge are not available. Global estimates of ballast water usage thus have large uncertainties but these numbers are not only linked to vessel size but also to port statistics. Hence, my approach connects the amount of global ballast water volume to the cargo throughput at each port site, i.e. the size of the harbour. The amount of cargo throughput is made available by the American Association of Port Authorities (AAPA) in the statistics of the world port ranking from 2016 (AAPA, 2016). This ranking lists the 100 largest ports in two categories: containerised and tonnaged cargo. Containerised cargo is usually measured in twenty-foot equivalent units (TEUs), which is a measure of the number of twenty-foot containers loaded and unloaded at a harbour. Cargo volume is given in tonnes and includes oil and gas tankers as well as dry bulk, such as iron ore, grain, or coal.
Both rankings have to be taken into account for a complete ranking of harbour size.

Therefore, I generate a modified world port ranking by calculating the percentage share of containerised and tonnaged good according to their global ratio in annual ship traffic. The Review of Maritime Transport publishes the global annual volume of goods loaded in 2016 to 10286.9 million tonnes, of which 16.6 % are containerised and 83.4 % are tonnaged goods (UNCTAD, 2017). According to the percentage share of their category and their individual size in the ranking, each container and bulk port is assigned its relative fraction under the simplified assumption that these ports account for all of the global commercial ship trade and thus receive all of the global ballast water. Since many harbours are among the 100 largest ports in both categories, the percentages are added to give their total cargo share and results in the modified world port ranking encompassing 144 ports (suppl. Table, Chapter 3).

An estimate of global ballast water volume is required to determine how much ballast water is discharged at each individual port. Current estimates range from 3–5 billion m^3 (Chapter 1.1.1). Furthermore, David (2015) stated that the discharged ballast water amounts on average to roughly 33 % of the loaded cargo volume. In this case, the global cargo volume of loaded goods is 10286.9 million tonnes which leads to a ballast water volume of 3.4 billion m^3, which agrees well with the estimates from previous studies. This volume is now distributed among all harbours according to the calculated percentages in the modified world port ranking and I obtain the estimated discharge volume of ballast water for each port (Fig. 2.1). The majority of harbours lies in the northern hemisphere (NH), with some sites in Australia and South America. The largest number of major ports is located in East-Southeast Asia making it the main area of treated ballast water input.

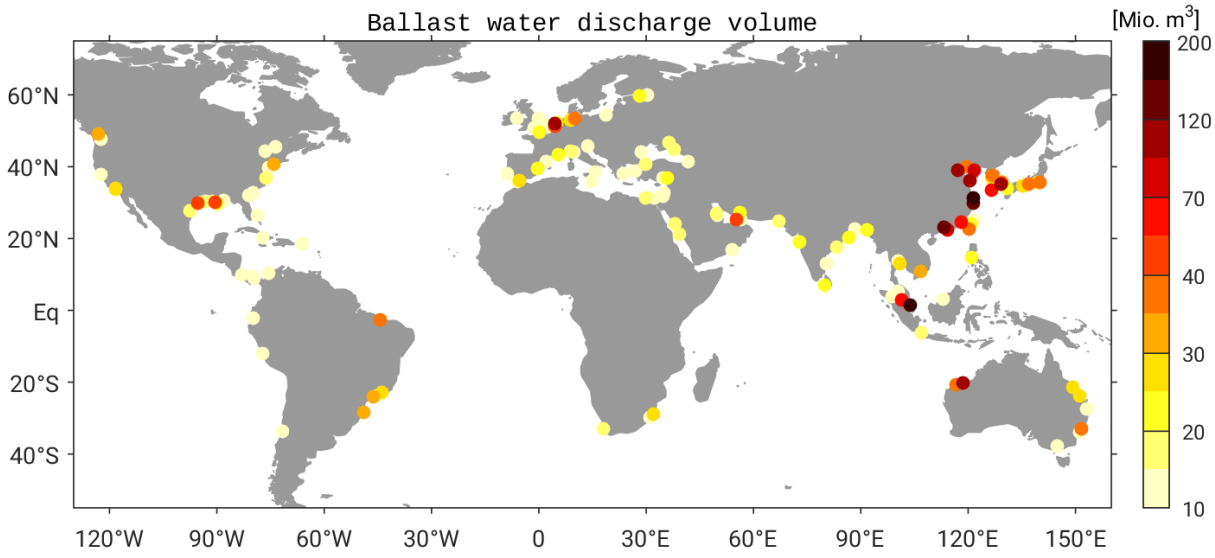

Figure 2.1: Estimated annual ballast water discharge volume ($10^6\ m^3$) from each harbour in the modified world port ranking.

Bromoform measurements from ballast water treatment

In this section, I derive the bromoform concentration from ballast water treatment. In order to know how much bromoform is discharged at each port, I estimate its concentration in the treated ballast water. Depending on the type of BWTS, the different treatment methods, water properties or residence times of the ballast water, the amount of produced bromoform can show large variations (Shah et al., 2015). Here I use ballast water samples taken during shipboard tests to determine a range of possible bromoform concentrations. Additionally, bromoform values from approved BWTSs are obtained from the reports for Final Approval by the Marine Environment Protection Committee (MEPC). To comply with the BWM Guidelines G9, each BWTS has to report its functionality through land-based tests and monitor the amount of residual oxidant, biological species and DBPs discharged after the treatment process (MEPC 57/21, 2008). This documentation for each BWTS can be accessed through the IMODOCS account (`https://docs.imo.org`). All systems obtaining Final Approval until 2017 that provide bromoform concentrations in seawater or brackish water are considered from a total of 29 BWTSs of which 22 use chlorine as the main disinfecting agent.

The shipboard samples were taken from the discharge of chlorinated ballast water from

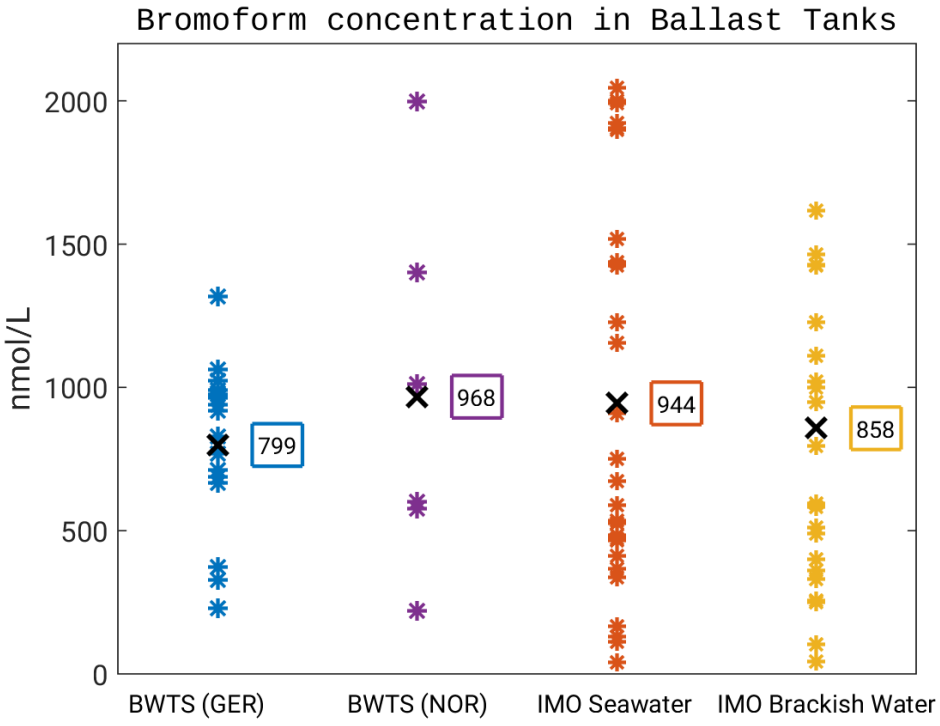

Figure 2.2: Bromoform concentrations in nmol L^{-1} and μg L^{-1} measured in ballast water samples from BWTSs in Germany and Norway, as well as measurements in seawater and brackish water from the MEPC reports for Final Approval of BWTSs, which use active substances.

Table 2.1: Three different scenarios for simulation of ballast water spread and its bromoform concentration.

Scenario	**% of vessels using chemical treatment**	**[μg/L]**
LOW	50	84
MODERATE	70	226
HIGH	90	368

three unnamed BWTSs, two in Norway and one in Germany. The samples from Germany are triplicates which were sampled during three different residence times in 15–20 min intervals. Bromoform concentrations of $202.0 \pm 74.0\,\mu g\,L^{-1}$ ($799.1 \pm 292.7\,nmol\,L^{-1}$) are found in nine ballast water samples taken in Germany from one BWTS (Fig 2.2). The particulate organic matter in the ballast water was 11.1–12.6 $mg\,L^{-1}$. The twelve ballast water samples of the two systems taken as triplicates in Norway have a bromoform concentration of $244.5 \pm 163.6\,\mu g\,L^{-1}$ ($967.6 \pm 647.4\,nmol\,L^{-1}$) (Fig. 2.2). All samples were measured in the lab with a purge-and-trap gas chromatograph-mass spectrometer (GC-MS) system which has a detection limit of around 0.1 $pmol\,L^{-1}$.

The average bromoform concentration of 226 ± 142 μg $CHBr_3$ L^{-1} (894 ± 560 nmol L^{-1}) serves as a range to determine different scenarios of ballast water discharge per volume. Thereby measured concentrations from ship-based samples are in good agreement with the values from the MEPC reports. To account for the unknown percentage of chemical BWTSs being installed onboard vessels, a range for its use needs to be given. Oxidative water treatment is more suited for larger vessels such as bulk carriers or tankers, which carry the largest volumes of ballast water (Maritime Impact, 2017). Thus, it is reasonable to assume that a minimum of 50 % of the global ballast water will be chemically treated. I choose three scenarios, LOW, MODERATE and HIGH, which represent the range of bromoform produced in the ballast water and the share of chemical BWTS used (Tab. 2.1). The lowest scenario (LOW) uses a mean $CHBr_3$ concentration minus one standard deviation and 50 % global ballast water, the middle scenario (MODERATE) the mean $CHBr_3$ concentration and 70 % of the ballast water, and the highest scenario (HIGH) uses a mean $CHBr_3$ concentration plus one standard deviation and 90 % of the ballast water. These scenarios will be used for the analyses of DBP discharge and bromoform emissions in Chapters 3 and 5.

Apart from bromoform, other brominated substances which contribute to the total amount of organic bromine are not included because their concentrations in treated water are negligible compared to bromoform concentrations (Rajagopal et al., 2012). Variations in the amount of bromine release, which depends on the composition of the DBP matrix for different treatment technologies, is included by the application of the three scenarios.

2.1.2 Cooling water

In analogy to the ballast water discharge (Chapter 2.1.1), I derive a global number of cooling water volumes and the DBPs within, with a focus on bromoform. The power plant database Enipedia (`enipedia.tudelft.nl`) lists a total number of 21297 power plants with coordinates, the electricity output capacity (in MWh), and for some the fuel type. The total capacity of the power plants in the database is 16980 TWh. I assume that all plants located at the coast use seawater for cooling purposes and as such have a once-through cooling system with no water consumption as described in Chapter 1.1.1. Coastal plants are selected by being located less than 0.02 degrees (or up to 2 km at low latitudes) away from any coastline. This results in 2903 coastal power plants with a capacity of 3880 TWh or 23 % of the total capacity.
Since the global electricity production is given as 24973 TWh in 2016 (IEA, 2018), and the average water use per MWh energy produced is 144 $m^3\,MWh^{-1}$ (Chapter 1.1.1), the global cooling water demand from coastal plants is 821.5 billion m^3 (2.1).

$$24973\,\frac{TWh}{a} \times 0.23 \times 144 \cdot 10^6\,\frac{m^3}{TWh} = 821.5 \cdot 10^9\,\frac{m^3}{a} \tag{2.1}$$

The distribution of annual cooling water among the individual coastal power plants is shown in Figure 2.3. Coastal power plants are represented at all continents in the statistics, but a high density is seen in the NH. Especially Europe and East Asia appear to have a high number of power plants and also some with a very large capacity and cooling water demand.
In contrast to ballast water treatment, the disinfection of cooling water is a well-established process and there is currently only weak scientific interest to investigate the side effects of treated cooling water on the environment. Only few scientific assessments of DBPs in cooling water effluents are available and the research locations are limited and mostly confined to European power plants (e.g. Jenner et al., 1997; Allonier et al., 1999; Taylor, 2006; Boudjellaba et al., 2016). In addition, some single studies are based on measurements from single power plants in Asia (e.g. Yang, 2001; Rajamohan et al., 2007; Padhi et al., 2012). The sampling method differs among the individual studies. Some measurements originate from coastal surface water at the power plant outlet (Fogelqvist and Krysell, 1991; Yang, 2001), while other studies have sampled in the undiluted effluent inside the power plant (Jenner et al., 1997; Rajamohan et al., 2007). All available measurements show bromoform to be the dominant DBP, however with a large range from 8–290 $\mu g\,L^{-1}$ (Tab. 2.2). Since the bromoform concentrations do not show a systematic difference between measurements in the undiluted effluent of the near-environment, all values are considered for estimating the average anthropogenic bromoform from cooling water treatment.
Additionally, the treatment methodology can differ between plants. Apart from the chlo-

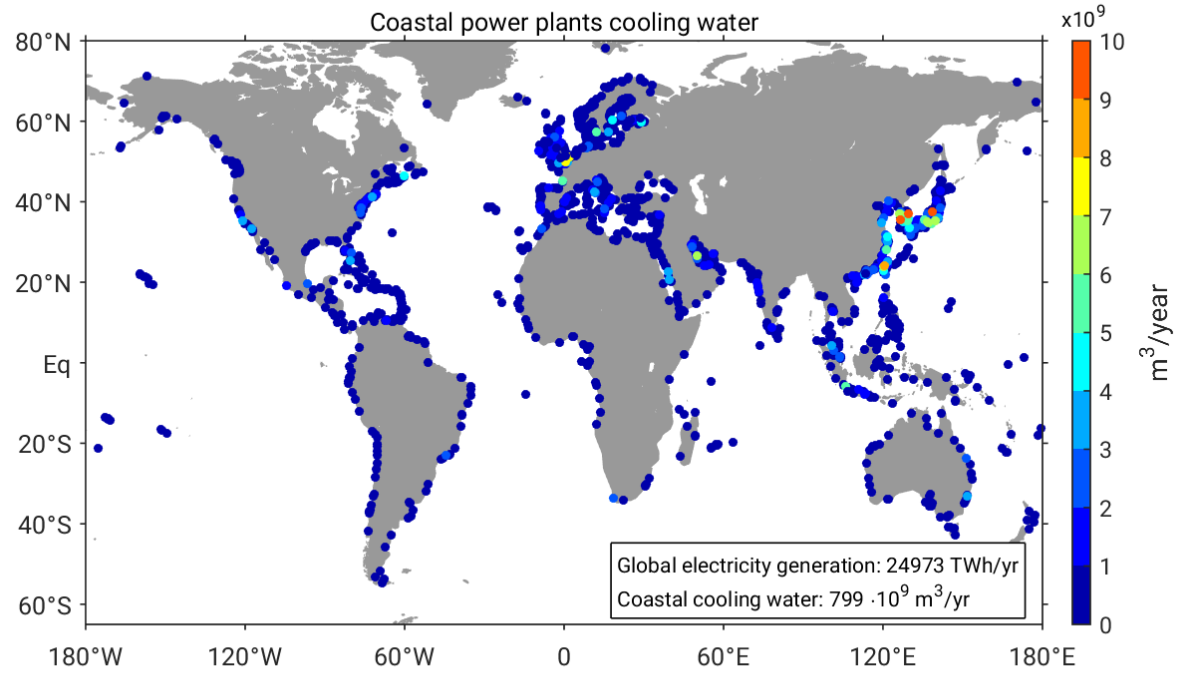

Figure 2.3: Estimated annual global cooling water discharge volume ($10^9\,m^3\,a^{-1}$) from coastal powerplants.

rine dosage, some power plants apply continuous low-dose chlorination while others perform shock-chlorination where a high chlorine dosage is used but only on a weekly to monthly frequency (Rajagopal et al., 2012). This can lead to very different measurement results depending on the sample timing relative to chlorine usage, but also the season or environmental factors. Bromoform generation also depends on the water condition such as temperature, salinity or DOM (Shah et al., 2015), all properties which vary seasonally. All these factors are reflected in the broad range of bromoform values given in literature (Tab. 2.2).

For the analysis in this thesis, I choose to scale the bromoform concentration in the cool-

Table 2.2: Bromoform concentrations in $\mu g\,L^{-1}$ from cooling water measurements as given in literature.

Effluent/ near outlet	**Location**	**Reference**
90-100	Gothenburg, Sweden, Kattegatt	Fogelqvist and Krysell (1991)
9-17	North Sea	Jenner et al. (1997)
8-27	English Channel	Allonier et al. (1999)
124	Youngkwang, South Korea, Yellow Sea	Yang (2001)
20-290	Kalpakkam, India, Bay of Bengal	Rajamohan et al. (2007)
12-41	Kalpakkam, India, Bay of Bengal	Padhi et al. (2012)
19	Gulf of Fos, France, Mediterranean	Boudjellaba et al. (2016)

ing water discharge according to three scenarios in analogy to the ballast water scenarios, LOW, MODERATE and HIGH. In these scenarios the initial bromoform concentration is $20\,\mu g\,L^{-1}$ (LOW), $60\,\mu g\,L^{-1}$ (MODERATE) and $100\,\mu g\,L^{-1}$ (HIGH) in the undiluted cooling water. Although there is no physical correlation between the ballast water and cooling water scenarios, the classification helps to give a possible range of bromoform input into the environment from the two anthropogenic sources. The cooling water scenarios will be used for the analyses of bromoform spread and emissions in Chapters 4 and 5.

2.2 Lagrangian simulations

To investigate the influence of anthropogenic bromoform in the surface ocean and the atmosphere on a regional to global scale, I simulate the pathway of the bromoform spread from the coastal sources into the environment. With Lagrangian particle trajectories, I model the 3-dimensional bromoform spread from the coastal sources into the open ocean, into the atmospheric boundary layer and the entrainment into the upper troposphere and lower stratosphere.

2.2.1 Oceanic simulations - ARIANE

For the ocean advection simulation of DBPs and especially bromoform on a regional to global scale, the offline ARIANE Lagrangian package is used (Blanke et al., 1999). ARIANE consists of particle advection within the analytically computed 3-dimensional streamlines using the time-varying velocity field of an ocean general circulation model (OGCM). The OGCM output stems from a hindcast experiment with the ORCA0083 model configuration developed within the DRAKKAR consortium based on the NEMO-ORCA code version 3.6 (Madec and the NEMO Team, 2008). The ORCA0083 configuration is a high-resolution, eddy-resolving model on a horizontal Arakawa C-grid with a $1/12^\circ \times 1/12^\circ$ resolution. In the vertical, there are 75 levels, with 46 levels in the upper 1000 m and spacing increasing with depth (see also Marzocchi et al., 2015; Durgadoo et al., 2017). The surface boundary conditions are derived from the atmospheric ERA-Interim reanalysis, which are included in the DFS5.2 forcing data set (Dussin et al., 2016) and varies on a range of time scales, from synoptic to interannual.
Model output is given at 5-day intervals for the years 1963-2012. In this thesis, the DBPs from oxidative water treatment are approximated as particles that are continuously released at 5-day intervals and passively advected with the simulated flow for up to two years. The streamline calculations are purely advective and no diffusivity is applied. The amount of particles is scaled to the size of the ports and coastal power plants, while each particle represents the same amount of DBP or bromoform. The release position of the particles is chosen as close as possible to the coast while ensuring that there is minimal

influence of the land boundaries on the simulation. This avoids numerically-related beaching of particles into the coast. Thus, particles are released approximately 8–40 km off the coast. Here, the resolution of the OGCM does not allow to capture smaller-scale coastal structures such as harbours or estuaries nor does it simulate the near-coastal exchange, e.g. through tides.
The 2-year Lagrangian simulations serve the purpose to identify the main pathways of the DBPs and also the hot-spots of bromoform air-sea exchange. Therefore, the seasonal and annual mean particle density maps from the upper 20 m are used, which show the most probable distribution of the DBPs at the surface. In order to allow for an accumulation period, the first 11 months (January–November) are used as a spin-up and the months December–November of the following year are analysed. Additionally, particles older than 11 months are not considered to ensure that the total particle number for each time step stays constant. Detailed description of the release positions and the individual ARIANE simulations can be found in Chapters 3 and 4.
Sink processes of bromoform such as constant gas exchange at the air-sea interface or chemical loss rates are taken into account. Oceanic sinks include degradation through halide substitution and hydrolysis with a half-life of 4.37 years (Hense and Quack, 2009), as well as remineralisation with a half-life of 5.72 years (Hense and Quack, 2009). The air-sea exchange calculation is described in detail in the next section.

2.2.2 Air-sea flux calculation

The air-sea flux of bromoform is calculated after the general flux equation at the air-sea interface:

$$Flux = (C_w - C_{eq}) \cdot k \tag{2.2}$$

Here $Flux$ is positive when it is directed from the ocean to the atmosphere and is given in pmol m^{-2} h^{-1}. C_w is the actual concentration in the surface mixed layer (pmol L^{-1}) and can consist of bromoform either originating from anthropogenic sources only or from a mixture of natural and anthropogenic sources. C_{eq} is the theoretical equilibrium concentration at the sea surface (pmol L^{-1}) calculated from the atmospheric mixing ratio C_{air} (converted from ppt to pmol L^{-1}) and the specific Henry constant H (Quack and Wallace, 2003):

$$C_{eq} = \frac{C_{air}}{H} \tag{2.3}$$

$$H = exp\left(13.16 - \frac{4973}{SST}\right) \tag{2.4}$$

The parameterisation from (Nightingale et al., 2000) is used to determine the gas transfer velocity k for bromoform (cm h^{-1}). Schmidt number (Sc) correction is applied by scaling

the empirical value of k_{CO_2} and a Schmidt number of 600 for CO_2 at 20°C water (2.5), (2.6). The transfer velocity k mainly depends on surface wind speed u and sea surface temperature (SST). The Schmidt number for bromoform Sc is calculated from the kinematic viscosity ν at the sea and the maas diffusivity D (2.7).

$$k = k_{CO_2} \cdot \sqrt{\frac{600}{Sc}} \tag{2.5}$$

$$k_{CO_2} = 0.222 \cdot u_{10}^2 + 0.333 \cdot u_{10} \tag{2.6}$$

$$Sc = \frac{\nu}{D} \tag{2.7}$$

The global distribution of k is shown in Figure 2.4. k is highest where the global wind bands are dominant, in the Southern Ocean, in the trade wind passages and the NH westerlies. Transfer velocities are strong in the respective winter hemisphere and in the Indian Ocean during the Indian summer monsoon.
Wind velocities at 10 m height (u_{10}) are given at 6-hourly time intervals from the NEMO-ORCA forcing data set DFS5.2 (Dussin et al., 2016), which is based on the ERA-Interim atmospheric data product. The resulting gas transfer velocities k (Figure 2.4) are calculated for the same 6-hourly time interval on a global $1° \times 1°$ horizontal grid. Afterwards k is averaged to match the 5-daily resolution of the ARIANE output to calculate the

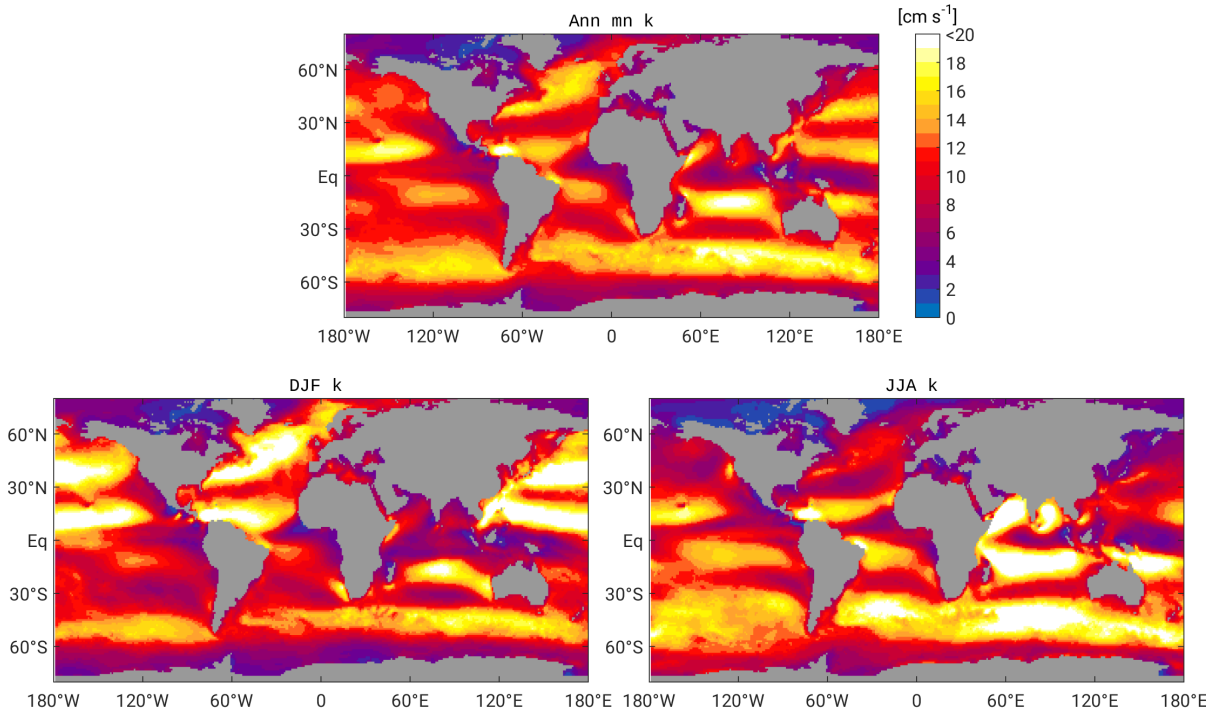

Figure 2.4: Annual and seasonal (DJF, JJA) mean gas transfer velocity (k) of bromoform in 2006 calculated on a $1° \times 1°$ horizontal grid.

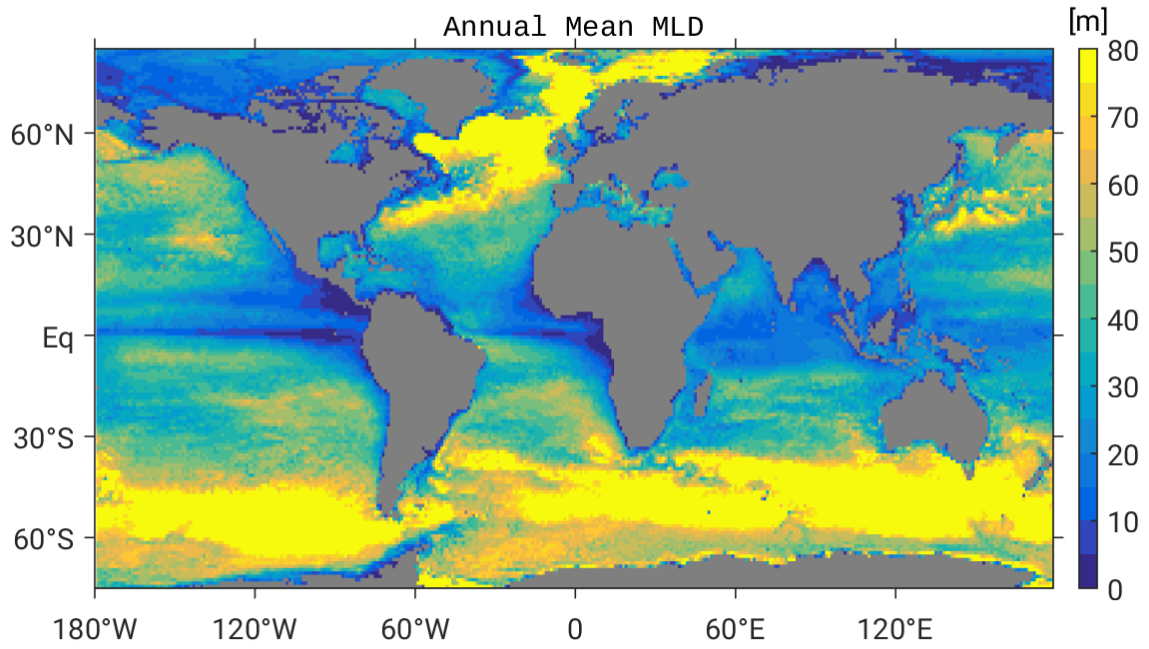

Figure 2.5: Annual mean mixed layer depth (MLD) in 2006 from NEMO-ORCA0083 interpolated on a $1° \times 1°$ horizontal grid.

bromoform air-sea exchange. For the air–sea gas exchange, all particles that are shallower than the mixed layer depth (MLD) at each model time step are taken into account and treated as 'surface particles'. The MLD from the NEMO-ORCA0083 model output is defined as the depth where the gradient of the potential density σ_θ exceeds $0.02\,\mathrm{kg\,m^{-3}}$ relative to the density at a reference depth of 10 m.

Along the coast line, the annual mean MLD is relatively shallow, often less than 20 m deep (Fig. 2.5). The MLD is constantly deep along the strong ocean currents, such as the Antarctic Circumpolar Current, the Kuroshio in the Pacific and the Gulf Stream in the Atlantic Ocean. Since particles are released in coastal vicinity at a 5-day temporal resolution, it is reasonable to assume that each particle in the MLD is in contact with the atmosphere at least once during each time step.

From the additive nature of the air-sea flux parameterisation (2.2), it is possible to calculate the flux of the anthropogenic part separately from the natural bromoform. Here, only the industrial sources in the surface ocean are considered and the air-sea flux in each grid box is calculated according to the anthropogenic bromoform portion. The resulting atmospheric mixing ratios from anthropogenic air-sea flux C_{air} would result in an equilibrium concentration C_{eq}, which is always lower than 8 % of the sea surface concentration C_w (at a water temperature of 20 °C and air pressure of 1015 hPa). C_{eq} is therefore assumed negligible for the flux calculations here. Hence, the atmospheric bromoform C_{air} is set to zero and (2.2) reduces to:

$$Flux = C_w \cdot k \tag{2.8}$$

Thus, the resulting bromoform air-sea flux from the sea surface to the atmospheric marine boundary layer is always positive. For comparison and simulation of atmospheric transport, the positive emissions from the ocean to the atmosphere from climatological emission maps are used, as well. The resulting bromine flux to the atmosphere from all bromoform sources is calculated as $3 \times CHBr_3$ (in Mmol Br a^{-1}).

2.2.3 Atmospheric simulation - FLEXPART

Bromoform surface emissions serve as a source function for simulations of the atmospheric transport. The simulations are performed with the **FLEX**ible **PART**icle dispersion model (FLEXPART), an offline model driven by 3-dimensional meteorological fields (Stohl et al., 2005). The meteorological input data are temperature and wind from the ERA-Interim reanalysis data set (Dee et al., 2011), which has a $1° \times 1°$ horizontal resolution, 61 vertical levels from the surface up to 0.1 hPa and 3-hour temporal resolution. The FLEXPART model includes parameterisations of moist convection, dry deposition and the simulation of chemical decay (Stohl et al., 2005). For bromoform, an atmospheric lifetime of 17 days is prescribed for all runs (Montzka and Reimann, 2010). Bromoform is seeded as particles in each surface box with a pre-defined mixing ratio depending on the emission strength for each grid box. A total of 1000 particles are randomly seeded inside each grid box at each model time step throughout the whole time period. The FLEXPART runs are performed for both boreal winter (DJF) and boreal summer (JJA) with a one month spin-up phase starting at the beginning of November (for DJF) and May (for JJA). The output from the FLEXPART runs is directly given as bromoform mixing ratio at the same horizontal resolution as the atmospheric fields and 33 vertical levels from 50 m up to 20000 m. In all simulations bromoform is treated as a passive tracer and is lost only through chemical decay.
The individual runs based on the scenarios presented in Chapter 2.1.1 and 2.1.2, as well as the climatological background based on the updated Ziska et al. (2013) bromoform emission inventory (Fiehn et al., 2018) are described in detail in the individual chapters (Chapter 4 and 5).

2.3 Statistical assessment

Ballast water concentrations and emissions in Singapore and the Pearl River Delta is averaged over three grid boxes, closest to the release spot. Furthermore the particle density distribution from the Lagrangian simulations shows the most probable pathways of the particles. Hence, the area where the 10 % of particles with the highest density are transported to, is the most probable pathway for the particles with a 10 % probability. In analogy this probability density is valid for all percentages. In Chapters 4 and 5, I use the

area of the most probable 90 % as the 'average' distribution and the most probable 10 % as the 'maximum' distribution by averaging over the respective area. This method is applied for sea surface concentration from ARIANE simulations, air-sea flux, and atmospheric mixing ratios from the FLEXPART simulations. To compare my modelled results with climatological values, I apply the same method to the sea surface concentration and air-sea flux from the Ziska et al. (2013) climatology (Fig. 1.2).

3 Simulating the spread of disinfection by-products and anthropogenic bromoform emissions from ballast water discharge in Southeast Asia

Published article in: *Ocean Sciences*, 15, 891-904, 2019, doi: 10.5194/os-15-891-2019

Josefine Maas[1], Susann Tegtmeier[1,2], Birgit Quack[1], Arne Biastoch[1,3], Jonathan V. Durgadoo[1], Siren Rühs[4], Stephan Gollasch[5] and Matej David[6,7]

In this chapter, I present a first analysis of the input of ballast water treatment to the environment for the industrialised region of Southeast Asia. The focus lies on the ports around Singapore and the Pearl River Delta. With the ARIANE software, I simulate the spread of DBPs in the surface ocean and also calculate the air-sea flux of anthropogenic bromoform. I obtain average bromoform concentrations around the ports and the annual bromine flux from ballast water treatment. While DBPs spread over a large area along the coasts, the volatile DBP bromoform is instantly outgassed into the atmosphere without large-scale ocean transport. This results in only very localised emissions confined to the direct area of the major harbours. In these areas, emissions can be very high in addition to the background emissions of bromoform. Hence, anthropogenic bromoform input from ballast water treatment can have a local impact around major harbours but with 13 $\mathrm{Mmol\,Br\,a^{-1}}$ does not have influence on the bromine budget on a global scale.

[1]GEOMAR Helmholtz Centre for Ocean Research Kiel, Kiel, Germany
[2]now at: Institute of Space and Atmospheric Studies, University of Saskatchewan, Saskatoon, Canada
[3]Christian-Albrechts-Universität zu Kiel, Kiel, Germany
[4]Ocean Frontier Institute, Dalhousie University, Halifax, Canada
[5]GoConsult, Hamburg, Germany
[6]Dr. Matej David Consult, Izola, Slovenia
[7]Faculty of Maritime Studies, University of Rijeka, Rijeka, Croatia

Ocean Sci., 15, 891–904, 2019
https://doi.org/10.5194/os-15-891-2019

Ocean Science Open Access EGU

Simulating the spread of disinfection by-products and anthropogenic bromoform emissions from ballast water discharge in Southeast Asia

Josefine Maas[1], Susann Tegtmeier[1], Birgit Quack[1], Arne Biastoch[1,2], Jonathan V. Durgadoo[1], Siren Rühs[1,a], Stephan Gollasch[3], and Matej David[4,5]

[1]GEOMAR Helmholtz Centre for Ocean Research Kiel, Kiel, Germany
[2]Christian-Albrechts-Universität zu Kiel, Kiel, Germany
[3]GoConsult, Hamburg, Germany
[4]Dr. Matej David Consult, Izola, Slovenia
[5]Faculty of Maritime Studies, University of Rijeka, Rijeka, Croatia
[a]now at: Ocean Frontier Institute, Dalhousie University, Halifax, Canada

Correspondence: Josefine Maas (jmaas@geomar.de)

Received: 19 December 2018 – Discussion started: 2 January 2019
Revised: 8 June 2019 – Accepted: 11 June 2019 – Published: 11 July 2019

Abstract. Ballast water treatment is required for vessels to prevent the introduction of potentially invasive neobiota. Some treatment methods use chemical disinfectants which produce a variety of halogenated compounds as disinfection by-products (DBPs). One of the most abundant DBPs from oxidative ballast water treatment is bromoform ($CHBr_3$), for which we find an average concentration of $894 \pm 560\,\mathrm{nmol\,L^{-1}}$ ($226 \pm 142\,\mu\mathrm{g\,L^{-1}}$) in the undiluted ballast water from measurements and the literature. Bromoform is a relevant gas for atmospheric chemistry and ozone depletion, especially in the tropics where entrainment into the stratosphere is possible. The spread of DBPs in the tropics over months to years is assessed here for the first time. With Lagrangian trajectories based on the NEMO-ORCA12 model velocity field, we simulate DBP spread in the sea surface and quantify the oceanic bromoform concentration and emissions to the atmosphere from ballast water discharge at major harbours in the tropical region of Southeast Asia. The exemplary simulations of two important regions, Singapore and the Pearl River Delta, reveal major transport pathways of DBPs and anthropogenic bromoform concentrations in the sea surface. Based on our simulations, we expect DBPs to spread into the open ocean, along the coast and through advection with monsoon-driven currents into the North Pacific and Indian Ocean. Furthermore, anthropogenic bromoform concentrations and emissions are predicted to increase locally around large harbours. In the sea surface around Singapore, we estimate an increase in bromoform concentration by 9 % compared to recent measurements. In a moderate scenario in which 70 % of the ballast water is chemically treated, bromoform emissions to the atmosphere can locally exceed $1000\,\mathrm{pmol\,m^{-2}\,h^{-1}}$ and double climatological emissions. In the Pearl River Delta all bromoform is directly outgassed, which leads to an additional bromine (Br) input into the atmosphere of $495\,\mathrm{kmol\,Br\,a^{-1}}$ ($\sim 42\,\mathrm{t\,CHBr_3}$). For Singapore ports the additional atmospheric Br input is calculated as $312\,\mathrm{kmol\,Br\,a^{-1}}$ ($\sim$ 26 t $CHBr_3$). We estimate a global anthropogenic Br input from ballast water into the atmosphere of up to $13\,\mathrm{Mmol\,a^{-1}}$. This is 0.1 % of global Br input from background bromoform emissions and thus not relevant for stratospheric ozone depletion.

Published by Copernicus Publications on behalf of the European Geosciences Union.

1 Introduction

1.1 Ballast water treatment

Ballast water is necessary for ships to maintain stability and draught during voyage and port operations. Usually, ballast water is taken up during cargo unloading and discharged during loading operations. However, the uptake and discharge of ballast water by commercial ships represent the main driver of the global spread of marine invasive species, which can cause negative impacts on ecosystems, economies and public health (Ruiz et al., 2000; Briski et al., 2012). In September 2017, the Ballast Water Management Convention (IMO, 2004) entered into force, aiming to minimise the survival of organisms carried in ballast water tanks. According to the convention, shipowners from ratified flag states have different options to manage their ballast water, one being the onboard operation of ballast water treatment systems (BWTSs), which are type approved by the member states. Over the next years, more than 75 000 vessels have to instal such BWTSs in order to control the transport of potentially harmful species (David and Gollasch, 2015).

Different BWTSs are available which can be separated into physical and chemical oxidation methods (e.g. David and Gollasch, 2015). Physical methods include filtration, cavitation and treatment with ultraviolet radiation. Chemical treatment is achieved via, e.g. electrolysis, chlorination or ozonation. Electrolysis makes use of electricity in the ballast water to generate sodium hypochlorite as an oxidant from the chemical reaction of salt in the seawater. During chlorination, a chemical such as sodium hypochlorite or chlorine dioxide is added in solution to the ballast water. Ozone treatment forms hydroxyl and oxyl radicals that react with bromide ions in seawater to hypobromous acid or to the hypobromite ion, which act as disinfecting agents (Werschkun et al., 2012). As of January 2019, 76 systems had received approval, 33 of which use chemical treatment (IMO, 2019). However, it is currently unknown which treatment methods will be applied most on ships over the next years.

Chemical BWTSs that apply oxidative treatment have been shown to produce a variety of so-called disinfection by-products (DBPs) including trihalomethanes, halogenated acetic acids and bromate (Delacroix et al., 2013; Werschkun et al., 2014; Shah et al., 2015). The generally proposed mechanism for generating DBPs is the reaction of oxidants such as chlorine and ozone with organic and inorganic substances, such as bromide (Br-) and iodide (I-), in the water via the formation of hypobromous (HOBr) and hypoiodous (HOI) acid. The nature and amount of DBPs generated in seawater depend on many factors including the type of oxidant, the injected concentration, the amount and composition of dissolved organic matter (DOM) (Liu et al., 2015), and the concentrations of the specific halide ions, i.e. salinity (Shah et al., 2015). The chlorination and ozonation of seawater, for example, have been shown to produce bromoform ($CHBr_3$) as one major DBP (Jenner et al., 1997; Padhi et al., 2012; Liu et al., 2015). Bromoform concentration is generally higher for chlorination than ozonation or other treatment methods. Moreover, in the presence of DOM mainly organohalogens are produced as DBPs (Shah et al., 2015), which is often the case for harbour seawater with a high influence from land use or river runoff.

DBPs like bromoform will spread in the marine environment once the ship discharges its ballast water. To receive approval with the Ballast Water Management Convention, BWTSs need to include a risk assessment according to the methodology of the Joint Group of Experts on the Scientific Aspects of Marine Environmental Protection – Ballast Water Working Group (GESAMP-BWWG) (IMO, 2017). The methodology tries to identify if the DBPs found in ballast water have an ecotoxicological effect on marine life as well as human health. The risk assessment uses a worst-case scenario in which the DBPs discharged into the harbour are modelled to calculate their predicted environmental concentration. A recent study by David et al. (2018) showed that the GESAMP-BWWG methodology does not fully account for potential environmental risks. To date, the GESAMP-BWWG methodology has not assessed the environmental impacts of volatile DBPs on atmospheric chemistry.

1.2 Brominated very short-lived substances

Trihalomethanes generated in BWTSs such as bromoform are also formed naturally in the oceans. Bromoform is of biological origin with both macroalgae and microalgae as potential producers, which oxidise primary metabolic compounds with haloperoxidases in the presence of hydrogen peroxide (e.g. Theiler et al., 1978; Moore et al., 1996). Currently available measurements of bromoform in seawater suggest a large spatial variability with elevated abundances in coastal, equatorial and upwelling regions due to biological sources (Quack and Wallace, 2003; Ziska et al., 2013; Fuhlbrügge et al., 2016).

Bromoform is the most important carrier of organic bromine from the ocean to the atmosphere, contributing together with dibromomethane (CH_2Br_2) up to 70 % of organic bromine to the marine troposphere (Hossaini et al., 2012). Both compounds have relatively short lifetimes of around 2 weeks ($CHBr_3$) and 3 months (CH_2Br_2) in the tropical boundary layer of the atmosphere and thus belong to the so-called very short-lived substances (VSLSs; Carpenter and Reimann et al., 2014). Given the highly variable oceanic production and its short lifetime, the atmospheric distribution of bromoform is characterised by strong variations (Quack and Wallace, 2003).

Upon their release into the atmosphere, bromoform and other brominated VSLSs impact atmospheric chemistry. VSLSs are quickly oxidised or photodissociated to reactive halogen species, which participate in the depletion of tropospheric ozone by catalytic cycles (Saiz-Lopez and von

Glasow, 2012). Furthermore, reactive halogen species reduce tropospheric NO_x by the formation of nitryl halides (XNO_2, where X=Cl, Br and I) (Simpson et al., 2015) and alter tropospheric HO_x ratios towards OH (Sherwen et al., 2016). Thereby, reactive halogens from VSLSs impact the atmospheric lifetimes of dimethyl sulfide (DMS), many pollutants and greenhouse gases, such as methane and mercury (Simpson et al., 2015; Saiz-Lopez and von Glasow, 2012).

In the stratosphere, VSLSs also contribute to the depletion of ozone. Due to their short lifetime, they are mostly oxidised and subsequently removed through tropospheric precipitation. However, in regions of deep convection, they can be entrained into the stratosphere through rapid vertical transport (e.g. Aschmann et al., 2009; Tegtmeier et al., 2015). Deep convective events are most common in the tropics near the Equator where solar irradiance is high throughout the year and the ocean is an efficient source of bromoform and other VSLSs (Quack and Wallace, 2003). Observational (e.g. Dorf et al., 2006) and modelling (e.g. Warwick et al. 2006; Liang et al., 2010) studies have suggested that VSLSs provide a significant contribution to stratospheric total bromine (Br_y), with current estimates ranging between 2 and 8 ppt (Carpenter and Reimann et al., 2014; Wales et al., 2018). Once brominated VSLSs have reached the stratosphere, they participate in ozone depletion at middle and high latitudes (Yang et al., 2014; Sinnhuber and Meul, 2015).

1.3 Motivation

Recent publications have analysed the production of DBPs from oxidative ballast water treatment and assessed its ecotoxicity (Delacroix et al., 2013; Shah et al., 2015; Werschkun et al., 2014). These studies focussed on risk assessments on board ships or in the near-ship environment. So far, the focus has been on the small-scale immediate exposure of DBPs to humans and the marine environment. The long-term effects of ballast water discharge on regional to global scales has not been assessed so far and the atmosphere, as a sink for volatile halocarbons, has not been considered in any existing risk assessment of oxidative ballast water treatment. In particular, brominated species such as bromoform are frequently produced in treated ballast water and are known to impact atmospheric chemistry. In this study, we provide a first analysis of how DBPs and any other passive substances contained in treated ballast water spread over a period of months to years around different harbours in Southeast Asia (Sect. 3). The derived spread can serve as a proxy for assessing the environmental impact of any chemical or biological species contained in treated or untreated ballast water. In a second step, we derive an estimate of bromoform released from ballast water into the marine environment and quantify its emission into the atmosphere (Sect. 4). We further discuss the methods and data used for this study including port statistics, DBP concentrations in ballast water and our Lagrangian simulations (Sect. 2).

2 Methods

2.1 Port statistics

For a regional to global analysis, volumes of ballast water discharge for individual ports and the typical bromoform concentration in the treated ballast water are needed. As ships are usually not required to report ballast water operations to harbour officials, exact numbers of localised ballast water discharge are not available. Thus, any approach to calculate such numbers from ship size or cargo is challenging (Seebens et al., 2013). Here, we derive estimates of the discharge volumes by linking the annual amount of global ballast water volume with the cargo throughput at each port. Global annual discharge volume is estimated to range from 3 to 5 billion m^3 (Tamelander et al., 2010; Endresen et al., 2004; David, 2015). In addition to the global ballast water amount, it is known that the discharged ballast water amounts on average to roughly 33 % of the loaded cargo volume (David, 2015). We use the global ballast water discharge as 33 % of the global 10 286.9 million tonnes of loaded goods (UNCTAD, 2017) to obtain a ballast water volume of 3.4 billion m^3, which agrees well with the estimates from the studies mentioned above.

The cargo throughput is obtained from the world port ranking 2016 published by the American Association of Port Authorities (AAPA, 2016). This statistic includes the 100 biggest ports for two categories: containerised and bulk cargo. Containerised cargo is given in twenty-foot equivalent units (TEUs), while bulk cargo is given in tonnes. In order to combine these two rankings, we generate a modified world port ranking and calculate the percentage share of containerised and tonnage goods according to their global ratio given by the Review of Maritime Transport (UNCTAD, 2017). The percentage share of containerised goods in 2016 amounts to 16.6 %, while the rest makes up 83.4 % of the total goods loaded (UNCTAD, 2017). According to the percentage share of their category and their individual size in the ranking, each container and bulk port is assigned its relative fraction under the simplified assumption that these ports account for all of the global commercial ship trade and receive all of the global ballast water. Since many of the harbours appear in both statistics (containerised and bulk), both percentage values are added to give their total cargo share, which forms our modified world port ranking encompassing 144 ports (Supplement table). We use the calculated percentages to divide global ballast water volume among all ports to derive the estimated discharge for each port.

Our study focus was set on the coastal region of Southeast Asia (10° S–40° N, 95–145° E) where 38 harbours from our modified world port ranking are located, comprising 57 % of the global shipping industry (Fig. 1). This region is to a major extent located in the tropics, which makes it very relevant for the entrainment of oceanic VSLS emissions into the stratosphere.

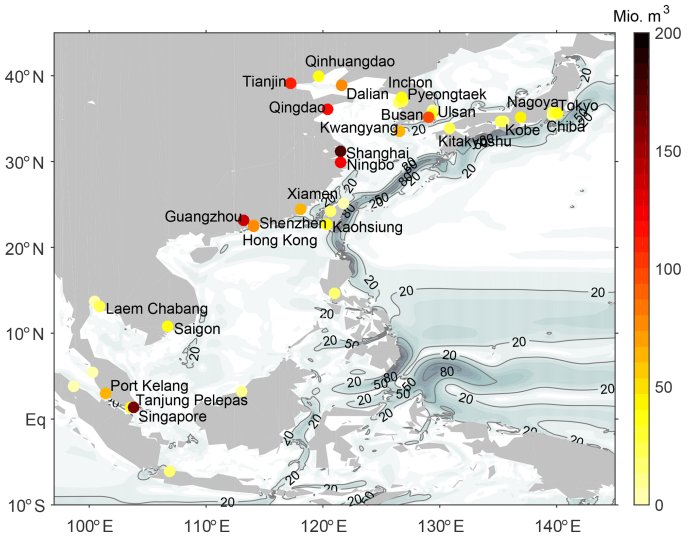

Figure 1. Estimated annual ballast water discharge volume (10^6 m^3) from each harbour in the modified world port ranking in Southeast Asia with the names of the 26 largest ports (Supplement table). Contours and black contour lines show climatological ocean surface velocities (cm s^{-1}) from NEMO-ORCA.

For our detailed analysis, we choose two different locations in the tropics that are characterised by large harbours and different ocean dynamics. The first area is Singapore, where the two ports of Singapore and Tanjung Pelepas (Malaysia) are located very close to the Equator. This location in the Maritime continent is characterised by sea surface currents of over 0.2 m s^{-1} in the climatological mean (Fig. 1). The other location is the Pearl River Delta where the harbour cities of Guangzhou, Hong Kong and Shenzhen are located. There, only weak coastal currents can be found in the climatology.

2.2 Bromoform production from oxidative ballast water treatment

In a second step, we derive estimates of the bromoform concentration produced during chemical ballast water treatment. Since there are many BWTSs that use different chemical treatment methods with different water parameters and residence times, the produced amount of bromoform can show large variations. Here, we determine a range of possible bromoform concentrations which can be used in our analysis to estimate the environmental input of bromoform. For this purpose we use measurements of chemically treated ballast water taken during shipboard tests, as well as literature data. The formation of disinfection by-products in BWTSs is most commonly investigated during land-based tests. In contrast, we have conducted one of the first shipboard tests of the formation of major halocarbons in treated ballast water. The samples were taken from the discharge of treated ballast water for three unnamed BWTSs, two in Norway and one in Germany, which use chlorination techniques. This allows us to obtain a more robust estimate of the initial bromoform concentrations in the ballast water. The bromoform measurements were carried out with a purge-and-trap gas chromatograph–mass spectrometer (GC–SM) system with a detection limit of around 0.1 pmol L^{-1}. Bromoform concentrations of 244.5 ± 163.6 µg L^{-1} (967.6 ± 647.4 nmol L^{-1}) were found in 12 ballast water samples taken in Norway from two different BWTSs (Table 1). Bromoform concentrations of 202.0 ± 74.0 µg L^{-1} (799.1 ± 292.7 nmol L^{-1}) were found in nine ballast water samples taken in Germany from one BWTS (Table 1). These samples were taken on board the vessel at three time periods during ballast water discharge in 15–20 min intervals. The particulate organic matter in the water was 11.1 to 12.6 mg L^{-1}.

In addition, we use bromoform concentrations given in the reports of the International Maritime Organization (IMO) Marine Environment Protection Committee (MEPC) for Final Approval of BWTSs (https://docs.imo.org, last access: 3 July 2019). Mean bromoform values for seawater and brackish water from the MEPC reports on 29 BWTSs, 22 of which use chlorine as the main disinfecting agent, are also given in Table 1.

Different chemical treatment systems show greatly varying bromoform concentrations, as illustrated by the large standard deviations in the MEPC data. This is due to different doses and types of oxidant, varying residence time in the tank, and different water properties such as salinity, temperature and the amount of DOM (Shah et al., 2015). In general, the systems using chlorination as the main disinfecting agent generate higher bromoform concentrations than ozonation systems. Samples of the same treatment system (German system in Table 1), show a smaller standard deviation. Overall, our shipboard DBP measurements are in the range of the land-based test results published in the MEPC reports, suggesting a similar amount of bromoform production. On average 226 ± 142 µg $CHBr_3$ L^{-1} can be expected in ballast water, which corresponds to 894 ± 560 nmol L^{-1} (Table 1) with the mean values of all four data sets in good agreement. The values shown here mainly stem from chlorination-based treatment systems. Therefore, we will focus on chlorination-based treatment in the following.

The exact percentage of vessels that will eventually use chemical BWTSs is unknown. Oxidative water treatment is more suited for larger vessels such as bulk carriers or tankers, which are typically the types of ships that carry the largest volumes of ballast water (Maritime Impact, 2017). Thus, we assume that 70 ± 20 % of the ballast water will be chemically treated, producing DBPs. In order to capture the range of uncertainty resulting from the variations of the bromoform concentrations in ballast water samples and from the unknown share of chemical BWTSs, we set up three scenarios: LOW, MODERATE and HIGH (Table 2). The scenarios are assigned an initial bromoform concentration corresponding to the mean and the mean ± 1 standard deviation, and they use different shares (50 %, 70 % and 90 %) of chemi-

Table 1. Bromoform ($CHBr_3$) data from samples of undiluted ballast water given as an average and standard deviation ($\mu g\,L^{-1}$; $nmol\,L^{-1}$). Samples 1 and 2 are measurements from shipboard tests of a chlorination BWTS. Samples 3 and 4 are data from the IMO Marine Environmental Protection Committee (MEPC) reports on approval for different BWTSs using chemical treatment.

	$CHBr_3$ concentration ($\mu g\,L^{-1}$)	$CHBr_3$ concentration ($nmol\,L^{-1}$)
1. Sample BWTS Norway	244.5 ± 163.6	967.6 ± 647.4
2. Sample BWTS Germany	202.0 ± 74.0	799.1 ± 292.7
3. MEPC report seawater	239.4 ± 173.3	947.1 ± 685.8
4. MEPC report brackish water	217.4 ± 155.1	860.0 ± 613.5
Mean	225.8 ± 141.5	893.5 ± 559.9

cally treated ballast water. Based on these two assumptions, we derive different amounts of annually discharged bromoform for the selected regions in Singapore and the Pearl River Delta (Table 2). In these scenarios, other brominated species like dibromomethane have been neglected because their concentrations in treated water were usually more than 10 times lower than bromoform concentrations. Variations in the usage of the different treatment methods will lead to variations of anthropogenic bromine release. We include these variations by applying the three scenarios in which we include a best- and a worst-case scenario, LOW and HIGH, respectively.

2.3 Lagrangian simulations

In contrast to earlier studies which focussed on the local effect of DBPs from ballast water (e.g. David et al., 2018), we investigate the long-term, large-scale influence of DBPs in the ocean and atmosphere. Therefore, we need regional to global ocean velocity and surface wind data, which can be obtained from high-resolution ocean general circulation models (OGCMs). We simulate the spread of treated ballast water and the DBPs contained within by applying a Lagrangian trajectory integration scheme to the 3-D velocity output from an eddy-resolving OGCM. The model output stems from a hindcast experiment with the ORCA0083 model configuration based on the NEMO-ORCA code version 3.6 (Madec, 2008). The ORCA0083 configuration from the European DRAKKAR consortium (The DRAKKAR Group, 2007) has a horizontal resolution of $1/12°$ and 75 vertical levels, with 46 levels in the upper 1000 m and spacing increasing with depth (see also Marzocchi et al., 2015; Durgadoo et al., 2017). Atmospheric forcing comes from the DFS5.2 data set (Dussin et al., 2016) and varies on a range of scales, from synoptic to interannual and longer. The experiment ORCA0083-N06 used in this study was run by the National Oceanography Centre, Southampton, UK. Model output is given at a temporal resolution of 5 d for the time period 1963 to 2012.

To simulate the spread of DBPs in the surface ocean, the ARIANE software was used (Blanke et al., 1999). ARIANE performs offline trajectory calculations by passively advecting virtual particles along analytically computed 3-D streamlines. This method has been developed and extensively used for analysing mean large-scale spreading of water masses or minor species from a known source over different time periods (e.g. Durgadoo et al., 2017; van Sebille et al., 2015; Rühs et al., 2019). In our study, the DBPs from ballast water discharge are approximated as particles that are passively advected with the simulated flow. The streamline calculations are purely advective and no diffusivity is applied. For both regions of interest, 10 individual simulations are conducted starting each year in January from 2001 to 2010. The 10 different simulations are used to obtain more robust ensemble results and avoid extremes from internal variability. In each simulation, particles are continuously released close to the port site at every model output time step (once every 5 d), which represents a continuous ballast water discharge at this location. Subsequently, the particle advection is simulated for 2 years. For the purpose of calculating seasonal and annual means and to allow for an initial accumulation period, only months 12 to 23 (December of one year to November of the following year) are analysed for each simulation. Additionally, all particles older than 11 months are not considered in the analysis so that the total particle number is constant at each time step.

The experiments were run for the Pearl River Delta region and the Singapore region. The Pearl River Delta region comprises three major ports, Hong Kong, Guangzhou and Shenzhen, for which we derive a total annual ballast water discharge volume of 271 million m^3 (8 % of the global ballast water discharge) from the modified world port ranking (Supplement table). The Singapore region comprises the ports of Singapore and Tanjung Pelepas, with a ballast water amount of 190 million m^3 (5.6 %) each year. The discharge location where particles are released has been chosen in the vicinity of the harbours at approximately 8 to 40 km off the coast, as the model resolution does not allow for the capture of small-scale coastal structures such as harbours. Our method ensures minimal influence of the land boundaries on the initialisation of the simulation. We assume that the DBPs are transported from the inner harbour into the adjacent coastal

Table 2. Scenarios for the simulation of ballast water (BW) spread with different initial bromoform concentration and annual bromoform amount for two regions in Southeast Asia, Singapore and the Pearl River Delta (PRD).

Scenario	$CHBr_3$ concentration in BW ($\mu g\,L^{-1}$)	Percentage of vessels using chemical BW treatment (%)	$CHBr_3$ Singapore		$CHBr_3$ PRD	
			(10^6 g a^{-1})	(kmol a^{-1})	(10^6 g a^{-1})	(kmol a^{-1})
MODERATE	226	70	30	119	43	170
LOW	84	50	8	32	11	45
HIGH	368	90	63	250	90	356

areas where our model simulations are initialised. For many ports this is reasonable since rivers and tidal flushing cause a steady turnover of coastal waters with the ocean.

For the analysis of the experiments, we distinguish (1) the passive spread of DBPs without any environmental sinks (hereafter PASSIVE) and (2) the spread of bromoform as a major volatile DBP accounting for atmospheric fluxes and oceanic sinks (hereafter FLUX). For the PASSIVE analysis, we consider the full history of simulated particle positions, which is equivalent to assuming no particles getting lost through sinks in the ocean or emission into the atmosphere. The resulting distribution shows where DBPs in ballast water or assumingly dimensionless and immotile species can be transported through ocean currents within 1 year.

For the FLUX analysis, each particle is given an initial mass of bromoform based on the ballast water volume of the harbour and the produced bromoform according to the three scenarios MODERATE, HIGH and LOW (Table 2). Moreover, different sinks of bromoform, such as constant exchange at the air–sea interface and chemical loss rates, are taken into account.

We calculate the bromoform air–sea exchange based on the flux parameterisation from Nightingale et al. (2000) for all particles that reach the mixed layer at a certain time step. The mixed layer depth (MLD) is defined as the ocean layer in which the vertical density gradient does not exceed $0.02\,kg\,m^{-3}$ referenced to the 10 m depth. According to ORCA, the annual mean MLD is less than 20 m deep within our research area. Since the results are given at a 5 d temporal resolution and the MLD is relatively shallow, it is reasonable to assume that the whole mixed layer is in contact with the atmosphere at least once during each time step. Treated ballast water provides an additional source of bromoform to the environment, adding to the natural bromoform occurring in the ocean and atmosphere. Given the additive nature of the ocean and atmospheric terms in the air–sea flux parameterisation, it is possible to calculate the flux of the anthropogenic and natural bromoform portions separately. For our simulations, we only consider bromoform from ballast water treatment and apply the air–sea flux parameterisation to the anthropogenic bromoform in water and air. We have conducted sensitivity tests with an atmospheric transport model which shows that outgassed anthropogenic bromoform is quickly advected from the sea surface to other areas and different heights. Therefore, we can assume that anthropogenic bromoform in the atmosphere is always zero at the ocean surface in the region of interest. The air–sea exchange is linearly proportional to the gas transfer velocity of bromoform, which depends on surface wind velocities and sea surface temperature and salinity. Surface wind velocities are taken from the NEMO-ORCA forcing data set DFS5.2 (Dussin et al., 2016).

Oceanic sinks are also taken into account, although they are negligible on the timescales considered in this study. These include degradation through halide substitution and hydrolysis with a half-life of 4.37 years (Hense and Quack, 2009), as well as remineralisation with a half-life of 5.72 years (Hense and Quack, 2009).

The particle density distribution is calculated on a $1^\circ \times 1^\circ$ horizontal grid over the upper 20 m of the ocean (further mentioned as the "surface"). The distribution is given as a percentage per grid box of the total particle number (PASSIVE) and as bromoform concentration (pmol L^{-1}; FLUX). Statistical values are calculated over three grid boxes with the highest concentration around the discharge location. Analyses on seasonal to interannual timescales were conducted by averaging and concatenating the simulations from the model years 2001 to 2010. For the calculation of time series, we use the smoothed 2-week (15 d) running mean of the concentration and emission rates from the three grid boxes around the discharge location for the three scenarios MODERATE, LOW and HIGH. Wind speed values from these boxes are also smoothed with a 15 d running mean in order to better show the seasonal to annual variations.

The global atmospheric input of bromoform from ballast water emissions can be estimated by multiplying the initial concentrations with the global ballast water volume for each scenario, taking into account different percentages of chemical treatment systems (Table 2). The global atmospheric bromine input from the source-gas bromoform is derived by multiplying the global annual emissions with the number of bromine (Br) atoms.

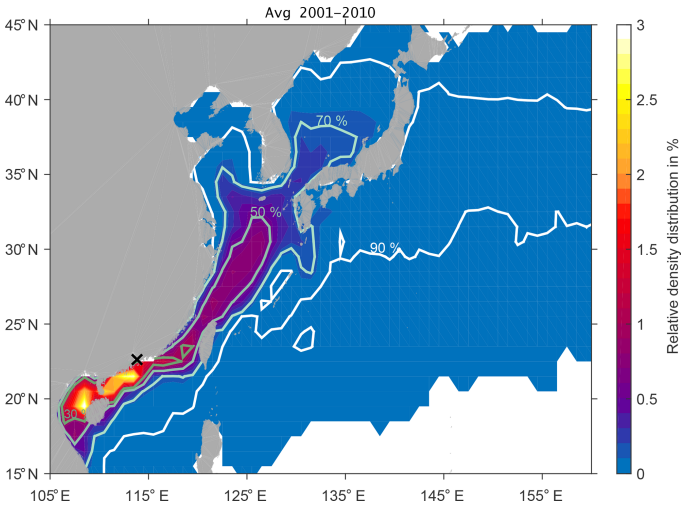

Figure 2. Annual mean surface (20 m) spread of DBPs from discharge in the Pearl River Delta relative to the total number of particles released. Contours show the area of the percentage of particles (30 %, 50 %, 70 % and 90 %) characterised by the highest density.

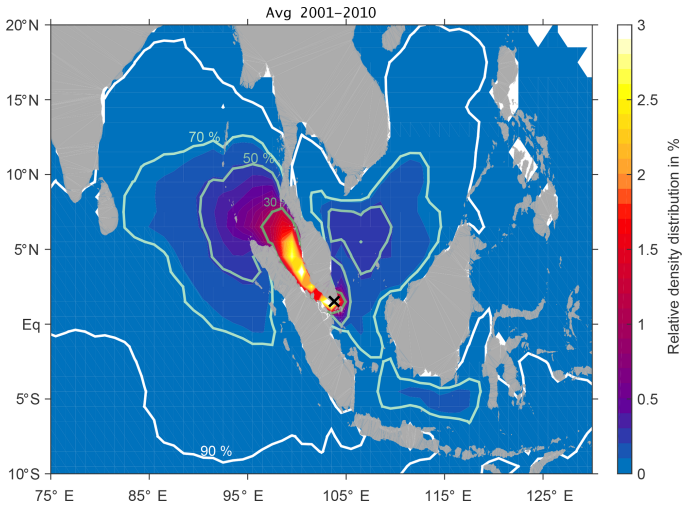

Figure 3. Annual mean surface (20 m) spread of DBPs from discharge in Singapore relative to the total number of particles released. Contours show the area of the percentage of particles (30 %, 50 %, 70 % and 90 %) characterised by the highest density.

3 Surface spread of DBPs – PASSIVE

Figure 2 shows the relative particle density distribution of DBPs averaged over 10 years released from the Pearl River Delta. We estimate the contour lines of the percentage of DBPs (30 %, 50 %, 70 % and 90 %) that are characterised by the highest particle density. The distribution shows that 90 % of DBPs spread past Japan and the Korean Peninsula, with the Kuroshio into the North Pacific, and southwards into the South China Sea towards the Philippines within 1 year. On average, 30 % of the DBPs with the highest density will stay southward of the Pearl River Delta along the coast and are now distributed in the Gulf of Tonkin west of the island of Hainan. There, the highest relative particle density distribution reaches up to 3 % locally with respect to total DBP discharge.

For the Singapore harbour region, the relative DBP distribution averaged over the years 2001–2010 is shown in Fig. 3. As for the Pearl River Delta, most of the DBPs stay in the close vicinity of the coastlines, with the highest relative density distribution of 4 %. On an annual mean basis, the 30 % of DBPs that are characterised by the highest particle density have been transported northwestward and accumulate in the Strait of Malacca, in close contact with the coastlines of the Malay Peninsula and the island of Sumatra. DBPs within the 50 %–70 % distribution expand mostly into the Indian Ocean towards Sri Lanka, but a small fraction is advected into the South China Sea between Borneo and Vietnam and even into the Java Sea. The main driver for the mean state of DBP transport from Singapore is the Indonesian throughflow, generally directed westward through the different passages of the Indonesian Archipelago (Gordon, 2001).

For the Pearl River Delta and Singapore, the areas of the 90 % of DBPs with the highest particle density expand over 5.0 and 8.6 million km^2, respectively, illustrating the large possible spread of longer-lived DBPs in ballast water. The size of the area and dominant direction of expansion are subject to variability on different timescales.

We investigate the interannual variations in the spread of DBPs by analysing the area extent of the 30 %, 50 %, 70 % and 90 % of particles with the highest density for the time period 2001–2010 (Fig. 4). The largest variations are found for the annual mean distribution of the 90 % area which expands over 6.6–10.2 million km^2 for the Pearl River Delta region depending on the surface velocity strength in the area. The extent of the 30 % and 50 % regions varies less on interannual timescales. Our results show that half of the longer-lived organisms and chemicals in ballast water can be expected to be spread over a relatively constant area of 0.5–1 million km^2 around the harbour, while the other 50 % is transported into a much larger region (up to 10.2 million km^2) that fluctuates depending on interannual variations of ocean surface transport.

Since a lot of the volatile DBPs will be emitted into the atmosphere and other short-lived non-volatile DBPs degrade in the ocean on relatively short timescales of weeks to months, the seasonal timescales are also of interest when evaluating the main pathways of DBP distribution. Depending on the season of discharge, the dominant atmospheric winds and oceanic currents can vary substantially in strength and direction in the region considered. We calculate seasonal anomalies of the particle density distribution for the time period 2001–2010 by subtracting the annual mean climatology from the seasonal mean climatologies.

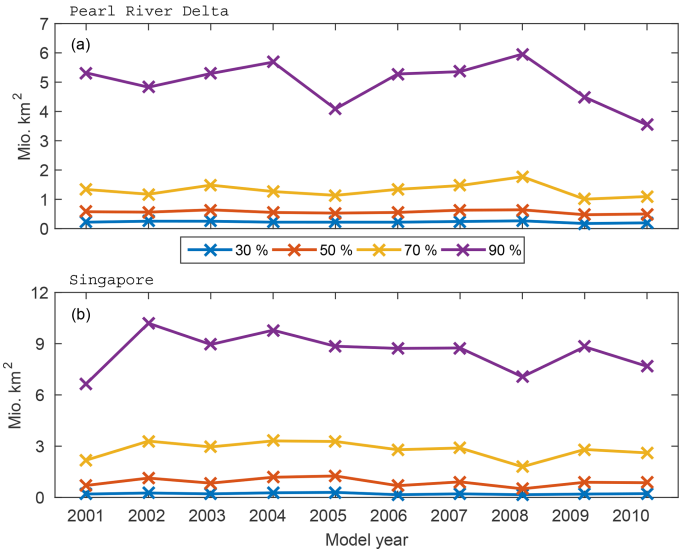

Figure 4. Annual mean area extent of DBP spread in the **(a)** Pearl River Delta and **(b)** Singapore based on 30 %, 50 %, 70 % and 90 % of the particles characterised by the highest density.

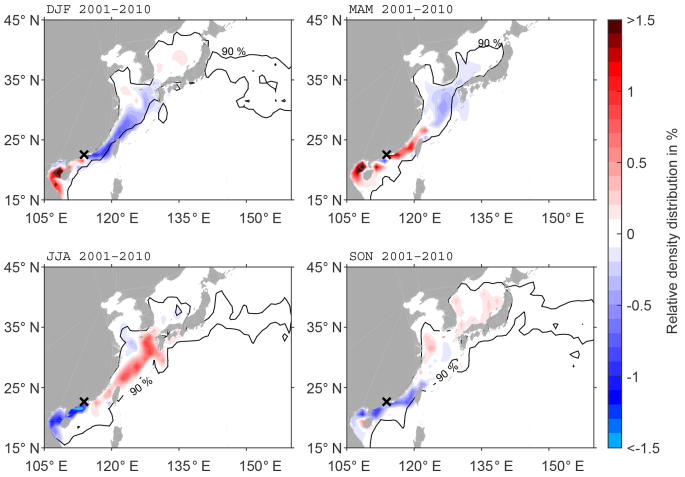

Figure 5. Anomaly of seasonal DBP spread compared to climatology (2001–2010) at the surface (20 m) for discharge in the Pearl River Delta. The black contour line shows the area of the 90 % of particles characterised by the highest density in the seasonal mean.

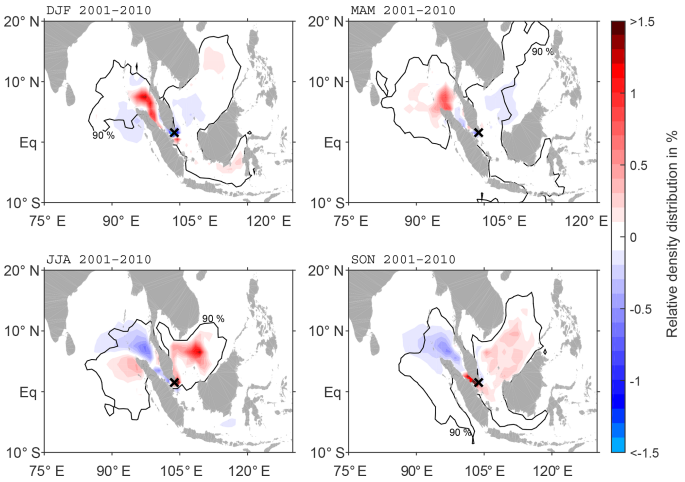

Figure 6. Anomaly of seasonal DBP spread compared to climatology (2001–2010) at the surface (20 m) for discharge in Singapore. The black contour line shows the area of the 90 % of particles characterised by the highest density in the seasonal mean.

Seasonal anomalies of the main pathways of ballast water spread from the Pearl River Delta region show a clear reversal of main spread from boreal winter (DJF) to summer (JJA) (Fig. 5). Surface currents in the South China Sea are wind-driven and seasonally affected by the northwest Pacific monsoon (Shaw and Chao, 1994). During DJF, the main pathway is towards the southwest, with an accumulation of DBPs west of Hainan and positive anomalies up to 9 %. There is a clear separation of these positive anomalies south of the Pearl River Delta and negative anomalies north of this region. Furthermore, the area of the 90 % DBP distribution is located in a narrower band towards the coast during DJF. This anomaly pattern reverses in JJA. More DBPs are transported northward, while there is less advection to the south. However, the northeast winter monsoon prevails much longer in the Pearl River Delta than the southwest summer monsoon, which explains why in the annual mean the largest part of DBPs is advected southward. During boreal spring (MAM) and autumn (SON) anomalies are less pronounced. In MAM, the anomalies are mostly positive around the discharge location, which means more DBP accumulation along the coast and slower transport than in the annual mean due to weaker currents. The opposite happens in SON with negative anomalies around the discharge location, indicating that the fastest transport occurs during SON.

A similar seasonality in DBP spread can be seen from discharge in the Singapore region (Fig. 6). Here, close to the Equator, the monsoon winds seasonally reverse from northwesterly winds in JJA to southeasterly winds in DJF. As a result, more DBPs are transported towards the northwest through the Strait of Malacca into the Indian Ocean in DJF, and Singapore ports show a negative anomaly. As expected from the reversed winds in JJA, fewer DBPs are advected towards the west and more towards the east so that the DBPs can reach the Pacific Ocean. During SON, the strongest positive anomalies can be found in the southern Strait of Malacca. Then winds transition and become very weak, and thus DBPs cannot be transported quickly and accumulate near the discharge location of Singapore. The lowest anomalies are found in MAM, with a slightly enhanced accumulation of DBPs north of Malaysia.

4 Concentration and emission of bromoform – FLUX

The oceanic distribution of bromoform from ballast water treatment and its emissions into the marine boundary layer are estimated from the FLUX analysis based on the simu-

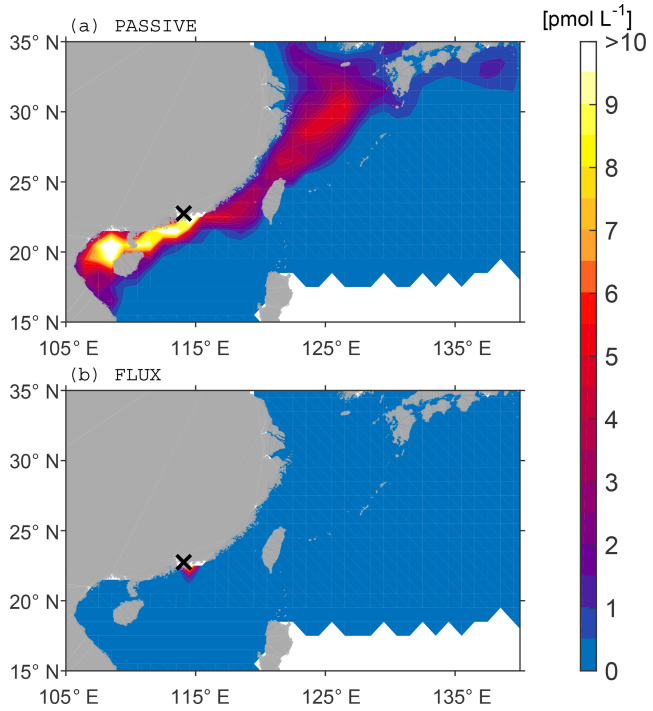

Figure 7. Surface bromoform concentration in the Pearl River Delta for the MODERATE scenario averaged over 1 year. **(a)** PASSIVE analysis without loss rates. **(b)** FLUX analysis with outgassing.

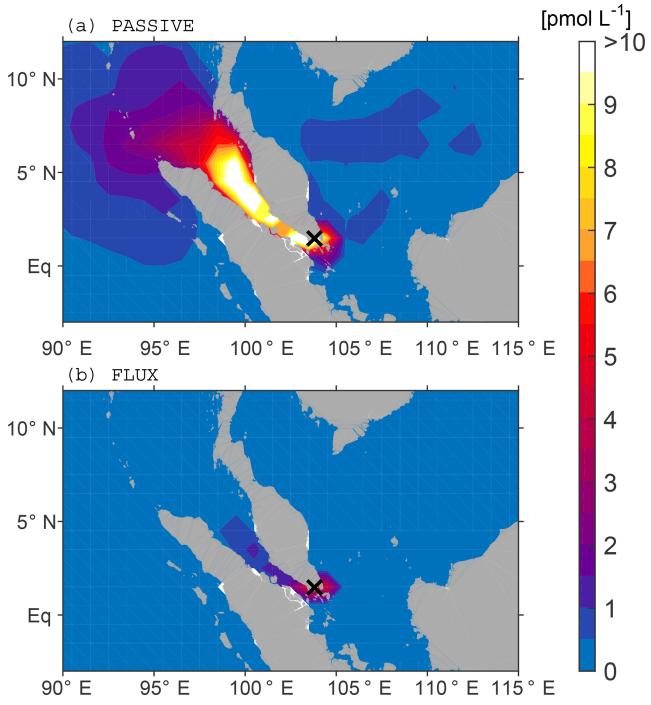

Figure 8. Surface bromoform concentration in Singapore for the MODERATE scenario averaged over 1 year. **(a)** PASSIVE analysis without loss rates. **(b)** FLUX analysis with outgassing.

lated velocity fields from 2006 and the corresponding Lagrangian experiments. As shown in Sect. 3, the interannual transport variability is small and therefore a 1-year simulation is sufficient to derive the representative emission estimates. Bromoform as a volatile gas can be outgassed into the marine atmospheric boundary layer, as long as it stays at the ocean–atmosphere interface. In the FLUX analysis, we calculate the bromoform outgassing rate for all particles within the mixed layer at every time step. We also calculate the bromoform surface concentration in the upper 20 m and the sea-to-air flux averaged over 1 year for the three scenarios MODERATE, HIGH and LOW. For comparison we calculate the bromoform concentrations that would prevail without outgassing into the atmosphere from the PASSIVE analysis.

We find that surface concentrations from the FLUX analysis are largely reduced compared to PASSIVE. In the Pearl River Delta region, bromoform only remains in the box around the discharge location due to the new input of ballast water at every time step (Fig. 7). Thus, the majority of released bromoform is instantly outgassed into the atmosphere, resulting in a relatively constant concentration of 10 pmol L^{-1} in the MODERATE scenario around the discharge location, ranging from 22 (HIGH) to 3 pmol L^{-1} (LOW) (Table 3).

Also, bromoform concentrations from Singapore ballast water stay much more centred around the discharge location when compared to the PASSIVE analysis without outgassing (Fig. 8). Small concentrations of 1 to 2 pmol L^{-1} can still be found in the Strait of Malacca. Average bromoform concentrations around Singapore add up to 11 pmol L^{-1} in the MODERATE scenario, ranging from 23 (HIGH) to 3 pmol L^{-1} (LOW). Measurements of bromoform in this region showed elevated surface concentrations of up to 130 pmol L^{-1} (Fuhlbrügge et al., 2016), most likely due to the combination of strong natural and already existing anthropogenic coastal sources. The additional bromoform input expected from ballast water discharge in Singapore would thus lead to a 9 % (18.5 %; 2.4 %) increase.

Evaluation of the time series shows that wind velocities are enhanced in the Pearl River Delta region with a strong seasonal cycle (Fig. 9). Such strong winds cause high exchange velocities, which in turn lead to high emission rates. The bromoform emission rate stays constant at 1690 pmol m^2 h^{-1} because everything discharged into the ocean is instantly outgassed into the atmosphere. Therefore, both oceanic concentrations and emissions into the atmosphere stay relatively constant throughout the time period, independent of the wind variations. The bromoform emissions in the Pearl River Delta region range between 440 and 3530 pmol m^2 h^{-1} for the three different scenarios (Table 3). This flux is much larger than in the Singapore region where the average range is 250 to 1940 pmol m^2 h^{-1}. Around Singapore, concentrations and emissions underlie a strong seasonality driven by the wind speed. Two times a year in summer and winter, wind velocities increase and cause bromoform emissions to increase as well. At the same time, oceanic bromoform concentrations

Table 3. Average values for the FLUX experiment in Singapore and the Pearl River Delta region for different scenarios. Values are calculated as the sum of three grid boxes around the discharge location.

Scenario	Singapore			Pearl River Delta		
	Concentration (pmol L^{-1})	Emission (pmol m^{-2} h^{-1})	Total Br flux (kmol a^{-1})	Concentration (pmol L^{-1})	Emission (pmol m^{-2} h^{-1})	Total Br flux (kmol a^{-1})
MODERATE	11	928	306	10	1687	511
LOW	3	246	81	3	448	136
HIGH	23	1943	641	22	3532	1070

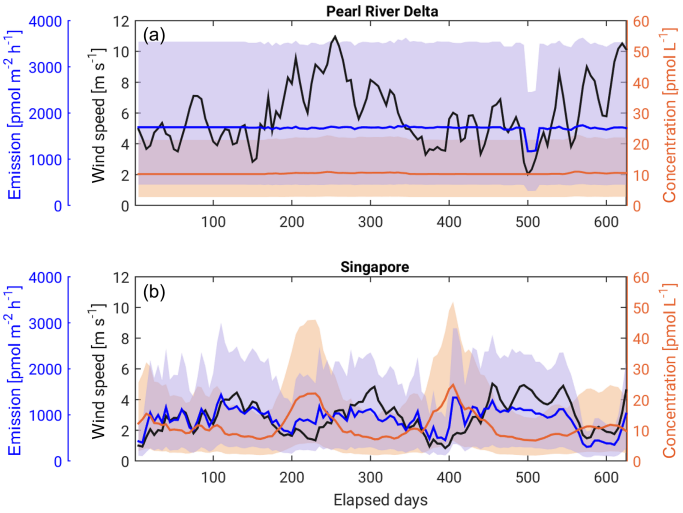

Figure 9. Time series of the 2-week running mean of wind speed (black), bromoform surface concentration (orange) and emissions (blue) for **(a)** Singapore and **(b)** Pearl River Delta. Solid lines show values from the MODERATE scenario. Shaded areas show the range between the HIGH and LOW scenarios for both bromoform concentration and emissions.

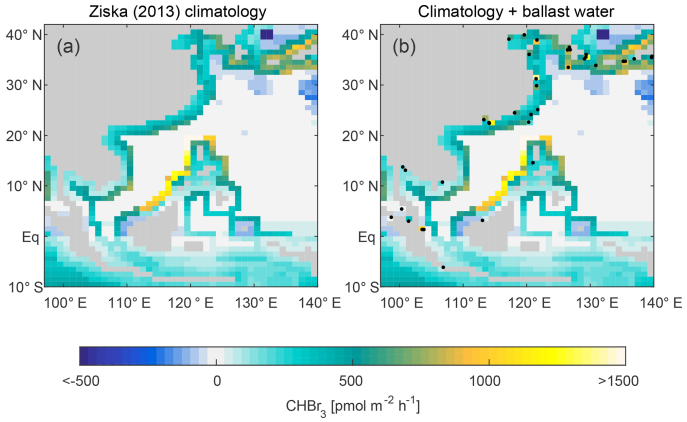

Figure 10. **(a)** Modelled bromoform emission rates updated from Ziska et al. (2013). **(b)** Same as **(a)** with additional anthropogenic emission rates calculated as 90 % of total bromoform release from ballast water treatment at each harbour. Black dots indicate the location of all harbours from the modified world port ranking in Southeast Asia.

around the discharge location drop due to the increased emissions and faster oceanic transport (Fig. 9). For weaker winds, the bromoform response is reversed with lower emissions and higher oceanic concentrations.

Adding up the air–sea flux rate of bromoform over 1 year, we derive the annual air–sea flux of bromine (Br) resulting from ballast water treatment. In Singapore, the total Br flux ranges from 80 to 640 kmol (7 to 55 t) Br a^{-1} from LOW to HIGH, which corresponds to an outgassing of roughly 85 % of the original 8 to 63 t Br produced as bromoform in ballast water (Table 3). The remaining 15 % is transported from the port site into the open ocean where it is either eventually outgassed into the atmosphere or transported into the deeper ocean. In the Pearl River Delta region, the flux ranges from 136 to 1070 kmol (12 to 92 t) Br a^{-1}, which corresponds to an outgassing of 100 % of the Br produced from ballast water treatment.

Given that 85 % of Singapore and 100 % of Pearl River Delta ballast water bromoform is directly outgassed into the atmosphere, we expect that on average 90 % of the anthropogenic bromoform is quickly outgassed after ballast water discharge in the Southeast Asia region. Based on this assumption, we estimate the anthropogenic outgassing rate of bromoform at each of the 38 harbours in the modified world port ranking in Southeast Asia according to its calculated ballast water volume for a MODERATE scenario. These emission rates are calculated on a $1° \times 1°$ horizontal grid box closest to the harbour so that the values can be compared to emission maps reconstructed from observations after Ziska et al. (2013) (Fig. 10). Note that anthropogenic emissions are always positive (from ocean to atmosphere) since they were calculated with zero concentration in the atmosphere. The climatological emissions can have negative (atmosphere to ocean) fluxes whereby the reconstructed atmosphere has higher concentrations than the sea surface. Thus, adding anthropogenic emissions to the climatology can theoretically reduce emissions. However, the climatology from Ziska et al. (2013) shows that bromoform emissions in coastal areas are generally characterised by high positive emissions with 500 to 1000 pmol m^2 h^{-1} wherein macroalgae act as efficient bromoform producers (Quack and Wallace, 2003) (Fig. 10a). When we add the estimated

anthropogenic bromoform emissions from ballast water to the climatological emissions, many of the grid boxes clearly show a strong increase in emissions, sometimes more than doubling the emission rates of bromoform (Fig. 10b). This is especially visible at very big harbours such as Shanghai, Singapore and the Pearl River Delta region where the new emission rates exceed 1000 pmol m^2 h^{-1}. These regions appear as local hot spots of anthropogenic bromoform emissions. Most of these areas are characterised by heavy industry and other anthropogenic activities, resulting in strong emissions of greenhouse gases like methane and ozone. The expected additional source of bromoform to the atmospheric environment can perturb the oxidising capacity and thus the atmospheric lifetime of greenhouse gases and other pollutants (Saiz-Lopez and von Glasow, 2012). The atmospheric chemistry around large ports is highly sensitive to additional emissions of volatile DBPs from treated ballast water.

5 Discussion and conclusion

We investigate a new source of halogenated disinfection by-products to the ocean and atmosphere from the release of chemically treated ballast water. Over the next years, more than 75 000 ships have to instal a ballast water treatment system to prevent the continued spread of harmful invasive species (David and Gollasch, 2015). As a side effect, halogenated DBPs at high concentrations will be produced in ballast water and released into coastal waters (Werschkun et al., 2012; Delacroix et al., 2013). In particular, bromoform shows concentrations in undiluted ballast water up to 1 million times higher than in the natural environment.

Our simulations of the DBP spread from the Singapore and Pearl River Delta harbours in the PASSIVE analysis show that within 1 year about half of the DBPs discharged with the ballast water spreads fast in the surface ocean, while the other half accumulates close to coastal areas around the discharge location with a relative abundance of 3 % to 4 % of DBPs per $1^\circ \times 1^\circ$ grid box. The currents determining the DBP spread in Southeast Asia are seasonally influenced by monsoon winds. In Singapore, the main driver of DBP transport throughout the year is the westward Indonesian throughflow, and most of the DBPs spread into the Strait of Malacca and the Indian Ocean. For the Pearl River Delta region, the majority of DBPs is transported southwestward during the northeast monsoon period in boreal winter and northeastward during the southwest monsoon period in boreal summer. Thus, non-volatile DBPs can either spread over large areas at the sea surface or accumulate in specific regions, such as the accumulation of DBPs from the Pearl River Delta in the Gulf of Tonkin. While interannual variations of the DBP spread are relatively small, the seasonal cycle in transport patterns leads to enhanced coastal accumulations depending on the region and time of year.

Based on our simulations in the FLUX analysis, we expect brominated VSLS concentrations and emissions to increase locally in regions with high industrial activity. Anthropogenic bromoform can locally add up to 23 pmol L^{-1} (0.006 µg L^{-1}) in the HIGH scenario around the port sites. Our simulations assume that DBPs are transported out of the harbour, thereby providing a lower boundary for environmental concentrations. Other studies like David et al. (2018), which use a port-based model approach to calculate the predicted environmental concentration, estimate higher bromoform values (e.g. 0.3 µg L^{-1}) due to the smaller areas considered and the missing air–sea exchange. Once ballast water treatment has been established globally, in situ measurements will be necessary to confirm if existing model-based results provide realistic estimates.

Our simulations reveal that bromoform emissions to the atmosphere can exceed 1000 pmol m^{-2} h^{-1} for the MODERATE scenario. This is caused by moderate to high wind speeds above 10 m s^{-1}, which occur especially in the Pearl River Delta. In this region the transfer velocity is sufficiently high so that all anthropogenic bromoform within the mixed layer is instantly outgassed into the atmosphere. Anthropogenic bromoform from ballast water discharge does not accumulate in the ocean but is rather an immediate additional input of Br to the atmosphere. This new source can locally double the climatological bromoform flux calculated from Ziska et al. (2013) around big harbours like Singapore, Shanghai and in the Pearl River Delta. Here, the bromoform emissions to the atmosphere are substantially larger than natural fluxes. For the HIGH scenario, emissions of up to 3500 pmol m^{-2} h^{-1} can occur, which is in the range of the highest natural emissions found in global shelf waters but does not exceed reported maximum values of 4450 pmol m^{-2} h^{-1} (Quack and Wallace, 2003). The area of Southeast Asia shown in Figure 10 gives a total Br input of 80 Mmol yr^{-1} for the Ziska et al. (2013) climatology, while anthropogenic bromoform leads to an additional 3 Mmol Br yr^{-1}.

Over the next decades, the impact of brominated VSLSs on climate and ozone depletion will increase due to changes in atmospheric transport and chemistry (Hossaini et al., 2015; Tegtmeier et al., 2015; Fernandez et al., 2017). Increasing VSLS production from anthropogenic activities needs to be investigated and monitored in order to quantify its input to atmospheric bromine. Measurements of VSLSs in coastal areas and ports can reveal the local impact of anthropogenic emissions. For some harbours, they can be even higher than our simulations suggest because our initialisation assumes a dilution of DBPs in the coastal ocean approximately 8 to 40 km off the coast. Moreover, anthropogenic sources like ballast water are always subject to economic fluctuations and trading policies and are thus likely to increase in the future. The choice of simulation scenarios covers a broad range of possible cases, and an increase of ballast water discharge ac-

cording to current economic growth of $\sim 2\,\%$ per year will not change the main results.

On a global scale the bromine emissions from ballast water treatment reach up to 13 Mmol Br a^{-1} in the HIGH scenario. Compared to current estimates of background emissions of 2 to 10 Gmol Br a^{-1} (see Ziska et al., 2013, and references therein) the anthropogenic bromine input is rather small, amounting to 0.1 %. Thus, we do not expect an impact of anthropogenic VSLSs from ballast water treatment on global atmospheric chemistry or the stratospheric ozone layer.

Ballast water, however, is not the only anthropogenic source of DBPs to the coastal oceans. DBPs are also produced through the oxidation of drinking water, wastewater, seawater in desalination plants and cooling water in power plants (e.g. Jenner et al., 1997; Werschkun et al., 2012). In contrast to drinking water for which by-products are strictly regulated (Richardson et al., 2007), the chemical treatment of seawater or brackish water containing high levels of inorganic bromine is not monitored regularly, although it can lead to much higher levels of brominated DBPs. Thus, it is of interest to investigate in future studies the combined effect of anthropogenic VSLSs from all types of oxidative water treatment on the environment.

Data availability. Data from the ARIANE simulations are available upon request from the corresponding author.

Supplement. The supplement related to this article is available online at: https://doi.org/10.5194/os-15-891-2019-supplement.

Author contributions. JM wrote the paper, performed the simulations and created the output. ST developed the research question and guided the research process. BQ helped in the formulation of the research question and analysed water samples. SG and MD provided water samples. AB and JVD provided the model data; SR and JVD set up the ARIANE environment and helped with the simulation. All authors took part in the process of paper preparation.

Competing interests. The authors declare that they have no conflict of interest.

Special issue statement. This article is part of the special issue "Shipping and the Environment – From Regional to Global Perspectives (ACP/OS inter-journal SI)". It is a result of the conference Shipping and the Environment – From Regional to Global Perspectives, Gothenburg, Sweden, 23–24 October 2017.

Acknowledgements. We thank Stephanie Delacroix for providing ship-based samples of ballast water. The authors would also like to thank Yue Jia for simulations of the atmospheric bromoform mixing ratios. Furthermore, we wish to thank Bruno Blanke and Nicolas Grima for realising and providing the Lagrangian software ARIANE. The OGCM and trajectory simulations were performed in the High-Performance Computing Centre at the Christian-Albrechts-Universität zu Kiel. The OGCM model data used for this study were kindly provided through collaboration within the DRAKKAR framework by the National Oceanographic Centre, Southampton, UK. We especially thank Andrew C. Coward, Adrian L. New and colleagues for making the data available. This study was carried out within the Emmy-Noether group AVeSH (A new threat to the stratospheric ozone layer from Anthropogenic Very Short-lived Halocarbons) funded by the Deutsche Forschungsgemeinschaft (DFG, German Research Foundation) – TE 1134/1. Siren Rühs received funding from the Cluster of Excellence 80 "The Future Ocean" within the framework of the Excellence Initiative by the Deutsche Forschungsgemeinschaft (DFG) on behalf of the German federal and state governments (grant CP1412). Finally, we thank the editor and two anonymous reviewers for their helpful comments to improve the paper.

Financial support. This research has been supported the Deutsche Forschungsgemeinschaft (DFG, German Research Foundation) – (grant no. TE 1134/1).

Review statement. This paper was edited by David Turner and reviewed by two anonymous referees.

References

AAPA: World Port Rankings 2016, Port Industry Statistics, Am. Assoc. Port Authorities, available at: http://www.aapa-ports.org/unifying/content.aspx?ItemNumber=21048, last access: 19 December 2018.

Aschmann, J., Sinnhuber, B. M., Atlas, E. L., and Schauffler, S. M.: Modeling the transport of very short-lived substances into the tropical upper troposphere and lower stratosphere, Atmos. Chem. Phys., 9, 9237–9247, https://doi.org/10.5194/acp-9-9237-2009, 2009.

Blanke, B., Arhan, M., Madec, G., and Roche, S.: Warm Water Paths in the Equatorial Atlantic as Diagnosed with a General Circulation Model, J. Phys. Oceanogr., 29, 2753–2768, 1999.

Briski, E., Ghabooli, S., Bailey, S. A., and MacIsaac, H. J.: Invasion risk posed by macroinvertebrates transported in ships' ballast tanks, Biol. Invasions, 14, 1843–1850, https://doi.org/10.1007/s10530-012-0194-0, 2012.

Carpenter, L. J., Reimann, S., (Lead Authors), Burkholder, J. B., Clerbaux, C., Hall, B. D., Hossaini, R., Laube, J. C., and Yvon-Lews, S. A.: Update on Ozone-Depleting Substances (ODSs) and Other Gases of Interest to the Montreal Protocol, Chapter 1 Sci. Assess. Ozone Deplet. 2014, (Global Ozone Research and Monitoring Project-Report No. 55), World Meteorological Organization, Geneva, Switzerland, 1.1–1.101, 2014.

David, M.: Vessels and Ballast Water, in: Glob. Marit. Transp. Ballast Water Manag., edited by: David, M. and Gollasch, S.,

Invading Nature-Springer Series, Invasion Ecology, 8, 13–34, https://doi.org/10.1007/978-94-017-9367-4_2, 2015.

David, M. and Gollasch, S.: Ballast Water Management Systems for Vessels, Glob. Marit. Transp. Ballast Water Manag., edited by: David, M. and Gollasch, S., Invading Nature-Springer Series, Invasion Ecology 8, 109–132, https://doi.org/10.1007/978-94-017-9367-4_6, 2015.

David, M., Linders, J., Gollasch, S., and David, J.: Is the aquatic environment sufficiently protected from chemicals discharged with treated ballast water from vessels worldwide? – A decadal environmental perspective and risk assessment, Chemosphere, 207, 590–600, https://doi.org/10.1016/j.chemosphere.2018.05.136, 2018.

Delacroix, S., Vogelsang, C., Tobiesen, A., and Liltved, H.: Disinfection by-products and ecotoxicity of ballast water after oxidative treatment – Results and experiences from seven years of full-scale testing of ballast water management systems, Mar. Pollut. Bull., 73, 24–36, 2013.

Dorf, M., Butler, J. H., Butz, A., Camy-Peyret, C., Chipperfield, M. P., Kritten, L., Montzka, S. A., Simmes, B., Weidner, F., and Pfeilsticker, K.: Long-term observations of stratospheric bromine reveal slow down in growth, Geophys. Res. Lett., 33, L24803, https://doi.org/10.1029/2006GL027714, 2006.

DRAKKAR Group: Eddy permitting ocean circulation hindcasts of past decades, CLIVAR Exchanges, 42, 8–10, 2007.

Durgadoo, J. V., Ruehs, S., Biastoch, A., and Boening, C. W. B.: Indian Ocean sources of Agulhas leakage, J. Geophys. Res.-Ocean., 122, 1–19, https://doi.org/10.1002/2016JC012676, 2017.

Dussin, R., Barnier, B., Brodeau, L., and Molines, J. M.: The Making Of the DRAKKAR FORCING SET DFS5, DRAKKAR/MyOcean Rep. 01-04-16, 1–34, 2016.

Endresen, Ø., Lee Behrens, H., Brynestad, S., Bjørn Andersen, A., and Skjong, R.: Challenges in global ballast water management, Mar. Pollut. Bull., 48, 615–623, https://doi.org/10.1016/j.marpolbul.2004.01.016, 2004.

Fernandez, R. P., Kinnison, D. E., Lamarque, J. F., Tilmes, S., and Saiz-Lopez, A.: Impact of biogenic very short-lived bromine on the Antarctic ozone hole during the 21st century, Atmos. Chem. Phys., 17, 1673–1688, https://doi.org/10.5194/acp-17-1673-2017, 2017.

Fuhlbrügge, S., Quack, B., Atlas, E., Fiehn, A., Hepach, H., and Krüger, K.: Meteorological constraints on oceanic halocarbons above the Peruvian upwelling, Atmos. Chem. Phys., 16, 12205–12217, https://doi.org/10.5194/acp-16-12205-2016, 2016.

Gordon, A. L.: Interocean Exchange, Interocean Exch. Int. Geophys. Ser., 77, 303–316, 2001.

Hense, I. and Quack, B.: Modelling the vertical distribution of bromoform in the upper water column of the tropical Atlantic Ocean, Biogeosciences, 6, 535–544, https://doi.org/10.5194/bg-6-535-2009, 2009.

Hossaini, R., Chipperfield, M. P., Dhomse, S., Ordóñez, C., Saiz-Lopez, A., Abraham, N. L., Archibald, A., Braesicke, P., Telford, P., Warwick, N., Yang, X., and Pyle, J.: Modelling future changes to the stratospheric source gas injection of biogenic bromocarbons, Geophys. Res. Lett., 39, GL053401, https://doi.org/10.1029/2012GL053401, 2012.

Hossaini, R., Chipperfield, M. P., Montzka, S. A., Rap, A., Dhomse, S., and Feng, W.: Efficiency of short-lived halogens at influencing climate through depletion of stratospheric ozone, Nat. Geosci., 8, 186–190, https://doi.org/10.1038/ngeo2363, 2015.

IMO: International Convention for the Control and Management of Ships' Ballast Water and Sediments, in: BWM/CONF/36, 1–38, 2004.

IMO: Methodology for information gathering and conduct of work of the GESAMMP-BWWG, BWM.2/Circ.13/Rev.4, 1–99, 2017.

IMO: List of ballast water management systems that make use of Active Substances which received Basic and Final Approval, BWM.2/Circ.34/Rev.7, 1–28, 2019.

Jenner, H. A., Taylor, C. J. L., van Donk, M., and Khalanski, M.: Chlorination by-products in chlorinated cooling water of some European coastal power stations, Mar. Environ. Res., 43, 279–293, https://doi.org/10.1016/S0141-1136(96)00091-8, 1997.

Liang, Q., Stolarski, R. S., Kawa, S. R., Nielsen, J. E., Douglass, A. R., Rodriguez, J. M., Blake, D. R., Atlas, E. L., and Ott, L. E.: Finding the missing stratospheric Bry: A global modeling study of $CHBr_3$ and CH_2Br_2, Atmos. Chem. Phys., 10, 2269–2286, https://doi.org/10.5194/acp-10-2269-2010, 2010.

Liu, Z., Wang, X., Luo, Z., Huo, M., Wu, J., Huo, H., and Yang, W.: Removing of disinfection by-product precursors from surface water by using magnetic graphene oxide, PLoS One, 10, e0143819, https://doi.org/10.1371/journal.pone.0143819, 2015.

Madec, G. and the NEMO team: NEMO ocean engine. Note du Pôle de modélisation, Institut Pierre-Simon Laplace (IPSL), France, No. 27, ISSN No. 1288–1619, 2008.

Maritime Impact: Treat Her Right, Issue 01, 18–19, https://issuu.com/dnvgl/docs/dnv_gl_maritime_impact_01-2017 (last access: 18 December 2018), 2017

Marzocchi, A., Hirschi, J. J. M., Holliday, N. P., Cunningham, S. A., Blaker, A. T., and Coward, A. C.: The North Atlantic subpolar circulation in an eddy-resolving global ocean model, J. Mar. Syst., 142, 126–143, https://doi.org/10.1016/j.jmarsys.2014.10.007, 2015.

Moore, R. M., Webb, M., Tokarczyk, R., and Wever, R.: Bromoperoxidase and iodoperoxidase enzymes and production of halogenated methanes in marine diatom cultures, J. Geophys. Res.-Ocean., 101, 20899–20908, https://doi.org/10.1029/96JC01248, 1996.

Nightingale, D., Malin, G., Law, C. S., Watson, A. J., Liss, P. S., Liddicoat, M. I., Boutin, J., and Upstill-Goddard, R. C.: In situ evaluation of air-sea gas exchange parameterizations using novel conservative and volatile tracers, Global Biogeochem. Cy., 14, 373–387, 2000.

Padhi, R. K., Subramanian, S., Mohanty, A. K., Bramha, S. N., Prasad, M. V. R., and Satpathy, K. K.: Trihalomethanes in the cooling discharge of a power plant on chlorination of intake seawater, Environ. Eng. Res., 17, 57–62, https://doi.org/10.4491/eer.2012.17.S1.S57, 2012.

Quack, B. and Wallace, D. W. R.: Air-sea flux of bromoform: Controls, rates, and implications, Global Biogeochem. Cy., 17, 1023, https://doi.org/10.1029/2002GB001890, 2003.

Richardson, S. D., Plewa, M. J., Wagner, E. D., Schoeny, R., and DeMarini, D. M.: Occurrence, genotoxicity, and carcinogenicity of regulated and emerging disinfection by-products in drinking water: A review and roadmap for research, Mutat. Res.-Rev. Mutat. Res., 636, 178–242, https://doi.org/10.1016/j.mrrev.2007.09.001, 2007.

Rühs, S., Schwarzkopf, F. U., Speich, S., and Biastoch, A.: Cold vs. warm water route – sources for the upper limb of the Atlantic Meridional Overturning Circulation revisited in a high-resolution ocean model, Ocean Sci., 15, 489–512, https://doi.org/10.5194/os-15-489-2019, 2019.

Ruiz, G. M., Rawlings, T. K., Dobbs, F. C., Drake, L. A., Mullady, T., Huq, A., and Colwell, R. R.: Global spread of microorganisms by ships, Nature, 408, 49–50, https://doi.org/10.1038/35040695, 2000.

Saiz-Lopez, A. and Von Glasow, R.: Reactive halogen chemistry in the troposphere, Chem. Soc. Rev., 41, 6448–6472, https://doi.org/10.1039/c2cs35208g, 2012.

Seebens, H., Gastner, M. T., and Blasius, B.: The risk of marine bioinvasion caused by global shipping, Ecol. Lett., 16, 782–790, https://doi.org/10.1111/ele.12111, 2013.

Shah, A. D., Liu, Z.-Q., Salhi, E., Höfer, T., Werschkun, B., and von Gunten, U.: Formation of disinfection by-products during ballast water treatment with ozone, chlorine, and peracetic acid: influence of water quality parameters, Environ. Sci. Water Res. Technol., 1, 465–480, https://doi.org/10.1039/C5EW00061K, 2015.

Shaw, P. T. and Chao, S. Y.: Surface circulation in the South China Sea, Deep-Sea Res. Pt. I, 41, 1663–1683, https://doi.org/10.1016/0967-0637(94)90067-1, 1994.

Sherwen, T., Schmidt, J. A., Evans, M. J., Carpenter, L. J., Großmann, K., Eastham, S. D., Jacob, D. J., Dix, B., Koenig, T. K., Sinreich, R., Ortega, I., Volkamer, R., Saiz-Lopez, A., Prados-Roman, C., Mahajan, A. S., and Ordóñez, C.: Global impacts of tropospheric halogens (Cl, Br, I) on oxidants and composition in GEOS-Chem, Atmos. Chem. Phys., 16, 12239–12271, https://doi.org/10.5194/acp-16-12239-2016, 2016.

Simpson, W. R., Brown, S. S., Saiz-Lopez, A., Thornton, J. A., and von Glasow, R.: Tropospheric Halogen Chemistry: Sources, Cycling, and Impacts, Chem. Rev., 115, 4035–4062, https://doi.org/10.1021/cr5006638, 2015.

Sinnhuber, B. M. and Meul, S.: Simulating the impact of emissions of brominated very short lived substances on past stratospheric ozone trends, Geophys. Res. Lett., 42, 2449–2456, https://doi.org/10.1002/2014GL062975, 2015.

Tamelander J., Riddering L., Haag F., and Matheickal J.: Guidelines for Development of National Ballast Water Management Strategies. GEF-UNDP-IMO GloBallast, London, UK and IUCN, Gland, Switzerland, GloBallast Monographs No. 18, 2010.

Tegtmeier, S., Ziska, F., Pisso, I., Quack, B., Velders, G. J. M., Yang, X., and Krüger, K.: Oceanic bromoform emissions weighted by their ozone depletion potential, Atmos. Chem. Phys., 15, 13647–13663, https://doi.org/10.5194/acp-15-13647-2015, 2015.

Theiler, R., Cook, J. C., Hager, L. P., and Siuda, J. F.: Halohydrocarbon synthesis by bromoperoxidase, Science, 202, 1094–1096, https://doi.org/10.1126/science.202.4372.1094, 1978.

UNCTAD: Review of Maritime Transport 2017, UN, New York, https://doi.org/10.18356/a9b345e7-en (last access: 4 July 2019), 2017.

Van Sebille, E., Scussolini, P., Durgadoo, J. V., Peeters, F. J. C., Biastoch, A., Weijer, W., Turney, C., Paris, C. B., and Zahn, R.: Ocean currents generate large footprints in marine palaeoclimate proxies, Nat. Commun., 6, 6521, https://doi.org/10.1038/ncomms7521, 2015.

Wales, P. A., Salawitch, R. J., Nicely, J. M., Anderson, D. C., Canty, T. P., Baidar, S., Dix, B., Koenig, T. K., Volkamer, R., Chen, D., Huey, L. G., Tanner, D. J., Cuevas, C. A., Fernandez, R. P., Kinnison, D. E., Lamarque, J. F., Saiz-Lopez, A., Atlas, E. L., Hall, S. R., Navarro, M. A., Pan, L. L., Schauffler, S. M., Stell, M., Tilmes, S., Ullmann, K., Weinheimer, A. J., Akiyoshi, H., Chipperfield, M. P., Deushi, M., Dhomse, S. S., Feng, W., Graf, P., Hossaini, R., Jöckel, P., Mancini, E., Michou, M., Morgenstern, O., Oman, L. D., Pitari, G., Plummer, D. A., Revell, L. E., Rozanov, E., Saint-Martin, D., Schofield, R., Stenke, A., Stone, K. A., Visioni, D., Yamashita, Y., and Zeng, G.: Stratospheric Injection of Brominated Very Short-Lived Substances: Aircraft Observations in the Western Pacific and Representation in Global Models, J. Geophys. Res.-Atmos., 123, 5690–5719, https://doi.org/10.1029/2017JD027978, 2018.

Warwick, N. J., Pyle, J. A., Carver, G. D., Yang, X., Savage, N. H., O'Connor, F. M., and Cox, R. A.: Global modeling of biogenic bromocarbons, J. Geophys. Res.-Atmos., 111, D24305, https://doi.org/10.1029/2006JD007264, 2006.

Werschkun, B., Sommer, Y., and Banerji, S.: Disinfection by-products in ballast water treatment: An evaluation of regulatory data, Water Res., 46, 4884–4901, https://doi.org/10.1016/j.watres.2012.05.034, 2012.

Werschkun, B., Banerji, S., Basurko, O. C., David, M., Fuhr, F., Gollasch, S., Grummt, T., Haarich, M., Jha, A. N., Kacan, S., Kehrer, A., Linders, J., Mesbahi, E., Pughiuc, D., Richardson, S. D., Schwarz-Schulz, B., Shah, A., Theobald, N., von Gunten, U., Wieck, S., and Höfer, T.: Emerging risks from ballast water treatment: The run-up to the International Ballast Water Management Convention, Chemosphere, 112, 256–266, https://doi.org/10.1016/j.chemosphere.2014.03.135, 2014.

Yang, X., Abraham, N. L., Archibald, A. T., Braesicke, P., Keeble, J., Telford, P. J., Warwick, N. J., and Pyle, J. A.: How sensitive is the recovery of stratospheric ozone to changes in concentrations of very short-lived bromocarbons?, Atmos. Chem. Phys., 14, 10431–10438, https://doi.org/10.5194/acp-14-10431-2014, 2014.

Ziska, F., Quack, B., Abrahamsson, K., Archer, S. D., Atlas, E., Bell, T., Butler, J. H., Carpenter, L. J., Jones, C. E., Harris, N. R. P., Hepach, H., Heumann, K. G., Hughes, C., Kuss, J., Krüger, K., Liss, P., Moore, R. M., Orlikowska, A., Raimund, S., Reeves, C. E., Reifenhäuser, W., Robinson, A. D., Schall, C., Tanhua, T., Tegtmeier, S., Turner, S., Wang, L., Wallace, D., Williams, J., Yamamoto, H., Yvon-Lewis, S., and Yokouchi, Y.: Global sea-to-air flux climatology for bromoform, dibromomethane and methyl iodide, Atmos. Chem. Phys., 13, 8915–8934, https://doi.org/10.5194/acp-13-8915-2013, 2013.

Supplement of Ocean Sci., 15, 891–904, 2019
https://doi.org/10.5194/os-15-891-2019-supplement

Ocean Science Open Access EGU

Supplement of

Simulating the spread of disinfection by-products and anthropogenic bromoform emissions from ballast water discharge in Southeast Asia

Josefine Maas et al.

Correspondence to: Josefine Maas (jmaas@geomar.de)

Supplement Table: Modified world port ranking and ballast water volumes derived from both the biggest 100 cargo and container ports with respect to annual throughput in 2016 (AAPA, 2016). Ballast water volume was calculated as 33 % of total goods loaded in 2016, which amounts to 3.4 billion m^3 and is divided among all ports listed. $CHBr_3$ is calculated for each scenario as the annual amount discharged from ballast water for different shares of chemical BWTS installed (70 % for MODERATE, 50 % for LOW and 90 % for HIGH).

				market volume	BW equivalent	$CHBr_3$ amount in kmol/a		
PORT	COUNTRY	Latitude	Longitude	share in %	in m^3/a	MODERATE	LOW	HIGH
Shanghai	China	31.230	121.474	5.11	173622371	108.7	29.0	227.2
Singapore	Singapore	1.352	103.820	4.59	155770045	97.5	26.0	203.8
Guangzhou	China	23.129	113.253	3.89	132210129	82.7	22.1	173.0
Ningbo	China	29.868	121.544	3.54	120107924	75.2	20.1	157.2
Qingdao	China	36.067	120.383	3.27	111095972	69.5	18.6	145.4
Rotterdam	Netherlands	51.924	4.478	3.20	108668142	68.0	18.1	142.2
Tianjin	China	39.084	117.201	3.06	103831507	65.0	17.3	135.9
Port Hedland	Australia	-20.312	118.575	2.95	100285267	62.8	16.7	131.2
Busan	South Korea	35.180	129.076	2.74	92914291	58.1	15.5	121.6
Dalian	China	38.914	121.615	2.25	76290834	47.7	12.7	99.8
Hong Kong	China	22.396	114.109	2.19	74275073	46.5	12.4	97.2
Shenzhen	China	22.543	114.063	1.91	64773732	40.5	10.8	84.8
Port Kelang	Malaysia	3.005	101.409	1.85	62817843	39.3	10.5	82.2
Kwangyang	South Korea	33.493	126.535	1.80	60997903	38.2	10.2	79.8
Xiamen	China	24.480	118.089	1.73	58747979	36.8	9.8	76.9
Antwerp	Belgium	51.219	4.402	1.62	55037257	34.4	9.2	72.0
Dubai Ports	United Arab Emirates	25.205	55.271	1.56	52796632	33.0	8.8	69.1
South Louisiana	United States	30.021	-90.471	1.45	49177886	30.8	8.2	64.4
Houston	United States	29.760	-95.370	1.44	48893230	30.6	8.2	64.0
Nagoya	Japan	35.181	136.906	1.26	42836935	26.8	7.2	56.1
Hamburg	Germany	53.551	9.994	1.12	38100756	23.8	6.4	49.9
Itaqui	Brazil	-2.578	-44.367	1.10	37239115	23.3	6.2	48.7
Qinhuangdao	China	39.929	119.620	1.10	37186541	23.3	6.2	48.7
Ulsan	South Korea	35.538	129.311	1.07	36297343	22.7	6.1	47.5
Inchon	South Korea	37.456	126.705	1.07	36245605	22.7	6.1	47.4

Kaohsiung	Taiwan	22.627	120.301	1.04	35302384	22.1	5.9	46.2
Chiba	Japan	35.607	140.106	1.04	35275262	22.1	5.9	46.2
Tanjung Pelepas	Malaysia	1.364	103.552	1.03	34876413	21.8	5.8	45.6
Newcastle	Australia	-32.927	151.779	1.02	34723238	21.7	5.8	45.4
Dampier	Australia	-20.664	116.708	1.02	34708749	21.7	5.8	45.4
Saigon	Viet Nam	10.750	106.742	0.98	33413647	20.9	5.6	43.7
New York/New Jersey	United States	40.713	-74.006	0.93	31718108	19.8	5.3	41.5
Metro Vancouver	Canada	49.197	-123.182	0.92	31179303	19.5	5.2	40.8
Tubarao	Brazil	-28.472	-49.015	0.82	27693686	17.3	4.6	36.2
Santos	Brazil	-23.968	-46.329	0.81	27360136	17.1	4.6	35.8
Algeciras - La Linea	Spain	36.141	-5.456	0.74	25149429	15.7	4.2	32.9
Gladstone	Australia	-23.852	151.264	0.73	24922393	15.6	4.2	32.6
Laem Chabang	Thailand	13.104	100.916	0.71	24144802	15.1	4.0	31.6
Kobe	Japan	34.690	135.196	0.69	23337570	14.6	3.9	30.5
Itaguai	Brazil	-22.863	-43.778	0.69	23262183	14.6	3.9	30.4
Pyeongtaek	South Korea	36.983	126.841	0.68	23226582	14.5	3.9	30.4
Tokyo	Japan	35.689	139.692	0.66	22325564	14.0	3.7	29.2
Hay Point	Australia	-21.306	149.292	0.65	22034361	13.8	3.7	28.8
Long Beach	United States	33.770	-118.194	0.64	21839071	13.7	3.6	28.6
Bremen/Bremerhaven	Germany	53.074	8.806	0.63	21445428	13.4	3.6	28.1
Los Angeles	United States	34.052	-118.244	0.62	21205994	13.3	3.5	27.8
Richards Bay	South Africa	-28.781	32.038	0.61	20578650	12.9	3.4	26.9
Kitakyushu	Japan	33.883	130.875	0.60	20393401	12.8	3.4	26.7
Valencia	Spain	39.470	-0.376	0.60	20266218	12.7	3.4	26.5
Amsterdam Ports	Netherlands	52.370	4.895	0.59	19877599	12.4	3.3	26.0
Ust-Luga	Russia	59.653	28.270	0.57	19324334	12.1	3.2	25.3
Osaka	Japan	34.694	135.502	0.56	19061373	11.9	3.2	24.9
Colombo	Sri Lanka	6.927	79.861	0.55	18724791	11.7	3.1	24.5
Chittagong	Bangladesh	22.348	91.812	0.54	18497631	11.6	3.1	24.2
Paradip	India	20.317	86.611	0.54	18411126	11.5	3.1	24.1

Bandar Abbas	Iran	27.183	56.267	0.54	18388178	11.5	3.1	24.1
Marseilles	France	43.296	5.370	0.53	18035493	11.3	3.0	23.6
Daesan	South Korea	36.940	126.434	0.52	17777758	11.1	3.0	23.3
Jawaharlal Nehru	India	18.950	72.951	0.52	17664711	11.1	3.0	23.1
Manila	Philippines	14.600	120.984	0.51	17363339	10.9	2.9	22.7
Taichung	Taiwan	24.148	120.674	0.51	17256258	10.8	2.9	22.6
New Orleans	United States	29.951	-90.072	0.50	16950597	10.6	2.8	22.2
Le Havre	France	49.494	0.108	0.48	16263062	10.2	2.7	21.3
Botas	Turkey	36.885	35.928	0.48	16236564	10.2	2.7	21.2
Novorossisk	Russia	44.715	37.762	0.47	15962518	10.0	2.7	20.9
Tanjung Priok	Indonesia	-6.132	106.871	0.47	15945438	10.0	2.7	20.9
Beaumont	United States	30.080	-94.127	0.47	15872245	9.9	2.7	20.8
Jeddah	Saudi Arabia	21.285	39.238	0.46	15511232	9.7	2.6	20.3
Corpus Christi	United States	27.801	-97.396	0.45	15393982	9.6	2.6	20.1
Yanbu	Saudi Arabia	24.023	38.190	0.41	13872405	8.7	2.3	18.2
Saldanha Bay	South Africa	-33.028	17.918	0.41	13769949	8.6	2.3	18.0
Baton Rouge	United States	30.458	-91.140	0.40	13707294	8.6	2.3	17.9
Jubail	Saudi Arabia	26.960	49.569	0.40	13681567	8.6	2.3	17.9
Izmit (Kocaeli)	Turkey	40.765	29.941	0.40	13660041	8.5	2.3	17.9
Primorsk	Russia	46.723	36.354	0.39	13335285	8.3	2.2	17.5
Bombay	India	19.076	72.878	0.38	13050063	8.2	2.2	17.1
Virginia	United States	36.912	-76.324	0.38	12981932	8.1	2.2	17.0
Karachi	Pakistan	24.861	67.010	0.38	12952244	8.1	2.2	16.9
Visakhapatnam	India	17.702	83.290	0.37	12696329	7.9	2.1	16.6
Alexandria and El-Dekheila	Egypt	31.200	29.919	0.37	12677791	7.9	2.1	16.6
Genoa	Italy	44.406	8.946	0.37	12615708	7.9	2.1	16.5
Constantza	Romania	44.160	28.635	0.36	12299957	7.7	2.1	16.1
Trieste	Italy	45.650	13.777	0.36	12261044	7.7	2.0	16.0
Barcelona	Spain	41.385	2.173	0.36	12160392	7.6	2.0	15.9
Chennai	India	13.084	80.290	0.36	12126121	7.6	2.0	15.9
St. Petersburg	Russia	59.934	30.335	0.35	11926082	7.5	2.0	15.6

London	United Kingdom	51.507	-0.128	0.35	11908807	7.5	2.0	15.6
Grimsby and Immingham	United Kingdom	53.567	-0.081	0.33	11260489	7.0	1.9	14.7
Sines	Portugal	37.957	-8.861	0.33	11230363	7.0	1.9	14.7
Mobile	United States	30.695	-88.040	0.32	10895508	6.8	1.8	14.3
Philadelphia	United States	39.813	-75.421	0.32	10856044	6.8	1.8	14.2
Pohang	South Korea	36.019	129.343	0.32	10770560	6.7	1.8	14.1
Plaquemines	United States	29.324	-89.474	0.31	10661975	6.7	1.8	14.0
Lake Charles	United States	30.227	-93.217	0.31	10523999	6.6	1.8	13.8
Calcutta	India	22.573	88.364	0.31	10414136	6.5	1.7	13.6
Aliaga	Turkey	38.800	26.971	0.31	10376051	6.5	1.7	13.6
Sao Sebastiao	Brazil	-23.806	-45.402	0.29	9744753	6.1	1.6	12.8
Dunkirk	France	51.034	2.377	0.28	9632362	6.0	1.6	12.6
Bintulu	Malaysia	3.171	113.042	0.28	9521005	6.0	1.6	12.5
Calais	France	50.951	1.859	0.27	9280698	5.8	1.5	12.1
Khor Fakkan	United Arab Emirates	25.337	56.343	0.15	5230532	3.3	0.9	6.8
Colon	Panama	9.335	-79.942	0.14	4593231	2.9	0.8	6.0
Gioia Tauro	Italy	38.426	15.899	0.12	4089343	2.6	0.7	5.4
Piraeus	Greece	37.943	23.647	0.12	3985329	2.5	0.7	5.2
Savannah	United States	32.084	-81.100	0.11	3887948	2.4	0.6	5.1
Felixstowe	United Kingdom	51.962	1.351	0.11	3877662	2.4	0.6	5.1
Northwest Seaport Alliance	United States	47.606	-122.332	0.11	3857258	2.4	0.6	5.0
Mina Raysu	Oman	16.970	53.981	0.10	3547086	2.2	0.6	4.6
East Port Said Port	Egypt	31.265	32.302	0.10	3417286	2.1	0.6	4.5
Marsaxlokk	Malta	35.840	14.545	0.10	3285001	2.1	0.5	4.3
Tanger	Morocco	35.759	-5.834	0.09	3162276	2.0	0.5	4.1
Keelung	Taiwan	25.128	121.739	0.09	3057715	1.9	0.5	4.0

Balboa	Panama	8.961	-79.563	0.09	3020852	1.9	0.5	4.0
Yokohama	Japan	35.444	139.638	0.09	2966353	1.9	0.5	3.9
Ambarli	Turkey	41.318	41.714	0.09	2965864	1.9	0.5	3.9
Durban	South Africa	-29.859	31.022	0.08	2795024	1.7	0.5	3.7
Melbourne	Australia	-37.814	144.963	0.08	2790294	1.7	0.5	3.7
Manzanillo	Mexico	20.333	-77.120	0.08	2751068	1.7	0.5	3.6
Dublin	Ireland	53.350	-6.260	0.08	2649232	1.7	0.4	3.5
Southampton	United Kingdom	50.910	-1.404	0.08	2623582	1.6	0.4	3.4
Oakland	United States	37.804	-122.271	0.07	2527916	1.6	0.4	3.3
Sydney Ports	Australia	-33.853	151.210	0.07	2521384	1.6	0.4	3.3
Cartagena	Colombia	10.391	-75.479	0.07	2454795	1.5	0.4	3.2
Callao	Peru	-12.051	-77.126	0.06	2192227	1.4	0.4	2.9
Charleston	United States	32.776	-79.931	0.06	2129613	1.3	0.4	2.8
Guayaquil	Ecuador	-2.171	-79.922	0.06	1943327	1.2	0.3	2.5
Dammam	Saudi Arabia	26.393	49.978	0.06	1908603	1.2	0.3	2.5
Kingston	Jamaica	44.231	-76.486	0.05	1672136	1.0	0.3	2.2
Gdansk	Poland	54.404	18.666	0.05	1663309	1.0	0.3	2.2
Bangkok	Thailand	13.756	100.502	0.05	1589441	1.0	0.3	2.1
La Spezia	Italy	44.102	9.824	0.05	1559103	1.0	0.3	2.0
Montreal	Canada	45.502	-73.567	0.05	1544253	1.0	0.3	2.0
Ashdod	Israel	31.804	34.655	0.05	1539463	1.0	0.3	2.0
Penang	Malaysia	5.415	100.330	0.05	1533109	1.0	0.3	2.0
Mersin	Turkey	36.812	34.641	0.04	1500337	0.9	0.3	2.0
Zeebrugge	Belgium	51.319	3.207	0.04	1492773	0.9	0.2	2.0
San Antonio	Chile	-33.593	-71.608	0.04	1373664	0.9	0.2	1.8
Haifa	Israel	32.794	34.990	0.04	1352627	0.8	0.2	1.8
San Juan	Puerto Rico	18.466	-66.106	0.04	1313309	0.8	0.2	1.7
Honolulu	United States	21.307	-157.858	0.04	1292949	0.8	0.2	1.7
Freeport	Bahamas	26.542	-78.646	0.04	1280151	0.8	0.2	1.7
Brisbane	Australia	-27.471	153.023	0.04	1262858	0.8	0.2	1.7
Limon-Moin	Costa Rica	9.991	-83.042	0.04	1256014	0.8	0.2	1.6
Belawan	Indonesia	3.784	98.694	0.04	1248633	0.8	0.2	1.6

4 Simulations of anthropogenic bromoform reveal high emissions at the coast of East Asia

Under review for: *Atmospheric Chemistry and Physics Discussions*

Josefine Maas[1], Yue Jia[1], Birgit Quack[1], Jonathan V. Durgadoo[1], Arne Biastoch[1,2] and Susann Tegtmeier[1,3]

This manuscript deals with bottom-up estimates of bromoform emissions which appear to under-represent the industrial sources of bromoform from East Asia. By means of Lagrangian analyses with the ARIANE software, the distribution in ocean and atmosphere of bromoform produced from power plant cooling water treatment in East-Southeast Asia is estimated and compared to observations. Based on the air-sea flux calculations, FLEXPART simulations provide atmospheric abundances of anthropogenic bromoform and are compared to simulations based on climatological bottom-up emission estimates. Anthropogenic bromoform emissions play a role in the marine boundary layer during both boreal summer and winter. Only during winter, the high mixing ratios from the northern hemisphere subtropics are advected equatorwards and can be transported into the upper troposphere/lower stratosphere. Bromoform from cooling water treatment in East Asia is a significant source of atmospheric bromine which is a missing factor in global bottom-up flux estimates of organic bromine. Because 90 % of this anthropogenic bromoform is discharged north of 20° N, only a small fraction reaches the stratosphere.

[1]GEOMAR Helmholtz Centre for Ocean Research Kiel, Kiel, Germany
[2]Christian-Albrechts-Universität zu Kiel, Kiel, Germany
[3]now at: Institute of Space and Atmospheric Studies, University of Saskatchewan, Saskatoon, Canada

https://doi.org/10.5194/acp-2019-1004
Preprint. Discussion started: 27 January 2020

Atmospheric Chemistry and Physics Discussions

Simulations of anthropogenic bromoform indicate high emissions at the coast of East Asia

Josefine Maas[1], Yue Jia[1], Birgit Quack[1], Jonathan V. Durgadoo[1], Arne Biastoch[1,2] and Susann Tegtmeier[1,*]

[1]GEOMAR Helmholtz Centre for Ocean Research Kiel, Kiel, Germany
[2]Kiel University, Kiel, Germany
*now at: Institute of Space and Atmospheric Studies, University of Saskatchewan, Saskatoon, Canada

Correspondence to: Josefine Maas (jmaas@geomar.de)

Abstract. Bromoform is the major by-product from chlorination of cooling water in coastal power plants. Power plants in East and Southeast Asian economies have increased rapidly exceeding global growth. Bottom-up estimates of bromoform emissions based on few measurements appear to under-represent the industrial sources of bromoform from East Asia. By means of Lagrangian analyses, we assess the amount of bromoform produced from power plant cooling water treatment in East and Southeast Asia. The spread of bromoform is simulated as passive particles that are advected using the 3-dimensional velocity fields from the high-resolution NEMO-ORCA0083 ocean general circulation model. Simulations are run for three scenarios with varying initial bromoform concentrations given by the range of measurements of bromoform in cooling water discharge. From comparison of our model results to observations, we expect initial bromoform concentrations between 20–60 µg L^{-1} used for the two lower scenarios, to be most realistic. From these two scenarios, we find elevated bromoform along the coastlines of East Asia with average concentrations of 23 and 68 pmol L^{-1} and maximum values in the Yellow, Japan and East China Seas. The industrially-produced bromoform is quickly emitted into the atmosphere with average air-sea flux of 3.1 and 9.1 nmol m^{-2} h^{-1}, respectively. Based on the emission estimates, atmospheric abundances of anthropogenic bromoform are derived from FLEXPART simulations and compared to simulations based on climatological bottom-up emission estimates. In the marine boundary layer of East Asia, anthropogenic bromoform amounts up to 0.5–1.6 ppt during boreal summer and is thus 2–7 times larger compared to the bottom-up estimates. During boreal winter some part of the anthropogenic bromoform is transported by the northeasterly winter monsoon towards the tropical regions, whereas during boreal summer anthropogenic bromoform is confined to the northern hemisphere subtropics. Convective events in the tropics entrain an additional 0.03 ppt of anthropogenic bromoform into the upper troposphere/lower stratosphere. We find that bromoform from cooling water treatment in East Asia is a significant source of atmospheric bromine responsible for annual emissions of 100–300 Mmol Br, which might be a missing factor in global flux estimates of organic bromine. About 90 % of this anthropogenic bromoform is discharged north of 20° N, while in the tropics natural sources dominate and only a small fraction of the anthropogenic bromoform reaches the stratosphere.

https://doi.org/10.5194/acp-2019-1004
Preprint. Discussion started: 27 January 2020

Atmospheric Chemistry and Physics Discussions

1 Introduction

Power plants require cooling water to regulate the temperature in the system. As their demand for cooling water is very high, power plants are often located at the coast to profit from an unlimited water supply. Seawater, however, needs to be disinfected to prevent biofouling and to control pathogens in effluents. The usual disinfection method, chlorination, is known to generate a broad suite of disinfection by-products (DBPs) including trihalomethanes, halogenated acetic acids and bromate (e.g. Helz et al., 1984; Jenner et al., 1997). DBPs develop when hypochlorous acid and organic matter react with the bromide and chloride ions contained in sea water (Allonier et al., 1999). Discharge of DBPs with the cooling water effluent can be harmful to the local ecosystem in combination with temperature and pressure gradients (Taylor, 2006). The composition and amount of generated DBPs depend on many factors including the type and concentration of the injected oxidant and the chemical characteristics of the treated water such as salinity, temperature and amount of dissolved organic matter (Liu et al., 2015). Cooling water effluents regularly discharge large volumes of water into the marine environment. This water is often warmer than the surrounding waters and decreases density at the sea surface. Chemicals such as DBPs contained in cooling water are likely to spread lateral across the sea surface which facilitates air-sea gas exchange for volatile DBPs.

One of the major DBPs is bromoform ($CHBr_3$), a halogenated volatile organic compound. Bromoform is also naturally produced in the ocean by macroalgae and phytoplankton and is the largest source of organic bromine to the atmosphere (Quack and Wallace, 2003). With an atmospheric lifetime of about 2–3 weeks, it belongs to the so-called very short-lived substances (VSLSs) (Engel and Rigby, 2018). Once bromoform is photolysed in the atmosphere, it can deplete ozone by catalytic cycles (Saiz-Lopez and von Glasow, 2012) or change the oxidising capacity of the atmosphere by shifting HO_x ratios towards OH (Sherwen et al., 2016). In the tropics, VSLSs such as bromoform can be entrained into the stratosphere through deep convection (e.g. Aschmann et al., 2009; Tegtmeier et al., 2015) and contribute to stratospheric ozone depletion (Hossaini et al., 2015). While the atmospheric abundance of chlorine and bromine species has started to decline as a result of the Montreal Protocol (Engel and Rigby, 2018), renewed productions and emissions of some long-lived ozone depleting substances (ODSs) have recently been discovered. The decline of CFC-11 has slowed unexpectedly, likely due to increasing emissions in eastern Asia (Montzka et al., 2018; Rigby et al., 2019). Atmospheric observations of carbon tetrachloride (CCl_4) also suggest ongoing anthropogenic emissions from feedstock and non-feedstock sources (Sherry et al., 2018). In contrast to the long-lived ODSs, emissions of halogenated VSLSs are not regulated by the Montreal Protocol, and their industrial contributions are not monitored. Current estimates of bromoform emissions suggest a global contribution to atmospheric bromine (Br) of 0.5–3.3 Gmol Br a^{-1} (Engel and Rigby, 2018). A bottom-up approach by Ziska et al. (2013) estimates 1.5 Gmol Br a^{-1}. Their analysis is based on the HalOcAt (Halocarbons in the Ocean and Atmosphere) database (https://halocat.geomar.de/) which contains VSLSs data in surface ocean and atmosphere from measurement campaigns. Based on physical and biogeochemical characteristics of the ocean and atmosphere, the data are classified into 21 regions and extrapolated to a regular grid within each region. Top-down bromoform emission estimates, on the other hand, are based on global model simulations adjusted to match available aircraft observations. They are in general, a factor of two larger than bottom-up emission estimates. Individual ship cruises, aircraft

https://doi.org/10.5194/acp-2019-1004
Preprint. Discussion started: 27 January 2020


Atmospheric Chemistry and Physics Discussions

campaigns and modelling studies have demonstrated a large spatio-temporal variability of bromoform in surface water and air (e.g. Fiehn et al., 2017; Fuhlbrügge et al., 2016; Jia et al., 2019). These pronounced variations combined with the poor temporal and spatial data coverage is a major challenge for deriving reliable emission estimates and may explain the large deviations between bottom-up and top-down estimates. Geographical regions with poor data coverage might not be well represented in the global emission scenarios. Furthermore, the anthropogenic input of bromoform might be under-estimated for large industrial regions (Boudjellaba et al., 2016).

Industrially produced bromoform will spread in the marine environment once the treated water is released and will be emitted into the atmosphere together with naturally produced bromoform. Atmospheric and oceanic measurements cannot distinguish between naturally and industrially produced bromoform and all top-down and bottom-up emission estimates discussed above automatically include the latter. A first comparison of natural and industrial bromoform sources from Quack and Wallace (2003) concluded a negligible global contribution of 3 % man-made bromoform. Their estimate was based on measurements of bromoform in disinfected water (80 nmol L^{-1}) from European power plants and cooling water use and projections of the global electricity production. In the meantime, the global electricity production has increased by almost 50 % from 16700 TWh in 2003 (IEA, 2005) to 25000 TWh in 2016 (IEA, 2018). Furthermore, new measurements of bromoform in disinfected cooling water have become available suggesting potentially higher concentrations of up to 500 nmol L^{-1} (Yang, 2001). Especially emerging economies in East Asia, such as China have experienced a massive growth over the last years exceeding the global economic growth. As the existing estimate of industrially produced bromoform is outdated, updated estimates taking into account new measurements are required to assess the impact of anthropogenic activities on the production and release of brominated VSLSs as well as their contribution to stratospheric ozone depletion.

We aim to quantify anthropogenic contributions to VSLSs, in form of bromoform emitted from regional industrial activities. As 50 % of global coastal cooling water is produced in East and Southeast Asia, we define these areas as our study region. We identify locations of high industrial activity along the coast of East and Southeast Asia and derive estimates of released cooling water and therein contained bromoform (Section 2). Based on Lagrangian simulations in the ocean, we derive the general marine distribution of non-volatile DBPs released with cooling water. For the case study of bromoform, we show oceanic distribution of the volatile DBP by taking air-sea exchange into account (Section 3). Based on the oceanic emissions, the atmospheric distribution of bromoform generated in industrial cooling water is simulated with a Lagrangian particle dispersion model (Section 4). Results are compared to existing observational atmospheric and oceanic distributions (Section 5). Methods are described in Section 2, while discussion and summary are provided in Section 6.

https://doi.org/10.5194/acp-2019-1004
Preprint. Discussion started: 27 January 2020

Atmospheric Chemistry and Physics Discussions

2 Methods

2.1 DBP production in cooling water from global power plants

In this study, we investigate the oceanic distribution of DBPs produced in power plants that chlorinate seawater. We assume that all power plants located at the coast use seawater for cooling purposes. Most of the seawater is only used once in the system as the ocean provides unlimited water supply. For the estimation of the cooling water volumes, we use the global power plant database Enipedia (enipedia.tudelft.nl, last access: 2017) where over 21,000 power plants are given together with location, electricity generation (in MWh) and sometimes fuel type. Based on the coordinates, we choose those power plants that are located less than 0.02 degrees (maximum 2 km at the equator) away from any coastline and refer to them as coastal. Based on this classification, 23 % of energy capacity from listed power plants in the database is generated by coastal power plants. The Key World Energy Statistics (IEA, 2018) give a total global electricity production of 24973 TWh in 2016. The average water use per MWh energy was given by Taylor (2006) to be 144 m^3 MWh^{-1} which leads to a global cooling water discharge of about 800 billion m^3 a^{-1} along the coast in 2016. For the individual coastal power plants in East and Southeast Asia, annual cooling water volumes are shown in Figure 1.

To determine the amount of bromoform produced in the cooling water, there are only a few measurements available and the locations are limited (Table 1). Most data originate from several power plants in Europe (Allonier et al., 1999; Boudjellaba et al., 2016; Jenner et al., 1997) and some studies are based on measurements from single power plants in Asia (Padhi et al., 2012; Rajamohan et al., 2007; Yang, 2001). Furthermore, the location where water is sampled is not consistent among the different studies. Some samples were taken in the coastal surface water at the power plant outlet (Fogelqvist and Krysell, 1991; Yang, 2001), while other studies sampled directly inside the power plant before dilution with the ocean (Jenner et al., 1997; Rajamohan et al., 2007). The measurements show a very large variability ranging from 8–290 µg L^{-1}. As there is no systematic difference between measurements inside the power plant and at the power plant outlet, both types of measurements are given in Table 1 together in column 1.

In addition to the sampling location, differences in the concentrations can result from water temperature, salinity and dissolved organic carbon content, which are seasonally dependent. Colder water from mid- to high latitudes during winter requires less water treatment as the settlement of pathogens takes longer compared to tropical or subtropical waters. The chlorination dosage and frequency of treatment also play a distinct role for the resulting DBP concentrations (Joint Research Council, 2001).

Given that available measurements are sparse and depend on many factors, the uncertainties in initial bromoform concentrations in cooling water are relatively high. For our analyses we chose to scale the bromoform discharge according to three scenarios (LOW, MODERATE and HIGH), which reflect the range of values given in available literature (Table 1). For our simulations, we use initial bromoform concentrations of 20 µg L^{-1} (LOW), 60 µg L^{-1} (MODERATE) and 100 µg L^{-1} (HIGH) in undiluted cooling water.

https://doi.org/10.5194/acp-2019-1004
Preprint. Discussion started: 27 January 2020

Atmospheric Chemistry and Physics Discussions

2.2 Lagrangian simulations in the ocean

For the assessment of the long-term, large-scale effect of DBPs from power plant cooling water on the environment, we simulate the distribution of non-volatile DBPs and the concentration and emission of the volatile DBP bromoform in the ocean. The Lagrangian model runs are based on velocity output from the high-resolution, eddy-rich ocean general circulation model (OGCM) NEMO-ORCA version 3.6 (Madec, 2008). The ORCA0083 configuration (The DRAKKAR Group, 2007) has a horizontal resolution of 1/12 degrees at 75 vertical levels and output is given at a temporal resolution of five days for the time period 1963–2012. Atmospheric forcing comes from the DFS5.2 data set (Dussin et al., 2016). The experiment ORCA0083-N06 used in this study was run by the National Oceanography Centre, Southampton, UK. Further details can be found in Moat et al. (2016).

We simulate the spread of the DBPs from treated cooling water, by applying a Lagrangian trajectory integration scheme to the 3D velocity fields with the ARIANE software (Blanke et al., 1999). We perform offline trajectory calculations by passively advecting virtual particles which represent the DBP amount discharged with the cooling water. The calculation of trajectories is purely advective without diffusivity. For each scenario we perform one simulation over the same time period. In each simulation, particles are continuously released close to the power plant locations at 5-day time steps over two years. We allow for an accumulation period of 11 months and show the results of the seasonal and annual mean of the second year starting in December. A detailed description of the applied method can be found in Maas et al., (2019) where it is also shown that interannual variability of surface velocity in the study region is small compared to seasonal variability.

Our study focusses on the region of East and Southeast Asia (90° E–165° E, 10° S–45° N), which comprises 50 % of the global coastal power plant capacity and cooling water discharge. The particle discharge locations have been chosen as close to the coastlines as possible (Figure 2). Particles are released approximately 8 to 40 km offshore, as the model-resolution does not allow to capture smaller-scale coastal structures such as harbours or estuaries nor does it simulate the near-costal exchange, e.g. through tides. Our approach ensures minimal influence of the land boundaries on the simulation in order to avoid numerically-related beaching of particles into the coastal boundary.

For the analysis of the experiments we distinguish 1) the passive spread of DBPs without any environmental sinks, and 2) the spread of bromoform as a major volatile DBP accounting for atmospheric fluxes and oceanic sinks. For the passive spread of non-volatile DBPs, we consider the full history of simulated particle positions which is equivalent to assuming no particles getting lost through sinks in the ocean or emission into the atmosphere. The resulting distribution shows locations where non-volatile DBPs such as bromoacetic acid are transported through the ocean currents within one year. For the spread of anthropogenic bromoform, each particle is assigned an initial mass of bromoform according to the amount of cooling water used by the respective power plant (Figure 1) and the bromoform concentration prescribed by the three scenarios, MODERATE,

https://doi.org/10.5194/acp-2019-1004
Preprint. Discussion started: 27 January 2020

HIGH and LOW. The particle density distribution is calculated at the sea surface down to 20 m on a 1°×1° grid. The distribution is given as particle density per grid box in percent for non-volatile DBPs and as concentration in pmol L^{-1} for bromoform.

Sink processes of bromoform such as constant gas exchange at the air-sea interface or chemical loss rates are taken into account. The air-sea flux of bromoform is calculated after the general flux equation at the air-sea interface:

$$Flux = (C_w - C_{eq}) \cdot k \quad (1)$$

Here Flux is positive when it is directed from the ocean to the atmosphere and is given in pmol m^{-2} h^{-1}. C_w is the actual concentration in the surface mixed layer in pmol L^{-1} and C_{eq} is the theoretical equilibrium concentration at the sea surface (in pmol L^{-1}) calculated from the atmospheric mixing ratio (in ppt), sea surface temperature and sea surface salinity (Quack and Wallace, 2003). The gas transfer velocity k (in cm h^{-1}) mainly depends on the surface wind speed and temperature and is calculated after Nightingale et al., (2000). Wind velocities at 10 m height are taken from the NEMO-ORCA forcing data set DFS5.2 (Dussin et al., 2016) which is based on the ERA-interim atmospheric data product.

As the oceanic and atmospheric terms in the air-sea flux parameterisation are of additive nature, it is possible to calculate the flux of anthropogenic and natural bromoform separately. For our simulations, we only consider bromoform from cooling water and apply the air-sea flux parameterisation to the anthropogenic portion of bromoform in water and air. We have conducted sensitivity tests (see section 2.3) to estimate the impact of atmospheric bromoform abundances on the flux calculations. The tests show that outgassed anthropogenic bromoform leads to atmospheric surface values C_{eq}, which are always below 8 % of the underlying sea surface concentration C_w (at a water temperature of 20°C). Such low equilibrium concentrations can be considered negligible for the flux calculation and therefore C_{eq} is set to zero in our study.

The sea surface concentration and air-sea flux from the three simulations are also compared to climatological maps of bromoform concentration and emissions from the updated Ziska et al. (2013) inventory (hereafter referred to as Ziska2013) (Fiehn et al., 2018).

Mean concentrations are calculated by averaging over the area where 90 % of bromoform, characterised by the highest local concentrations, accumulate. Maximum concentrations are calculated by averaging over the area where 10 % of the highest bromoform values accumulate. Mean and maximum fluxes are calculated based on the same principle. The annual mean atmospheric bromine input from industrial bromoform emissions in East and Southeast Asia is derived from the air-sea flux maps of the whole domain.

2.3 Lagrangian simulation in the atmosphere

Based on the seasonal mean emission maps, we obtain a source function of atmospheric bromoform. We simulate the atmospheric transport and distribution of bromoform for the three scenarios with the Lagrangian particle dispersion model FLEXPART

https://doi.org/10.5194/acp-2019-1004
Preprint. Discussion started: 27 January 2020

(Stohl et al., 2005). Bromoform emissions derived from the three scenarios are used as input data at the air-sea interface over the East and Southeast Asia area defined as our study region. The meteorological input data (temperature, wind) stem from the ERA-Interim reanalysis (Dee et al., 2011) and are given on a 1°×1° horizontal grid, at 61 vertical model levels and a 3-hourly temporal resolution. The chemical decay of bromoform in the atmosphere was accounted for by prescribing a half-life of 17 days during all runs (Montzka and Reimann, 2010). Output mixing ratios are given at the same horizontal resolution and 33 vertical levels from 50 to 20000 m. Detailed descriptions of model settings are described in Jia et al. (2019). The FLEXPART simulations were performed for the boreal winter (December–February, DJF) and summer (June–August, JJA) seasons, respectively, for a total of three months with a one-month spin-up.

We perform three additional FLEXPART runs based on the updated Ziska2013 emission inventory with the same FLEXPART configuration as described above for both seasons, DJF and JJA. As the Ziska2013 inventory currently presents our best knowledge of bottom-up derived bromoform emissions, it is of interest to analyse how much of these emissions can be explained by industrial sources and how much stems from natural sources.

The first run uses only the Ziska2013 emissions over the East and Southeast Asia area defined as our study region. This run is named Ziska2013-EastAsia and is used to compare the resulting mixing ratios in the atmospheric boundary layer to results driven by our anthropogenic emissions in the East and Southeast Asia region.

For comparisons of mixing ratios in the free troposphere and upper troposphere/lower stratosphere (UTLS) approximately above 17 km, emissions from other parts of the tropics also need to be taken into account as the time scales for horizontal transport are often shorter than the ones for vertical transport. Therefore, we set up two additional runs using the Ziska2013 emissions for the global tropics and subtropics between 45° S and 45° N. This configuration is used as input for the first of the two runs, which is named Ziska2013-Tropics.

As the Ziska2013 emissions are based on extrapolation of very few northern hemispheric coastal data, it likely neglects anthropogenic emissions in some regions. Therefore, the second run, Ziska2013-Mixed, uses the same Ziska2013 emissions between 45° S and 45° N, except for the East and Southeast Asia region. Here, the Ziska2013 emissions are replaced by the MODERATE emission values for every grid box where the MODERATE emissions are larger than Ziska2013. These two runs, Ziska2013-Mixed and Ziska2013-Tropics, are used to compare additional anthropogenic bromoform based on the MODERATE scenario to bromoform based on the Ziska2013 climatology for the UTLS region.

Mean mixing ratios from the whole domain in the marine boundary layer and in the UTLS are given as the average over the 90 % area characterised by the highest local values, and maximum mixing ratios as the average over the largest 10 % (see Section 2.2). In a second step, we identify two regions in order to analyse the vertical transport of bromoform into the free troposphere and into the UTLS. For the height profiles of the Ziska-Tropics and the Ziska-Mixed runs, we average mixing ratios over a region

https://doi.org/10.5194/acp-2019-1004
Preprint. Discussion started: 27 January 2020

Atmospheric Chemistry and Physics Discussions

above the maritime continent which we refer to as the tropical box (10° S–20° N, 90° E–120° E), and another region from China to Japan which we refer to as the subtropical box (30° N–40° N, 120° E–145° E) (Figure 2).

3 Oceanic spread of DBPs and bromoform

The particle density distribution shows the annual mean DBP accumulation pattern in the research area of interest (Figure 3). Non-volatile DBPs from cooling water usually accumulate around the coast and in the marginal seas. There is a clear latitudinal gradient with only little DBP distribution south of 20° N, except for higher values in the Strait of Malacca. In contrast to the relatively low DBP density in the inner tropics, the subtropics show a very high accumulation of DPBs with a centre in the marginal seas between 25° N and 40° N. While power plants can be found along all coastlines (Figure 1), the power plant capacity and therefore the amount of treated cooling water is much higher along the subtropical coasts of China, Korea and Japan leading to the DBP distribution pattern shown in Figure 3. Hot spots are around the coast of Shanghai and Incheon with a DBP density of 1 %. A relatively high DBP density of 0.8 % can also be found in the East China Sea, the Yellow Sea, the southern Japan Sea, the Gulf of Tonkin and the Strait of Malacca. Medium to low DBP density in the South China Sea suggest only small contributions of cooling waters to this region. Since Japan and Korea have a large number of power plants with high volumes of cooling water discharge, a relatively large amount of DBPs is transported with the Kuroshio Current into the North Pacific.

The distribution of bromoform, as a volatile DBPs in the surface ocean differs from the DBP accumulation pattern shown in Figure 3, as the volatile DBPs are outgassed into the atmosphere. The annual mean sea surface concentration of bromoform from cooling water is shown in Figure 4 (panel a-c) for the three scenarios LOW, MODERATE and HIGH and with a substantially smaller spread compared to non-volatile DBPs. The area which contains the 90 % highest bromoform concentrations does not vary between the three scenarios, as the air-sea flux, which determines how much bromoform remains in the water, is linearly proportional to the sea surface concentration. Higher surface concentrations result in higher fluxes into the atmosphere, which limits the spread of bromoform substantially compared to non-volatile DBPs. Bromoform concentrations are around 23, 68, and 113 pmol L^{-1} (LOW, MODERATE and HIGH) averaged over the region where the 90 % of bromoform with the highest concentrations accumulate (Table 2). This region is to a large degree limited to latitudes north of 20° N as a result of the power plant distribution. As in the case of the non-volatile DBPs, most of the bromoform is centred along the Chinese, Korean and Japanese coast line with a larger spread into the marginal seas for the latter two. One exception to this latitudinal gradient is the Strait of Malacca where local power plants result in average bromoform concentrations of 3.4, 10.3 and 16.7 pmol L^{-1} (LOW, MODERATE, and HIGH).

Observational based oceanic bromoform concentrations from Ziska2013 (Figure 4, panel d) are relatively evenly spread along the coastlines of the region and do not show the latitudinal gradient found for the anthropogenic concentrations. North of 20° N the anthropogenic bromoform is much higher than the oceanic distribution from Ziska2013, where the maximum lies around 21 pmol L^{-1}. Our simulations reach maximum values (averaged over the 10 % highest bromoform concentrations) of 112, 338

https://doi.org/10.5194/acp-2019-1004
Preprint. Discussion started: 27 January 2020

Atmospheric Chemistry and Physics Discussions

and up to 563 pmol L^{-1} (LOW, MODERATE and HIGH, Table 2) in the Japan Sea. These concentrations are all above 100 pmol L^{-1} and are very high compared to observational values from Ziska2013 (Figure 4, panel d).

Emissions of anthropogenic bromoform show a similar distribution as the oceanic concentrations (Figure 5, panel a-c). Flux rates averaged over the region of the 90 % highest flux values are 3, 9 and 15 nmol m^{-2} h^{-1} (LOW, MODERATE and HIGH). Maximum flux rates (averaged over the highest 10 %) even reach 13, 41 and 68 nmol m^{-2} h^{-1} in the Japan Sea near the Korean and Japanese coast for the three scenarios (Table 2). In contrast, the existing observational based estimates from the Ziska2013 climatology peak with 1.1 nmol m^{-2} h^{-1} located in the South China Sea along the west coast of the Philippines (Figure 5, panel d).

The annual bromine input from bromoform into the atmosphere in the East and Southeast Asia region is 118 Mmol according to the observation-based inventories from Ziska2013 (Table 2). Our simulations suggest that the anthropogenic input alone amounts to 100, 300 and 500 Mmol Br a^{-1} (LOW, MODERATE, HIGH) for the same region, which is almost 99 % of the bromine produced as bromoform during cooling water treatment in the power plant. While average and maximum emissions are much higher for anthropogenic bromoform as discussed above, the Ziska emissions spread out over a larger area thus resulting in similar total emissions as the LOW scenario. 90 % of the atmospheric bromine input from anthropogenic bromoform occurs north of 20° N where 89–447 Mmol Br are released over one year, compared to the regions south of 20° N where only 10–52 Mmol Br a^{-1} enter the atmosphere (from LOW to HIGH). In contrast, only 29 % of bromine is released into the atmosphere north of 20° N for the Ziska2013 climatology.

4 Anthropogenic bromoform in the atmosphere

4.1 Mixing ratios in the marine boundary layer

Atmospheric mixing ratios of anthropogenic bromoform are derived from FLEXPART runs driven by the seasonal emission estimates discussed in section 3. Atmospheric bromoform from industrial emissions is shown for a 5-day average at 50 m height for JJA for all three scenarios (Figure 6, panel a-c). Mean mixing ratios are 0.5, 1.6 and 2.4 ppt (LOW, MODERATE, HIGH, Table 2). Overall, high atmospheric mixing ratios are found around the coastlines of Japan, South Korea and northern China. Although maximum emissions are located in the Japan Sea, maximum mixing ratios are mostly located south of Japan with values up to 4.6, 13.9 and 23.3 ppt (LOW, MODERATE, HIGH, Table 2). Here, the westerlies lead to bromoform transport from the Japan Sea into the Northwest Pacific. We also localise hot spots of strong anthropogenic bromoform accumulations due to enhanced emissions over Shanghai, Singapore or the Pearl River Delta, respectively (Figure 6, panel a). During boreal summer, the West Pacific and Maritime Continent are influenced by southwesterly winds and the anthropogenic bromoform experiences northward transport, bringing some smaller portion of the subtropical emissions into the mid-latitudes (Figure 6, panel a, b and c).

https://doi.org/10.5194/acp-2019-1004
Preprint. Discussion started: 27 January 2020


Atmospheric Chemistry and Physics Discussions

During boreal winter (DJF, Figure 7, panel a-c), anthropogenic bromoform shows somewhat lower atmospheric mixing ratios with a mean of 0.3, 0.9 and 1.5 ppt and maximum values of 3.2, 9.5 and 15.9 ppt for the three scenarios (Table 2). In contrast to boreal summer, the atmospheric transport is dominated by winds from the northeast and higher bromoform values are confined to tropical and subtropical regions (Figure 7). Thus, tropical mixing ratios show a clear seasonal variability and are on average over 3 times higher for DJF than for JJA without large shifts in the location of the bromoform emissions (Figure S1).

In order to compare the atmospheric impact of industrial emissions with existing results, we repeat our analysis for the bottom-up emissions scenario Ziska2013 for the same region, which has been frequently used in past studies (e.g. Hossaini et al., 2013, 2016). Atmospheric mixing ratios are derived from seasonal FLEXPART runs driven by Ziska2013-EastAsia and shown for a 5-day average at 50 m height for JJA (Figure 6d). For both seasons, atmospheric bromoform based on industrial emissions is larger than atmospheric bromoform based on the Ziska2013 emissions. These differences maximise in the subtropical regions, where anthropogenic bromoform dominates especially during JJA when anthropogenic mixing ratios are 2–7 times larger than from climatological emissions (for LOW and MODERATE). In the tropical regions, the situation is more complicated. Atmospheric abundances driven by the industrial emissions reach higher peak values of up to 2 ppt especially in the Strait of Malacca (MODERATE, Figure 6b) while mixing ratios driven by the observationally based emissions from Ziska2013-EastAsia are smaller only reaching peak values of up to 0.8 ppt, but are spread over a much wider area (Figure 6d). Given the comparison of the boundary layer values, it is not clear which emission scenario will result in a larger contribution to stratospheric halogen budget.

4.2 Vertical transport of bromoform in the troposphere

In order to analyse atmospheric transport from the marine boundary layer into the free troposphere and UTLS, bromoform mixing rations are averaged over a subtropical box (30° N–40° N, 120° E–145° E, Figure 2) and a tropical box (10° S–20° N, 90° E–120° E, Figure 2) from the Ziska2013-Tropics and Ziska2013-Mixed simulations for DJF and JJA. Both simulations are based on global climatological Ziska2013 emissions between 45° S and 45° N, with Ziska2013-Mixed including additional anthropogenic bromoform emissions in East and Southeast Asia.

In the subtropical box (Figure 8), there is a strong dominance of anthropogenic bromoform in the marine boundary layer during JJA several times higher compared to bromoform of climatological bottom-up emissions (Figure 8). Our simulations suggest that during convective events in JJA, anthropogenic bromoform from the subtropical marine boundary layer can be transported into the UTLS region up to 17 km, the approximate height of the cold point. In our example, convective events occur during the second half of the summer bringing occasionally higher bromoform of over 0.3 ppt into the UTLS (Figure 8a).

During DJF (Figure S2), there is only very little transport of bromoform out of the boundary layer, and entrainment of anthropogenic bromoform into the subtropical UTLS is confined to boreal summer when the intertropical convergence zone (ITCZ) is located north of 10° N (Waliser and Gautier, 1993).

https://doi.org/10.5194/acp-2019-1004
Preprint. Discussion started: 27 January 2020


Atmospheric Chemistry and Physics Discussions

In the tropical box, atmospheric bromoform mixing ratios in the marine boundary layer are weaker than in the subtropics for the simulation based on Ziska2013-Mixed emissions (Figure 9, panel a and b). However, the vertical transport for the two simulations Ziska2013-Mixed and Ziska2013-Tropics are in the same range from 0.2–0.5 ppt (Figure 9) even though the spatial distribution of emissions between Ziska2013 and the MODERATE scenario differs strongly (Figure 5). The seasonal difference between DJF and JJA is very pronounced in the marine boundary layer where tropical mixing ratios during DJF exceed 0.5 ppt throughout the whole time period (Figure 9a). Thus, convective events during DJF bring more bromoform into the UTLS compared to JJA, especially for the run Ziska2013-Mixed which include the anthropogenic bromoform emissions (Figure 9). While the air-sea fluxes in the tropics hardly change from DJF to JJA (Figure S1), the prevailing northeasterly winds during DJF advect the bromoform from the high emissions in East Asia towards the maritime continent which increases tropical abundances substantially. This can be seen for Ziska2013 and even stronger in the MODERATE run where the East Asian emissions dominate over the Southeast Asian region (Figure 7, panel b and d).

4.3 Mixing ratios in the upper troposphere/lower stratosphere

Atmospheric processes over the maritime continent, which encloses the tropical box, are characterised by deep convective events which can lead to entrainment of VSLS into the stratosphere (Aschmann and Sinnhuber, 2013; Tegtmeier et al., 2019). For our case study, convective events reaching the UTLS occur frequently in both seasons sometimes persisting over several days (Figure 9). There is a clear anthropogenic signal in the free troposphere in both seasons, which is more pronounced during DJF (Figure 9a) than during JJA (Figure 9b) in agreement with the elevated mixing ratios in the marine boundary layer.

In addition to the mixing ratios averaged over two boxes, we show the spatial distribution of bromoform at 17 km for the whole domain as a 5-day snapshot (Figure 10) based on the bottom-up Ziska emissions only (Ziska2013-Tropics), and emissions estimates taking anthropogenic sources into account (Ziska2013-Mixed). During DJF (Figure 10, panel a and c), there is a clear anthropogenic signal over the Bay of Bengal, across the equator towards Indonesia. Mixing ratios for the Ziska2013-Mixed run are 0.19 ppt averaged over the area of 90 % highest mixing ratios and 0.16 ppt for Ziska2013-Tropics, corresponding to 0.03 ppt being of anthropogenic origin (Table S1). Again, the stronger advective transport in the boundary layer during DJF bringing higher bromoform abundances from the subtropics into the tropics plays an important role here. As a result more bromoform is picked up by convection and transported into the UTLS during DJF than during JJA. Bromoform mixing ratios are slightly smaller during JJA, with 0.17 ppt and 0.15 ppt based on the Ziska2013-Mixed and Ziska2013-Tropics emissions, respectively (Table S1). Here, more anthropogenic bromoform stays in the northern hemisphere and convection is confined to few areas in the Bay of Bengal and Thailand (Figure 10, panel b and d). Although over 90 % of anthropogenic bromoform is outgassed north of 20° N, we find that these emissions contribute 0.02–0.03 ppt to the stratospheric bromine budget which is an increase of 14–19 % in the MODERATE scenario compared to the Ziska2013 climatology.

https://doi.org/10.5194/acp-2019-1004
Preprint. Discussion started: 27 January 2020

Atmospheric Chemistry and Physics Discussions

5 Comparison with observations

5.1 Bromoform measurements in the ocean

Observations in the surface ocean and atmosphere from East and Southeast Asia can help to determine which scenario (LOW, MODERATE, HIGH) offers the best fit for simulating anthropogenic bromoform in this region. Recent measurement campaigns show elevated bromoform concentrations in the coastal waters of the East China and Yellow Seas (He et al., 2013a, 2013b; Yang et al., 2014, Yang et al., 2015). Average values of 6–13 pmol L^{-1} were measured in the Yellow and East China Seas during boreal spring and summer (Yang et al., 2014; Yang et al., 2015), and of 17 pmol L^{-1} were measured in boreal winter (He et al., 2013b). Particularly high concentrations were detected by He et al. (2013a) during spring in the East China Sea with a mean of 134 pmol L^{-1}. Highest bromoform concentration over 34 pmol L^{-1} (He et al., 2013b) and over 200 pmol L^{-1} He et al. (2013a) were observed near the estuaries of the Yangtse River, which the authors attributed to anthropogenic activities including coastal water treatment in the Shanghai region. Our simulations also show mean surface concentrations around Shanghai of 14–71 pmol L^{-1} (LOW to HIGH), in the range of the observations by He et al. (2013a).

Measurements in the South China and Sulu Seas (Fuhlbrügge et al., 2016) show a high variability of bromoform in the surface seawater with average concentrations of 19.9 pmol L^{-1}. Highest values of up to 136.9 pmol L^{-1} are found close to the Malaysian Peninsula and especially in the Singapore Strait suggesting industrial contributions. Maximum anthropogenic bromoform from our simulations in the Singapore Strait ranges from 36–178 (LOW to HIGH), in good agreement with maximum values reported by Fuhlbrügge et al., (2016).

Average anthropogenic bromoform concentrations for the three scenarios are around 23–113 pmol L^{-1} (averaged over the region of the 90 % highest values, Table 2) and are larger than the observational average values. The larger model values might be due to the fact that the cooling water effluents do not distribute far into the marginal seas but stay near the coast as observed by Yang (2001) and confirmed by our simulations. Our simulated anthropogenic bromoform concentrations stay usually within 100 km of the coast, the averaged observational values, however, include also measurements that are up 200 km away from the coastline and can therefore be expected to be lower. While observational mean values are slightly lower than the model results, maximum values found close to the coast line show very good agreement with the model results.

5.2 Bromoform measurements in the marine boundary layer

Atmospheric mixing ratios are 0.9 ppt and 0.3 ppt in the subtropical East China Sea during boreal winter and summer, respectively (Yokouchi et al., 2017). Our simulations in the East China Sea suggest anthropogenic bromoform contributions of 1.7–5.1 ppt near Shanghai, being on the upper side of the observations. Nadzir et al. (2014) observed relatively high values in the South China Sea (1.5 ppt) and the Strait of Malacca (3.7 ppt) during boreal summer. Our simulations show average mixing ratios of 0.5–1.8 ppt at the surface (LOW to MODERATE) near the Pearl River Delta in the South China Sea, in good agreement

https://doi.org/10.5194/acp-2019-1004
Preprint. Discussion started: 27 January 2020

with Nadzir et al. (2014). In the Strait of Malacca, our simulations suggest 0.2–0.7 ppt (LOW to MODERATE) which is lower than the observations.

Further south in the South China and Sulu Seas, Fuhlbrügge et al. (2016) measured atmospheric bromoform mixing ratios of 2 ppt during November. Near Singapore, the authors reported 3.4 ppt consistent with the high oceanic concentrations observed in the same region. Our simulations result in peak mixing ratios around Singapore during DJF of up to 1.7 and 5.3 ppt for the LOW and MODERATE scenario, respectively, in good agreement with Fuhlbrügge et al. (2016). Especially the high atmospheric bromoform mixing ratios found near Singapore and the Pearl River Delta can be associated with anthropogenic activity.

The HIGH scenario shows average mixing ratios which are in general too high for the whole domain. Thus, it is not likely that cooling water treatment produces anthropogenic bromoform with average concentrations of 100 µg L^{-1}. Nevertheless, such concentrations can occur at some locations and produce extremely high bromoform abundances near the coast of industrial regions, as confirmed by the observations presented here.

6 Discussion and conclusion

We find that there is a strong anthropogenic source of bromoform along the coast of East Asia with particular large contributions north of 20° N from the East China, Yellow and Japan Seas. This anthropogenic source results from local cooling water treatment in power plants and leads to extremely high annual mean air-sea flux rates of 3.1–9.1 nmol m^{-2} h^{-1} in coastal waters in East Asia. Atmospheric bromoform originating from industrial sources accumulates in the marine boundary layer and result in mixing ratios of up to 5–14 ppt. It shows a strong seasonal variability with the 'cloud of high bromoform abundances' being transported into the mid-latitudes during boreal summer and to the tropics during boreal winter.

In comparison, the bottom-up inventory by Ziska2013 shows much lower values along the coast of East Asia, but higher mean sea surface concentrations in Southeast Asia. Comparisons with individual campaigns suggest that our averaged anthropogenic values are higher than campaign-averaged estimates in surface water and air. This discrepancy of the mean values is possibly related to the regional extent of the campaign data, given the very sharp bromoform gradients from the coast into the open ocean waters. Maximum values found in surface water and air during the campaigns, however, agree very well with our estimates based on industrial sources for the LOW and MODERATE scenarios. Therefore, anthropogenic activities can be expected to cause extremely high bromoform concentrations and air-sea fluxes in locations relatively close to the source. Estimating the exact regional extent and distribution will require further targeted measurement campaigns.

Concentrations of bromoform in chemically treated cooling water from power plants depend on many different factors and observational studies provide a range of 8–290 µg L^{-1}. Based on the comparison of our model results to observations, we expect initial bromoform concentrations between 20–60 µg L^{-1} given by the two scenarios LOW and MODERATE. In consequence, oceanic and atmospheric abundances based on the HIGH scenario are most likely too high and only results based on the two lower scenarios are presented in this summary.

https://doi.org/10.5194/acp-2019-1004
Preprint. Discussion started: 27 January 2020

Atmospheric Chemistry and Physics Discussions

Our results indicate that cooling water from power plants provide a substantial and growing source of anthropogenic bromoform. Depending on the scenario, 100 to 300 Mmol bromine (Br) a^{-1} are released into the atmosphere from the coastal regions in Southeast and East Asia (LOW to MODERATE) in form of anthropogenic bromoform. The largest part, about 90 %, are emitted in coastal regions north of 20° N. In comparison, Ziska2013 estimates bromoform emissions of 34 Mmol Br a^{-1} for the same region north of 20° N. The high emissions of industrially produced bromoform in East Asia are most likely underrepresented in existing bottom-up estimates by Ziska et al. (2013) and Stemmler et al. (2015) and might explain some of their differences when compared to top-down estimates.

If bromoform is entrained into the stratosphere, it will contribute to ozone depletion driven by catalytic cycles. Atmospheric transport simulations show that during boreal winter strong northeasterly winds advect the anthropogenic bromoform from the East China Sea towards the tropics. Here it can be taken up by deep convection and reach the UTLS region. On average 0.19 ppt of bromoform are entrained above 17 km, the approximate altitude of the cold point, based on climatological and additional anthropogenic emissions. For the same configuration during boreal summer, the large amounts of anthropogenic bromoform emitted over the East China Sea do not reach the tropics, resulting in average mixing ratios of 0.17 ppt at 17 km. In comparison, the bottom-up Ziska2013 emissions are on average smaller, but spread out over a larger area thus resulting in similar total emissions, and only slightly less bromoform (0.15–0.16 ppt) is transported into the UTLS region during both seasons. In summary, the high anthropogenic bromoform emissions in the East China, Yellow and Japan Seas do not efficiently reach the stratosphere, unless the anthropogenic bromoform is advected with the Asian winter monsoon into the tropics, in which case it can lead to an increased entrainment of 14–19 % over this area.

Ashfold et al. (2015) and Oram et al. (2017) showed for chlorine-based VSLSs that pollution from East Asia can be efficiently entrained into the upper troposphere during DJF. Chlorine-based VSLSs concentrations of 50–250 ppt were measured at 10–12 km height (Oram et al., 2017). While chlorine-based species are still the largest contributor to ODSs, an increase in anthropogenic emission of brominated VSLSs is nevertheless of concern since bromine is about 60 times more effective in destroying ozone than chlorine (Sinnhuber et al., 2009). In particular during the northeasterly winter monsoon, many anthropogenic VSLSs from industrial emissions in East Asia can be entrained into the UTLS above the tropics.

While this study exclusively looks at the DBPs from cooling water treatment in power plants, other anthropogenic sources also contribute to local and global emissions of organic bromine, like desalination plants or ballast water from commercial ships which produce DBPs in chemically treated water. Desalination is mostly done at the Arabian Peninsula (Jones et al., 2019), and ballast water volumes with 3–5 billion m^3 a^{-1} (Tamelander et al., 2010) are globally negligible compared to cooling water volumes from coastal power plants but can locally increase DBP discharge (Maas et al., 2019). For assessing the total impact of anthropogenic VSLSs on a local industrial area, such as Singapore or the Pearl River Delta region, all sources of chemical water treatment need to be taken into account. Comparison of these two regions show that the bromoform from cooling water dominates

https://doi.org/10.5194/acp-2019-1004
Preprint. Discussion started: 27 January 2020

above ballast water, leading to emissions of around 990 pmol m^{-2} h^{-1} in Singapore and 6430 pmol m^{-2} h^{-1} in the Pearl River Delta (MODERATE, Figure 5b), while bromoform from ballast water is expected to cause 900 and 2000 pmol m^{-2} h^{-1} for these two areas (Maas et al., 2019). Direct outgassing during treatment of circulating water through the cooling towers into the atmosphere can also occur which has not been quantified yet and is therefore not considered here. Overall, cooling water from power plants can be assumed to be the largest global source of anthropogenic bromoform as it has by far the largest water volumes and is present in all regions and climate zones. The contribution of bromoform from anthropogenic sources should be considered as relevant next to natural sources for future estimates of the atmospheric bromine input.

Acknowledgements

The OGCM model data used for this study were kindly provided through collaboration within the DRAKKAR framework by the National Oceanographic Centre, Southampton, UK. We especially thank Andrew C. Coward, Adrian L. New and colleagues for making the data available. The OGCM and trajectory simulations were performed in the High-Performance Computing Centre at the Christian-Albrechts-Universität zu Kiel. Furthermore, we wish to thank Bruno Blanke and Nicolas Grima for realising and providing the Lagrangian software ARIANE; and Siren Rühs for helping with the set-up of the ARIANE environment. This study was carried out within the Emmy-Noether group AVeSH (A new threat to the stratospheric ozone layer from Anthropogenic Very Short-lived Halocarbons) funded by the Deutsche Forschungsgemeinschaft (DFG, German Research Foundation) – TE 1134/1. JVD acknowledges the Helmholtz-Gemeinschaft and the GEOMAR Helmholtz Centre for Ocean Research Kiel (grant IV014/GH018).

Author contribution

JM wrote the manuscript, performed the Lagrangian ocean simulations and created the output. YJ performed the Lagrangian simulations in the atmosphere. ST developed the research question and guided the research process. BQ developed the research question and gave input on the observational data. AB and JVD provided the NEMO-ORCA model data and gave input on the ocean simulations. All authors took part in the process of the manuscript preparation.

The authors declare that they have no conflict of interest.

Data availability

Data from the ARIANE and FLEXPART simulations are available upon request from the corresponding author.

https://doi.org/10.5194/acp-2019-1004
Preprint. Discussion started: 27 January 2020

Atmospheric Chemistry and Physics Discussions

References

Allonier, A.-S., Khalanski, M., Camel, V. and Bermond, A.: Characterization of Chlorination By-products in Cooling Effluents of Coastal Nuclear Power Stations, Mar. Pollut. Bull., 38(12), 1232–1241, doi:10.1016/S0025-326X(99)00168-X, 1999.

Aschmann, J. and Sinnhuber, B.-M.: Contribution of very short-lived substances to stratospheric bromine loading: uncertainties and constraints, Atmos. Chem. Phys., 13(3), 1203–1219, doi:10.5194/acp-13-1203-2013, 2013.

Aschmann, J., Sinnhuber, B.-M., Atlas, E. L. and Schauffler, S. M.: Modeling the transport of very short-lived substances into the tropical upper troposphere and lower stratosphere, Atmos. Chem. Phys., 9(23), 9237–9247, doi:10.5194/acp-9-9237-2009, 2009.

Ashfold, M. J., Pyle, J. A., Robinson, A. D., Meneguz, E., Nadzir, M. S. M., Phang, S. M., Samah, A. A., Ung, H. E., Peng, L. K., Yong, S. E. and Harris, N. R. P.: Rapid transport of East Asian pollution to the deep tropics, Atmos. Chem. Phys., 15, 3565–3573, doi:10.5194/acp-15-3565-2015, 2015.

Blanke, B., Arhan, M., Madec, G. and Roche, S.: Warm Water Paths in the Equatorial Atlantic as Diagnosed with a General Circulation Model, J. Phys. Oceanogr., 29(11), 2753–2768, doi:10.1175/1520-0485(1999)029<2753:WWPITE>2.0.CO;2, 1999.

Boudjellaba, D., Dron, J., Revenko, G., Démelas, C. and Boudenne, J.-L.: Chlorination by-product concentration levels in seawater and fish of an industrialised bay (Gulf of Fos, France) exposed to multiple chlorinated effluents, Sci. Total Environ., 541, 391–399, doi:10.1016/j.scitotenv.2015.09.046, 2016.

Dee, D. P., Uppala, S. M., Simmons, A. J., Berrisford, P., Poli, P., Kobayashi, S., Andrae, U., Balmaseda, M. A., Balsamo, G., Bauer, P., Bechtold, P., Beljaars, A. C. M., van de Berg, L., Bidlot, J., Bormann, N., Delsol, C., Dragani, R., Fuentes, M., Geer, A. J., Haimberger, L., Healy, S. B., Hersbach, H., Hólm, E. V., Isaksen, L., Kållberg, P., Köhler, M., Matricardi, M., McNally, A. P., Monge-Sanz, B. M., Morcrette, J.-J., Park, B.-K., Peubey, C., de Rosnay, P., Tavolato, C., Thépaut, J.-N. and Vitart, F.: The ERA-Interim reanalysis: configuration and performance of the data assimilation system, Q. J. R. Meteorol. Soc., 137(656), 553–597, doi:10.1002/qj.828, 2011.

Dussin, R., Barnier, B., Brodeau, L. and Molines, J. M.: The Making Of the DRAKKAR FORCING SET DFS5, DRAKKAR/MyOcean Rep. 01-04-16, 2016(April), 1–34, 2016.

Engel, A., Rigby, M. (Lead A., Burkholder, J. B., Fernandez, R. P., Froidevaux, L., Hall, B. D., Hossaini, R., Saito, T., Vollmer, M. K. and Yao, B.: Update on Ozone-Depleting Substances (ODSs) and Other Gases of Interest to the Montreal Protocol, Chapter 1, in Scientific Assessment of Ozone Depletion: 2018, Global Ozone Research and Monitoring Project – Report No. 58., 2018.

Fiehn, A., Quack, B., Hepach, H., Fuhlbrügge, S., Tegtmeier, S., Toohey, M., Atlas, E. and Krüger, K.: Delivery of halogenated very short-lived substances from the west Indian Ocean to the stratosphere during the Asian summer monsoon, Atmos. Chem. Phys., 17(11), 6723–6741, doi:10.5194/acp-17-6723-2017, 2017.

Fiehn, A., Quack, B., Stemmler, I., Ziska, F. and Krüger, K.: Importance of seasonally resolved oceanic emissions for bromoform delivery from the tropical Indian Ocean and west Pacific to the stratosphere, Atmos. Chem. Phys., 18(16), 11973–11990, doi:10.5194/acp-18-11973-2018, 2018.

Fogelqvist, E. and Krysell, M.: Naturally and anthropogenically produced bromoform in the Kattegatt, a semi-enclosed oceanic basin, J. Atmos. Chem., 13(4), 315–324, doi:10.1007/BF00057749, 1991.

Fuhlbrügge, S., Quack, B., Tegtmeier, S., Atlas, E., Hepach, H., Shi, Q., Raimund, S. and Krüger, K.: The contribution of oceanic halocarbons to marine and free tropospheric air over the tropical West Pacific, Atmos. Chem. Phys., 16(12), 7569–7585, doi:10.5194/acp-16-7569-2016, 2016.

He, Z., Yang, G.-P., Lu, X.-L. and Zhang, H.-H.: Distributions and sea-to-air fluxes of chloroform, trichloroethylene, tetrachloroethylene, chlorodibromomethane and bromoform in the Yellow Sea and the East China Sea during spring, Environ. Pollut., 177, 28–37, doi:10.1016/j.envpol.2013.02.008, 2013a.

https://doi.org/10.5194/acp-2019-1004
Preprint. Discussion started: 27 January 2020

He, Z., Yang, G.-P. and Lu, X.-L.: Distributions and sea-to-air fluxes of volatile halocarbons in the East China Sea in early winter, Chemosphere, 90(2), 747–757, doi:10.1016/j.chemosphere.2012.09.067, 2013b.

Helz, G. R., Sugam, R. and Sigleo, A. C.: Chemical modifications of estuarine water by a power plant using continuous chlorination, Environ. Sci. Technol., 18(3), 192–199, doi:10.1021/es00121a011, 1984.

Hossaini, R., Mantle, H., Chipperfield, M. P., Montzka, S. A., Hamer, P., Ziska, F., Quack, B., Krüger, K., Tegtmeier, S., Atlas, E., Sala, S., Engel, A., Bönisch, H., Keber, T., Oram, D., Mills, G., Ordóñez, C., Saiz-Lopez, A., Warwick, N., Liang, Q., Feng, W., Moore, F., Miller, B. R., Marécal, V., Richards, N. A. D., Dorf, M. and Pfeilsticker, K.: Evaluating global emission inventories of biogenic bromocarbons, Atmos. Chem. Phys., 13(23), 11819–11838, doi:10.5194/acp-13-11819-2013, 2013.

Hossaini, R., Chipperfield, M. P., Montzka, S. A., Rap, A., Dhomse, S. and Feng, W.: Efficiency of short-lived halogens at influencing climate through depletion of stratospheric ozone, Nat. Geosci., 8(3), 186–190, doi:10.1038/ngeo2363, 2015.

Hossaini, R., Patra, P. K., Leeson, A. A., Krysztofiak, G., Abraham, N. L., Andrews, S. J., Archibald, A. T., Aschmann, J., Atlas, E. L., Belikov, D. A., Bönisch, H., Carpenter, L. J., Dhomse, S., Dorf, M., Engel, A., Feng, W., Fuhlbrügge, S., Griffiths, P. T., Harris, N. R. P., Hommel, R., Keber, T., Krüger, K., Lennartz, S. T., Maksyutov, S., Mantle, H., Mills, G. P., Miller, B., Montzka, S. A., Moore, F., Navarro, M. A., Oram, D. E., Pfeilsticker, K., Pyle, J. A., Quack, B., Robinson, A. D., Saikawa, E., Saiz-Lopez, A., Sala, S., Sinnhuber, B. M., Taguchi, S., Tegtmeier, S., Lidster, R. T., Wilson, C. and Ziska, F.: A multi-model intercomparison of halogenated very short-lived substances (TransCom-VSLS): Linking oceanic emissions and tropospheric transport for a reconciled estimate of the stratospheric source gas injection of bromine, Atmos. Chem. Phys., 16(14), 9163–9187, doi:10.5194/acp-16-9163-2016, 2016.

IEA: Key world energy statistics 2005, Int. Energy Agency, 2005.

IEA: Key world energy statistics 2018, Int. Energy Agency, 2018.

Jenner, H. A., Taylor, C. J. L., van Donk, M. and Khalanski, M.: Chlorination by-products in chlorinated cooling water of some European coastal power stations, Mar. Environ. Res., 43(4), 279–293, doi:10.1016/S0141-1136(96)00091-8, 1997.

Jia, Y., Tegtmeier, S., Atlas, E. and Quack, B.: How marine emissions of bromoform impact the remote atmosphere, Atmos. Chem. Phys., 19(17), 11089–11103, doi:10.5194/acp-19-11089-2019, 2019.

Joint Research Council: Integrated Pollution Prevention and Control (IPPC) Reference Document on the application of Best Available Techniques to Industrial Cooling Systems, Eur. Comm., (December), 335, 2001.

Jones, E., Qadir, M., Vliet, M. T. H. Van, Smakhtin, V. and Kang, S.: Science of the Total Environment The state of desalination and brine production : A global outlook, Sci. Total Environ., 657, 1343–1356, doi:10.1016/j.scitotenv.2018.12.076., 2019.

Liu, Z., Wang, X., Luo, Z., Huo, M., Wu, J., Huo, H. and Yang, W.: Removing of Disinfection By-Product Precursors from Surface Water by Using Magnetic Graphene Oxide, edited by Y. K. Mishra, PLoS One, 10(12), e0143819, doi:10.1371/journal.pone.0143819, 2015.

Maas, J., Tegtmeier, S., Quack, B., Biastoch, A., Durgadoo, J. V., Rühs, S., Gollasch, S. and David, M.: Simulating the spread of disinfection by-products and anthropogenic bromoform emissions from ballast water discharge in Southeast Asia, Ocean Sci., 15(4), 891–904, doi:10.5194/os-15-891-2019, 2019.

Madec, G. and the N. T.: NEMO ocean engine, Note du Pôle modélisation l'Institut Pierre-Simon Laplace No 27, (27), 2008.

Moat, B. I., Josey, S. A., Sinha, B., Blaker, A. T., Smeed, D. A., McCarthy, G. D., Johns, W. E., Hirschi, J. J. M., Frajka-Williams, E., Rayner, D., Duchez, A. and Coward, A. C.: Major variations in subtropical North Atlantic heat transport at short (5 day) timescales and their causes, J. Geophys. Res. Ocean., doi:10.1002/2016JC011660, 2016.

Montzka, S. a. and Reimann, S.: Ozone-Depleting Substances (ODSs) and Related Chemicals, Sci. Assess. Ozone Deplet. 2010, Chapter 1, 1–108, 2010.

https://doi.org/10.5194/acp-2019-1004
Preprint. Discussion started: 27 January 2020

Atmospheric Chemistry and Physics Discussions

Montzka, S. A., Dutton, G. S., Yu, P., Ray, E., Portmann, R. W., Daniel, J. S., Kuijpers, L., Hall, B. D., Mondeel, D., Siso, C., Nance, J. D., Rigby, M., Manning, A. J., Hu, L., Moore, F., Miller, B. R. and Elkins, J. W.: An unexpected and persistent increase in global emissions of ozone-depleting CFC-11, Nature, doi:10.1038/s41586-018-0106-2, 2018.

Nadzir, M. S. M., Phang, S. M., Abas, M. R., Abdul Rahman, N., Abu Samah, A., Sturges, W. T., Oram, D. E., Mills, G. P., Leedham, E. C., Pyle, J. A., Harris, N. R. P., Robinson, A. D., Ashfold, M. J., Mead, M. I., Latif, M. T., Khan, M. F., Amiruddin, A. M., Banan, N. and Hanafiah, M. M.: Bromocarbons in the tropical coastal and open ocean atmosphere during the 2009 Prime Expedition Scientific Cruise (PESC-09), Atmos. Chem. Phys., 14(15), 8137–8148, doi:10.5194/acp-14-8137-2014, 2014.

Nightingale, D., Malin, G., Law, C. S., Watson, A. J., Liss, P. S., Liddicoat, M. I., Boutin, J. and Upstill-Goddard, R. C.: In situ evaluation of air-sea gas exchange parameterizations using novel conservative and volatile tracers, Global Biogeochem. Cycles, 14(1), 373–387, 2000.

Oram, D. E., Ashfold, M. J., Laube, J. C., Gooch, L. J., Humphrey, S., Sturges, W. T., Leedham-Elvidge, E., Forster, G. L., Harris, N. R. P., Iqbal Mead, M., Samah, A. A., Phang, S. M., Ou-Yang, C. F., Lin, N. H., Wang, J. L., Baker, A. K., Brenninkmeijer, C. A. M. and Sherry, D.: A growing threat to the ozone layer from short-lived anthropogenic chlorocarbons, Atmos. Chem. Phys., 17(19), 11929–11941, doi:10.5194/acp-17-11929-2017, 2017.

Padhi, R. K., Subramanian, S., Mohanty, A. K., Bramha, S. N., Prasad, M. V. R. R. and Satpathy, K. K.: Trihalomethanes in the Cooling Discharge of a Power Plant on Chlorination of Intake Seawater, Environ. Eng. Res., 17(S1), 57–62, doi:10.4491/eer.2012.17.S1.S57, 2012.

Quack, B. and Wallace, D. W. R.: Air-sea flux of bromoform: Controls, rates, and implications, Global Biogeochem. Cycles, 17(1), 1023, doi:10.1029/2002GB001890, 2003.

Rajamohan, R., Vinnitha, E., Venugopalan, V. P. and Narasimhan, S. V: Chlorination by-products and their discharge from the cooling water system of a coastal electric plant, Curr. Sci., 93(11), 1608–1612, 2007.

Rigby, M., Park, S., Saito, T., Western, L. M., Redington, A. L., Fang, X., Henne, S., Manning, A. J., Prinn, R. G., Dutton, G. S., Fraser, P. J., Ganesan, A. L., Hall, B. D., Harth, C. M., Kim, J., Kim, K.-R., Krummel, P. B., Lee, T., Li, S., Liang, Q., Lunt, M. F., Montzka, S. A., Mühle, J., O'Doherty, S., Park, M.-K., Reimann, S., Salameh, P. K., Simmonds, P., Tunnicliffe, R. L., Weiss, R. F., Yokouchi, Y. and Young, D.: Increase in CFC-11 emissions from eastern China based on atmospheric observations, Nature, 569(7757), 546–550, doi:10.1038/s41586-019-1193-4, 2019.

Saiz-Lopez, A. and von Glasow, R.: Reactive halogen chemistry in the troposphere, Chem. Soc. Rev., 41(19), 6448, doi:10.1039/c2cs35208g, 2012.

Sherry, D., McCulloch, A., Liang, Q., Reimann, S. and Newman, P. A.: Current sources of carbon tetrachloride (CCl 4) in our atmosphere, Environ. Res. Lett., 13(2), 024004, doi:10.1088/1748-9326/aa9c87, 2018.

Sherwen, T., Schmidt, J. A., Evans, M. J., Carpenter, L. J., Großmann, K., Eastham, S. D., Jacob, D. J., Dix, B., Koenig, T. K., Sinreich, R., Ortega, I., Volkamer, R., Saiz-Lopez, A., Prados-Roman, C., Mahajan, A. S. and Ordóñez, C.: Global impacts of tropospheric halogens (Cl, Br, I) on oxidants and composition in GEOS-Chem, Atmos. Chem. Phys., 16(18), 12239–12271, doi:10.5194/acp-16-12239-2016, 2016.

Sinnhuber, B.-M., Sheode, N., Sinnhuber, M., Chipperfield, M. P. and Feng, W.: The contribution of anthropogenic bromine emissions to past stratospheric ozone trends: a modelling study, Atmos. Chem. Phys., 9(8), 2863–2871, doi:10.5194/acp-9-2863-2009, 2009.

Stemmler, I., Hense, I. and Quack, B.: Marine sources of bromoform in the global open ocean – global patterns and emissions, Biogeosciences, 12(6), 1967–1981, doi:10.5194/bg-12-1967-2015, 2015.

Stohl, A., Forster, C., Frank, A., Seibert, P. and Wotawa, G.: Technical note: The Lagrangian particle dispersion model FLEXPART version 6.2, Atmos. Chem. Phys., 5(9), 2461–2474, doi:10.5194/acp-5-2461-2005, 2005.

https://doi.org/10.5194/acp-2019-1004
Preprint. Discussion started: 27 January 2020

Atmospheric Chemistry and Physics Discussions

Tamelander, J., Riddering, L., Haag, F. and Matheickal, J.: Guidelines for development of a national ballast water management strategy, GEF-UNDP-IMO Glob. London, UK IUCN, Gland. Switz., GloBallast(No. 18) [online] Available from: http://globallast.imo.org/wp-content/uploads/2014/11/Mono18_English.pdf, 2010.

Taylor, C. J. L.: The effects of biological fouling control at coastal and estuarine power stations, Mar. Pollut. Bull., 53(1–4), 30–48, doi:10.1016/j.marpolbul.2006.01.004, 2006.

Tegtmeier, S., Ziska, F., Pisso, I., Quack, B., Velders, G. J. M., Yang, X. and Krüger, K.: Oceanic bromoform emissions weighted by their ozone depletion potential, Atmos. Chem. Phys., 15(23), 13647–13663, doi:10.5194/acp-15-13647-2015, 2015.

Tegtmeier, S., Atlas, E., Quack, B., Ziska, F. and Krüger, K.: Variability and long-term changes of brominated VSLS at the tropical tropopause, Atmos. Chem. Phys. Discuss., 1–44, doi:10.5194/acp-2019-490, 2019.

Waliser, D. E. and Gautier, C.: A satellite-derived climatology of the ITCZ, J. Clim., 6(11), 2162–2174, doi:10.1175/1520-0442(1993)006<2162:ASDCOT>2.0.CO;2, 1993.

Yang, B., Yang, G.-P., Lu, X.-L., Li, L. and He, Z.: Distributions and sources of volatile chlorocarbons and bromocarbons in the Yellow Sea and East China Sea, Mar. Pollut. Bull., 95(1), 491–502, doi:10.1016/j.marpolbul.2015.03.009, 2015.

Yang, G.-P., Yang, B., Lu, X.-L., Ding, H.-B. and He, Z.: Spatio-temporal variations of sea surface halocarbon concentrations and fluxes from southern Yellow Sea, Biogeochemistry, 121(2), 369–388, doi:10.1007/s10533-014-0007-x, 2014.

Yang, J. S.: Bromoform in the effluents of a nuclear power plant: A potential tracer of coastal water masses, Hydrobiologia, 464, 99–105, doi:10.1023/A:1013922731434, 2001.

Yokouchi, Y., Saito, T., Zeng, J., Mukai, H. and Montzka, S.: Seasonal variation of bromocarbons at Hateruma Island, Japan: implications for global sources, J. Atmos. Chem., 74(2), 171–185, doi:10.1007/s10874-016-9333-9, 2017.

Ziska, F., Quack, B., Abrahamsson, K., Archer, S. D., Atlas, E., Bell, T., Butler, J. H., Carpenter, L. J., Jones, C. E., Harris, N. R. P. P., Hepach, H., Heumann, K. G., Hughes, C., Kuss, J., Krüger, K., Liss, P., Moore, R. M., Orlikowska, A., Raimund, S., Reeves, C. E., Reifenhäuser, W., Robinson, A. D., Schall, C., Tanhua, T., Tegtmeier, S., Turner, S., Wang, L., Wallace, D., Williams, J., Yamamoto, H., Yvon-Lewis, S. and Yokouchi, Y.: Global sea-to-air flux climatology for bromoform, dibromomethane and methyl iodide, Atmos. Chem. Phys., 13(17), 8915–8934, doi:10.5194/acp-13-8915-2013, 2013.

https://doi.org/10.5194/acp-2019-1004
Preprint. Discussion started: 27 January 2020

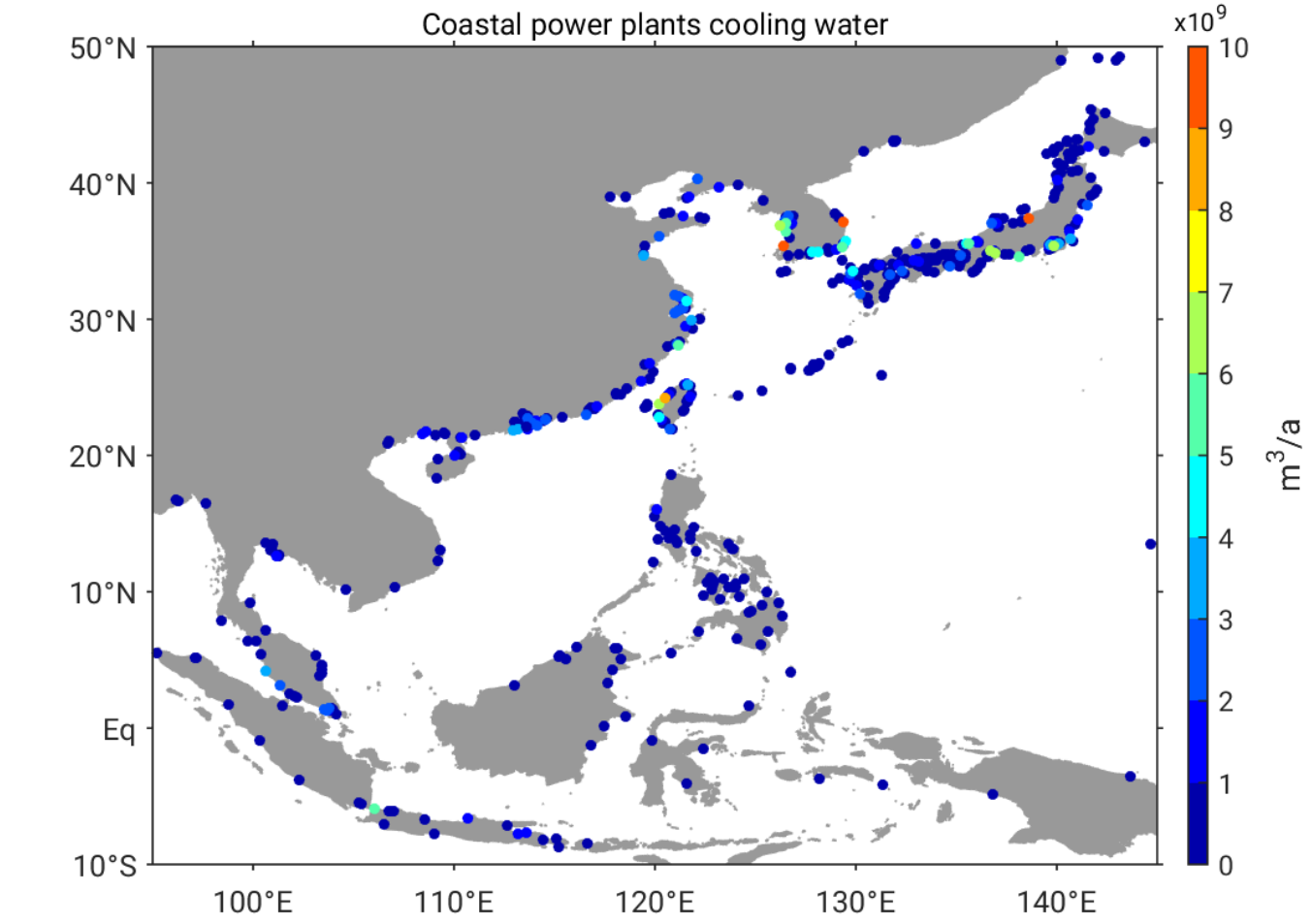

Figure 1: Location and annual cooling water volume [billion m^3 a^{-1}] of coastal power plants in East and Southeast Asia extracted from the enipedia-database and color-coded by the cooling water discharge.

https://doi.org/10.5194/acp-2019-1004
Preprint. Discussion started: 27 January 2020

Atmospheric Chemistry and Physics Discussions

Table 1: Bromoform concentrations measured in water samples from power plant cooling water and surrounding waters. Measurements in the power plant effluent can refer to both, samples of the undiluted water stream or sea water samples at the outlet.

Power plant effluent/ near outlet		Surroundings		Location	Reference
µg L^{-1}	nmol L^{-1}	µg L^{-1}	nmol L^{-1}		
90-100	356-396	1-20	4-79	Gothenburg, Sweden, Kattegatt	Fogelqvist, 1991
9-17	35-67	0.1-5	0.4-20	North Sea	Jenner, 1997
8-27	32-107	n/a	n/a	English Channel	Allonier, 1999
124	495	1-50	4-200	Youngkwang, South Korea, Yellow Sea	Yang, 2001
20-290	79-1147	0-54	0-214	Kalpakkam, India, Bay of Bengal	Rajamohan, 2007
12-41	47-162	n/a	n/a	Kalpakkam, India, Bay of Bengal	Padhi, 2012
19	75	0.5-2.2	2-9	Gulf of Fos, France, Mediterranean	Boudjellaba, 2016

https://doi.org/10.5194/acp-2019-1004
Preprint. Discussion started: 27 January 2020

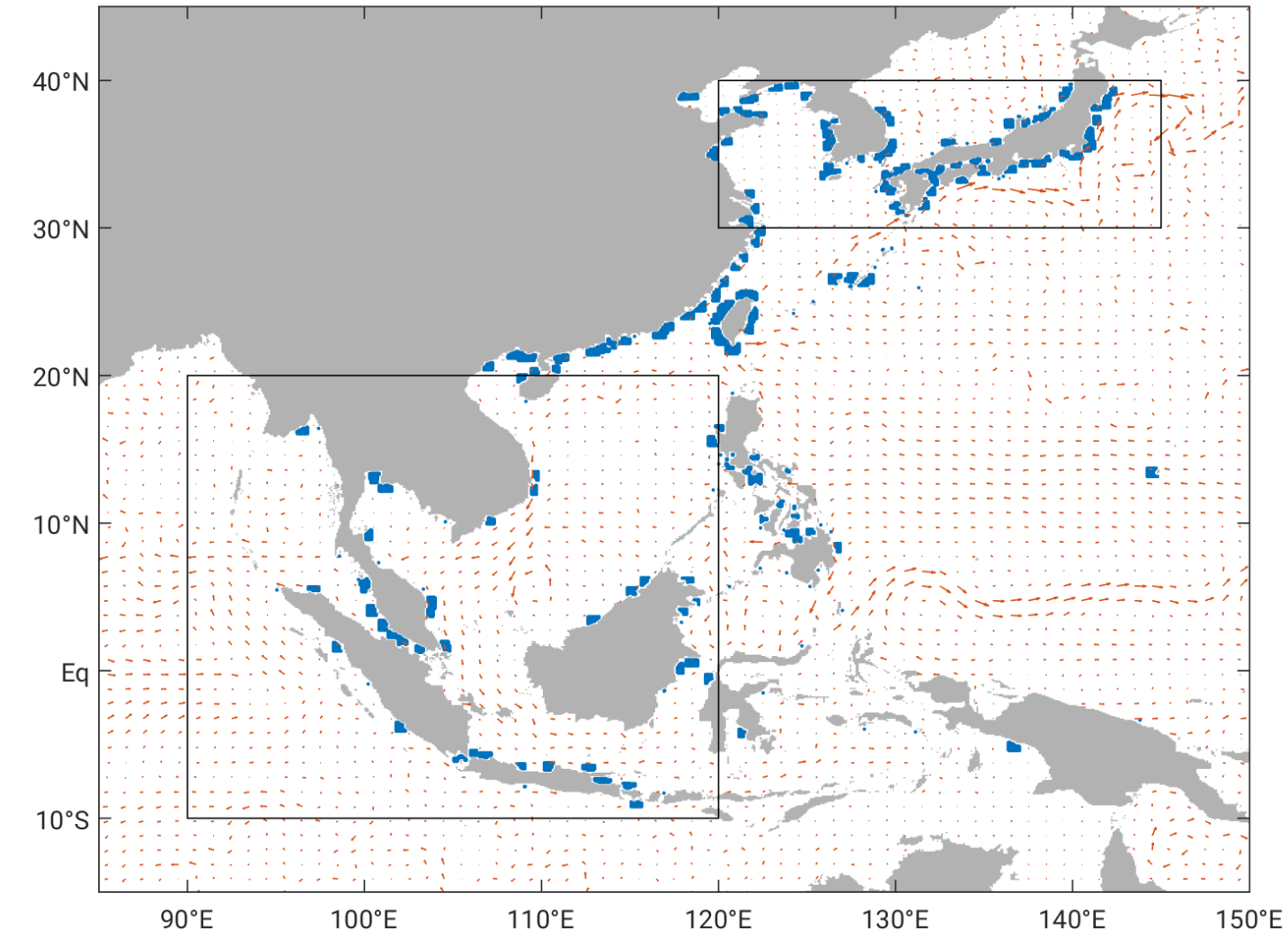

Figure 2: Initial position of particles in East and Southeast Asia (blue dots). NEMO-ORCA12 ocean currents from the initialisation time in January 2005 (red arrows); and the two boxes which mark the region referred to as tropics and subtropics as described in section 2.3.

https://doi.org/10.5194/acp-2019-1004
Preprint. Discussion started: 27 January 2020

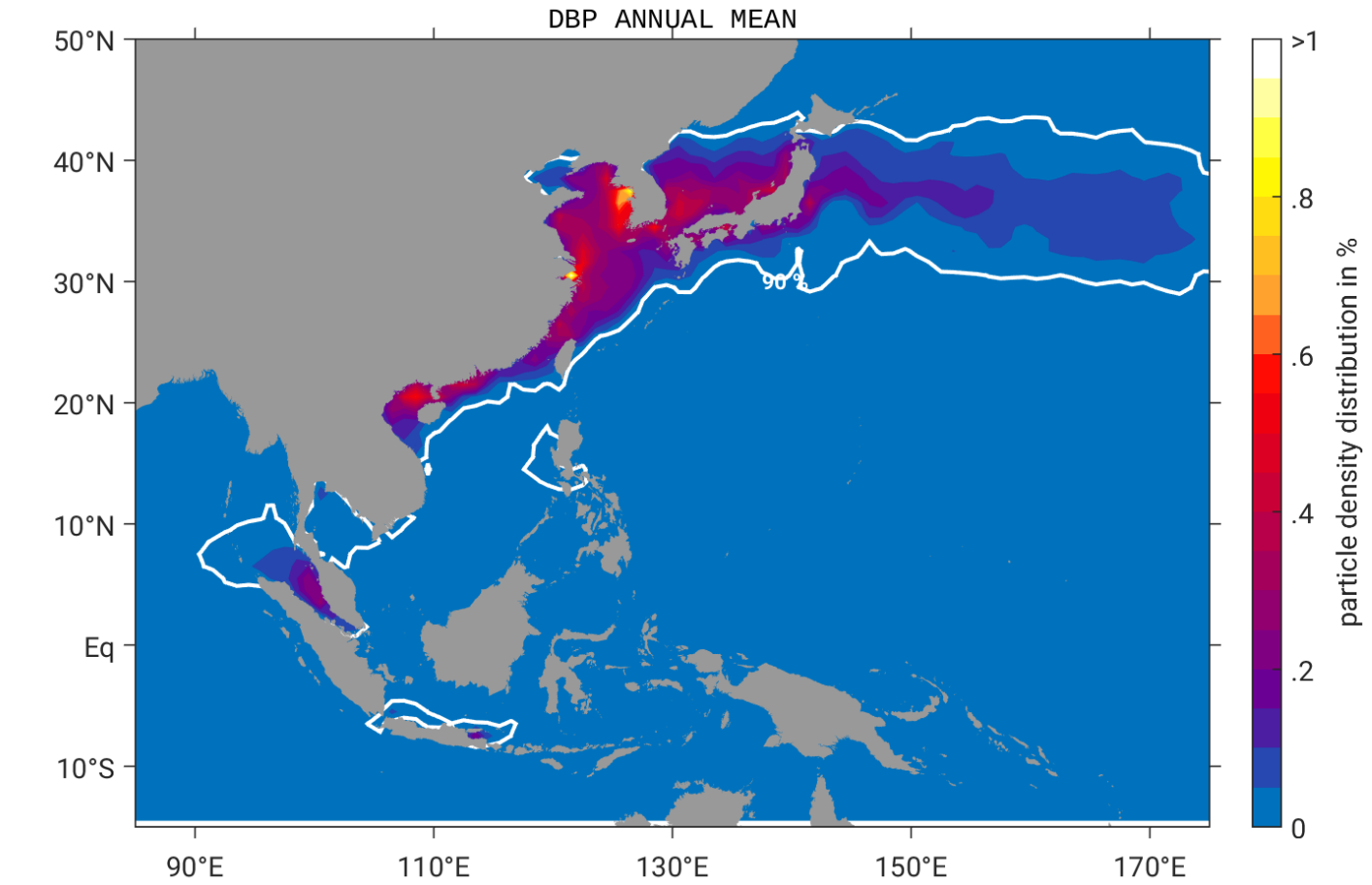

Figure 3: Annual mean particle density distribution in % of DBPs from cooling water treatment in coastal power plants in East and Southeast Asia. The white contour line shows the patches where 90 % of the largest particle density are located.

https://doi.org/10.5194/acp-2019-1004
Preprint. Discussion started: 27 January 2020

Atmospheric Chemistry and Physics Discussions

Table 2: Average values for the three scenarios LOW, MODERATE, HIGH, as well as the climatological values from the Ziska2013 bottom-up estimate in East and Southeast Asia. Sea surface concentrations [pmol L^{-1}], air-sea flux [pmol m^{-2} h^{-1}] and atmospheric mixing ratios from Ziska-EastAsia in the marine boundary layer [ppt] are given as the mean and the standard deviation over the largest 90 % (referred to as mean values) and over the largest 10 % (referred to as maximum values). The annual mean bromine flux [Mmol Br a^{-1}] is derived from the air-sea flux of the total domain in East and Southeast Asia.

Scenario	Sea surface concentration		Air-sea flux		Br flux	Atmospheric mixing ratio JJA		DJF	
	Mean	Max	Mean	Max	Total	Mean	Max	Mean	Max
LOW	23±24	112.1±6.3	3.1±3.4	13.7±0.9	100	0.5±0.6	4.6±1.2	0.3±0.4	3.2±1.5
MODERATE	68±74	338.3±16.6	9.1±10.2	41.1±2.9	300	1.6±2.0	13.9±3.4	0.9±1.3	9.5±4.6
HIGH	113±122	563.6±28.8	15.1±16.9	68.5±4.7	500	2.4±3.3	23.3±5.5	1.5±2.2	15.9±8.3
Ziska-EastAsia	7±6	21.3±1.3	0.4±0.2	1.1±0.2	118	0.2±0.2	0.8±0.1	0.2±0.1	0.5±0.1

https://doi.org/10.5194/acp-2019-1004
Preprint. Discussion started: 27 January 2020

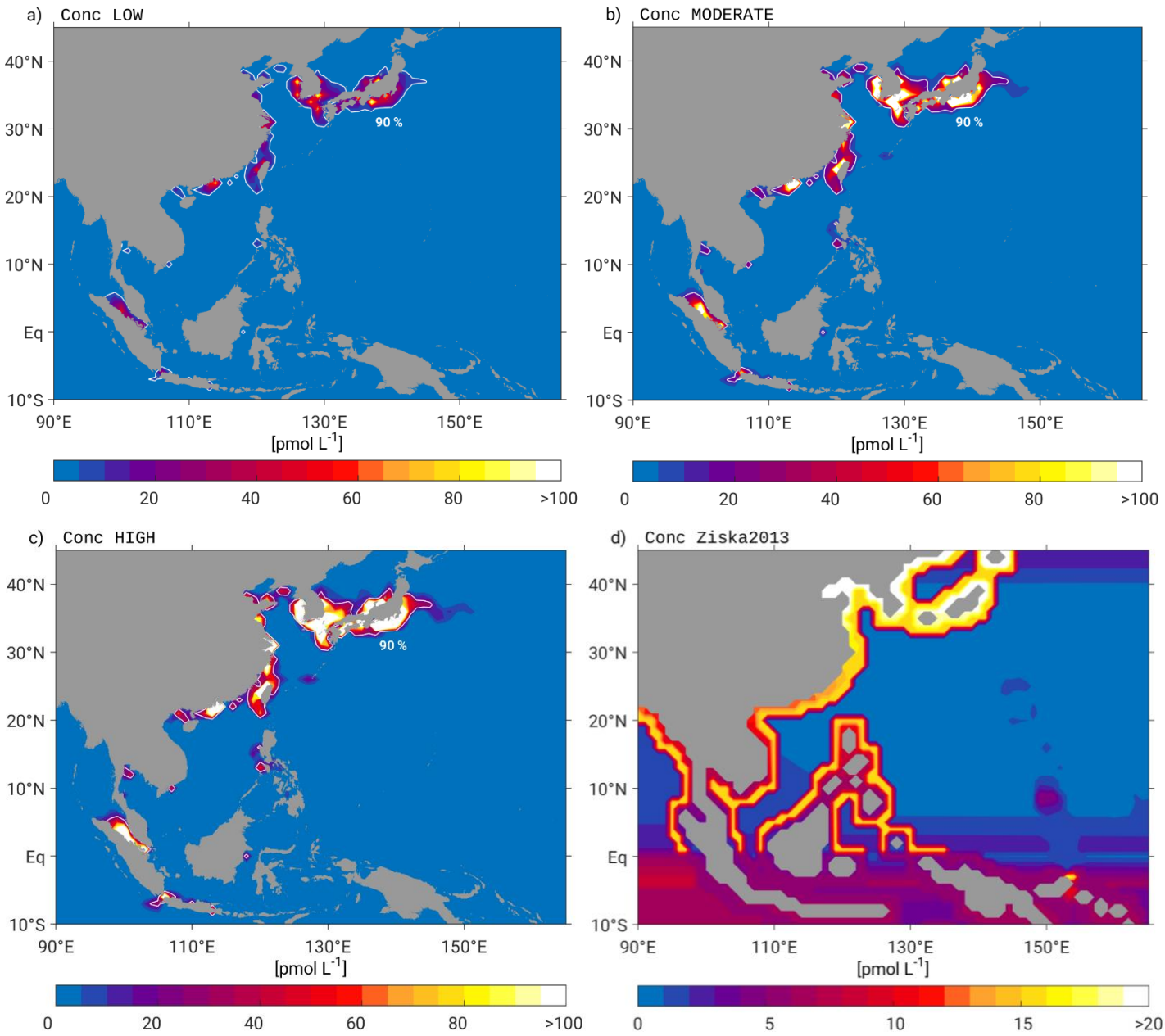

Figure 4: Annual mean surface bromoform concentration in pmol L^{-1} for the three scenarios a) LOW, b) MODERATE and c) HIGH as well as d) the bromoform surface map updated from Ziska2013. Note, that the colorbar for d) varies from the limits in a)-c). The white contour line in panel a)-c) shows the patches where 90 % of the largest concentrations are located.

https://doi.org/10.5194/acp-2019-1004
Preprint. Discussion started: 27 January 2020

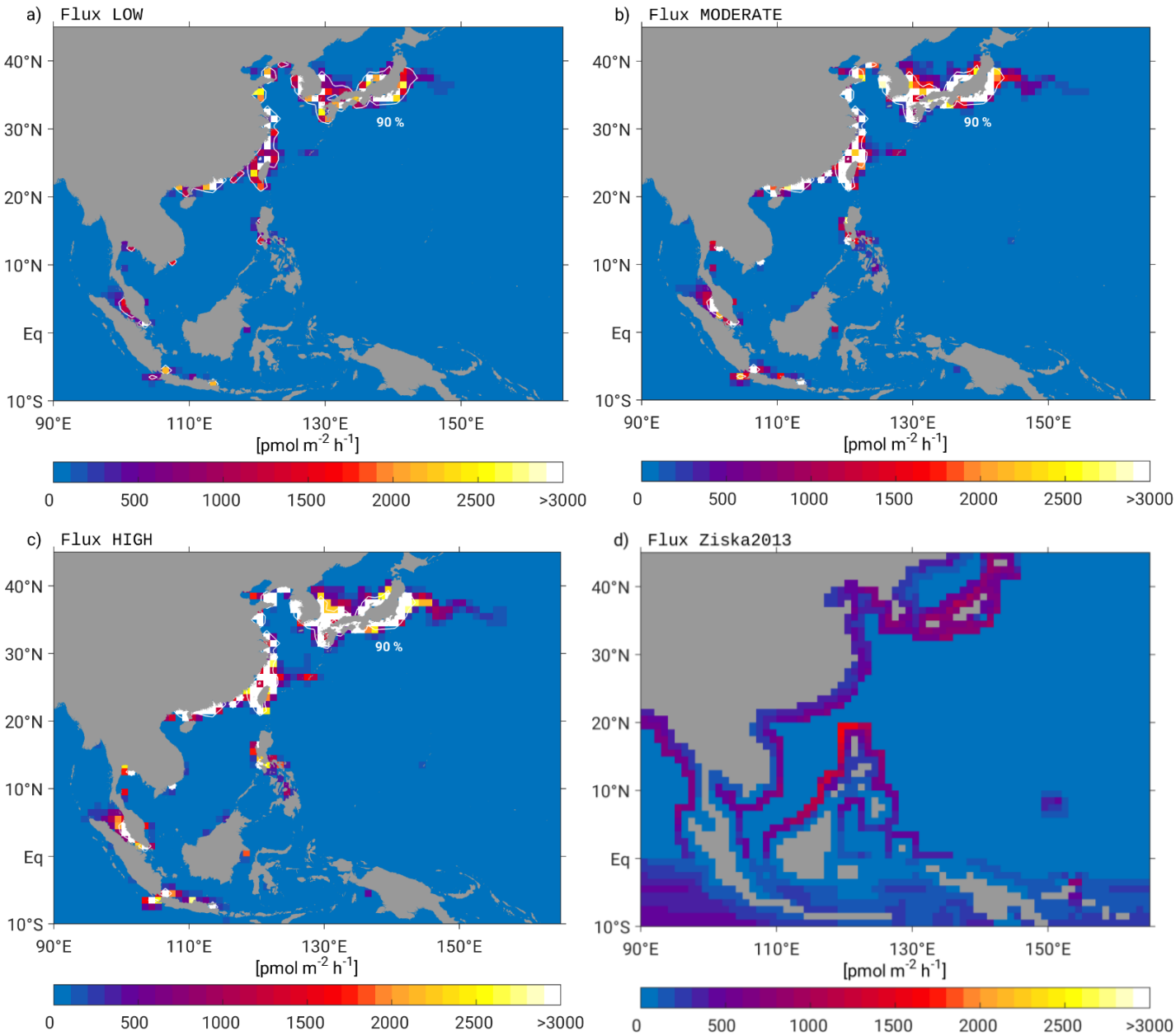

Figure 5: Annual mean air-sea flux of bromoform in pmol m^{-2} h^{-1} for the three scenarios a) LOW, b) MODERATE, c) HIGH, as well as d) the air-sea flux calculated from updated ocean and atmospheric maps after Ziska2013. The white contour line in panel a)-c) shows the patches where 90 % of the largest emissions are located.

https://doi.org/10.5194/acp-2019-1004
Preprint. Discussion started: 27 January 2020

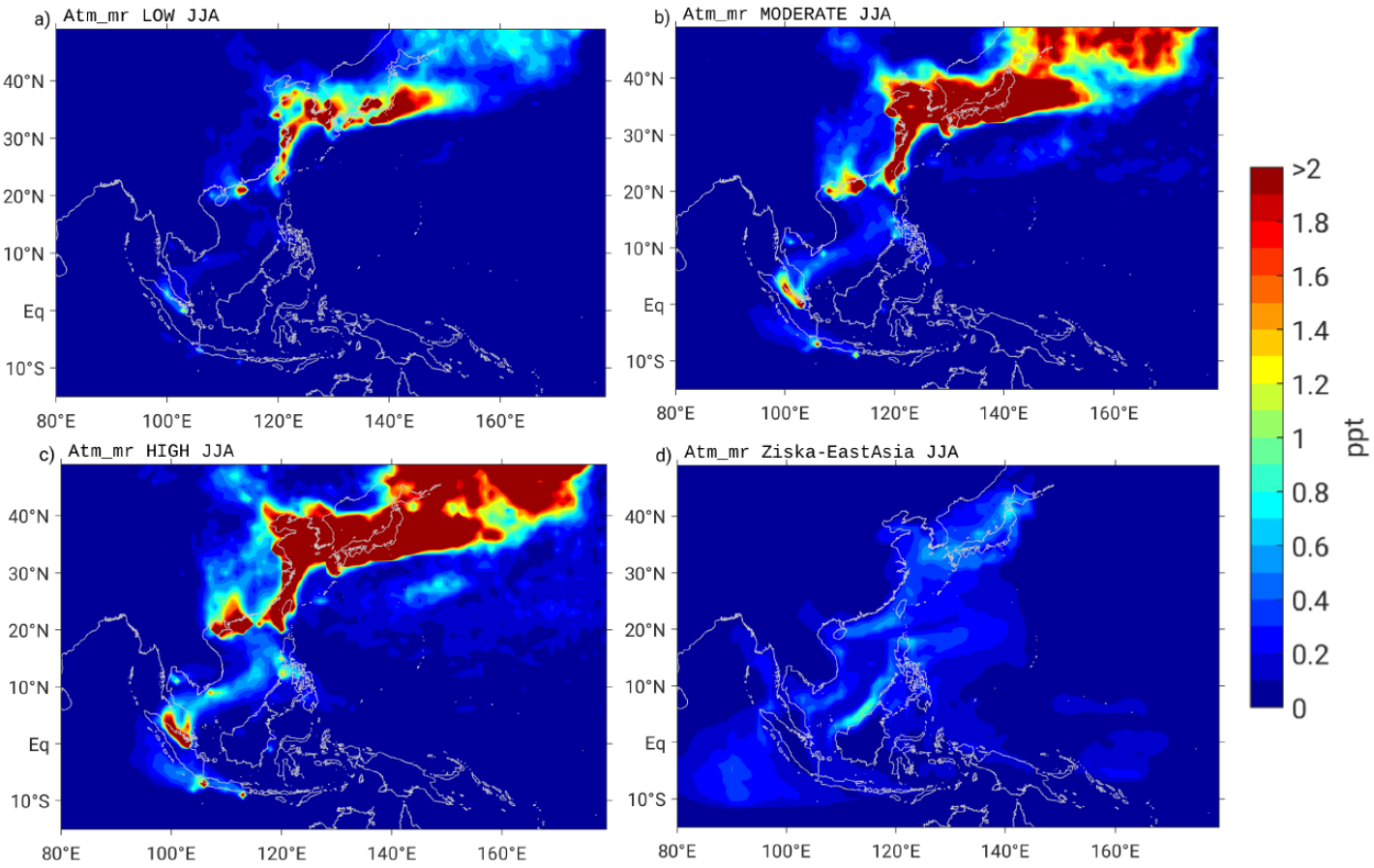

Figure 6: 5-day mean bromoform mixing ratios [ppt] in 50 m height during JJA derived from FLEXPART runs driven by the three scenarios a) LOW, b) MODERATE, c) HIGH, and d) Ziska2013-EastAsia.

https://doi.org/10.5194/acp-2019-1004
Preprint. Discussion started: 27 January 2020

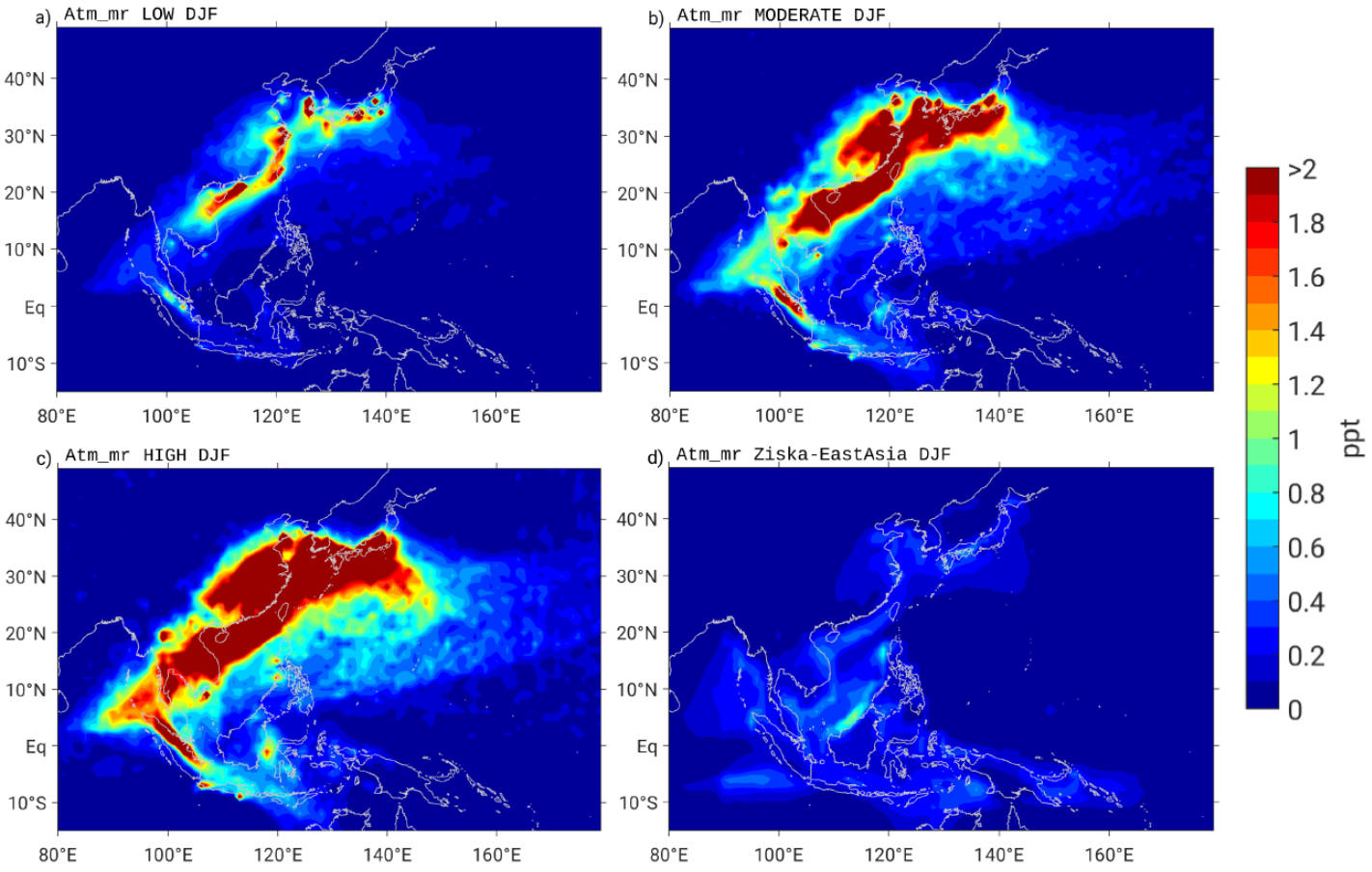

Figure 7: Same as Figure 6 only during DJF.

https://doi.org/10.5194/acp-2019-1004
Preprint. Discussion started: 27 January 2020

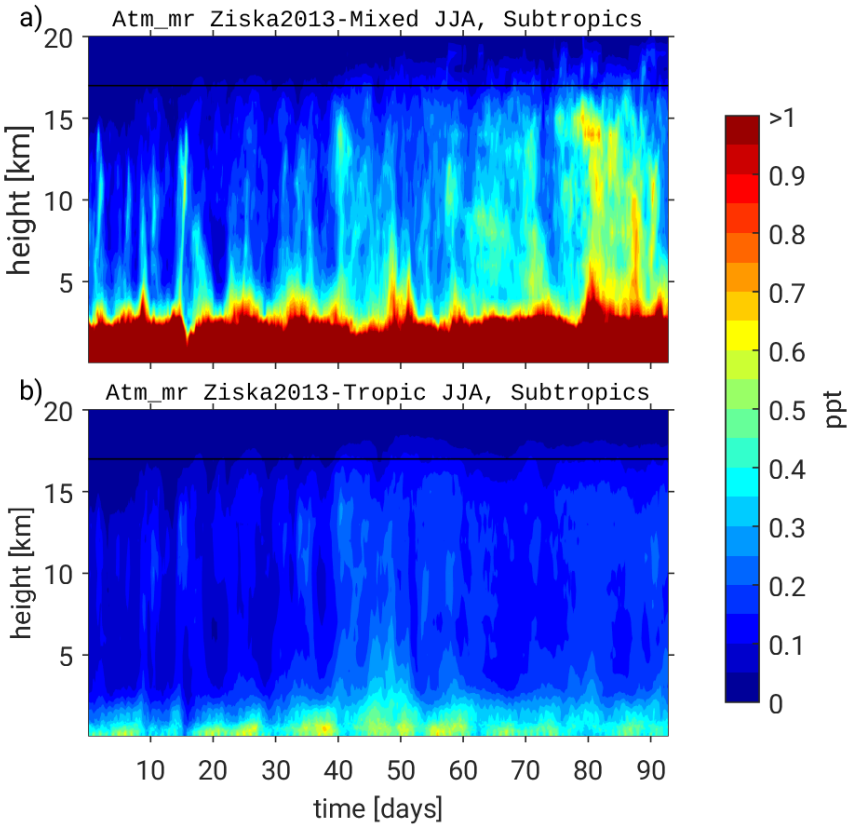

Figure 8: Time series of bromoform mixing ratio [ppt] in the subtropics (30° N–40° N, 120° E–145° E) during JJA for a) the Ziska2013-Mixed run and b) the Ziska2013-Tropics run. The black line marks the approximate location of the cold point tropopause at 17 km.

https://doi.org/10.5194/acp-2019-1004
Preprint. Discussion started: 27 January 2020

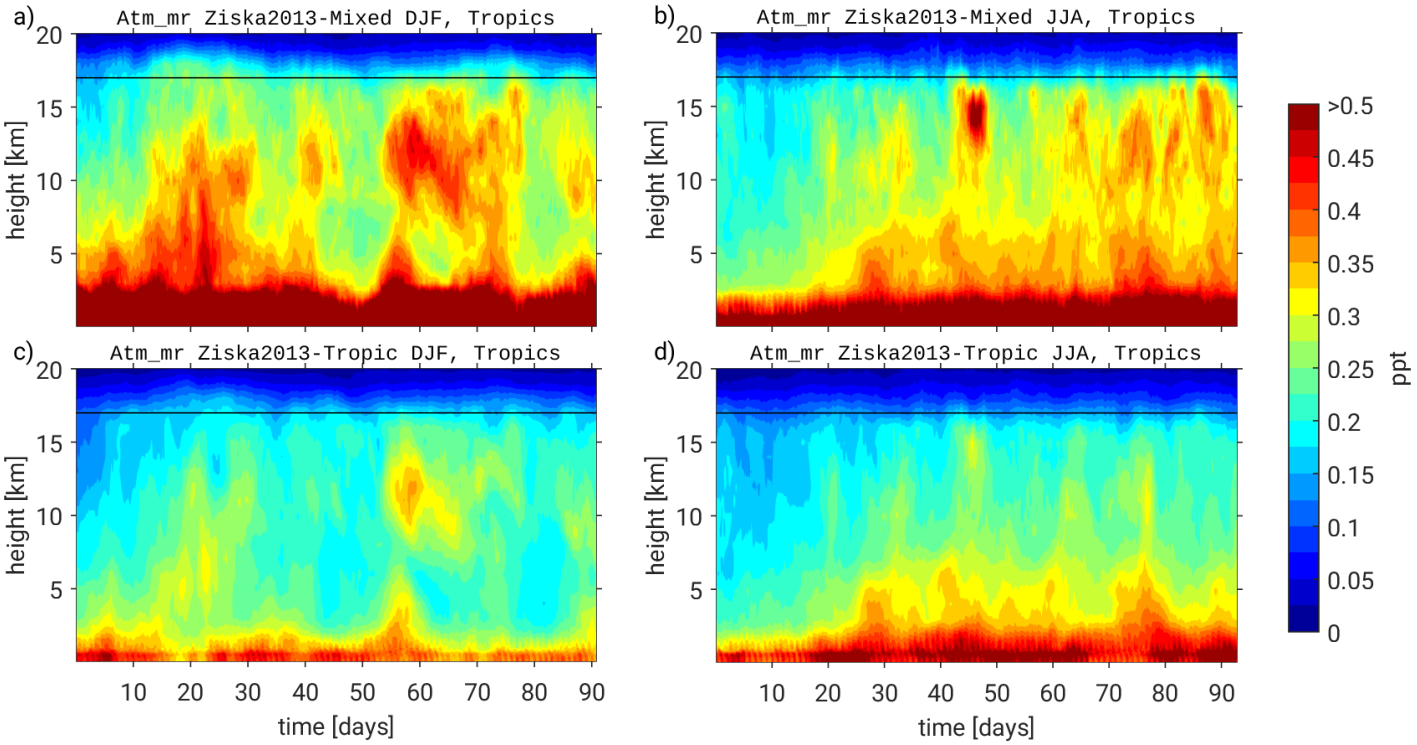

Figure 9: Time series of bromoform mixing ratio [ppt] in the tropics (10° S–20° N, 90° E–120° E) for a) and b) the Ziska2013-Mixed run and c) and d) Ziska2013-Tropics run for both DJF (left) and JJA (right). The black line marks the approximate location of the cold point tropopause at 17 km.

https://doi.org/10.5194/acp-2019-1004
Preprint. Discussion started: 27 January 2020

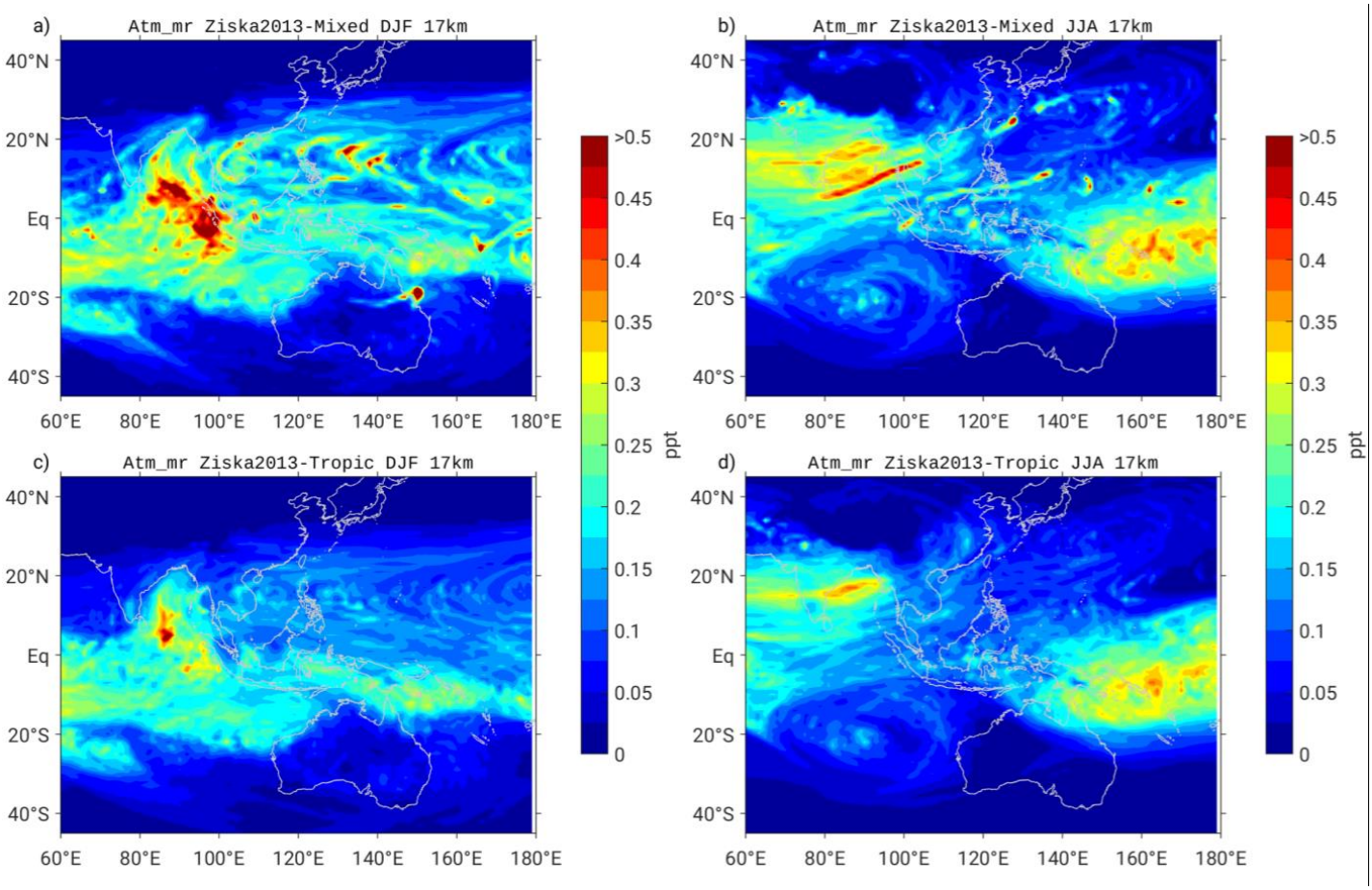

Figure 10: 5-day mean atmospheric mixing ratios [ppt] for a) and b) the Ziska2013-Mixed and c) and d) Ziska2013-Tropics simulation at 17 km height for DJF (left) and JJA (right).

Supplement to: Simulations of anthropogenic bromoform reveal high emissions at the coast of East Asia

Josefine Maas[1], Yue Jia[1], Birgit Quack[1], Jonathan V. Durgadoo[1], Arne Biastoch[1,2] and Susann Tegtmeier[1,*]

[1]GEOMAR Helmholtz Centre for Ocean Research Kiel, Kiel, Germany
[2]Kiel University, Kiel, Germany
*now at: Institute of Space and Atmospheric Studies, University of Saskatchewan, Saskatoon, Canada

Correspondence to: Josefine Maas (jmaas@geomar.de)

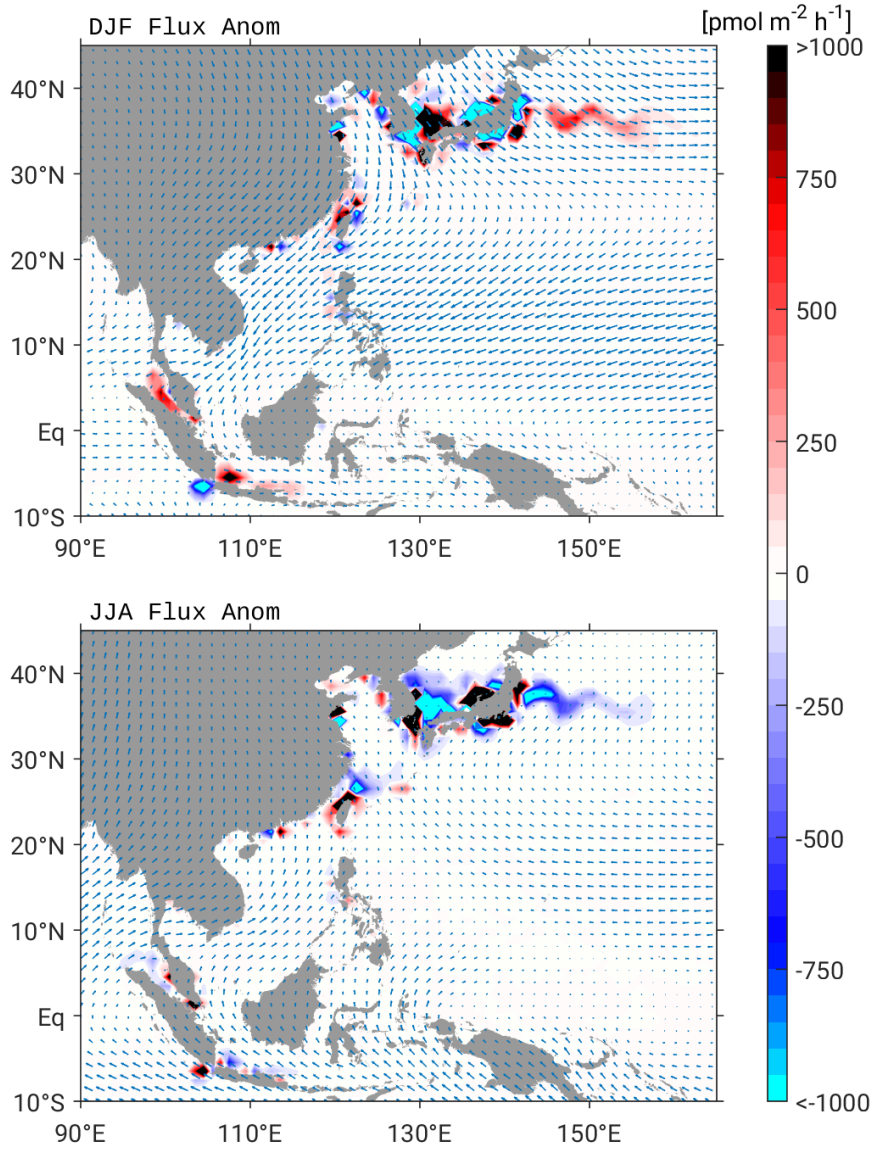

Figure S1: Seasonal anomaly of sea-air flux for the MODERATE scenario in boreal winter (DJF) and summer (JJA) (in pmol m^{-2} h^{-1}). Blue arrows show the seasonal mean surface winds from the forcing data of the simulation time period.

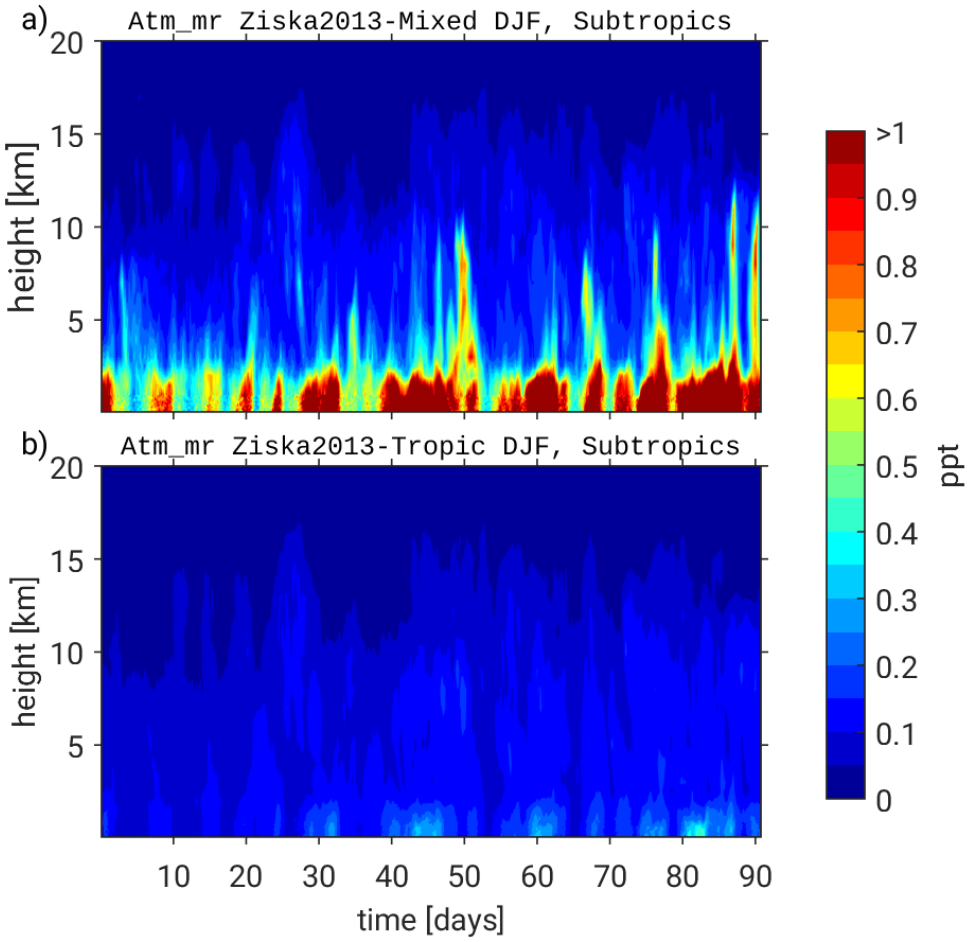

Figure S2: Time series of bromoform mixing ratio [ppt] in the Subtropics (30°N – 40°N, 120°E – 140°E) during DJF for a) the Ziska2013-Mixed run and b) the Ziska2013-Tropics run.

Table S1: Average atmospheric mixing ratios [ppt] from Ziska2013-Mixed and Ziska2013-Tropics in the UTLS at 17 km are given as the mean and the standard deviation over the largest 90 % (referred to as mean values) and over the largest 10 % (referred to as maximum values).

Scenario	Atmospheric mixing ratio [ppt] at 17 km			
	JJA		DJF	
	90 %	10 %	90 %	10 %
Ziska2013-Mixed	0.17 ± 0.08	0.36 ± 0.05	0.19 ± 0.08	0.41 ± 0.10
Ziska2013-Tropics	0.15 ± 0.07	0.31 ± 0.02	0.16 ± 0.06	0.38 ± 0.06

5 Global emissions of anthropogenic bromoform from industrial seawater treatment

In preparation.

Josefine Maas[1], Susann Tegtmeier[1,2], Yue Jia[1], and Birgit Quack[1]

Abstract. Global estimates of bromoform emissions from the surface ocean to the atmosphere have large uncertainties being based on sparse observational data. An improved emission inventory of short-lived bromocarbons such as bromoform is crucial for quantifying their entrainment into the stratosphere where they participate in ozone depletion. A missing source in the global estimate might be the bromoform production by disinfection of industrial seawater used in power plants and ballast water. We estimate the global anthropogenic bromoform production distributed among the coastal power plants and major harbours. We use these anthropogenic emissions of bromoform combined in a global bottom-up emission inventory and simulate the atmospheric transport pathways on a global scale. Two scenarios of anthropogenic emission strength are analysed in different regions where anthropogenic emissions are particularly strong. We find that the biggest contribution to the atmosphere originates from East-Southeast Asia, and Europe. Transport of anthropogenic bromoform into the stratosphere happens in the northern hemisphere subtropics and the tropics. While tropospheric emissions over Europe around the North Sea are very strong, there is no transport into the stratosphere. In contrast, tropical bromoform mixing ratios including anthropogenic bromoform contribute to an average of 0.4–0.5 ppt in the marine boundary layer from which 37–40 % are transported above 17 km. The anthropogenic emissions contribute 4–25 % to stratospheric bromoform entrainment. In East-Southeast Asia, anthropogenic emissions from coastal power plants increase the climatological background by 97–320 %. A small part reaches the tropical stratosphere through convective transport over the Maritime Continent and the West

[1]GEOMAR Helmholtz Centre for Ocean Research Kiel, Kiel, Germany
[2]now at: Institute of Space and Atmospheric Studies, University of Saskatchewan, Saskatoon, Canada

Pacific during boreal winter. The most efficient regions for stratospheric entrainment of bromoform can be found over the Indian Ocean and the equatorial West Pacific. Over the northern Indian Ocean, there is the largest input to stratospheric bromoform of up to 0.3 ppt during boreal summer with an entrainment efficiency of 40–50 %, because of rapid tropical convection and the monsoon circulation. The anthropogenic contribution to stratospheric bromoform is 10–43 % over the Indian Ocean in addition to background entrainment. The novel anthropogenic sources from coastal power plants in the bottom-up emission inventory increase the global bromine input by 8–35 % to 1.9–2.2 Gmol Br a^{-1}. The anthropogenic bromoform sources improve the current bottom-up estimate with significant increase of stratospheric entrainment over East-Southeast Asia, the Maritime Continent, India and the Arabian Peninsula.

5.1 Introduction

Over the last years several attempts have been made to calculate the input of organic bromine from its marine sources into the atmosphere (e.g. Liang et al., 2010; Ordóñez et al., 2012; Ziska et al., 2013). Bromocarbons are source gases for reactive bromine in the stratosphere, which destroys ozone very efficiently through catalytic cycles (Carpenter and Liss, 2000). Bromocarbons with atmospheric lifetimes of less than six months belong to the very short-lived substances (VSLSs). The largest carrier of organic bromine to the atmosphere is bromoform ($CHBr_3$) (Quack and Wallace, 2003) contributing 0.4–4.0 ppt to the marine boundary layer (Engel and Rigby, 2018). Bromoform emission budgets range from 2–10 Gmol Br a^{-1} (Chapter 1.2). Thereby, the air-sea fluxes which are calculated from global extrapolated surface observations for the bottom-up estimates, lie at the lower end of the emissions (Ziska et al., 2013). For top-down estimates, air-sea fluxes are calculated to be consistent with atmospheric observations and are usually higher (e.g. Warwick et al., 2006; Liang et al., 2010; Ordóñez et al., 2012). All global calculations lack a satisfying data coverage and rely on assumptions and extrapolations which include large uncertainties. One possibility for an under-representation in the bottom-up estimates can be missing sources from the sea surface.

The location and emission strength of bromoform is important to assess its atmospheric transport and the amount which enters into the stratosphere. Upon stratospheric entrainment, bromoform is degraded to reactive bromine species which can deplete ozone through catalytic cycles. Bromoform has both natural and anthropogenic sources in the ocean and the size of these sources is highly uncertain. Mostly natural bromoform sources have been considered relevant for stratospheric entrainment, while anthropogenic sources were assumed to have only minor contribution. Quack and Wallace (2003) made one attempt to quantify the global input of anthropogenic bromoform from water treatment facilities based on very simplified assumptions and few measurements. They found a con-

tribution of 300 Mmol Br a^{-1} from cooling water treatment in power plants.
One hypothesis to explain the large differences between top-down and bottom-up emission estimates, is that anthropogenic input of organic bromine might be larger than previously thought and not included in the latter. Especially in the rapidly growing industries in East Asia (Chapter 4, Maas et al., 2020), there are indications for a large source of bromoform from industrial activities (He et al., 2013). Bromoform is the largest by-product from chemical seawater treatment, which is extensively done in power plants to prevent bio-fouling and maintain the operability of the plant (Rajagopal et al., 2012). Power plants require large amounts of cooling water and are therefore often located at the coast where cooling water supply is unlimited.
The amount of bromoform discharged from power plants is highly uncertain and the few available measurements range between 30–1160 nmol L^{-1} (Chapter 4). Over the next years, the bromoform input from ballast water treatment at major harbours will also contribute to the global budget. Ballast water discharge volumes are low with currently about 3.4 billion m^3 a^{-1} but produce very high bromoform concentrations of 890 nmol L^{-1}. The total emissions are only minor with up to 13 Mmol Br a^{-1} but locally this can change the bromoform abundance near large harbours (Maas et al., 2019). In contrast to cooling water treatment, which is being applied in industry for many decades, ballast water treatment is an emerging source of bromoform. Although ballast water treatment has not reached its full impact yet, as the retrofitting of ships with treatment systems will be an ongoing process over the next years (David, 2015), it is considered here as well. Including as many sources as possible, is important for providing realistic estimates of the total pressure of industrial activity onto the environment. This way, it is possible to detect if and where high anthropogenic bromoform emissions exist, if these emissions have been included in previous estimates and if they are important for stratospheric ozone chemistry.
The total amount of bromoform discharged is scaled by the concentration of bromoform in treated cooling water and ballast water with the volumes of water discharged along the coast (Chapter 5.3). The anthropogenic bromoform is outgassed into the atmosphere where we will simulate the atmospheric transport pathways on a global scale. We localise regions where anthropogenic bromoform emissions influence tropospheric chemistry (Chapter 5.4) and where they are transported into the upper troposphere/lower stratosphere (UTLS) region and can participate in stratospheric ozone depletion (Chapter 5.5 and 5.6).

5.2 Methods

Coastal anthropogenic bromoform from both ballast water and cooling water treatment does not spread far into the open ocean, as oceanic transport simulations of the sources

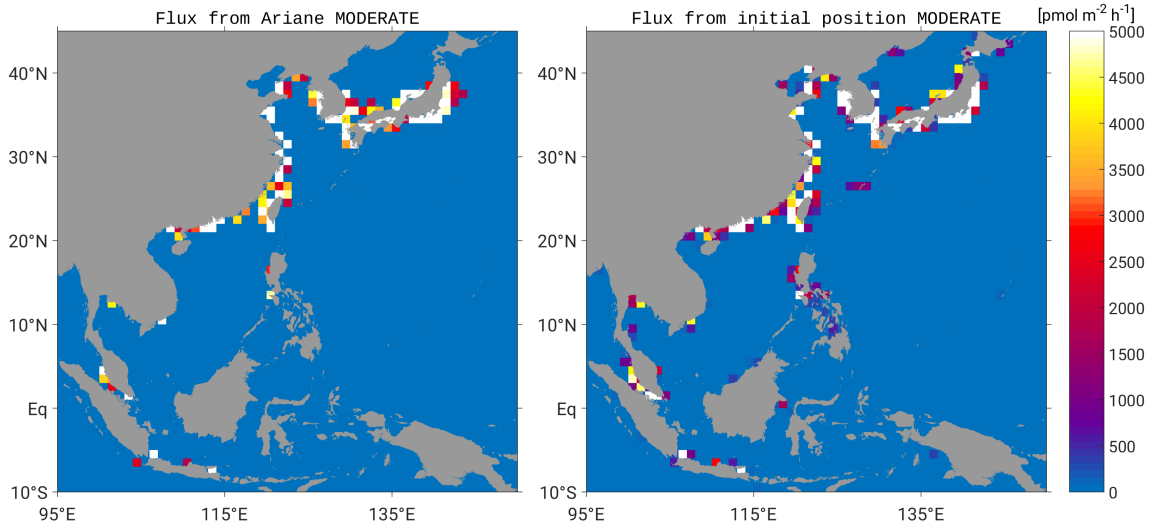

Figure 5.1: Air-sea flux of bromoform from cooling water in calculated from a) the 90 % largest area in the MODERATE scenario in Chapter 4 and b) direct air-sea flux of bromoform at the initial positions used here for the simplified global air-sea flux estimate.

in the East-Southeast Asia region revealed (Chapters 3 and 4). Instead about 99 % of bromoform from cooling water is instantly outgassed into the atmosphere upon discharge. The air-sea flux rate of bromoform from ballast water discharge was almost 100 % in the Pearl River Delta region and 85 % in Singapore (Maas et al., 2019).
Given the immediate outgassing of anthropogenic bromoform, we simplify our approach for the global scale and estimate the direct air-sea flux on a 1° × 1° grid, based on the initial oceanic discharge locations without taking into account oceanic transport and decay of bromoform. We first test our approach for the region East-Southeast Asia where we can compare the direct air-sea flux based on the simplified approach with the emissions derived from oceanic transport simulations of the previous chapter. From the old emission map derived from the oceanic transport simulations, only the area based on the highest 90 % of flux values are used and scaled to 100 %. The resulting flux distribution resembles very much the new direct air-sea flux at the coastal discharge location (Fig. 5.1). The main part of bromoform stays in the area of discharge until outgassing, thus it is reasonable to use the initial distribution for the air-sea flux calculation of bromoform.

5.2.1 Global anthropogenic emissions

We combine the ballast water and cooling water volumes from global sources, and create a map of the discharge location in analogy to the initial positions for the oceanic distribution (Fig. 5.2). Based on our simplified approach, these discharge locations serve as the direct anthropogenic outgassing locations where we calculate the air-sea flux of bromoform on a 1° × 1° grid. We use two scenarios, LOW and MODERATE, which have different initial bromoform concentrations. LOW uses a concentration of 80 nmol L^{-1} in

cooling water and 170 nmol L^{-1} in ballast water, and MODERATE uses 240 nmol L^{-1} in cooling water and 630 nmol L^{-1} in ballast water. The two scenarios capture the range of most likely bromoform abundances for different seawater treatment methods and water conditions. For atmospheric simulations, we combine the anthropogenic emission maps with updated climatological background emissions (Fiehn et al., 2018; Ziska et al., 2013, hereafter Ziska2013).

5.2.2 Combining natural and anthropogenic emissions

We combine our global anthropogenic bromoform emissions with the existing bottom-up emission scenario from Ziska2013. However, given that the coastal grid boxes of the Ziska2013 climatology are based on extrapolation of very few near-shore data points from the northern hemisphere (NH), we expect that a large part of the anthropogenic sources is not included. The anthropogenic emissions on the other hand are only relevant for industrialised coastal regions and do not include natural open ocean and coastal sources. As the Ziska2013 climatology contains some observations of elevated bromoform concentrations near the coast or in marginal seas, e.g. the North Sea, anthropogenic bromoform is to some part already included in the estimate.
There are two options for combining the two emission scenarios, either by adding the anthropogenic bromoform to the Ziska2013 climatology, or by replacing the Ziska2013

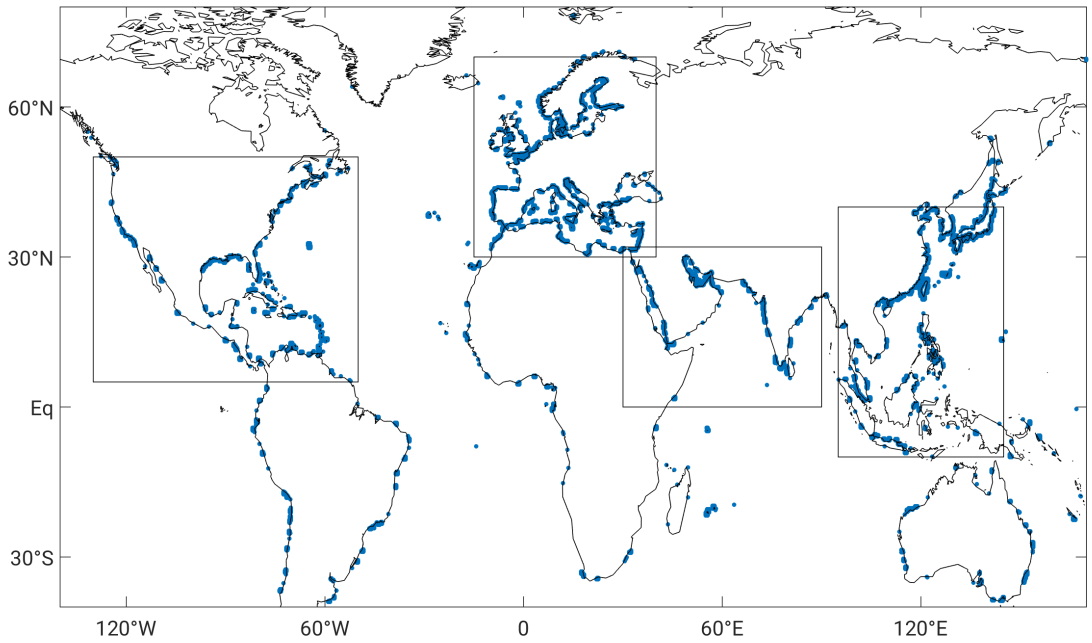

Figure 5.2: Release position of particles that serve to calculate air-sea flux directly on a $1° \times 1°$ grid. The boxes mark the four regions, Europe (30° N–70° N, 15° E–40° W), North America (5° N–50° N, 130° W–50° W), India and Arabia (0–32° N, 30° E–90° E), and East-Southeast Asia (10° S–40° N, 95° E–145° E), where the atmospheric impact of anthropogenic bromoform is assessed.

climatological flux values in the grid boxes where the coastal anthropogenic emissions are higher. Adding the anthropogenic emissions might lead to an over-estimation of the air-sea flux at the coast since they might be already included in the Ziska2013 climatology. Replacing the flux values integrates high anthropogenic fluxes into the existing observation-based climatology from Ziska2013 but only in locations where our anthropogenic estimates are larger. This means, possible natural sources in such an area will not be considered hence the resulting map could be an under-estimation. On the other hand, in some coastal locations, the anthropogenic fluxes are not taken into account because natural fluxes are very high, again resulting in an under-estimation of the total fluxes.
We have tested the difference between the two approaches by both adding the emissions and replacing them. In the global marine boundary layer, mixing ratios differ by 4–5 % between the two methods. Such a difference is considerably smaller than the one resulting from uncertainties in the bromoform concentrations and in the used water volumes, and it is therefore justified to use either method. Since both natural and anthropogenic sources underlie large uncertainties and it is not possible to distinguish them in measurements, we have decided for the more conservative approach of replacing the Ziska2013 emissions in grid cells where anthropogenic values exceed the climatological ones. From the replacement method, we get two new mixed emission maps for both scenarios LOW and MODERATE: Ziska+LOW and Ziska+MODERATE.

5.2.3 Flexpart simulations

The newly created emission maps serve as a source function for simulating atmospheric transport and decay of bromoform with the FLEXPART model (Stohl et al., 2005). FLEXPART is a Lagrangian offline model driven by 3-dimensional meteorological fields from the ERA-Intermin reanalysis data set (Dee et al., 2011). For bromoform, an atmospheric lifetime of 17 days is prescribed for all runs (Montzka and Reimann, 2010). Bromoform is seeded as particles between 50° S and 70° N in each surface box and mixing ratios are derived from the number of particles in each grid box. The FLEXPART runs are performed for boreal winter (DJF) and boreal summer (JJA) with a two month spin-up phase starting at the beginning of October (for DJF) and April (for JJA). The output is given as bromoform mixing ratios (in ppt) at the same horizontal resolution and 33 vertical levels from 50 m up to 20000 m. In the simulations, bromoform is treated as a passive tracer and is lost through chemical decay. We perform two model runs, Ziska+LOW and Ziska+MODERATE, based on the respective combined emission maps. Furthermore, the Ziska2013 emissions are used as bromoform source in a third run in order to compare mixed anthropogenic model runs with the current climatological background. Apart from global emissions and atmospheric transport simulations, we choose four regions to assess the regional impact of anthropogenic bromoform: (i) Europe (30° N–70° N, 15° E–40° W),

(ii) North America (5° N–50° N, 130° W–50° W), (iii) India and Arabia (0–32° N, 30° E–90° E), and (iv) the region of East-Southeast Asia (10° S–40° N, 95° E–145° E) (Fig. 5.2). The FLEXPART simulations use the same configuration as in Chapter 4. Statistics for average and maximum values are calculated as the mean over the most probable 90 % (average) and over the most probable 10 % (maximum) values (see Chapter 2.3). The range for modelled mixing ratios is based on the averages from the Ziska+LOW and the Ziska+MODERATE analyses.

5.3 Global input of bromoform to the atmosphere

The generated mixed emission maps including the background emission of Ziska2013 and anthropogenic bromoform from seawater treatment yield global input of bromine (Br) to the atmosphere of 1.9 (Ziska+LOW) and 2.2 Gmol Br a^{-1} (Ziska+MODERATE). Compared to the 1.7 Gmol Br a^{-1} from Ziska2013 this is an additional anthropogenic input of 0.14–0.51 Gmol Br a^{-1} (Tab. 5.1). The emission from anthropogenic sources alone add up to 0.20 and 0.60 Gmol Br a^{-1} (LOW and MODERATE).
Since all these values are based on assumptions, we give the potential global anthropogenic input between 0.14–0.60 Gmol Br a^{-1} from bromoform which is 8–35 % additional bromine missing in the Ziska2013 estimate. Quack and Wallace (2003) have estimated about 0.3 Gmol Br a^{-1} based on broad assumptions and different methods yielding a similar result.
Global anthropogenic bromoform mainly originates from four regions: Europe, North America, India and Arabia, and East-Southeast Asia (Fig. 5.2). Over 96 % of anthropogenic bromoform is released from these regions. In contrast, for the Ziska2013 background flux, only 28 % of bromoform originates from these four regions.
Even though Europe has a small area compared to the other areas, it contributes 25 % of anthropogenic bromoform emission with a total bromine flux of 177–263 Mmol Br a^{-1} (Ziska+LOW to Ziska+MODERATE). Compared to the Ziska2013 emission estimate, this is a 18–75 % increase compared to the climatological background emissions in this re-

Table 5.1: Global and regional atmospheric input from bromoform emissions per year in Mmol Br a^{-1} for the anthropogenic emissions in the LOW and MODERATE scenario and the resulting emission maps Ziska2013, Ziska+LOW and Ziska+MODERATE.

Region	LOW	MODERATE	Ziska2013	Ziska+LOW	Ziska+MODERATE
Global	196.84	595.65	1712.3	1857.3	2226.2
Europe	48.73	148.12	150.49	176.69	263.15
N America	22.45	68.82	139.58	154.52	191.73
India & Arabia	15.92	47.92	95.52	105.99	136.24
E-SE Asia	102.63	308.78	90.99	179.98	383.37

gion. Based on Ziska2013, Europe has the largest bromoform emission of the four regions but contributes only 9 % to the global bromine input (Tab. 5.1).
The main source of anthropogenic bromine is situated in East-Southeast Asia where over 50 % of bromoform from seawater treatment is released. Relative to the Ziska2013 climatology, where this region is only a minor source, the anthropogenic bromoform input increases the annual bromine in East-Southeast Asia by 98–320 % from Ziska+LOW and Ziska+MODERATE.

5.4 Bromoform in the marine boundary layer

The seasonal mean atmospheric bromoform distribution is presented for three FLEXPART runs, based on the combined emission scenarios Ziska+LOW, Ziska+MODERATE, and on the Ziska2013 climatology. In the marine boundary layer at 50 m, the hot-spots of bromoform emissions are clearly visible for both seasons, DJF and JJA (Fig. 5.3). High bromoform mixing ratios can generally be found over the Indian Ocean and the Maritime Continent, Europe, East Asia and the equatorial regions. Mostly, coastal regions show a clear signal of high bromoform abundances in the lower atmosphere, while open ocean mixing ratios are largest in the Indian Ocean and along the Intertropical Convergence Zone (ITCZ). There is a clear anthropogenic signal over East Asia and Europe in the two mixed runs (Fig. 5.3, a–d) compared to the Ziska2013 mixing ratios (Fig. 5.3, e–f). For DJF, global average bromoform is 0.41–0.52 ppt from Ziska+LOW to Ziska+MODERATE and 0.36 ppt for Ziska2013. During JJA, average mixing ratios are 0.39–0.50 ppt and 0.36 ppt, respectively.
Regions with high industrial emissions are discussed in the following to analyse seasonal transport pathways of bromoform.

Europe

In Europe, the high density of coastal power plants dominates the bromoform distribution in the marine boundary layer over the North Sea (Fig. 5.4). There are no large seasonal differences in the distribution at the surface since bromoform does not spread far from its source regions. Mixing ratios during JJA are slightly higher probably due to warmer air temperature and less precipitation. Bromoform stays in the lower troposphere and is removed from the atmosphere through wet deposition. In the marine boundary layer, mixing ratios reach up to 0.89–1.34 ppt in DJF and 0.95–1.34 ppt in JJA for the Ziska+LOW and Ziska+MODERATE scenarios. By subtracting the average of Ziska2013 from the Ziska+LOW and Ziska+MODERATE mixing ratios, we find that anthropogenic bromoform adds 0.12–0.60 ppt to the climatology in this region. The anthropogenic input makes

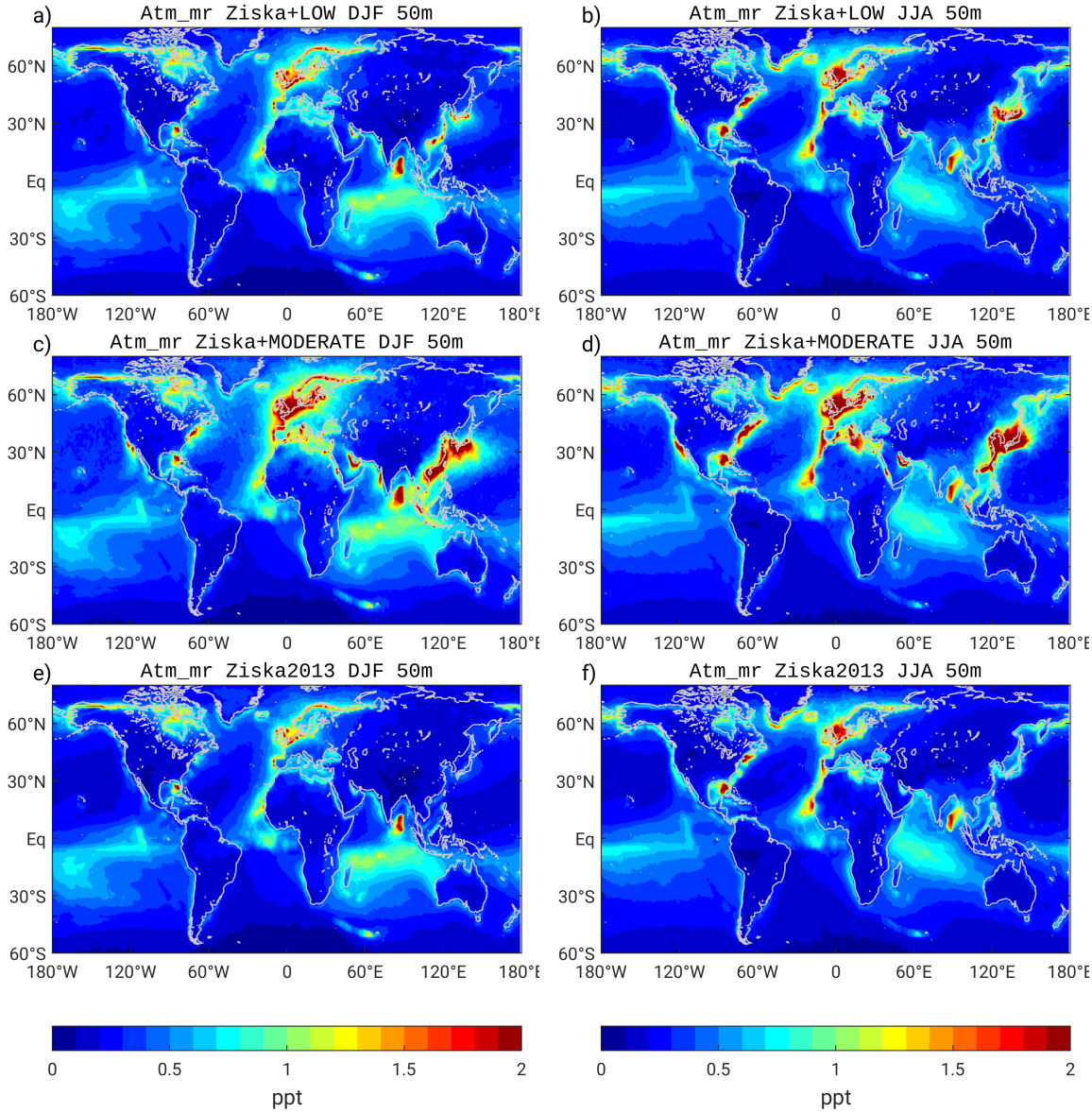

Figure 5.3: Global atmospheric mixing ratio of bromoform [ppt] in the marine boundary layer at 50 m height for the three FLEXPART-simulations Ziska+LOW, Ziska+MODERATE and Ziska2013 during the seasons DJF and JJA.

nearly half of the mean mixing ratios in Europe. Some local hot-spots of high bromoform can be localised over the Mediterranean Sea which mark large industrial areas and major harbours. However, European emission hot-spots are too remote from tropical convection into the stratosphere, so that bromoform can only impact tropospheric chemistry.

North America

Bromoform mixing ratios are abundant along the east and west coast of North America. In the West Atlantic, mixing ratios are dominated by a very large hot-spot in the Gulf of Mexico (Fig. 5.5). Since it is visible in all three runs, it could be both a natural

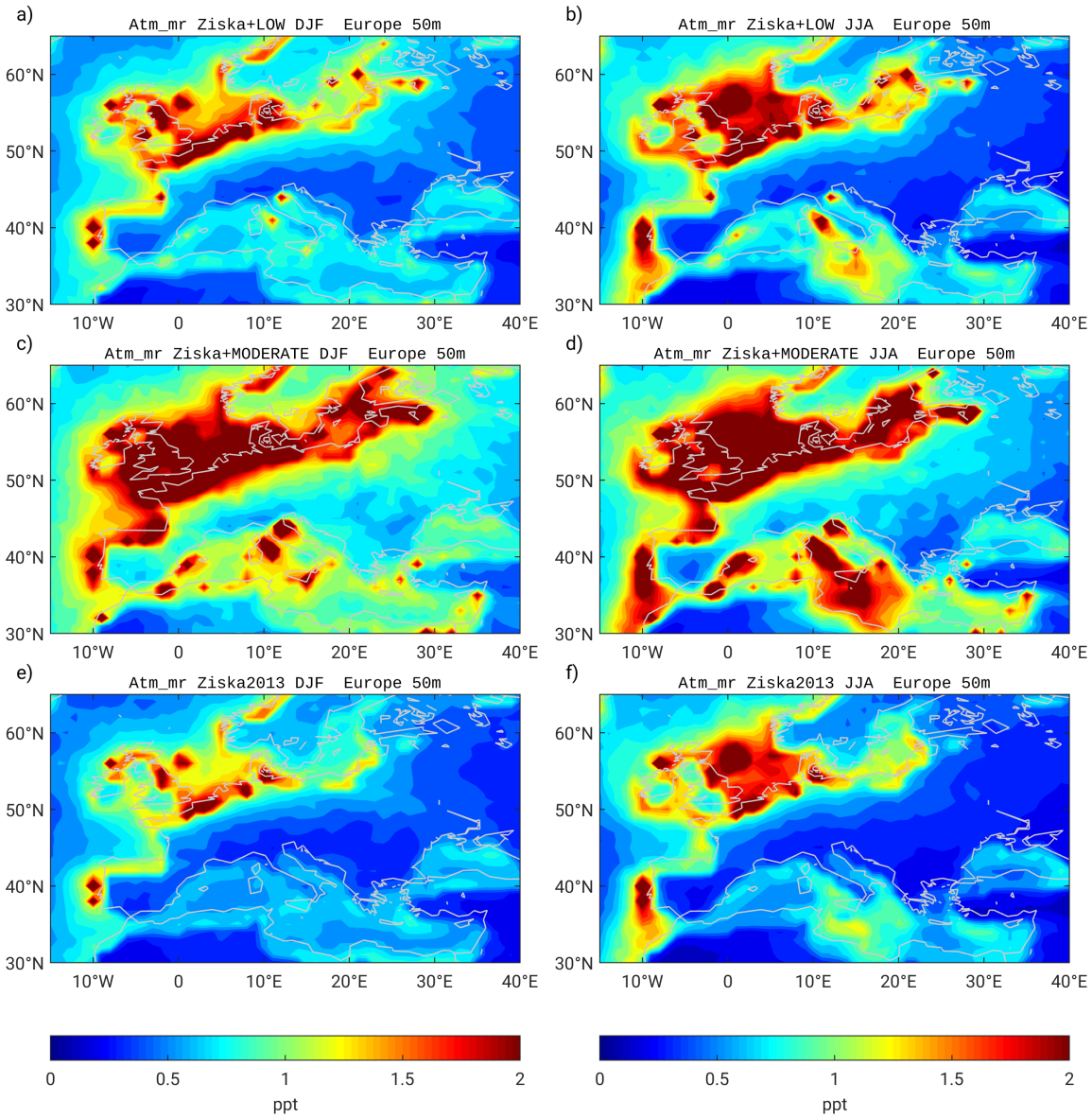

Figure 5.4: Atmospheric mixing ratio of bromoform [ppt] in the marine boundary layer at 50 m height for the three FLEXPART-simulations Ziska+LOW, Ziska+MODERATE and Ziska2013 during the seasons DJF and JJA in Europe.

and anthropogenic source. The Gulf of Mexico is surrounded by highly urbanised regions where anthropogenic input of bromoform from cooling water treatment is likely (Liu et al., 2011). Moreover, massive nutrient input from the coasts can simulate algal blooms which also contribute to the abundances of brominated VSLSs (Liu et al., 2011). Human activity plays a substantial role in the strength of bromoform abundances in the Gulf.

Average mixing ratios of 0.39–0.52 ppt in the marine boundary layer over the whole region during DJF for Ziska+LOW and Ziska+MODERATE are similar to the global mean mixing ratios. During JJA, mixing ratios are 0.51–0.63 ppt. However, the large continental area masks the high emissions along the coasts, where maximum mixing ratios are only

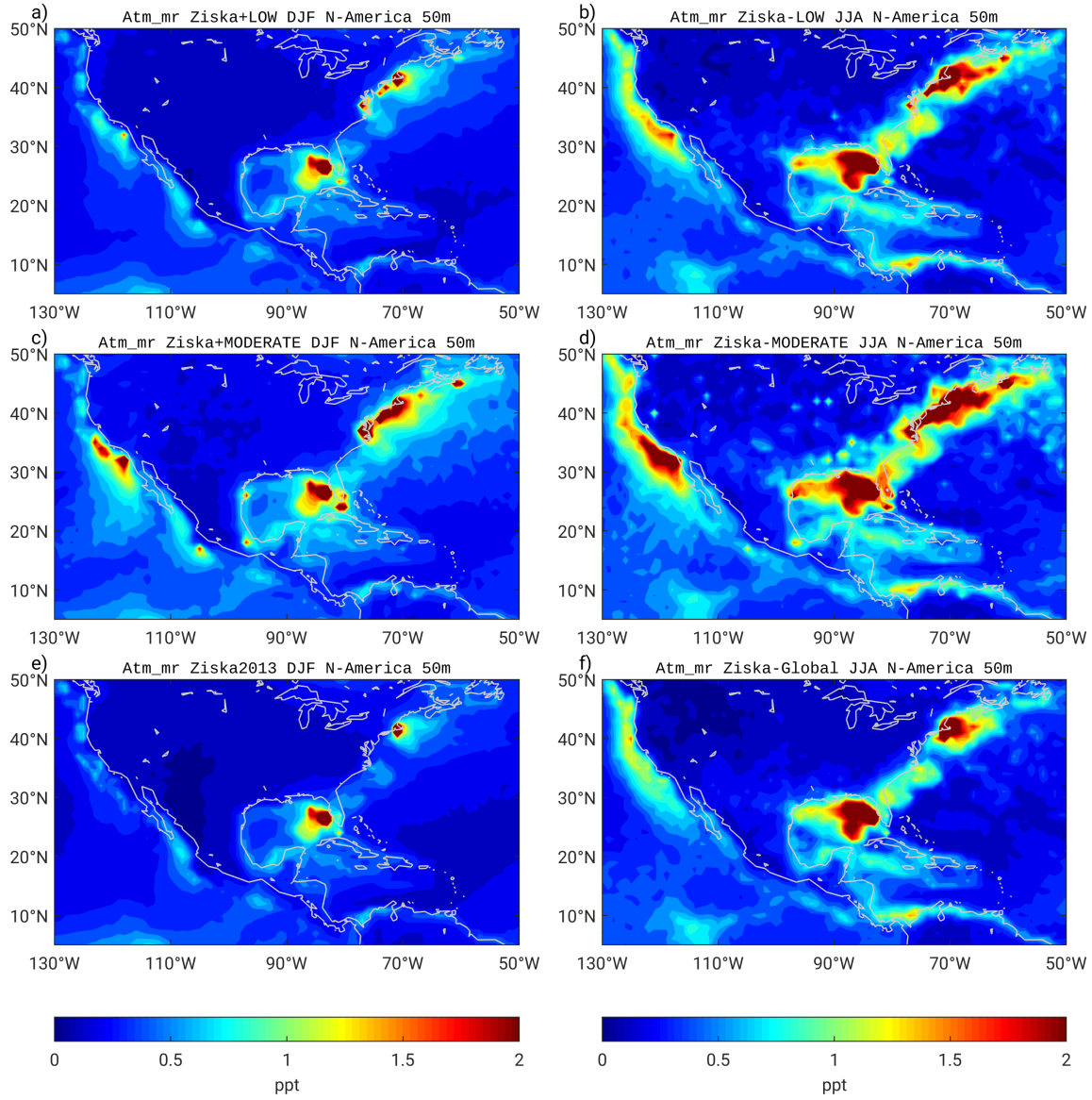

Figure 5.5: Atmospheric mixing ratio of bromoform [ppt] in the marine boundary layer at 50 m height for the three FLEXPART-simulations Ziska+LOW, Ziska+MODERATE and Ziska2013 during the seasons DJF and JJA in North America.

sightly lower compared to Europe. The additional anthropogenic contribution is small for Ziska+LOW (Fig. 5.5). Furthermore, the east coast has elevated abundances which are enhanced during JJA. Anthropogenic influence can be seen for the Ziska+MODERATE simulation along the North American west coast north of 30° N, and along the east coast with maximum mixing ratios up to 3.93 ppt in JJA (Ziska+MODERATE). Anthropogenic bromoform is dominant mostly north of 25° N (Fig. 5.5, a–d) and is thus not significant for additional entrainment into the stratosphere.

Only the region southward of the Gulf is influenced by tropical convection in JJA, and vertical transport of bromoform from the marine boundary layer into the UTLS region can occur (shown below).

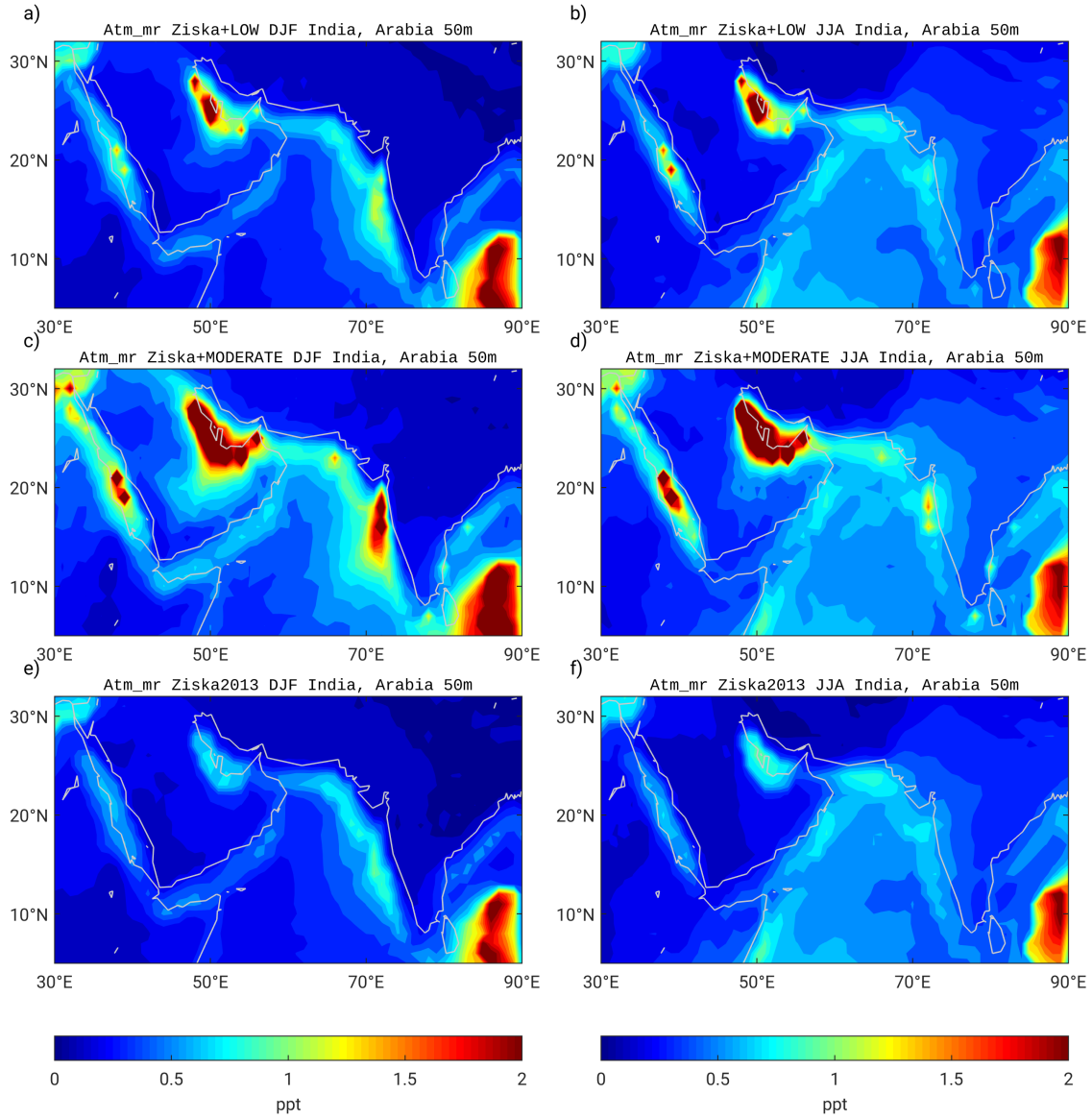

Figure 5.6: Atmospheric mixing ratio of bromoform [ppt] in the marine boundary layer at 50 m height for the three FLEXPART-simulations Ziska+LOW, Ziska+MODERATE and Ziska2013 during the seasons DJF and JJA in India and Arabia.

India and Arabia

The atmospheric boundary layer of the northern Indian Ocean is characterised by strong coastal bromoform in the Red Sea, Arabian Sea and Persian Gulf in all three FLEXPART runs (Fig. 5.6). Furthermore, there are very strong bromoform abundances in the central Bay of Bengal which originate from measurements by Yamamoto et al. (2001). Anthropogenic bromoform leads to significantly enhanced mixing ratios in the Persian Gulf, Red Sea and Indian west coast (Fig. 5.6, a–d) compared to the Ziska2013 simulation. During DJF, winds are directed from the Indian subcontinent southward and advect bromoform towards the open Indian Ocean and the convection region of the ITCZ. The winter monsoon brings bromoform from the coast towards the open ocean during DJF between 5°–

10° N compared to JJA, especially along the west coast of India for Ziska+MODERATE). During JJA, bromoform is transported over the continent. There is additional bromoform input over the Arabian Sea from the central Indian Ocean, which is transported along the African coast northward (Fig. 5.3d). Around the northern Indian Ocean, there are average mixing ratios of 0.51–0.73 ppt for Ziska+LOW and Ziska+MODERATE.
Stronger winds are prevailing during the Indian summer monsoon. During JJA, northward winds bring more bromoform over the Arabian Sea and the Indian subcontinent with an average mixing ratio of 0.56–0.67 ppt for the two mixed simulations.

5.5 Stratospheric entrainment of bromoform

Regional variations of the bromoform emission and transport pathways determine the bromine input of the source gas bromoform into the UTLS at 17 km. The tropics are the main entrainment region for air masses travelling from the troposphere into the stratosphere with transport time scales comparable to bromoform lifetime. The stratospheric entrainment of bromoform is seasonally varying with location of the ITCZ being shifted towards the southern hemisphere (SH) during DJF and towards the NH during JJA (Fig. 5.7).
In comparison to the climatological simulation Ziska2013, there is a clear anthropogenic influence to stratospheric bromoform entrainment in the tropics for Ziska+MODERATE, which is most pronounced over the Indian Ocean. The anthropogenic input can be calculated as the difference between the Ziska+MODERATE and the Ziska2013 simulation at 17 km relative to the difference in the marine boundary layer. The same applies for the anthropogenic input of Ziska+LOW simulation. In total 10–13 % of global anthropogenic bromoform is brought from the marine boundary layer into the UTLS region.
Global average mixing ratios at 17 km for both seasons are 0.12 ppt (Ziska2013), 0.13 ppt (Ziska+LOW) and 0.15 ppt (Ziska+MODERATE). Stratospheric entrainment is most efficient over the Indian Ocean and the West Pacific confirming results from other studies (Tegtmeier et al., 2012; Fiehn et al., 2017). Here, seasonal variations of the convective transport are strongest. Over the Maritime continent, entrainment is enhanced during DJF, especially for the Ziska+MODERATE run. This is related to the northeasterly winds, which transport anthropogenic bromoform from East Asia towards the tropics and agrees with the results presented in (Chapter 4).
The transport pathways over the northern Indian Ocean are strongly influenced by the monsoon circulation. During DJF, the Indian winter monsoon is directed southward from the land to the ocean. The ITCZ lies further south, so that all emissions from the coasts are advected towards the central Indian Ocean where strong convection happens above the whole ocean basin (Fig. 5.7).

The strong differences between DJF and JJA in bromoform transport can be seen even

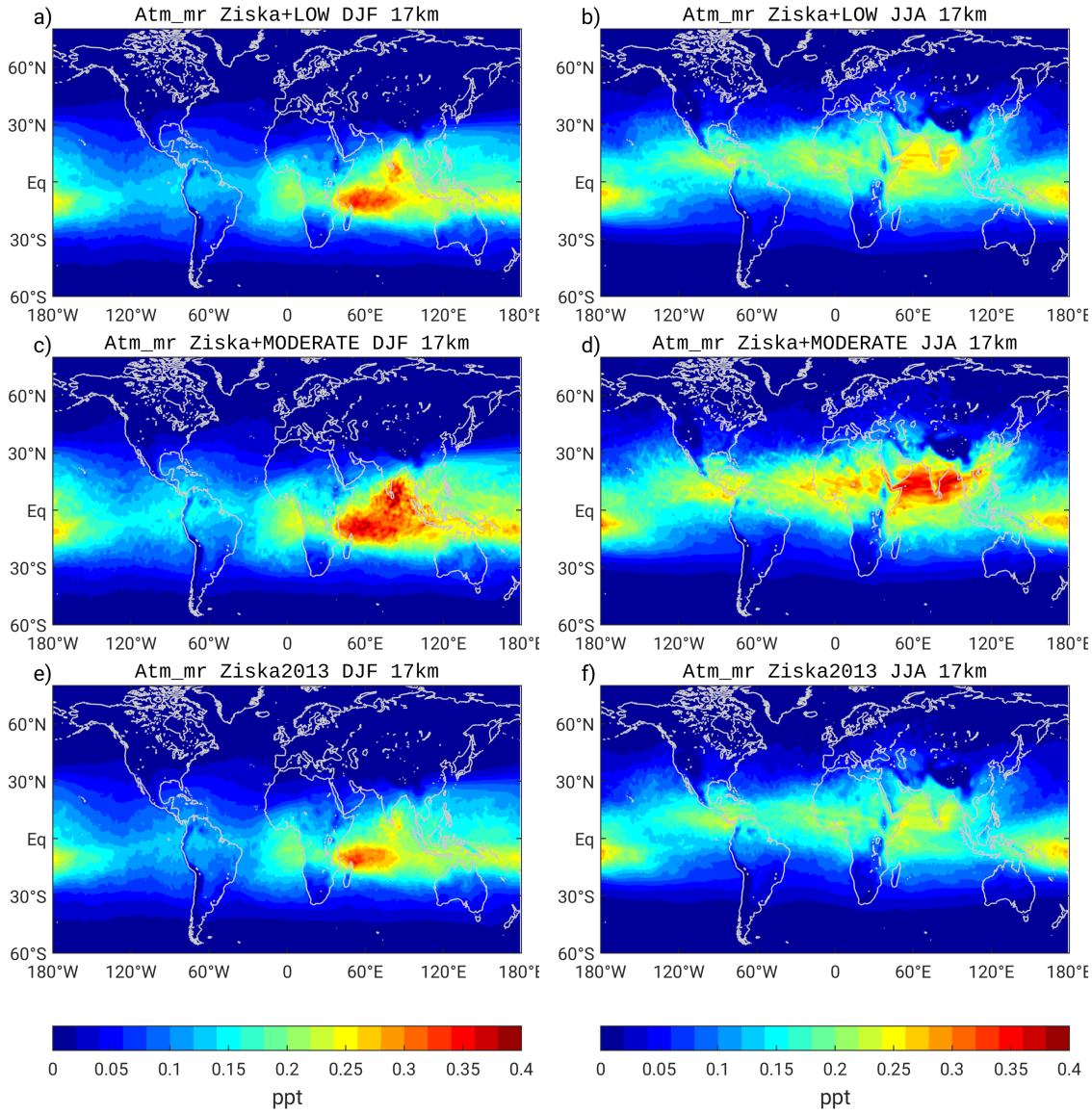

Figure 5.7: Global atmospheric mixing ratio of bromoform [ppt] in the marine boundary layer at 50 m height for the three FLEXPART-simulations Ziska+LOW, Ziska+MODERATE and Ziska2013 during the seasons DJF and JJA.

more pronounced over the northern Indian Ocean (Fig. 5.8). In the region around India and the Arabian Peninsula, up to 0.28–0.37 ppt are entrained into the UTLS for the Ziska+LOW and Ziska+MODERATE simulation during DJF but on a rather small area. Average mixing ratios are around 0.16–0.19 ppt, which is a 10–37 % enhancement compared to the Ziska2013 stratospheric entrainment.

Mixing ratios in the UTLS during JJA are slightly higher with an average of 0.22–0.27 ppt from Ziska+LOW to Ziska+MODERATE. During JJA, the Indian summer monsoon is directed northward and convection happens above the whole northern Indian Ocean from the Red Sea and Arabian Sea to the Bay of Bengal. Thus, over the Indian Ocean up to 23 % of anthropogenic bromoform can be brought from the surface into the UTLS.

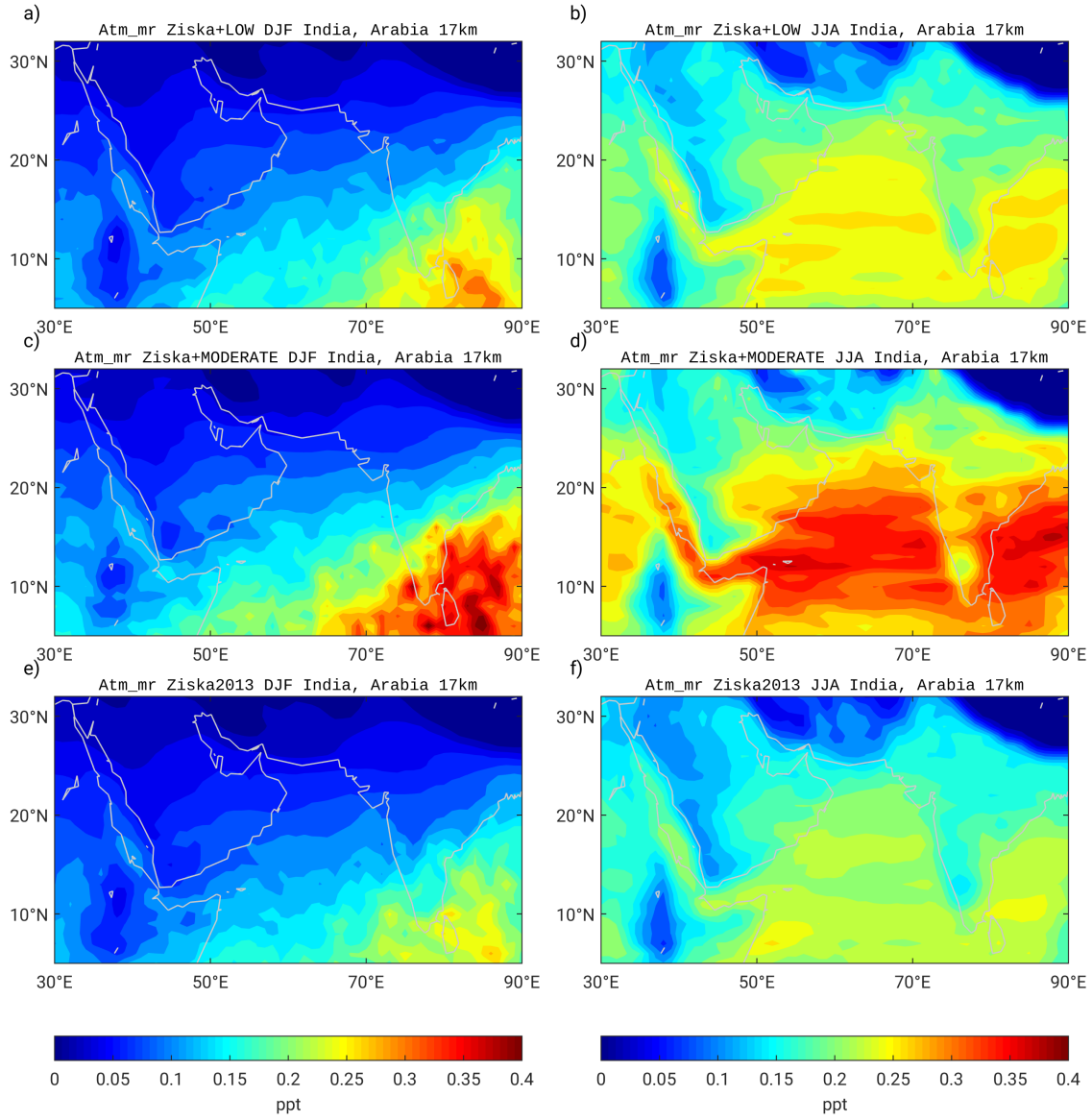

Figure 5.8: Atmospheric mixing ratio of bromoform [ppt] in the UTLS at 17 km height for the three FLEXPART simulations Ziska+LOW, Ziska+MODERATE and Ziska2013 during the seasons DJF and JJA in India and Arabia.

5.6 Vertical profiles

5.6.1 Bromoform profiles from FLEXPART simulations

The vertical transport of bromoform from the surface into the UTLS can be shown with height profiles averaged over the whole inner tropics (10° S–10° N), as well as for different regions in the tropics (Fig. 5.9). The profiles show a strong gradient in the marine boundary layer up to 4–5 km due to deposition. In the free troposphere at 5–15 km, mixing ratios are constant, and start declining in the tropical tropopause layer above 15 km. Vertical transport into the UTLS at 17 km is equally efficient during both seasons over

the whole tropics with 0.19 ppt reaching the UTLS for Ziska+MODERATE. Compared to mixing ratios of 0.16 ppt for Ziska2013, the entrainment of anthropogenic bromoform into the UTLS is 0.04 ppt (0.03 ppt), which is an additional entrainment of 25 % (16 %) for Ziska+MODERATE during DJF (JJA) (Tab. 5.2). The anthropogenic bromoform input from industrial water treatment into the tropical UTLS is estimated as the difference between Ziska+MODERATE (Ziska+LOW) and Ziska2013 relative to the total input of the respective scenario. For the inner tropics, the contribution of anthropogenic bromoform to the UTLS is 4–25 % depending on scenario and season (Ziska+LOW to Ziska+MODERATE).

The efficiency of anthropogenic bromoform to reach the UTLS above 17 km depends on the entrainment region. The anthropogenic bromoform input is not equally distributed as mentioned above, nor is tropical convection equally efficient over different regions. In the region of the northern Indian Ocean around India and the Arabian Peninsula, the vertical profile shows large differences between DJF and JJA (Fig. 5.9). The average mixing ratio in the boundary layer is elevated with 0.60 ppt during DJF, and 0.57 ppt during JJA for

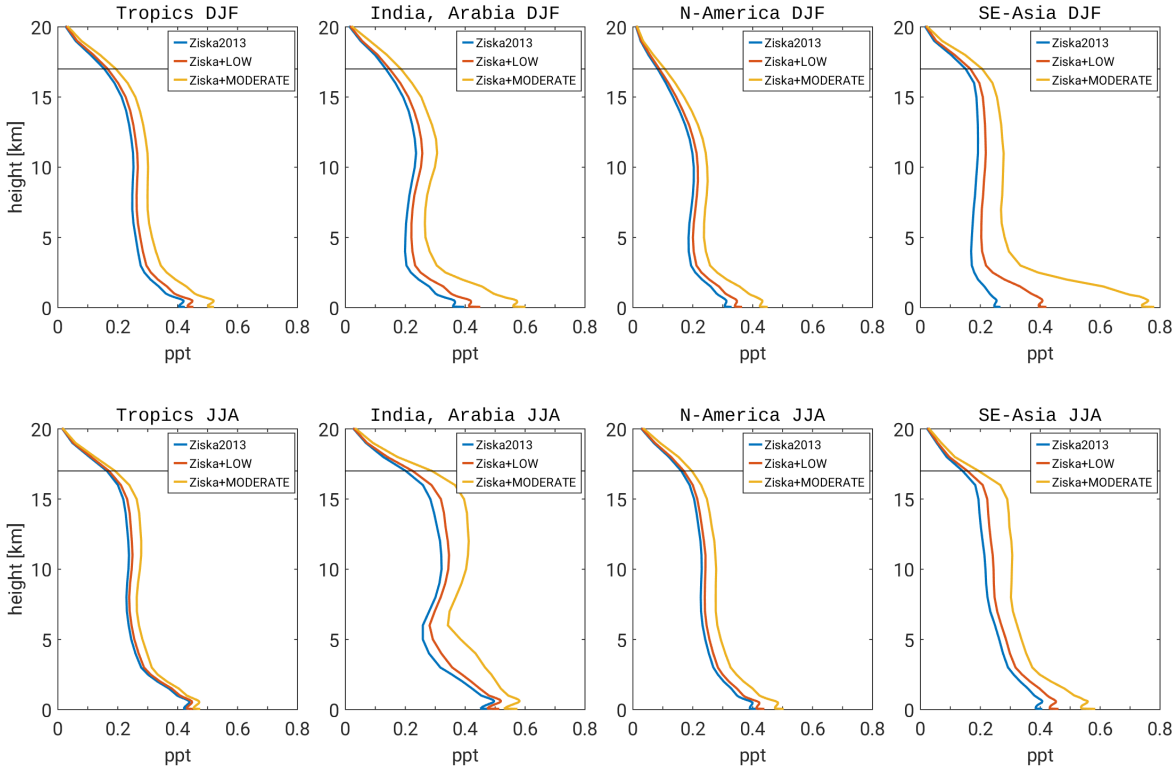

Figure 5.9: Vertical profiles of bromoform mixing ratios [ppt] for the three scenarios Ziska+LOW, Ziska+MODERATE, Ziska2013 averaged over different areas: Global tropics (10° S–10° N), India and Arabia (30° E–90° E, 5° N–20° N), North America (130° W–50° W, 5° N–25° N), and Southeast Asia (95° E–145° E, 0–20° N) for the seasons DJF (top) and JJA (bottom). The black line indicates the 17 km height which is about the height of the tropopause.

Table 5.2: Atmospheric mixing ratios [in ppt] of the FLEXPART simulation in the marine boundary layer at 50 m and in the UTLS at 17 km averaged over the same tropical regions as in Figure 5.9.

		Ziska+LOW		Ziska+MODERATE		Ziska2013	
Region	Height	DJF	JJA	DJF	JJA	DJF	JJA
Tropics	50m	0.449	0.446	0.518	0.471	0.420	0.437
	17km	0.166	0.171	0.194	0.191	0.155	0.164
N America	50m	0.361	0.435	0.446	0.500	0.326	0.412
	17km	0.088	0.170	0.107	0.197	0.083	0.161
Indian Ocean	50m	0.447	0.510	0.598	0.571	0.393	0.487
	17km	0.148	0.225	0.185	0.289	0.135	0.202
E-SE Asia	50m	0.417	0.457	0.777	0.580	0.263	0.403
	17km	0.167	0.157	0.206	0.195	0.151	0.141

Ziska+MODERATE (Tab. 5.2). Above the boundary layer, there is a strong vertical gradient in the transport during DJF and 0.19 ppt reach the UTLS at 17 km.
During JJA, there is strong vertical transport up to 17 km. In the tropical northern Indian Ocean, 0.29 ppt for Ziska+MODERATE reach the UTLS at 17 km. A relative amount of 51 % of bromoform from the marine boundary layer reaches the UTLS, which is the strongest entrainment for the regions displayed here. For all scenarios the stratospheric entrainment is about 41–51 %. The difference between Ziska+MODERATE and Ziska2013 is 0.09 ppt and 0.02 ppt between Ziska+LOW and Ziska2013, which corresponds to additional anthropogenic entrainment of 43 and 10 % at 17 km in JJA.
The only region shown here, where entrainment is stronger during DJF than during JJA, is in Southeast Asia over the Maritime Continent. We find elevated mixing ratios in the marine boundary layer during DJF of 0.78 ppt for Ziska+MODERATE (Tab. 5.2). This is three times stronger than mixing ratios of Ziska2013 corresponding to the anthropogenic increase in the air-sea flux of 320 % in this region.
Bromoform abundances of 0.21 ppt for Ziska+MODERATE reach the UTLS over this region, even though the majority is degraded in the troposphere during DJF. Although vertical transport is not very efficient in Southeast Asia during DJF, together with the northern Indian Ocean, it is the most important region for entrainment of anthropogenic bromoform into the UTLS.

5.6.2 Comparison with observations

Observations of atmospheric bromoform have been done in the marine boundary layer mostly during ship campaigns and in the upper troposphere from aircraft measurements. We now compare the aircraft observations to our simulations in the upper troposphere, since we are most interested in the anthropogenic contribution to the stratospheric bromine

budget. Observations at the sea surface have already been discussed in Chapter 4 (Maas et al., 2020).

Measured aircraft profiles from the global tropics show an average bromoform mixing ratio of 0.19 ppt at the tropopause, ranging between 0.01–0.54 ppt at 17 km (Engel and Rigby, 2018). Our simulations from the inner tropics lie with 0.19 ppt in the global mean for the Ziska+MODERATE simulations and slightly lower with 0.17 and 0.16 ppt for Ziska+LOW and Ziska2013, for both DJF and JJA respectively. Thus, our addition of anthropogenic bromoform to the Ziska2013 bromoform emission estimate has improved the simulation of stratospheric bromoform entrainment in the tropics. However, measurements over specific regions, such as the tropical Pacific find larger mixing ratios of 0.35 ppt in the UTLS than our simulations suggest (Hossaini et al., 2016).

Recently, Feng et al. (2018) compared observations in the West Pacific from aircraft campaigns to chemistry transport model output. Observations of bromoform mixing ratios in the tropical West Pacific are around 1 ppt at the surface to 0.4–0.5 ppt at the maximum altitude of 14 km. Our FLEXPART simulation Ziska+MODERATE gives an average mixing ratio of about 0.3 ppt at 14 km in Southeast Asia (Fig. 5.9). Compared to the 0.2 ppt in the Ziska2013 simulation, the results from Ziska+MODERATE improve the bromoform mixing ratios and emission estimate in this region with respect to the observations.

Other modelling studies, which also use the Ziska2013 inventory, mostly lie around 0.2–0.3 ppt at the UTLS in the West Pacific (Hossaini et al., 2016). Other emission inventories, which are characterised by strong emissions in the tropics (e.g. Liang et al., 2010; Warwick et al., 2006; Ordóñez et al., 2012), tend to overestimate the tropical profile of bromoform transport compared to observations (Hossaini et al., 2013). Other aircraft campaigns over the tropical Pacific showed large observed bromoform mixing ratios of 1–2 ppt between 14–18 km (Navarro et al., 2015). At 17 km, bromoform is around 1 ppt in both the West and East Pacific.

Our FLEXPART simulation Ziska+MODERATE shows an improvement in the tropical transport into the UTLS but still under-estimates the entrainment over the West Pacific and the emissions from Southeast Asia. It is unclear whether these emissions, which result in elevated mixing ratios measured in the tropical upper troposphere of the West Pacific have natural or anthropogenic origin.

5.7 Discussion

In this study, we have investigated additional anthropogenic sources from industrial water treatment and analysed whether these sources are relevant for tropospheric and stratospheric bromine budgets. Combined bromoform emission maps from anthropogenic and climatological air-sea flux estimates for two scenarios (Ziska+LOW and Ziska+MODERATE)

are the source function for atmospheric bromoform simulations. The resulting combined bromoform mixing ratios are compared to the climatological mixing ratios (Ziska2013) which do not include these anthropogenic sources directly due to extreme data sparsity at the coasts.

The atmospheric bromine input increases by 8–35 % compared to the bottom-up emission inventory by Ziska2013 due to the addition of anthropogenic bromoform. Our estimate suggests a total atmospheric bromine input of 1.9–2.2 Gmol Br a^{-1} by bromoform including our anthropogenic emissions from industrial water treatment. This improves the bottom-up emission inventory and reduces the gap between top-down estimates. However, it does not completely explain the difference between top-down and bottom-up emission estimates.

We find that anthropogenic emissions play only a role for large-scale atmospheric transport in the NH and the tropics. From around 0.4–0.5 ppt in the marine boundary layer, about 40–50 % is transported into the UTLS above 17 km in the tropical regions. The anthropogenic contribution to stratospheric bromine entrainment from bromoform source gas is 0.03–0.12 ppt Br in the inner tropics. Compared to the entrainment of 0.47–0.49 ppt Br for the Ziska2013 simulation, the anthropogenic sources bring additional 4–25 % of bromine into the UTLS region.

Considering that about half of the bromine entrainment originates from the source gas injection (Hossaini et al., 2010; Engel and Rigby, 2018), the total bromine contribution of both source gas and product gases from the anthropogenic sources alone is 0.06–0.24 ppt Br, and 1.15 ppt Br for the Ziska+MODERATE simulation. Compared to a total stratospheric bromine estimate from all VSLSs of about 3–7 ppt Br (Engel and Rigby, 2018), the anthropogenic input provides only a minor contribution to stratospheric bromine levels.

It has previously been shown that East-Southeast Asia is a large source of anthropogenic bromoform (Chapter 4). This study confirms that this region contributes more than 50 % to the anthropogenic budget and contributes, next to the northern Indian Ocean, most to bromoform transport into the UTLS. In East-Southeast Asia, there are also the largest differences between the Ziska2013 emission climatology and the anthropogenic emissions. The atmospheric bromoform input from the Ziska+MODERATE emissions increases by 320 % compared to the Ziska2013 emissions (Tab. 5.1). Anthropogenic bromoform from industrial water treatment is highly centred along the coasts of large industrial regions, especially in the NH. The four regions, Europe, North America, India and Arabia, and East-Southeast Asia, comprise over 96 % of anthropogenic bromoform emissions from water treatment. However they are responsible for only 28 % of the emissions in the Ziska2013 climatology.

In Europe, there is strong anthropogenic input into the marine boundary layer but no convective transport into the UTLS region. North America has large sources in the Gulf

of Mexico and anthropogenic sources along the coast north of 30° N especially during JJA. Therefore vertical transport into the UTLS above 17 km is enhanced in JJA.
Around India and Arabia, there are anthropogenic sources along the Persian Gulf and the Arabian Sea. Seasonal variability of vertical transport between DJF and JJA is strongest over the Indian Ocean due to the monsoon circulation (Fiehn et al., 2017). While the Indian winter monsoon advects surface bromoform southward into the Indian Ocean, there is very strong and localised entrainment into the UTLS over the West Indian Ocean. During the Indian summer monsoon, bromoform is transported over the Indian sub-continent where over 50 % reaches the UTLS above 17 km. This corresponds to an additional anthropogenic bromoform input into the UTLS of 10–40 % compared to the climatological background. The region of India and Arabia has the lowest bromoform air-sea flux of the four regions shown here. Due to its tropical location and the influence of monsoon winds, however it is very important in respect of stratospheric bromine entrainment.
There is a clear anthropogenic signal visible in the regions of the NH, in particular in East-Southeast Asia. The addition of the anthropogenic sources lead to the largest increase of atmospheric bromoform abundances compared to the Ziska2013 climatology in this region. Seasonally dependent bromoform emissions could help to improve the convective transport into the stratosphere in models compared to observations (Fiehn et al., 2018). Although the climatological estimate, as well as the assessment of anthropogenic bromoform from seawater treatment contains large uncertainties, including missing bromoform emissions from seawater treatment improves the Ziska2013 bottom-up estimate. Compared to observations of tropical bromoform mixing ratios at the UTLS (e.g. Hossaini et al., 2016; Navarro et al., 2015; Feng et al., 2018), our simulations including anthropogenic emissions, are still lower. On the one hand, this might be from under-estimating the emissions of these regions in the Ziska+anthropogenic simulations. On the other hand, one factor for smaller mixing ratios in the tropical UTLS region, might be the lifetime estimate which stays constant over height in our simulations. We did not apply interactive chemistry but a simplified bromoform chemistry, which only depends on the lifetime.
Additional uncertainties in bromoform mixing ratios arise from the initial concentration in the treated seawater. To some degree, this is displayed in the two scenarios and the large range of the results shown here. Additional measurements of VSLSs in the cooling water effluent of fossil fuel and nuclear power plants could reduce the uncertainty of the anthropogenic source. Regional estimates can be further improved by taking into account the water treatment facilities in desalination plants, of which the majority are located in the Middle East and Arabia. The number of coastal plants in our database is also relatively low compared to population and economies' sizes around the Arabian Sea. The input of cooling water in this region might be higher than assumed here.
The stratospheric ozone layer is predicted to recover by the second half of the 21st century

(Engel and Rigby, 2018). A continuing increase of anthropogenic emission of brominated ozone-depleting substances (ODSs) can alter the stratospheric bromine input and influence future ozone abundances. Therefore, a special focus should be given on the development of anthropogenic sources of bromocarbons.

The atmospheric input of anthropogenic bromoform is directly linked to the industrial activity which depends on economic growth, population size and the demographic development of countries. Therefore, countries with a large growth and an increasing energy demand might lead to a strong increase of power plant activity in the future. The global energy demand is projected to increase annually by 1 % until 2040 (IEA, 2016). However, energy demand in India, Southeast Asia, Middle East and Africa is expected to grow annually by over 2 %. These regions have been shown to be the main location for bromoform entrainment into the UTLS. This implies a rise in cooling water volumes by the same rate as long as electricity generation is mainly based on fossil fuels, which is projected not to change significantly until 2040 (IEA, 2016). Moreover, the implementation of ballast water treatment can become an additional local source of anthropogenic bromoform to the atmosphere over the next years (Maas et al., 2019).

With the results presented here, we improved the bottom-up emission estimate by Ziska2013 including missing anthropogenic sources, especially in East-Southeast Asia. We show that additional bromoform sources from seawater treatment are a relevant factor for the whole budget which is continuing to increase over the next years. It is uncertain if a continuing anthropogenic increase of brominated VSLSs can have an influence on the stratospheric ozone layer. Additional observations are necessary to minimise the uncertainties of anthropogenic bromoform in the ocean and atmosphere.

6 Conclusion and outlook

The aim of my thesis was to derive the first detailed estimate of anthropogenic sources of brominated VSLSs from industrial water treatment and to quantify their contribution to tropospheric and stratospheric bromine. The focus lay on bromoform, which is both the main DBP from industrial water treatment, as well as the major contributor of organic bromine to the atmosphere from both natural and anthropogenic sources. Due to its short lifetime in the lower atmosphere of around two-weeks, bromoform entrainment into the stratosphere occurs only via deep convective events close to the oceanic sources. Once in the stratosphere, bromoform releases the halogen radicals, which deplete ozone through catalytic cycles. Thus, the ozone depletion potential of bromoform strongly depends on time and location of its emission into the atmosphere. The quantification of anthropogenic bromoform sources is important for assessing their impact on stratospheric ozone levels. In the scope of this thesis, three research questions were addressed (Chapter 1.3), which are answered in the following by summarising my findings:

1. **Will treated ballast water from ships become an additional and relevant source of brominated VSLSs to the atmosphere?**
   Ballast water treatment is now required on-board ships after the ratification of the BWM Convention in 2017. Chemical ballast water treatment produces large amounts of DBPs and mainly bromoform. Here, I quantified this new source of bromoform and its emission from the ocean to the atmosphere.
   My analysis reveals that ballast water treatment will have no substantial impact on the amount of brominated VSLSs in the atmosphere. Global ballast water discharge volumes were quantified to be 3.4 billion $m^3\,a^{-1}$. The global bromine input by bromoform from treated ballast water was estimated to be 3–13 Mmol Br a^{-1}, which is negligible compared to current global emission estimates of 2–10 Gmol Br a^{-1} (Tab. 1.1). However, bromoform concentration in treated ballast water was measured to be about 890 ± 560 nmol L^{-1}, which is up to 10^5 times higher compared to average concentrations of 10–20 pmol L^{-1} in coastal waters. Bromoform as the dominant DBP in treated ballast water serves as a representative parameter to assess the impact of ballast water in the ocean and atmosphere. The discharge of bromoform leads to an inhomogeneous distribution, mainly around large harbours in Southeast Asia where over 57 % of the global shipping industry is located. The local to regional impact of this source was analysed with a modelling study in the surface ocean. While

non-volatile DBPs in the ballast water spread widely along the coast, bromoform is quickly outgassed into the atmosphere upon discharge. Ballast water is found to be a strong point source of bromoform with an air-sea flux up to 3500 pmol m^{-2} h^{-1}, while the coastal air-sea flux usually ranges between 500 and 1500 pmol m^{-2} h^{-1} in climatological inventories. Hence, it is to be expected that ballast water treatment can increase local abundances of brominated VSLSs in the upcoming years.

2. **How strong is the air-sea flux of bromoform produced from power plant cooling water treatment in comparison to recent bottom-up estimates?**
In contrast to ballast water, cooling water treatment in coastal power plants is a well-established technique. Therefore, the separation between anthropogenic and natural bromoform emissions is not possible based on available measurements. In order to identify the anthropogenic contribution from cooling water treatment, I quantified the water volumes and the bromoform concentration in analogy to the ballast water. I derived a global estimate of coastal cooling water use of over 800 billion m^3 a^{-1}, which is about 240 times higher than ballast water volumes. Concentrations of bromoform in cooling water were estimated to range from 80–240 nmol L^{-1}. Hence, global bromine input of bromoform from cooling water treatment ranges between 200–600 Mmol Br a^{-1}.
The global bromine flux of a recent bromoform bottom-up emission inventory based on observations was estimated to be 1.7 Gmol Br a^{-1} (Ziska et al., 2013). So far, most of the anthropogenic bromoform from cooling water treatment has not been included in existing emission estimates due to gaps in measurements. Incorporating the anthropogenic bromoform from industrial water treatment into the climatological bottom-up emission estimate leads to a global bromine flux of 1.9–2.2 Gmol Br a^{-1} (i.e. 156–188 Gg $CHBr_3$ a^{-1}). The novel anthropogenic sources increase the global bromine input by 8–35 %. The global anthropogenic bromine flux is mainly determined by bromoform produced from cooling water treatment. Including the bromine flux from ballast water treatment does not change the estimate given here.
The anthropogenic sources are inhomogeneously distributed, and very high emissions concentrate over relatively small areas along the coasts (Fig. 6.1). Over 96 % of anthropogenic bromoform is released into the atmosphere around Europe, East-Southeast Asia, the northern Indian Ocean, and North America. European coastal power plants produce about one quarter of the anthropogenic bromoform in this estimate. About half of the anthropogenic bromoform emissions originate from industrial water treatment in East-Southeast Asia, which is thus the most important region for anthropogenic emissions to the atmosphere. In this region, anthropogenic bromoform leads to the most pronounced increase of the bottom-up air-sea flux inventory by 98–320 % (Tab. 5.1, Fig. 6.1).

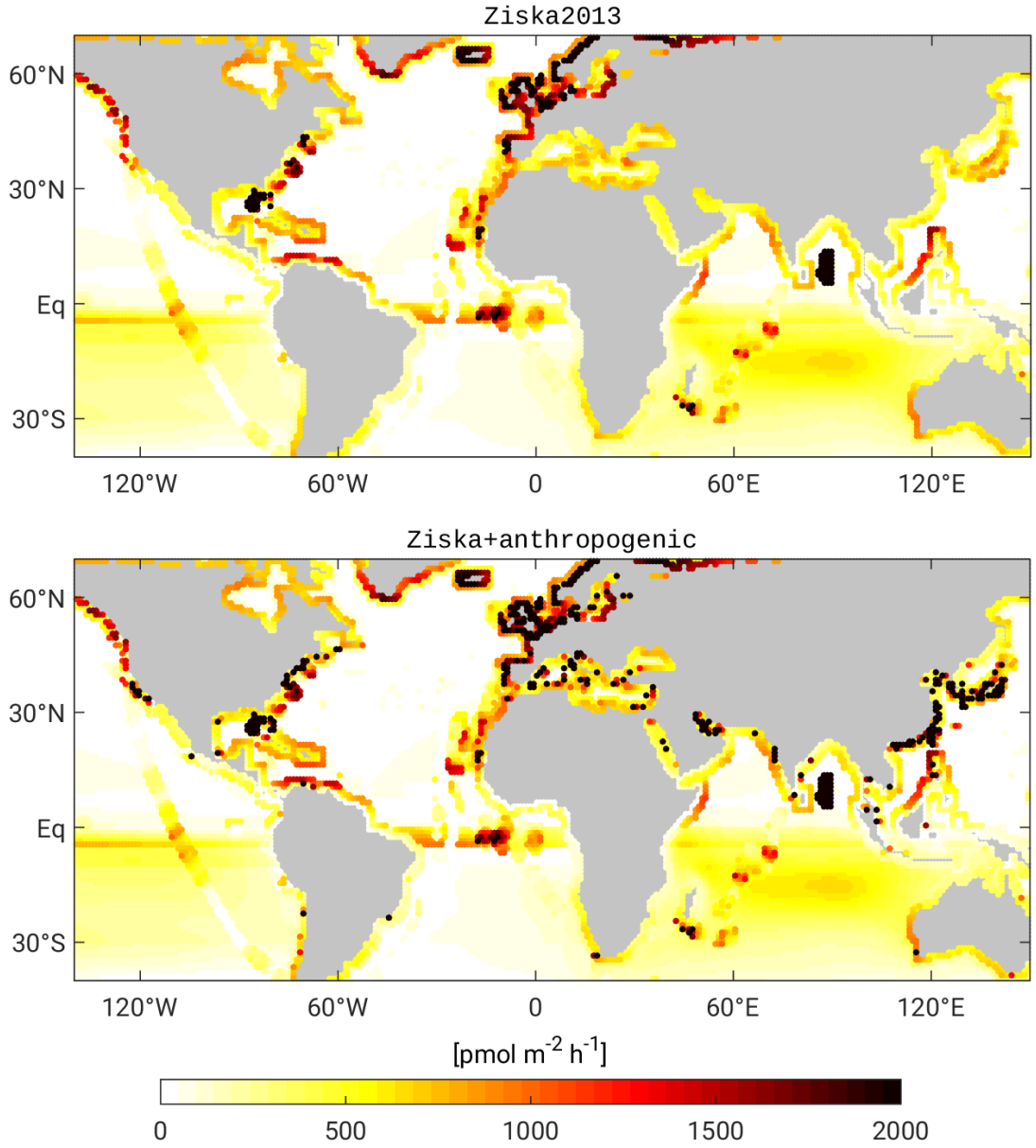

Figure 6.1: (Upper panel) Global distribution of bromoform air-sea flux [pmol m^{-2} h^{-1}] from a bottom-up estimate (updated from Ziska et al., 2013), and (lower panel) the same air-sea flux combined with anthropogenic emissions (Chapter 5.2.2).

3. **What is the contribution of anthropogenic bromoform from industrial water treatment to stratospheric bromine entrainment?**
   Due to the short lifetime of bromoform, an effective transport into the stratosphere mainly takes place in the convective areas of the tropics. In the tropical marine boundary layer, global bromoform emissions including anthropogenic sources lead to an average bromine mixing ratio of 1.2–1.5 ppt Br, of which around 40 % are transported above 17 km into the UTLS. The stratospheric bromine from anthropogenic bromoform source and product gases is estimated to be 0.06–0.24 ppt Br, of which half is added as product gas injection. The anthropogenic bromoform

from industrial water treatment contributes about 4–25 % to stratospheric bromine entrainment depending on season and scenario compared to the bottom-up based entrainment. However, in comparison to the total stratospheric bromine inventory from all VSLSs of about 3–7 ppt Br, the contribution of anthropogenic bromoform is rather small.

The tropical West Pacific and the Indian Ocean have been identified as the most efficient regions for stratospheric entrainment of bromoform. Transport over the northern Indian Ocean is influenced by the Indian monsoon circulation with strong seasonal variations. During the Indian summer monsoon, transport into the stratosphere is strongest with a bromoform entrainment of over 50 % from the marine boundary layer to the UTLS, of which 10–43 % are of anthropogenic origin.

Highest mixing ratios in the marine boundary layer are found in East Asia. However, the majority of the anthropogenic bromoform emission occurs outside of the tropics along the Yellow, Japan and East China Seas. My simulations reveal strong seasonal differences of VSLS transport towards the convective regions in the tropics. Stratospheric entrainment is enhanced during boreal winter, when northeasterly winds bring large anthropogenic bromoform abundances from the East Asian coast towards the convective region over the Maritime Continent and West Pacific. About 20 % of this anthropogenic bromoform is entrained into the stratosphere. In contrast, the high emissions along the European coast are not relevant for source gas injection into the stratosphere, since they are too remote from the deep convective regions in the tropics.

My analyses show, that entrainment of anthropogenic bromoform is most effective during boreal summer over the northern Indian Ocean, and during boreal winter over the West Pacific and the Maritime Continent. However, in most cases the industrial sources do not occur close to strong convection areas, so that the majority of up to 90 % of globally emitted anthropogenic bromoform does not reach the stratosphere but is degraded in the troposphere.

The assessment of anthropogenic bromoform from industrial water treatment in this thesis was realised based on current climate conditions and the present state of global industry. Many factors that determine the production, emissions, and transport of brominated VSLSs will change in the future.

Industrial growth in terms of global energy demand is projected to increase anually by 1 % until 2040 (IEA, 2016). Global economies are continuing to grow, resulting in an increased use of seawater for cooling purpose and in the shipping industry. As long as energy generation depends on coal, oil and nuclear power, the demand for industrial cooling water will likewise increase, alongside the anthropogenic emissions of VSLSs and other DBPs. For some regions the energy demand is expected to increase above average by 2 % per year, such as India, the Maritime Continent and Africa (IEA, 2016). My results

demonstrate that these regions are also most important for entrainment of VSLSs into the stratosphere, which will make the increasing emissions particularly important for the stratospheric bromine budget.

In consequence of global warming and growing populations, desalination will become more important in the course of the 21st century as tropical expansion is expected to cause a decline of freshwater sources in tropical and subtropical regions (Seidel et al., 2008). Currently, the Arabian Peninsula and the Middle East are the main regions where desalination is in use but expansion into other regions is predicted (Sowers et al., 2011). Desalination has not been included in this thesis but the expected growing importance of the sector strongly motivates to include future VSLS emissions from water treatment in desalination plants in follow-up studies.

Apart from economic challenges, climate change will also have environmental effects influencing generation, transport and degradation of VSLSs over the next decades. The marine environment and atmospheric processes will face many changes under global warming. Formation rate of brominated VSLSs in the ocean depends amongst other things on water temperature and nutrients (Quack et al., 2004), while the air-sea flux of VSLSs is driven by wind stress (Wanninkhof, 1992). All of these factors are sensitive to climate change. Air-sea flux of VSLSs is predicted to increase under future climate change scenarios due to an increase in SST and stronger winds, even when surface concentrations of VSLSs are considered to stay constant (Ziska et al., 2017). Moreover, the rise of atmospheric temperatures, as well as stronger convection associated with climate change, will lead to an enhanced impact of VSLSs on ozone in the troposphere and stratosphere (Hossaini et al., 2012; Salawitch, 2006). Changes in circulation patterns are predicted for both troposphere and stratosphere, which can alter both distributions of ODSs, as well as ozone (Dessens et al., 2009). The tropospheric lifetime of brominated VSLSs can also be altered due to changes in OH, which can have either a positive or negative trend for different climate change scenarios (Hossaini et al., 2012). Furthermore, the influence of brominated VSLSs on the stratospheric ozone depends on chlorine levels (Yang et al., 2015). Recent evidence of increasing emissions of chlorinated ODSs in East Asia (Montzka et al., 2018) could slow down the decline of stratospheric chlorine abundances.

Nevertheless, long-lived ODSs are projected to decrease accompanied by a recovery of the global ozone layer, thus VSLSs will become more important for stratospheric chemistry (Engel and Rigby, 2018). A rise of anthropogenic VSLSs from industrial water treatment in addition to increasing convective transport could eventually affect the recovery of the stratospheric ozone layer. The quantification of anthropogenic emissions and individual sources of VSLSs presented in this thesis is an important step towards understanding the full impact of anthropogenic halogens on the atmosphere. To ensure a full recovery of the stratospheric ozone layer, it is likewise important to monitor both ozone, as well as the development of ODSs, which includes the VSLSs and their here identified sources.

Acronyms

AAPA	American Association of Port Authorities
BWM	Ballast Water Management
BWTS	ballast water treatment system
CFC	chlorofluorocarbon
DBP	disinfection by-product
DJF	boreal winter
DMS	dimethyl sulfide
DOM	dissolved organic matter
DWT	dead weight tonnage
GC-MS	gas chromatograph-mass spectrometer
GHG	greenhouse gas
GESAMP-BWWG	Joint Group of Experts on the Scientific Aspects of the Marine Environmental Protection - Ballast Water Working Group
HCFC	hydrogenated chlorofluorocarbon
IMO	International Maritime Organization
ITCZ	Intertropical Convergence Zone
JJA	boreal summer
MAM	boreal spring
MEPC	Marine Environment Protection Committee
MLD	mixed layer depth
NH	northern hemisphere
ODS	ozone-depleting substance
OGCM	ocean general circulation model
PRD	Pearl River Delta

SH	southern hemisphere
SON	boreal autumn
SST	sea surface temperature
TEU	twenty-foot equivalent unit
THM	trihalomethane
UTLS	upper troposphere/lower stratosphere
UV	ultraviolet
VSLS	very short-lived substance
WHO	World Health Organisation

List of Chemicals

$\mathbf{BrO_3^-}$	bromate
BrO	hypobromite
$\mathbf{BrNO_2}$	nitryl bromide
ClO	hypochlorite
$\mathbf{CBr_2O}$	carbonyl bromide
CHBrO	formyl bromide
$\mathbf{CH_3Br}$	methyl bromide
$\mathbf{CHBr_3}$	bromoform
$\mathbf{CH_2Br_2}$	dibromomethane
$\mathbf{Cl_2}$	molecular chlorine
$\mathbf{H_2O_2}$	hydrogen peroxide
HOBr	hypobromous acid
HOCl	hypochlorous acid
$\mathbf{N_2}$	molecular nitrogen
NaOCl	sodium hypochlorite
$\mathbf{O_2}$	molecular oxygen
$\mathbf{O_3}$	ozone
OH	hydroxyl radical

List of Figures

List of Tables

Bibliography

The bibliography covers references for Chapters 1, 2, 5 and 6. Chapters 3–4 have their own references included at the end of the respective chapter.

AAPA (2016). Port Industry Statistics: World Port Rankings 2016. *American Association of Port Authorities*, (http://www.aapa-ports.org/unifying/content.aspx?ItemNumber=21048):last access: 28.09.2019.

Allonier, A.-S., Khalanski, M., Camel, V., and Bermond, A. (1999). Characterization of Chlorination By-products in Cooling Effluents of Coastal Nuclear Power Stations. *Marine Pollution Bulletin*, 38(12):1232–1241.

Aschmann, J., Sinnhuber, B.-M., Atlas, E. L., and Schauffler, S. M. (2009). Modeling the transport of very short-lived substances into the tropical upper troposphere and lower stratosphere. *Atmospheric Chemistry and Physics*, 9(23):9237–9247.

Blanke, B., Arhan, M., Madec, G., and Roche, S. (1999). Warm Water Paths in the Equatorial Atlantic as Diagnosed with a General Circulation Model. *Journal of Physical Oceanography*, 29(11):2753–2768.

Boudjellaba, D., Dron, J., Revenko, G., Démelas, C., and Boudenne, J.-L. (2016). Chlorination by-product concentration levels in seawater and fish of an industrialised bay (Gulf of Fos, France) exposed to multiple chlorinated effluents. *Science of The Total Environment*, 541:391–399.

Brioude, J., Portmann, R. W., Daniel, J. S., Cooper, O. R., Frost, G. J., Rosenlof, K. H., Granier, C., Ravishankara, A. R., Montzka, S. A., and Stohl, A. (2010). Variations in ozone depletion potentials of very short-lived substances with season and emission region. *Geophysical Research Letters*, 37(19):n/a–n/a.

Briski, E., Ghabooli, S., Bailey, S. A., and MacIsaac, H. J. (2012). Invasion risk posed by macroinvertebrates transported in ships' ballast tanks. *Biological Invasions*, 14(9):1843–1850.

Butler, J. H., King, D. B., Lobert, J. M., Montzka, S. A., Yvon-Lewis, S. A., Hall, B. D., Warwick, N. J., Mondeel, D. J., Aydin, M., and Elkins, J. W. (2007). Oceanic distributions and emissions of short-lived halocarbons. *Global Biogeochemical Cycles*, 21(1):GB1023.

Carpenter, L. J. and Liss, P. S. (2000). On temperate sources of bromoform and other reactive organic bromine gases. *Journal of Geophysical Research: Atmospheres*, 105(D16):20539–20547.

Carpenter, L. J., Reimann, S., (Lead Authors), Burkholder, J. B., Clerbaux, C., Hall, B. D., Hossaini, R., Laube, J. C., and Yvon-Lews, S. A. (2014). Update on Ozone-Depleting Substances (ODSs) and Other Gases of Interest to the Montreal Protocol.

Chapter 1 in Scientific Assessment of Ozone Depletion: 2014, (Global Ozone Research and Monitoring Project-Report No. 55):World Meteorological Organization, Geneva, Switzer.

David, M. (2015). Vessels and Ballast Water. In David, M. and Gollasch, S., editors, *Global Maritime Transport and Ballast Water Management*, number Invading Nature - Springer Series in Invasion Ecology 8, chapter 2, pages 13–34. Springer Netherlands, Dordrecht.

David, M. and Gollasch, S. (2015). Ballast Water Management Systems for Vessels. In *Global Maritime Transport and Ballast Water Management*, number Invading Nature - Springer Series in Invasion Ecology 8, pages 109–132. Springer Netherlands, Dordrecht.

Dee, D. P., Uppala, S. M., Simmons, A. J., Berrisford, P., Poli, P., Kobayashi, S., Andrae, U., Balmaseda, M. A., Balsamo, G., Bauer, P., Bechtold, P., Beljaars, A. C. M., van de Berg, L., Bidlot, J., Bormann, N., Delsol, C., Dragani, R., Fuentes, M., Geer, A. J., Haimberger, L., Healy, S. B., Hersbach, H., Hólm, E. V., Isaksen, L., Kållberg, P., Köhler, M., Matricardi, M., McNally, A. P., Monge-Sanz, B. M., Morcrette, J.-J., Park, B.-K., Peubey, C., de Rosnay, P., Tavolato, C., Thépaut, J.-N., and Vitart, F. (2011). The ERA-Interim reanalysis: configuration and performance of the data assimilation system. *Quarterly Journal of the Royal Meteorological Society*, 137(656):553–597.

Delacroix, S., Vogelsang, C., Tobiesen, A., and Liltved, H. (2013). Disinfection by-products and ecotoxicity of ballast water after oxidative treatment – Results and experiences from seven years of full-scale testing of ballast water management systems. *Marine Pollution Bulletin*, 73(1):24–36.

Dessens, O., Zeng, G., Warwick, N., and Pyle, J. (2009). Short-lived bromine compounds in the lower stratosphere; impact of climate change on ozone. *Atmospheric Science Letters*, 10(3):201–206.

Durgadoo, J. V., Ruehs, S., Biastoch, A., and Boening, C. W. B. (2017). Indian Ocean sources of Agulhas leakage. *Journal of Geophysical Research: Oceans*, 122:1–19.

Dussin, R., Barnier, B., Brodeau, L., and Molines, J. M. (2016). The Making Of the DRAKKAR FORCING SET DFS5. *DRAKKAR/MyOcean Report 01-04-16*, 2016(April):1–34.

Endresen, Ø., Lee Behrens, H., Brynestad, S., Bjørn Andersen, A., and Skjong, R. (2004). Challenges in global ballast water management. *Marine Pollution Bulletin*, 48(7-8):615–623.

Engel, A., Rigby, M. (Lead Authors), Burkholder, J. B., Fernandez, R. P., Froidevaux, L., Hall, B. D., Hossaini, R., Saito, T., Vollmer, M. K., and Yao, B. (2018). Update on Ozone-Depleting Substances (ODSs) and Other Gases of Interest to the Montreal Protocol, Chapter 1. In *Scientific Assessment of Ozone Depletion: 2018, Global Ozone Research and Monitoring Project – Report No. 58.*

Feng, L., Palmer, P. I., Butler, R., Andrews, S. J., Atlas, E. L., Carpenter, L. J., Donets, V., Harris, N. R. P., Salawitch, R. J., Pan, L. L., and Schauffler, S. M. (2018). Surface fluxes of bromoform and dibromomethane over the tropical western Pacific inferred from

airborne in situ measurements. *Atmospheric Chemistry and Physics*, 18(20):14787–14798.

Fernandez, R. P., Kinnison, D. E., Lamarque, J.-F., Tilmes, S., and Saiz-Lopez, A. (2017). Impact of biogenic very short-lived bromine on the Antarctic ozone hole during the 21st century. *Atmospheric Chemistry and Physics*, 17(3):1673–1688.

Fiehn, A., Quack, B., Hepach, H., Fuhlbrügge, S., Tegtmeier, S., Toohey, M., Atlas, E., and Krüger, K. (2017). Delivery of halogenated very short-lived substances from the west Indian Ocean to the stratosphere during the Asian summer monsoon. *Atmospheric Chemistry and Physics*, 17(11):6723–6741.

Fiehn, A., Quack, B., Stemmler, I., Ziska, F., and Krüger, K. (2018). Importance of seasonally resolved oceanic emissions for bromoform delivery from the tropical Indian Ocean and west Pacific to the stratosphere. *Atmospheric Chemistry and Physics*, 18(16):11973–11990.

Fogelqvist, E. and Krysell, M. (1991). Naturally and anthropogenically produced bromoform in the Kattegatt, a semi-enclosed oceanic basin. *Journal of Atmospheric Chemistry*, 13(4):315–324.

Fuhlbrügge, S., Quack, B., Atlas, E., Fiehn, A., Hepach, H., and Krüger, K. (2016). Meteorological constraints on oceanic halocarbons above the Peruvian upwelling. *Atmospheric Chemistry and Physics*, 16(18):12205–12217.

Geigert, J. and Neidleman, S. L. (1986). *Biohalogenation: principles, basic roles and applications*. New York, Ellis Horwood Limited.

GloBallast (2013). Identifying and Managing Risks from Organisms Carried in Ships ' Ballast Water. *GEF-UNDP-IMO GloBallast Partnerships, London, UK and WMU, Malmö, Sweden.*, GloBallast(No. 21).

He, Z., Yang, G.-P., Lu, X.-L., and Zhang, H.-H. (2013). Distributions and sea-to-air fluxes of chloroform, trichloroethylene, tetrachloroethylene, chlorodibromomethane and bromoform in the Yellow Sea and the East China Sea during spring. *Environmental Pollution*, 177:28–37.

Hegglin, M. I. (2018). Evidence of illegal emissions of ozone-depleting chemicals. *Nature*, 557(7705):317–318.

Hegglin, M. I. L. A., Fahey, D. W., McFarland, M., Montzka, S. A., and Nash, E. R. (2015). Twenty Questions and Answers About the Ozone Layer: 2014 Update. Technical report.

Hense, I. and Quack, B. (2009). Modelling the vertical distribution of bromoform in the upper water column of the tropical Atlantic Ocean. *Biogeosciences*, 6:535–544.

Hossaini, R., Chipperfield, M. P., Dhomse, S., Ordóñez, C., Saiz-Lopez, A., Abraham, N. L., Archibald, A., Braesicke, P., Telford, P., Warwick, N., Yang, X., Pyle, J., Saiz-Lopez, A., Abraham, N. L., Archibald, A., Braesicke, P., Telford, P., Warwick, N., Yang, X., and Pyle, J. (2012). Modelling future changes to the stratospheric source gas injection of biogenic bromocarbons. *Geophysical Research Letters*, 39(20):2012GL053401.

Hossaini, R., Chipperfield, M. P., Monge-Sanz, B. M., Richards, N. a. D., Atlas, E., and Blake, D. R. (2010). Bromoform and dibromomethane in the tropics: a 3-D model study of chemistry and transport. *Atmospheric Chemistry and Physics*, 10:719–735.

Hossaini, R., Chipperfield, M. P., Montzka, S. A., Rap, A., Dhomse, S., and Feng, W. (2015). Efficiency of short-lived halogens at influencing climate through depletion of stratospheric ozone. *Nature Geoscience*, 8(3):186–190.

Hossaini, R., Mantle, H., Chipperfield, M. P., Montzka, S. A., Hamer, P., Ziska, F., Quack, B., Krüger, K., Tegtmeier, S., Atlas, E., Sala, S., Engel, A., Bönisch, H., Keber, T., Oram, D., Mills, G., Ordóñez, C., Saiz-Lopez, A., Warwick, N., Liang, Q., Feng, W., Moore, F., Miller, B. R., Marécal, V., Richards, N. A., Dorf, M., and Pfeilsticker, K. (2013). Evaluating global emission inventories of biogenic bromocarbons. *Atmospheric Chemistry and Physics*, 13(23):11819–11838.

Hossaini, R., Patra, P. K., Leeson, A. A., Krysztofiak, G., Abraham, N. L., Andrews, S. J., Archibald, A. T., Aschmann, J., Atlas, E. L., Belikov, D. A., Bönisch, H., Carpenter, L. J., Dhomse, S., Dorf, M., Engel, A., Feng, W., Fuhlbrügge, S., Griffiths, P. T., Harris, N. R., Hommel, R., Keber, T., Krüger, K., Lennartz, S. T., Maksyutov, S., Mantle, H., Mills, G. P., Miller, B., Montzka, S. A., Moore, F., Navarro, M. A., Oram, D. E., Pfeilsticker, K., Pyle, J. A., Quack, B., Robinson, A. D., Saikawa, E., Saiz-Lopez, A., Sala, S., Sinnhuber, B. M., Taguchi, S., Tegtmeier, S., Lidster, R. T., Wilson, C., and Ziska, F. (2016). A multi-model intercomparison of halogenated very short-lived substances (TransCom-VSLS): Linking oceanic emissions and tropospheric transport for a reconciled estimate of the stratospheric source gas injection of bromine. *Atmospheric Chemistry and Physics*, 16(14):9163–9187.

IEA (2016). World Energy Outlook 2016. *International Energy Agency*.

IEA (2018). Key world energy statistics 2018. *International Energy Agency*.

IMO (2004). International Convention for the Control and Management of Ships' Ballast Water and Sediments. In *BWM/CONF/36*, pages 1–38.

Jacob, D. J. (1999). *Introduction to atmospheric chemistry*. Princeton University Press.

Jenner, H., Taylor, C., van Donk, M., and Khalanski, M. (1997). Chlorination by-products in chlorinated cooling water of some European coastal power stations. *Marine Environmental Research*, 43(4):279–293.

Jenner, H. A., Whitehouse, J. W., Taylor, C. J. L., and Khalanski, M. (1998). Cooling water management in European power stations Biology and control of fouling.\rBiologie et contrôle des salissures dans les circuits de refroidissement des centrales thermiques européennes. *Resources and Energy*.

Joint Research Council (2001). Integrated Pollution Prevention and Control (IPPC) Reference Document on the application of Best Available Techniques to Industrial Cooling Systems. *European Commission*, (December):335.

Jones, E., Qadir, M., van Vliet, M. T., Smakhtin, V., and Kang, S.-m. (2019). The state of desalination and brine production: A global outlook. *Science of The Total Environment*, 657:1343–1356.

Khalanski, M. and Jenner, H. A. (2012). Chlorination Chemistry and Ecotoxicology of the Marine Cooling Water Systems in: Operational and Environmental Consequences of Large Industrial Cooling Water Systems, Ch. 9. *Springer*.

Liang, Q., Stolarski, R. S., Kawa, S. R., Nielsen, J. E., Douglass, A. R., Rodriguez, J. M., Blake, D. R., Atlas, E. L., and Ott, L. E. (2010). Finding the missing stratospheric Bry: A global modeling study of CHBr3 and CH2Br2. *Atmospheric Chemistry and Physics*, 10(5):2269–2286.

Liu, Y., Yvon-Lewis, S. A., Hu, L., Salisbury, J. E., and O'Hern, J. E. (2011). CHBr 3 , CH 2 Br 2 , and CHClBr 2 in U.S. coastal waters during the Gulf of Mexico and East Coast Carbon cruise. *Journal of Geophysical Research*, 116(C10):C10004.

Liu, Z., Wang, X., Luo, Z., Huo, M., Wu, J., Huo, H., and Yang, W. (2015). Removing of Disinfection By-Product Precursors from Surface Water by Using Magnetic Graphene Oxide. *PLOS ONE*, 10(12):e0143819.

Maas, J., Jia, Y., Quack, B., Durgadoo, J. V., Biastoch, A., and Tegtmeier, S. (2020). Simulations of anthropogenic bromoform reveal high emissions at the coast of East Asia. Submitted to:. *Atmospheric Chemistry and Physics Discussions*, acp-2019-1004 (in review).

Maas, J., Tegtmeier, S., Quack, B., Biastoch, A., Durgadoo, J. V., Rühs, S., Gollasch, S., and David, M. (2019). Simulating the spread of disinfection by-products and anthropogenic bromoform emissions from ballast water discharge in Southeast Asia. *Ocean Science*, 15(4):891–904.

Madec, G. and the NEMO Team (2008). NEMO ocean engine. *Note du Pôle de modélisation de l'Institut Pierre-Simon Laplace No 27*, (27).

Maritime Impact (2017). Treat Her Right. 18-19(https://issuu. com/dnvgl/docs/dnv_-gl_maritime_impact_01-2017):last access: 28 September 2019.

Marzocchi, A., Hirschi, J. J., Holliday, N. P., Cunningham, S. A., Blaker, A. T., and Coward, A. C. (2015). The North Atlantic subpolar circulation in an eddy-resolving global ocean model. *Journal of Marine Systems*, 142:126–143.

MEPC 57/21 (2008). Procedure for Approval of Ballast Water Management Systems That Make Use of Active Substances (G9). *IMO*, 169(57):1–15.

Montzka, S. and Reimann, S. (2010). Ozone-Depleting Substances (ODSs) and Related Chemicals. *Scientific Assessment of Ozone Depletion: 2010*, Chapter 1:1–108.

Montzka, S. A., Dutton, G. S., Yu, P., Ray, E., Portmann, R. W., Daniel, J. S., Kuijpers, L., Hall, B. D., Mondeel, D., Siso, C., Nance, J. D., Rigby, M., Manning, A. J., Hu, L., Moore, F., Miller, B. R., and Elkins, J. W. (2018). An unexpected and persistent increase in global emissions of ozone-depleting CFC-11. *Nature*.

Moore, R. M., Webb, M., Tokarczyk, R., and Wever, R. (1996). Bromoperoxidase and iodoperoxidase enzymes and production of halogenated methanes in marine diatom cultures. *Journal of Geophysical Research C: Oceans*, 101(C9):20899–20908.

Nadzir, M. S. M., Phang, S. M., Abas, M. R., Abdul Rahman, N., Abu Samah, A., Sturges, W. T., Oram, D. E., Mills, G. P., Leedham, E. C., Pyle, J. A., Harris, N. R. P., Robinson, A. D., Ashfold, M. J., Mead, M. I., Latif, M. T., Khan, M. F., Amiruddin, A. M., Banan, N., and Hanafiah, M. M. (2014). Bromocarbons in the tropical coastal and open ocean atmosphere during the 2009 Prime Expedition Scientific Cruise (PESC-09). *Atmospheric Chemistry and Physics*, 14(15):8137–8148.

Navarro, M. A., Atlas, E. L., Saiz-Lopez, A., Rodriguez-Lloveras, X., Kinnison, D. E., Lamarque, J.-F., Tilmes, S., Filus, M., Harris, N. R. P., Meneguz, E., Ashfold, M. J., Manning, A. J., Cuevas, C. A., Schauffler, S. M., and Donets, V. (2015). Airborne measurements of organic bromine compounds in the Pacific tropical tropopause layer. *Proceedings of the National Academy of Sciences*, 112(45):13789–13793.

Nightingale, D., Malin, G., Law, C. S., Watson, A. J., Liss, P. S., Liddicoat, M. I., Boutin, J., and Upstill-Goddard, R. C. (2000). In situ evaluation of air-sea gas exchange parameterizations using novel conservative and volatile tracers. *Global Biogeochemical Cycles*, 14(1):373–387.

Ordóñez, C., Lamarque, J.-F., Tilmes, S., Kinnison, D. E., Atlas, E. L., Blake, D. R., Sousa Santos, G., Brasseur, G., and Saiz-Lopez, A. (2012). Bromine and iodine chemistry in a global chemistry-climate model: description and evaluation of very short-lived oceanic sources. *Atmospheric Chemistry and Physics*, 12(3):1423–1447.

Padhi, R. K., Subramanian, S., Mohanty, A. K., Bramha, S. N., Prasad, M. V. R., and Satpathy, K. K. (2012). Trihalomethanes in the Cooling Discharge of a Power Plant on Chlorination of Intake Seawater. *Environmental Engineering Research*, 17(S1):57–62.

Pyle, J. A., Ashfold, M. J., Harris, N. R. P., Robinson, A. D., Warwick, N. J., Carver, G. D., Gostlow, B., O'Brien, L. M., Manning, A. J., Phang, S. M., Yong, S. E., Leong, K. P., Ung, E. H., and Ong, S. (2011). Bromoform in the tropical boundary layer of the Maritime Continent during OP3. *Atmospheric Chemistry and Physics*, 11(2):529–542.

Quack, B., Atlas, E., Petrick, G., Stroud, V., Schauffler, S., and Wallace, D. W. R. (2004). Oceanic bromoform sources for the tropical atmosphere. *Geophysical Research Letters*, 31(23):1–4.

Quack, B. and Wallace, D. W. R. (2003). Air-sea flux of bromoform: Controls, rates, and implications. *Global Biogeochemical Cycles*, 17(1):1023.

Rajagopal, S., Jenner, H. A., and Venugopalan, V. P. (2012). *Operational and Environmental Consequences of Large Industrial Cooling Water Systems*. Springer US, Boston, MA.

Rajamohan, R., Vinnitha, E., Venugopalan, V. P., and Narasimhan, S. V. (2007). Chlorination by-products and their discharge from the cooling water system of a coastal electric plant. *Current Science*, 93(11):1608–1612.

Richardson, S. D., Plewa, M. J., Wagner, E. D., Schoeny, R., and DeMarini, D. M. (2007). Occurrence, genotoxicity, and carcinogenicity of regulated and emerging disinfection by-products in drinking water: A review and roadmap for research.

Rigby, M., Park, S., Saito, T., Western, L. M., Redington, A. L., Fang, X., Henne, S., Manning, A. J., Prinn, R. G., Dutton, G. S., Fraser, P. J., Ganesan, A. L., Hall, B. D., Harth, C. M., Kim, J., Kim, K.-R., Krummel, P. B., Lee, T., Li, S., Liang, Q., Lunt, M. F., Montzka, S. A., Mühle, J., O'Doherty, S., Park, M.-K., Reimann, S., Salameh, P. K., Simmonds, P., Tunnicliffe, R. L., Weiss, R. F., Yokouchi, Y., and Young, D. (2019). Increase in CFC-11 emissions from eastern China based on atmospheric observations. *Nature*, 569(7757):546–550.

Ruiz, G. M., Rawlings, T. K., Dobbs, F. C., Drake, L. a., Mullady, T., Huq, a., and Colwell, R. R. (2000). Global spread of microorganisms by ships. *Nature*, 408(6808):49–50.

Saiz-Lopez, A. and von Glasow, R. (2012). Reactive halogen chemistry in the troposphere. *Chemical Society Reviews*, 41(19):6448.

Salawitch, R. J. (2006). Biogenic bromine. *Nature*, 439(7074):275–277.

Salawitch, R. J., Weisenstein, D. K., Kovalenko, L. J., Sioris, C. E., Wennberg, P. O., Chance, K., Ko, M. K. W., and McLinden, C. A. (2005). Sensitivity of ozone to bromine in the lower stratosphere. *Geophysical Research Letters*, 32(5):1–5.

Seidel, D. J., Fu, Q., Randel, W. J., and Reichler, T. J. (2008). Widening of the tropical belt in a changing climate. *Nature Geoscience*, 1(1):21–24.

Shah, A. D., Liu, Z.-Q., Salhi, E., Höfer, T., Werschkun, B., and von Gunten, U. (2015). Formation of disinfection by-products during ballast water treatment with ozone, chlorine, and peracetic acid: influence of water quality parameters. *Environmental Science: Water Research & Technology*, 1(4):465–480.

Sherwen, T., Schmidt, J. A., Evans, M. J., Carpenter, L. J., Großmann, K., Eastham, S. D., Jacob, D. J., Dix, B., Koenig, T. K., Sinreich, R., Ortega, I., Volkamer, R., Saiz-Lopez, A., Prados-Roman, C., Mahajan, A. S., and Ordóñez, C. (2016). Global impacts of tropospheric halogens (Cl, Br, I) on oxidants and composition in GEOS-Chem. *Atmospheric Chemistry and Physics*, 16(18):12239–12271.

Simpson, W. R., Brown, S. S., Saiz-Lopez, A., Thornton, J. A., and von Glasow, R. (2015). Tropospheric Halogen Chemistry: Sources, Cycling, and Impacts. *Chemical Reviews*, 115(10):4035–4062.

Sinnhuber, B.-M. and Meul, S. (2015). Simulating the impact of emissions of brominated very short lived substances on past stratospheric ozone trends. *Geophysical Research Letters*, 42(7):2449–2456.

Sinnhuber, B.-M., Sheode, N., Sinnhuber, M., Chipperfield, M. P., and Feng, W. (2009). The contribution of anthropogenic bromine emissions to past stratospheric ozone trends: a modelling study. *Atmospheric Chemistry and Physics*, 9(8):2863–2871.

Solomon, S. (1999). Stratospheric ozone depletion: A review of concepts and history. *Reviews of Geophysics*, 37(3):275–316.

Sowers, J., Vengosh, A., and Weinthal, E. (2011). Climate change, water resources, and the politics of adaptation in the Middle East and North Africa. *Climatic Change*, 104(3-4):599–627.

Stohl, A., Forster, C., Frank, A., Seibert, P., and Wotawa, G. (2005). Technical note: The Lagrangian particle dispersion model FLEXPART version 6.2. *Atmospheric Chemistry and Physics*, 5(9):2461–2474.

Tamelander, J., Riddering, L., Haag, F., and Matheickal, J. (2010). Guidelines for development of a national ballast water management strategy. *GEF-UNDP-IMO GloBallast, London, UK and IUCN, Gland, Switzerland*, GloBallast(No. 18).

Taylor, C. J. (2006). The effects of biological fouling control at coastal and estuarine power stations. *Marine Pollution Bulletin*, 53(1-4):30–48.

Tegtmeier, S., Krüger, K., Quack, B., Atlas, E. L., Pisso, I., Stohl, A., and Yang, X. (2012). Emission and transport of bromocarbons: from the West Pacific ocean into the stratosphere. *Atmospheric Chemistry and Physics*, 12(22):10633–10648.

Tegtmeier, S., Ziska, F., Pisso, I., Quack, B., Velders, G. J. M., Yang, X., and Krüger, K. (2015). Oceanic bromoform emissions weighted by their ozone depletion potential. *Atmospheric Chemistry and Physics*, 15(23):13647–13663.

Theiler, R., Cook, J. C., Hager, L. P., and Siuda, J. F. (1978). Halohydrocarbon Synthesis by Bromoperoxidase. *Science*, 202(4372):1094–1096.

Thompson, A. M. (1992). The Oxidizing Capacity of the Earth's Atmosphere: Probable Past and Future Changes. *Science*, 256(5060):1157–1165.

UNCTAD (2017). *Review of Maritime Transport 2017*. Number United Nations, New York/Geneva in Review of Maritime Transport. UN.

UNCTAD (2018). Review of Maritime Transport 2018. *Report by the UNCTAD secretariat*, (United Nations, New York/Geneva):1–116.

Wales, P. A., Salawitch, R. J., Nicely, J. M., Anderson, D. C., Canty, T. P., Baidar, S., Dix, B., Koenig, T. K., Volkamer, R., Chen, D., Huey, L. G., Tanner, D. J., Cuevas, C. A., Fernandez, R. P., Kinnison, D. E., Lamarque, J.-F., Saiz-Lopez, A., Atlas, E. L., Hall, S. R., Navarro, M. A., Pan, L. L., Schauffler, S. M., Stell, M., Tilmes, S., Ullmann, K., Weinheimer, A. J., Akiyoshi, H., Chipperfield, M. P., Deushi, M., Dhomse, S. S., Feng, W., Graf, P., Hossaini, R., Jöckel, P., Mancini, E., Michou, M., Morgenstern, O., Oman, L. D., Pitari, G., Plummer, D. A., Revell, L. E., Rozanov, E., Saint-Martin, D., Schofield, R., Stenke, A., Stone, K. A., Visioni, D., Yamashita, Y., and Zeng, G. (2018). Stratospheric Injection of Brominated Very Short-Lived Substances: Aircraft Observations in the Western Pacific and Representation in Global Models. *Journal of Geophysical Research: Atmospheres*, 123(10):5690–5719.

Wanninkhof, R. (1992). Relationship Between Wind Speed and Gas Exchange Over the Ocean. *Journal of Geophysical Research*, 97(C5):7373–7382.

Warwick, N. J., Pyle, J. A., Carver, G. D., Yang, X., Savage, N. H., O'Connor, F. M., and Cox, R. A. (2006). Global modeling of biogenic bromocarbons. *Journal of Geophysical Research*, 111(D24):D24305.

Werschkun, B., Sommer, Y., and Banerji, S. (2012). Disinfection by-products in ballast water treatment: An evaluation of regulatory data. *Water Research*, 46(16):4884–4901.

WHO (2011). Guidelines for drinking-water quality. *4th Edition*, WHO, Genev.

Wisher, A., Oram, D. E., Laube, J. C., Mills, G. P., van Velthoven, P., Zahn, A., and Brenninkmeijer, C. A. M. (2014). Very short-lived bromomethanes measured by the CARIBIC observatory over the North Atlantic, Africa and Southeast Asia during 2009–2013. *Atmospheric Chemistry and Physics*, 14(7):3557–3570.

Yamamoto, H., Yokouchi, Y., Otsuki, A., and Itoh, H. (2001). Depth profiles of volatile halogenated hydrocarbons in seawater in the Bay of Bengal. *Chemosphere*, 45(3):371–377.

Yang, B., Yang, G.-P., Lu, X.-L., Li, L., and He, Z. (2015). Distributions and sources of volatile chlorocarbons and bromocarbons in the Yellow Sea and East China Sea. *Marine Pollution Bulletin*, 95(1):491–502.

Yang, J. S. (2001). Bromoform in the effluents of a nuclear power plant: A potential tracer of coastal water masses. *Hydrobiologia*, 464:99–105.

Yang, X., Abraham, N. L., Archibald, A. T., Braesicke, P., Keeble, J., Telford, P. J., Warwick, N. J., and Pyle, J. A. (2014). How sensitive is the recovery of stratospheric ozone to changes in concentrations of very short-lived bromocarbons? *Atmospheric Chemistry and Physics*, 14(19):10431–10438.

Yang, X., Cox, R. A., Warwick, N. J., Pyle, J. A., Carver, G. D., O'Connor, F. M., and Savage, N. H. (2005). Tropospheric bromine chemistry and its impacts on ozone: A model study. *Journal of Geophysical Research*, 110(D23):D23311.

Yokouchi, Y., Hasebe, F., Fujiwara, M., Takashima, H., Shiotani, M., Nishi, N., Kanaya, Y., Hashimoto, S., Fraser, P., Toom-Sauntry, D., Mukai, H., and Nojiri, Y. (2005). Correlations and emission ratios among bromoform, dibromochloromethane, and dibromomethane in the atmosphere. *Journal of Geophysical Research*, 110(D23):D23309.

Ziska, F., Quack, B., Abrahamsson, K., Archer, S. D., Atlas, E., Bell, T., Butler, J. H., Carpenter, L. J., Jones, C. E., Harris, N. R. P., Hepach, H., Heumann, K. G., Hughes, C., Kuss, J., Krüger, K., Liss, P., Moore, R. M., Orlikowska, A., Raimund, S., Reeves, C. E., Reifenhäuser, W., Robinson, A. D., Schall, C., Tanhua, T., Tegtmeier, S., Turner, S., Wang, L., Wallace, D., Williams, J., Yamamoto, H., Yvon-Lewis, S., and Yokouchi, Y. (2013). Global sea-to-air flux climatology for bromoform, dibromomethane and methyl iodide. *Atmospheric Chemistry and Physics*, 13(17):8915–8934.

Ziska, F., Quack, B., Tegtmeier, S., Stemmler, I., and Krüger, K. (2017). Future emissions of marine halogenated very-short lived substances under climate change. *Journal of Atmospheric Chemistry*, 74(2):245–260.

Acknowledgements

For of obtaining a doctorate, there were a few ingredients necessary, and when mixed together resulted in a well-prepared and ready-served thesis.
First of all, I needed a brilliant supervisor. The great 'Doktormutter' Susann formed the basis of the whole project and worked as both the main ingredient as well as the necessary spiciness. Her expertise and commitment created the right texture and made sure the thesis succeeded.
More taste was added by my ISOS committee members Birgit and Arne, who brought new flavours into the thesis. The right dosage of chemistry and physics by the observer and modeller was the perfect balance. The thesis could only be successfully finished because it was prepared in the right kitchen. A good working environment and helpful co-workers were essential. Yue, Tania, Silke, Katja and the Happy-ME did a great job. The rest was only heating, stirring, compiling, writing, resilience and endurance.
A well-dosed crash-course about basic chemistry was provided by Michael and a thoughtful care-package by Katharina. The stress ball relieved me from my world problems.
Reaching this milestone could only be accomplished because of my friends. They shared the same fate and accompanied me during my formation from a fresher to a scientist: Wilma, Christian, Svenja, Kristin, Gesa, Niklas, Matthias, Heiko and Annika (in reverse order of physical distance). You are the best crew that carried me through ten years of academic life and shared the best experiences. Looking forward to even more memorable moments yet to come.
My career as a scientist was only possible with support from Cordula and Christof. They encouraged me my whole life to complete everything that I started and thought I had the brains for anything. My whole family provided me with delicious side-dishes of empathy, humour and optimism. In remembrance of Miki and her infinite optimism.
Johannes was the guardian angel of my thesis. Thanks! For everything.

Eidesstattliche Erklärung

Hiermit erkläre ich, Josefine Maas, dass ich die vorliegende Arbeit eigenständig verfasst habe und alle Referenzen und Hilfsmittel als solche gekennzeichnet habe. Die Doktorarbeit wurde unter Einhaltung der Regeln guter wissenschaftlicher Praxis der Deutschen Forschungsgemeinschaft erstellt. Ich habe die Arbeit weder ganz noch zum Teil an anderer Stelle zur Prüfung vorgelegt, nirgendwo veröffentlicht, noch zur Veröffentlichung eingereicht. Mir wurde kein akademischer Grad entzogen.

Datum, Unterschrift